Terms and Conditions of Use of Digitised Theses from Trinity College Library Dublin

Copyright statement

All material supplied by Trinity College Library is protected by copyright (under the Copyright and Related Rights Act, 2000 as amended) and other relevant Intellectual Property Rights. By accessing and using a Digitised Thesis from Trinity College Library you acknowledge that all Intellectual Property Rights in any Works supplied are the sole and exclusive property of the copyright and/or other IPR holder. Specific copyright holders may not be explicitly identified. Use of materials from other sources within a thesis should not be construed as a claim over them.

A non-exclusive, non-transferable licence is hereby granted to those using or reproducing, in whole or in part, the material for valid purposes, providing the copyright owners are acknowledged using the normal conventions. Where specific permission to use material is required, this is identified and such permission must be sought from the copyright holder or agency cited.

Liability statement

By using a Digitised Thesis, I accept that Trinity College Dublin bears no legal responsibility for the accuracy, legality or comprehensiveness of materials contained within the thesis, and that Trinity College Dublin accepts no liability for indirect, consequential, or incidental, damages or losses arising from use of the thesis for whatever reason. Information located in a thesis may be subject to specific use constraints, details of which may not be explicitly described. It is the responsibility of potential and actual users to be aware of such constraints and to abide by them. By making use of material from a digitised thesis, you accept these copyright and disclaimer provisions. Where it is brought to the attention of Trinity College Library that there may be a breach of copyright or other restraint, it is the policy to withdraw or take down access to a thesis while the issue is being resolved.

Access Agreement

By using a Digitised Thesis from Trinity College Library you are bound by the following Terms & Conditions. Please read them carefully.

I have read and I understand the following statement: All material supplied via a Digitised Thesis from Trinity College Library is protected by copyright and other intellectual property rights, and duplication or sale of all or part of any of a thesis is not permitted, except that material may be duplicated by you for your research use or for educational purposes in electronic or print form providing the copyright owners are acknowledged using the normal conventions. You must obtain permission for any other use. Electronic or print copies may not be offered, whether for sale or otherwise to anyone. This copy has been supplied on the understanding that it is copyright material and that no quotation from the thesis may be published without proper acknowledgement.

Modulation of the Blood-Brain Barrier for Therapeutic Benefit

A Thesis Submitted to the Trinity College Dublin, the University of Dublin, for the Degree of Doctor of Philosophy

By

Finnian Hanrahan

February 2014

Under the supervision of Prof. Pete Humphries

Department of Genetics

University of Dublin

Trinity College

Declaration

I declare that this thesis has not been submitted as an exercise for a degree at this or any other university and it is entirely my own work, except where noted.

I agree to deposit this thesis in the University's open access institutional repository or allow the library to do so on my behalf, subject to Irish Copyright Legislation and Trinity College Library conditions of use and acknowledgement.

Finnian Hanrahan

September 2013

Summary

To date this lab has carried out novel work in the area of low-molecular weight (<1 kDa) drug delivery to the retina (Campbell, Nguyen et al. 2009; Tam, Kiang et al. 2010). This work was carried by suppression of claudin-5 (CL5), a tight junction protein expressed on endothelial cells of the inner blood-retina barrier, by delivery of small interfering RNA molecules. Recently this work has been extended to include a limited study on suppression of claudin-5 at the blood-brain barrier (BBB), and this resulted in successful delivery of a low-molecular weight compound to the brain (Campbell, Humphries et al. 2011). The primary goal of the study presented here is to extend this BBB modulation to a comprehensive exploration of the benefits of barrier modulation to conditions affecting the brain.

This study is divided into four separate results chapters, which separate different areas of focus as well as representing a roughly chronological record of projects that were undertaken. The first of these chapters focuses on establishing protocols demonstrating the effective suppression of CL5 using CL5 siRNA. Successful suppression was observed both in vitro and in vivo in mice, and this was matched by observed BBB modulation, which peaked 48hrs after siRNA injection. Furthermore, in this chapter it is demonstrated that CL5 siRNA administration fails to provoke an interferon-response in vitro or in vivo.

In the next chapter barrier modulation is employed in a model of glioblastomas inoculated into immune-deficient mice. To develop a model of glioblastoma in the lab a

number of brain tumour cell lines were first characterised for their ability to grow in vitro and to reconstitute a tumour in vivo. Following this a number of experiments were carried out to modulate the BBB in mice with inoculated glioblastomas. This was done in order to observe an increased range of delivery of a low-molecular weight compound to the tumour regions, and following this to deliver a number of chemotherapeutics in animals in the presence or absence of CL5 suppression.

The third results chapter focussed on a different hypothesised benefit of BBB modulation. Here instead of delivery a compound to the brain, traumatic brain injury (TBI) was employed in order to explore if CL5 suppression could release the water build-up that is characteristic of TBI-associated oedema. To this end a model of cold-induced TBI was established and characterised. Following this the effect of CL5 siRNA on oedema volume and brain water content was analysed, as were cognitive outcomes following injury and siRNA administration. A number of MRI analyses were also carried in order to elucidate the effect that CL5 siRNA was having on the BBB in the proximity of a TBI. Furthermore alterations were made to the siRNA dose and time of delivery, in order to attempt to ascertain the clinical parameters that would need to be specified would this work succeed in progressing from the lab.

The final results chapter studied inflammation following TBI. The expression level of a number of cytokines and growth factors were measured following TBI with or without CL5 siRNA delivery. When some factors were found to be differentially regulated in the two groups this analysis was extended to include 40 different inflammatory markers. Following these analyses TBIs were administered in a number of murine knockouts of

core elements of sterile inflammation, with lesion volume and cognitive outcome being recorded for each.

Acknowledgements

Many thanks to my supervisor Prof. Peter Humphries, who provided invaluable support and direction throughout my years in his lab. The door to his office was always open, whether to talk about inspiration for upcoming projects, problems with current ones, or about sailing around Mizen Head. The friendly atmosphere that this created made working in the Humphries lab a fantastic and an extremely memorable experience.

Thank you also to Dr. Matthew Campbell, for providing huge amounts of direct input into the projects on which I worked. Matt is a tireless worker and he taught me a huge amount over my four years working closely with him. I hugely appreciate his candid attitude and his patience with my many pestering questions.

Thanks also go to Dr. Marian Humhpries, Dr. Anna-Sophia Kiang, Dr. Anh Nguyen, Lawrence Tamm, Ema Ozaki, James Keaney, Kelly Mulfaul, Mayu Suzuki, Dr. Christoph Blau, Dr. Oliviero Gobbo and Rustam Rakhmatullin for immeasurable amount of help provided and great times had. Also, thank you to the people of the Farrar lab for all the help, support and good times over the past four years.

Finally, I want to thank from the bottom of my heart all the people who made this thesis possible, through their friendship and their support. Cathal Daly and Kevin Crowley for the great times out and amazing holidays away from it all, as well as advice for my over-complicated life; Alistair Wilson for being my friend through good times and bad, and for all the Sundays playing Starcraft and drinking coffee; Simon Mc Keagney and Michael Pidgeon for being amazing friends for so many years, for drunken ramblings and a sobering perspective on things; Gareth O'Dwyer and Claire Kilty for so much support and

friendship, and most of all for listening to me complain during the four years of my PhD. I want to also thank Stéphanie O'Keeffe for all of her kindness and love. Stéphanie, you made what should be one of the most difficult years of someone's life into the best I've yet had. Thank you.

Finally, thank you to my parents, Elisabeth Muller and Derek Hanrahan, and my sisters Alanna and Fidelma. Family is a person's core, their foundation, and I'm so proud to have the family that I do.

Table of Contents

Chapter 1: General Introduction

The brain and retina are energy-demanding tissues that are suffused with capillaries, no neuron in fact, being more than a 40^{th} of a millimetre away from a supplying blood vessel (Pardridge 2005). The endothelial cells lining the brain and inner retinal vasculatures are sealed by so-called 'tight junctions' (TJs) comprising over 40 proteins – these representing the blood-brain and inner blood retina barriers (Anderson and Van Itallie 2009), and they have evolved for the very important purpose of preventing harmful blood-borne agents such as antibodies, anaphylatoxins, small enzymes, pathogens etc from entering the highly delicate cerebral and retinal environments. Notwithstanding this critically important protective function, these same barriers have prevented an estimated 98% of systemically administrable low molecular weight potentially therapeutic drugs from entering the brain (Pardridge 2005), and in cases of cerebral oedema, they prevent fluid moving from the cerebral compartment into the peripheral circulation. For this reason, it has proven to be extremely difficult to systemically treat brain malignancies with low molecular weight cytotoxic drugs that are normally in widespread use for treatment of other forms of malignancy, and for the same reason, methods for alleviation of cerebral oedema induced by traumatic brain injury (TBI) are inadequate and have hardly changed in the last eighty years. In the studies reported in this thesis the hypothesis was addressed that it is possible, by RNAi-mediated down-regulation of selected TJ transcripts, to marginally increase permeability at the BBB such as to allow entry from the bloodstream into the brain of potentially therapeutic low molecular weight compounds, or to allow fluid out in a safe and controllable manner in murine models of brain malignancy and TBI. In this introductory chapter I provide a detailed

account of our knowledge of the BBB, of the clinical features of glioblastoma and TBI, of the inadequacies of current treatments, and of the RNAi-mediated strategy that has been developed to address such deficiencies.

1.1 The Blood-Brain Barrier

The delicate tissue of the brain requires a highly regulated environment, with fluctuations in the concentrations of particular ions, such as Na^+, K^+ and Ca^{2+}, being detrimental to neuronal function (Hawkins and Davis 2005). The CNS is also an organ that is slow to repair, if repair is possible at all, and governs all the major functions of the body that keep us functioning and alive. As such, conditions that might be mildly damaging to peripheral organs, such as bacterial or viral infection, inflammation or complement activation, could be hugely detrimental if they occurred in the CNS. In this regard, the necessity for a distinct separation of the CNS from the circulating bloodstream is of fundamental importance, and it is this separation that underlies the key function and presence of the BBB, ensuring strict homeostasis of the brain environment to keep neurons in good functional state.

The first evidence of the BBB was described by Paul Ehrlich and his student Edwin Goldmann (Mott 1913). Ehrlich found that injection of water-soluble dyes into the circulatory system stained all organs except for the brain and spinal cord. He attributed this to nervous tissue having low affinity for the dye, however in 1913 Goldmann

discovered that injection of trypan blue directly into the cerebrospinal fluid (CSF) stained the CNS but not the bloodstream. Golmann's findings are illustrated in *Figure 1.1*.

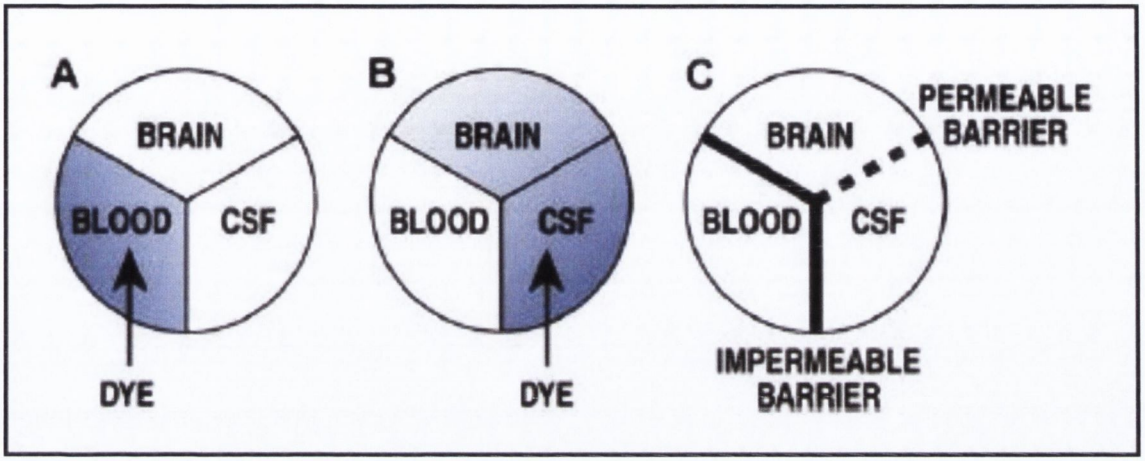

Figure 1.1: The results and conclusions of Goldmann's experiments on the BBB. *(A) Goldmann first injected trypan blue into the bloodstream, resulting in colouration of the blood but not the brain and CSF; (B) the reverse experiment was carried out whereby dye was injected into the CSF resulting in a blue CNS but normally coloured blood; (C) Goldmann concluded that a barrier permeable to trypan blue existed between the CSF and the brain, while an impermeable one existed between the blood and the CNS. (Zlokovic 2008)*

In subsequent years Goldmann's experiments received much criticism, with many researchers concluding that the different compositions of blood and CSF influenced the speed at which diffusion from one to the other took place. The field reached a turning point however in experiments by Hugh Davson which measured the rates of diffusion of Ringer solution into brain and skeletal muscle excised from bodies. Equilibration occurred at a comparable rate in both tissues, indicating that a barrier existed between the two in

the living body, rather than a fundamental difference in the makeup of the tissues (Davson and Spaziani 1959).

The cause for this barrier to delivery to the CNS is that blood capillaries in the brain are 50-100 times more resistant to transport across them than microvessels in other major organs (Abbott 2002). This resistance develops over time during development, with the blood-brain barrier (BBB) in 17-20 day foetal rats having a trans endothelial electrical resistance (TER) of 310 Ωcm^2 – still somewhat leaky; from 21 days gestation, the resistance was measured at 1128 Ωcm^2, indicating a tight BBB and low ion permeability. Following birth this had increased slightly more to 1462 Ωcm^2 in 28-33 day old rats, and this was found to be higher in arterial vessels than in veins (Butt, Jones et al. 1990). This latter observation concurs with another study that found that arterial endothelial cells express 18-fold protein and 9-fold mRNA of some tight junction (TJ) constituents as their venous counterparts (Kevil, Okayama et al. 1998), which may be a requirement in the face of higher pressure present in the arteries.

Endothelial cells of the brain and of peripheral blood vessels, such as the aorta, are morphologically similar (Antonov, Lukashev et al. 1986), although aorta endothelial cells appear to more regularly demonstrate large multinuclear cells, with increasing frequency in adult aortas and in aortas affected by atherosclerosis (Antonov, Lukashev et al. 1986; Antonov, Nikolaeva et al. 1986). TER values, in contrast, differ greatly with peripheral endothelial cells demonstrating resistance of only 10-50 Ωcm^2, and are permeable to both small and large molecules. This difference in barrier properties between endothelial cells of different origins coincides with the microscopy observation that tight barrier-forming

endothelial cells have filamentous actin structures associated with junctional complexes laid out in tight belt-like structures, whereas in peripheral endothelial cells these actin structures are diffusely spread (Rubin, Hall et al. 1991). The similarity in morphology and non-barrier characteristics between endothelial cells in the CNS and in the rest of the body suggest that it is the microenvironment in which they reside that dictates their differing characteristics. Indeed it has been demonstrated in a number of studies that when cultured with factors that would be present in the brain, peripheral endothelial cells obtain many of the characteristics specific to those that form the BBB, including increased barrier strength (Hurst and Fritz 1996; Kuchler-Bopp, Delaunoy et al. 1999).

1.1.1 Cellular Composition of the Blood-Brain Barrier

Despite the importance of endothelial cells to the BBB, many other cell types and structures in and surrounding the blood vessels of the brain have been found to contribute to its function. In blood vessels themselves the basement membrane on the ablumenal side of endothelial cells must be crossed following crossing of the endothelial cell layer. In veins and arteries smooth muscle cells and pericytes surround the vessels and must also be breached by cells or substances to gain access to the brain, while in capillaries the former cell type is not present. Final to the blood vessel component of the BBB there is the outer vascular basement membrane, another membrane consisting of connective tissue proteins such as collagen and integrins. Surrounding the veins and arteries of the brain is the perivascular compartment, consisting of perivascular fluid and cells occupying the perivascular space – usually leptomeningeal cells and macrophages. Finally, before entering the brain parenchyma proper, the last barrier to cellular or

molecular entry to or exit from the brain is the glia limitans. This is formed by a further basement membrane as well as astrocytic and microglial endfeet (Bechmann, Galea et al. 2007) (*Figure 1.2*).

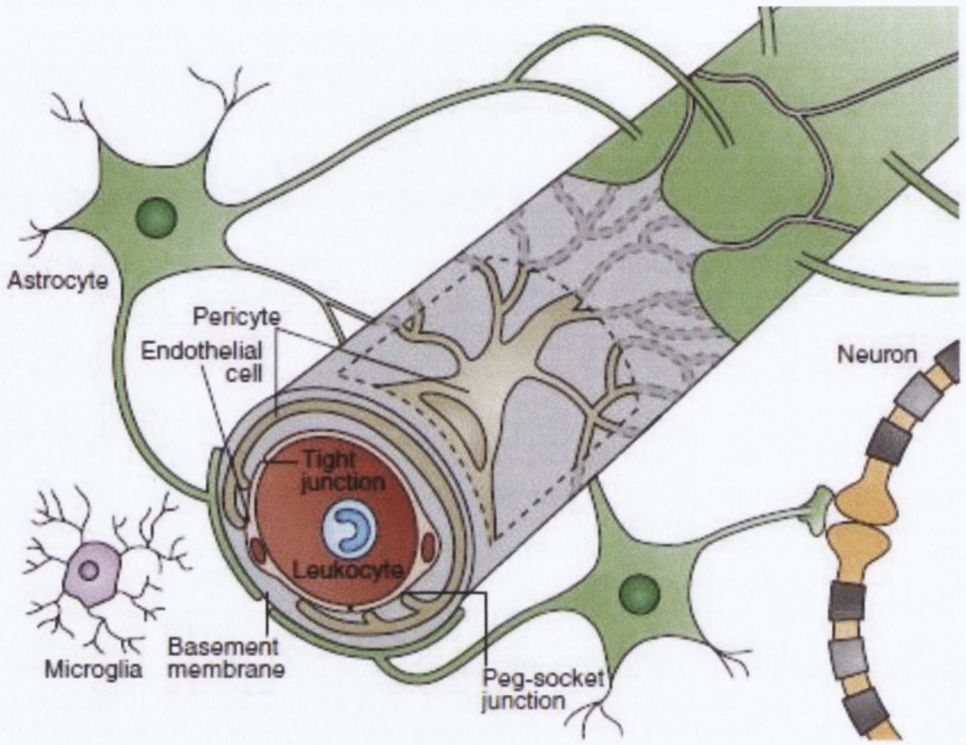

Figure 1.2: Cellular composition of the BBB. *Endothelial cells, joined by tight junctions, are surrounded by pericytes within a basement membrane. Outside of this astrocyte end-feet surround the entire BBB unit. (Obermeier, Daneman et al. 2013)*

Endfeet of astrocytic glial cells are observed to surround the endothelial cells of the BBB (Kacem, Lacombe et al. 1998) (*Figure 1.2*), and the proximity of these cells appears to be crucial for BBB integrity. This is observed to be true as brain vessels grown amidst peripheral tissue become more leaky to tracer molecules, whereas the initially leaky blood vessels of other tissues increase their tightness when grown amidst brain tissue (Bauer and Bauer 2000). Also, brain endothelial cells isolated and grown in culture

generally have some loss of barrier characteristics, and some of these properties can be restored by co-culture with glial cells (Abbott 2002). This effect of astrocytes on barrier strength is not dependent on contact between endothelial cells and astrocytes, but instead appears to be a result of factor released by the latter. Neither is their effect solely to strengthen the barrier – ATP, endothelin-1, glutamate, nitric oxide and cytokines such as IL-1β are all substances released by astrocytes under certain conditions which temporarily increase BBB permeability (Abbott 2002).

Interestingly some parts of the brain do not have a BBB at all, or have a diminished barrier. Chemokine expression in response to systemic injection of LPS, IL-1β, and TNF-α is confined in the brain to the circumventricular organs, choroid plexus, leptomeninges, and cerebral blood vessels (Thibeault, Laflamme et al. 2001). Together these structures form the interface between systemic circulating molecules and the brain. The circumventricular organs have secretory and sensory functions, such as the area postrema which initiates vomiting in response to toxins in the bloodstream (Maolood and Meister 2009), and in these cases this tissue must be exposed to all the substances present in the blood in order to carry out their functions. Otherwise however, the BBB is an essential barrier required to maintain a stable and controlled microenvironment for sensitive neural tissue to function.

1.1.2 Development and Maintenance of the Blood-Brain Barrier

Central to the development of the BBB is the Wnt-β-catenin signalling pathway. This pathway is active in endothelial cells of the CNS, but not in peripheral regions of the

developing embryo (Daneman, Agalliu et al. 2009). Within the CNS different elements of the Wnt-β-catenin signalling pathway play roles in distinct regions, with Wnt 1, 3 and 3b being expressed in the dorsal spinal cord and hindbrain, and Wnt7a and 7b expression in the forebrain and ventral neural tube. Interference with Wnt signalling during development results in death of the developing embryo due to brain haemorrhages, with abnormal vessel growth being observed in the CNS but not elsewhere (Daneman, Agalliu et al. 2009).

Wnt-β-catenin signalling functions initially by the binding of Wnt to Fzd receptors located on the cell membrane of endothelial cells, and this binding results in the accumulation of β-catenin due to inhibition of its degradation. B-catenin then translocates to the nucleus where it induces the transcription of genes involved in BBB function (Logan and Nusse 2004; Reis, Czupalla et al. 2012). This signalling pathway results in the expression of the distinct transcriptome specific to the BBB (Daneman, Zhou et al. 2010), with BBB-specific genes such as Slc2a1 (which encodes Glut-1) (Stenman, Rajagopal et al. 2008), Stra6 (Szeto, Jiang et al. 2001), Pvlap, and Claudin-3 (Liebner, Corada et al. 2008).

Sonic Hedgehog (Shh) is another major signalling factor which initiates BBB development in the developing embryo. This protein is produced and secreted by astrocytes, and its absence also results in embryonic death associated with deficits in the formation of blood vessels in the brain (Alvarez, Dodelet-Devillers et al. 2011). Shh appears to play a role not only in the development of the BBB, but also in its maintenance, with endothelial cells exposed to this form of astrocytic signalling demonstrating increased expression of TJ proteins and a consequent increase in barrier strength (Alvarez, Dodelet-Devillers et al.

2011). The importance of Shh and other astrocyte-produced factors in the maintenance of BBB characteristics is backed up by findings that the characteristics are lost by endothelial cells when astrocytes are depleted from the brain, and that this change is reversible (Willis, Leach et al. 2004; Willis 2012). Barrier properties are also increased in cells grown in vitro by their co-culture with astrocytes (Hayashi, Nomura et al. 1997). Similarly pericytes have been found to be essential for BBB integrity, with observations of negative correlations between pericyte coverage of blood vessels and barrier permeability (Armulik, Genove et al. 2010).

1.1.3 Traversing the Blood-Brain Barrier

Transport across the BBB is, to a great extent, confined to transcellular pathways. Some substances can cross the barrier paracellularly but these are usually extremely small or employ specific mechanisms in order to move between endothelial and other cell types, such as T-cell migration across the BBB by means of a process initiated by leucocyte binding to ICAM-1 and -2 expressed on endothelial cell surfaces (Steiner, Coisne et al. 2010).

Transcellular transport pathways make use of receptors that recognise and transport specific molecules that are required for neuronal function. For instance the brain's energy needs are met by proteins such as GLUT1 which transports glucose across the endothelial cell layer (Pardridge and Oldendorf 1975). Peptides that are required, such as hormones, are recognised by specific receptors, for example PST-1 which recognises vasopressin (Banks 2006). Ion concentrations are kept constant by proteins such as Na^+, K^+, ATPase

which exchanges sodium and potassium ions (Betz 1983). Organic anions, meanwhile, are transported by OAT-family proteins, such as OAT1 which is found in the brush border of the choroid plexus (Sugiyama, Kusuhara et al. 1999), which functions to make the cerebrospinal fluid that occupies the ventricular space in the brain and surrounds the spinal cord.

As well as needing to enable the transport of substances required by the brain, the BBB actively effluxes compounds which might be dangerous to the delicate neuronal microenvironment. P-glycoprotein was the first protein observed to transport chemotherapeutic agents out of cancerous cells (Ling 1995) and is expressed at the BBB (Schinkel, Smit et al. 1994) where it plays an active role in preventing access of many drugs to the brain. Other transporters participate in this process too, particularly the multi-drug-resistance-related protein (MRP) family. MRP-4, for instance, is expressed in endothelial cells of the BBB and prevents accumulation of the anti-cancer drug topotecan (Leggas, Adachi et al. 2004) or oseltamivir, a drug targeting the influenza virus (Ose, Ito et al. 2009). More detailed analysis of transport and efflux across the BBB is reviewed in Ueno, Nakagawa et al. 2010.

1.1.4 Tight junctions

Tight junctions (TJs), also known as occluding junctions or zonula occludens, are contact points between the plasma membranes of adjacent cells, observed under electron microscopy such as in *Figure 1.3 (a)*.

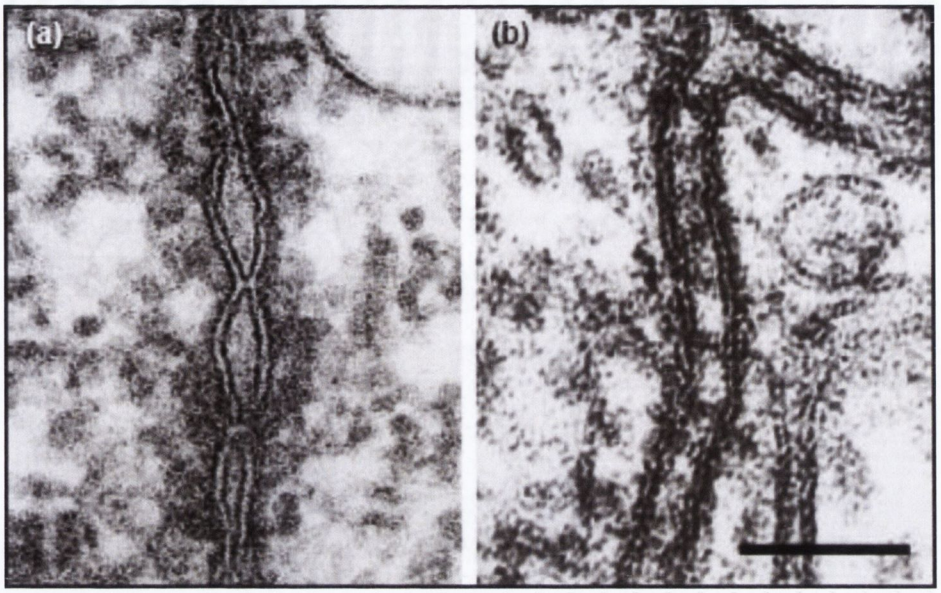

Figure 1.3: Electron micrographs of paracellular junctions in vertebrates and invertebrates. *(a) Vertebrate tight junctions; (b) invertebrate septate junctions. (Furuse and Tsukita 2006)*

TJs are positioned at the apical end of the plasma membrane, and as observed in *Figure 1.3 (a)* each TJ is paired to and associates with another TJ on the membrane of the adjacent cell. TJs function as sites for vesicle targeting, proliferation and transcription signals, defining cell polarity, and most crucially it is these structures which limit paracellular transport across the BBB, as well as the BRB and to a lesser extent other endothelial barriers (Anderson and Van Itallie 2008).

All metazoans have some form of paracellular barrier, however TJs are specific to vertebrates. *Figure 1.3 (b)* shows an image from an electron microscope of the related invertebrate septate junction. These two structures appear to share similar functions in reducing permeability between cells of the BBB, although septate junctions have been

reported to be readily permeable to certain small molecules such as sucrose (Skaer, Maddrell et al. 1987), which cannot travel across vertebrate TJs (Johansson, Dziegielewska et al. 2006).

Each TJ actually consists of at least three different types of protein – occludin, members of the junction adhesion molecule (JAM) family of proteins, and claudin proteins (Ben-Yosef, Belyantseva et al. 2003) – but can consist of over 40 individual proteins between support proteins, structural proteins, transport proteins, and other more unique proteins such as tricellulin, a homologue of occludin that concentrates when three cells come together (Anderson and Van Itallie 2008). The actin cytoskeleton of the cell appears to be key to TJ formation, as onto this framework of actin strands bind the PDZ-domain containing support proteins including ZO-1, ZO-2, ZO-3, MAGI-1, PatJ, PALS1 and MUPP1. It is onto these proteins that the transmembrane proteins that form the TJ pore bind – these are occludin, JAM proteins, and primarily the claudin protein family (Anderson and Van Itallie 2008). The current model of TJ structure is illustrated in *Figure 1.4*.

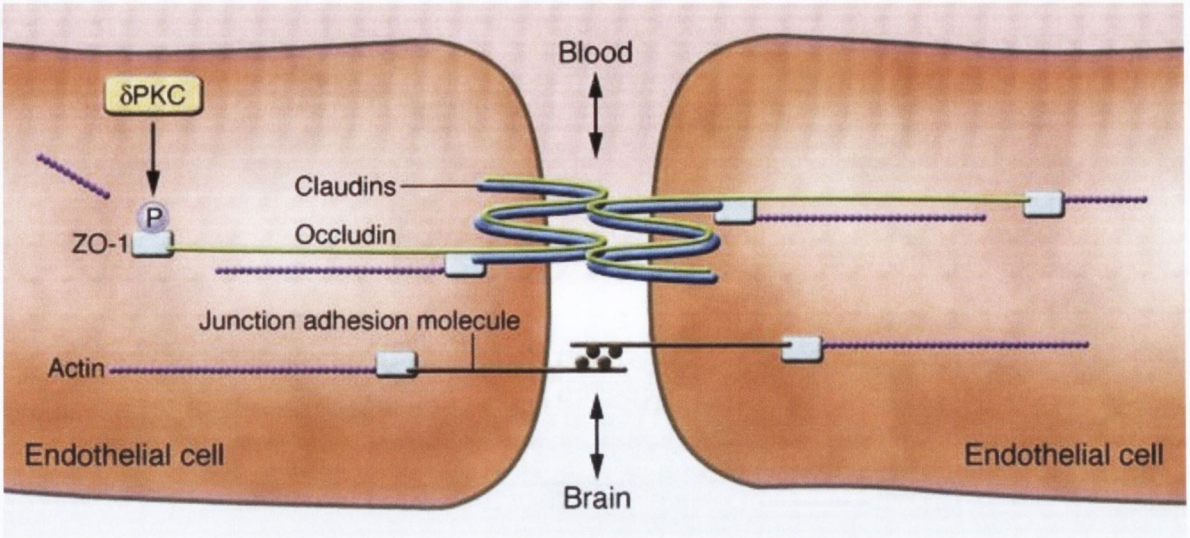

Figure 1.4: ***Model of a tight junction at the BBB.***

TJs form at the apical end of adjacent endothelial cells. Claudin tails bind PDZ-domains of scaffolding proteins which bind actin filaments, possibly resulting in regulation of the barrier by the cytoskeleton. (Image sourced from: http://www.brainfrontier.or.kr/newsletter/vol.29/Vol_07.html)

The TJ is also strongly linked in function to the more basolateral-positioned cadherin-based adherens junction. At adherens junctions, the protein VE-cadherin can act as a mediator of intracellur signalling via its interaction with phosphatidylinositol-3-OH kinase or indeed various growth factor receptors. VE-cadherin has also been shown to interact directly with the known transcription factor β-catenin, which can then regulate cellular homeostasis or responses to cellular stress (Taddei, Giampietro et al. 2008).

Paracellular transport of molecules is exclusively passive, driven by electro-osmotic or concentration gradients (Van Itallie and Anderson 2004). The resistance of the BBB to paracellular transport of all but a very few molecules is matched by the observation that

endothelial cells of the barrier contain 2-4 times the number of mitochondria compared with their peripheral counterparts (Oldendorf, Cornford et al. 1977). This fuels the increased transcellular transport across specific transporters in order to bypass the paracellular TJs. Also, while infections of the CNS are an important cause of illness and death worldwide, the majority of the infectious agents in these diseases have methods to bypass TJs. For instance transcellular traversal of the BBB is the major route for many of the meningitis-causing bacteria, such as E. coli, which attach to and invade human brain microvascular endothelial cells, and traverse them in enclosed vacuoles (Kim 2008). In fact one of the only studied cases of paracellular traversal of the BBB by pathogens is that of the Trypansoma family of protozoa – the cause of sleeping sickness endemic in some parts of Africa – and this is due to the pathogens exploiting IFN-γ signalling by T-cells, a mechanism that results in TJ-loosening to allow leukocyte traversal of the BBB (Masocha, Rottenberg et al. 2007).

Some non-pathogenic diseases of the brain also are believed to occur due to dysfunction in the BBB. For instance new angiogenic blood vessels in the hippocampus have been reported to be linked to epilepsy, as vessels stimulated by VEGF do not form a proper BBB and enable access to the CNS to substances which are damaging to neurons (Rigau, Morin et al. 2007). These substances include albumin, which has been shown to cause epilepsy in animal models when applied to neuronal tissue (Seiffert, Dreier et al. 2004; Ivens, Kaufer et al. 2007). Also, in multiple sclerosis BBB dysfunction or damage appears to enable greater leucocyte passage into the CNS which can then lead to inflammation and progressive demyelination (Alvarez, Cayrol et al. 2011). A similar situation exists in the retina where many inflammatory eye diseases result in BRB dysfunction, permeability and

monocyte infiltration into the retina which in turn leads to significant oxidation and tissue damage (Rajesh, Sulochana et al. 2004). It is clear that the BBB and BRB represent a formidable and essential barrier to unwanted organisms, cells and substances.

1.1.5 Claudins

The permeability of TJs varies considerably among different tissue types, with some tissues varying in electrical conductance, charge selectivity, non-charged solute permeability, and size discrimination. This variation is reflected in TJ compositional heterogeneity, particularly the claudin proteins that are found to be present.

Despite the structural differences between TJs and invertebrate septate junctions, recent studies have identified Drosophila claudin homologues, such as Sinuous and Megatrachea. Septate junctions in null mutants for these genes were found not to exclude a 10 kDa fluorescent tracer, in contrast to wild-type Drosophila which excluded the molecule (Behr, Riedel et al. 2003; Wu, Schulte et al. 2004). Similarly in Caenorhabditis elegans a gene showing sequence similarity to claudins, CLC-1, was shown to be found at septate junctions, and to also allow permeability to a 10 kDa tracer when knocked down (Asano, Asano et al. 2003). It has been suggested however that in contrast to TJs in vertebrates, the invertebrate septate gap of 20 nm is too wide to be crossed by claudin homologues, and that they might function in these animals only in a signalling function (Stork, Engelen et al. 2008). Vertebrate TJs, with a reported width of less than 1 nm (Karakotchian and Fraser 2007), are certainly spanned by claudin family proteins.

Compared with the six reported claudin homologues in Drosophila (Van Itallie and Anderson 2004), and the 5 claudin-like proteins in C. elegans (Asano, Asano et al. 2003), vertebrates have many more claudin proteins with 56 being reported in the puffer fish Fugu rubripes (Loh, Christoffels et al. 2004). Both humans and mice have 24 members of the claudin family, although proteins exist in the 'pfam00822' protein family that share many of claudin family signature features (Van Itallie and Anderson 2004). Structurally claudins are integral membrane proteins with four transmembrane domains and two extracellular and one intracellular loops. In the first extracellular loop claudins have a common WGLWCC motif, and they also possess a C-terminus PDZ domain. This motif binds to the PDZ domains of the TJ support proteins, such as ZO-1, ZO-2, ZO-3 (Itoh, Furuse et al. 1999) and MUPP-1 (Hamazaki, Itoh et al. 2002). The C-terminus tail, but not the PDZ domain, is the region which confers stability to claudins, and swapping the C-terminus tails has been found to coincide with a reversal of protein half-lives (Van Itallie, Colegio et al. 2004). The structure of claudins is illustrated in *Figure 1.5*.

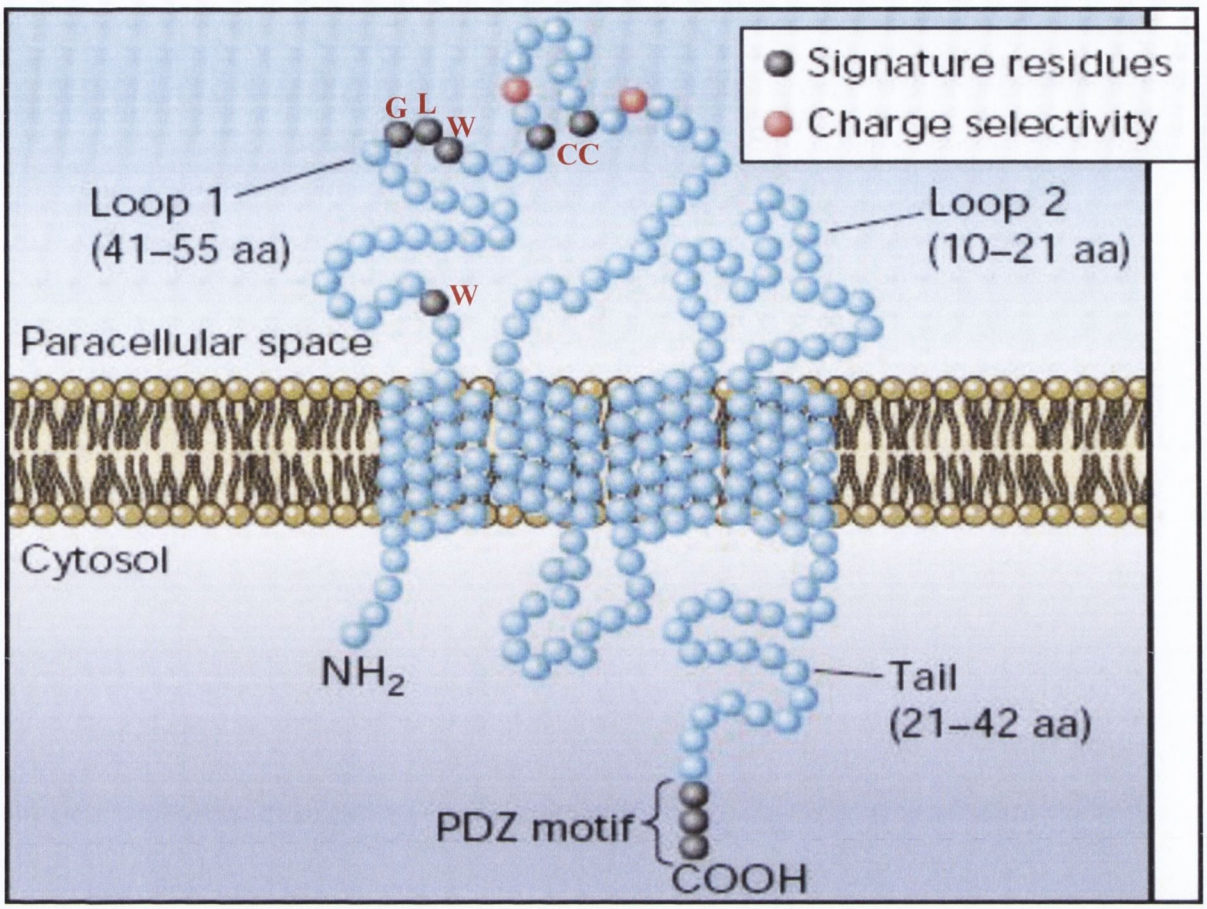

Figure 1.5: Generalised structure of claudin proteins. *Observable are the 4 transmembrane domains, the 2 extracellular and 1 intracellular loops. The C-terminus PDZ motif is highlighted in black, as is the conserved WGLWCC motif in the first extracellular loop. It is likely that the two cysteine residues form a disulphide bond. Two residues believed to be involved in charge selectivity of the claudin pore are highlighted in red. (Van Itallie and Anderson 2004)*

Various post-translational modifications have also been implicated in claudin function. For instance phosphorylation has been shown to increase claudin-1-4 permeability to chloride ions (Yamauchi, Rai et al. 2004), and loss of palmitoylation sites on claudin-14 results in reduced localisation of the protein to the membrane (Van Itallie, Gambling et al.

2005). It is possible that this observation was due to alteration of the protein's shape, however a role for palmitoylation in the assembly of integral membrane protein structures has been previously described (Berditchevski, Odintsova et al. 2002).

Some claudins, such as claudin-1, are widely expressed (Van Itallie and Anderson 2004), whereas other claudin proteins are expressed only in certain cell types or periods of development (Turksen and Troy 2001). This, together with the large number of different claudins in mammals, suggests that they possess varied functions in TJs. Indeed the permeability of TJs vary considerably among different tissue types, with different tissues varying in electrical conductance, charge selectivity, noncharged solute permeability, and size discrimination (Van Itallie and Anderson 2004), and this is reflected in their compositional heterogeneity. This variation in claudin composition and permeability is reflected in the nephron, as *Table 1.1* illustrates:

	Bowman's capsule	Proximal tubule	Thin descending limb	Thin ascending limb	Thick ascending limb	Distal tubule	Collecting duct
Claudin-1	X						
Claudin-2	X	X	~				
Claudin-3				X	~	~	~
Claudin-4				X			X
Claudin-7			~			X	X
Claudin-8			~			X	X
Claudin-10		X			X		
Claudin-11		X			X		
Claudin-16					X		

Table 1.1: *Expression of claudins in different regions of the nephron. 'X' indicates that the claudin in question was detected in that region of the nephron; '~' indicates that the claudin was detected in part of the region. (Furuse and Tsukita 2006)*

In fact each claudin studied thus far has demonstrated a characteristic influence on TJ function. A number of studies expressing different combination of claudins in Madin-Darby canine kidney (MDCK) cells found that overexpression of claudin-7 increased paracellular permeability to cations, while reducing it to anions. Claudin-4, -8 and -14 overexpression reduced permeability to cations but not anions, while overexpression of claudin-2 actually decreased barrier strength without reducing the number of TJ strands, as well as resulting in higher permeability to cations (Ben-Yosef, Belyantseva et al. 2003; Furuse and Tsukita 2006). Site-directed mutagenesis demonstrated that charge selectivity was determined by a small number of residues in the first extracellular loop of the protein

(*Figure 1.6*, red), and one study even found that swapping negative residues in this loop for positive ones in claudin-15 reversed its permeability from Na^+ to Cl^- in these cells (Colegio, Van Itallie et al. 2002).

The finding that claudin-14 reduces permeability to cations fits with its abundant in vivo expression in the outer hair cells of the cochlea in the ear. Here TJs function to separate the K^+-rich endolymph and Na^--rich perilymph, a separation essential for hearing. The importance of claudin-14 for this role is seen in the deafness observed in mice and humans with claudin-14 mutations (Ben-Yosef, Belyantseva et al. 2003). Claudin-11-null mice also exhibit deafness, and this is due to a similar role of claudin-11 in maintaining the endocochlear potential in the ear (Kitajiri, Miyamoto et al. 2004). Interestingly claudin-11-null Sertoli cells in these mice also leads to a lack of spermatozoa and consequent sterility, likely due to failure to establish or maintain a microenvironment suitable for spermatocyte maturation (Gow, Southwood et al. 1999). Mutations in claudin-16, expressed in the thick ascending limb of the nephron (*Table 1.1*), cause a series of hereditary defects in Mg^{2+} reabsorption in humans and cattle, resulting in deficiency of the ion. Similar to claudin-15, claudin-16 contains a number of negatively charged residues in its first extracellular loop, which appear to electrostatically interact with soluble ions, enabling or barring their passage (Simon, Lu et al. 1999).

As well as discriminating on the basis of charge, claudins also play a central role in determining the maximum size of molecules that can cross an endothelial or epithelial cell layer via the paracellular pathway. For instance, claudin-1 knockout mice die within one day of birth due to excessive water loss across the skin. In the study on claudin-1

knockout mice a small, 600 Da tracer was found to passively diffuse across the epithelium of these animals (Furuse, Hata et al. 2002). Interestingly, mutations in claudin-1 are associated in humans with ichthyosis – a condition manifested by skin dehydration (Hadj-Rabia, Baala et al. 2004). These observed phenotypes in humans and other animals lacking, or with mutations in claudin proteins demonstrate their indispensible nature in proper TJ function in preventing paracellular transport of molecules as small as water.

1.2 Glioblastomas

1.2.1 Epidemiology and Classification of Glioblastomas

Glioblastomas are a type of glioma, a tumour subtype which arise from glial cells, and include oligodendrogliomas, ependymomas, astrocytomas, and glioblastomas. Tumours of glial origin account for 32% of all tumours of the CNS, as well as 80% of malignant tumours that arise in central nervous tissue. Of these glioblastomas make up 15.8% of all primary brain tumours, with incidence highest among older patients; this frequency was second only to meningiomas, however these tumours are largely not malignant. When incidence of malignant brain tumours alone was analysed glioblastomas occurred at a rate of 3.19 per 100,000 in the US, with astrocytomas second at 0.58 per 100,000 (Dolecek, Propp et al. 2012).

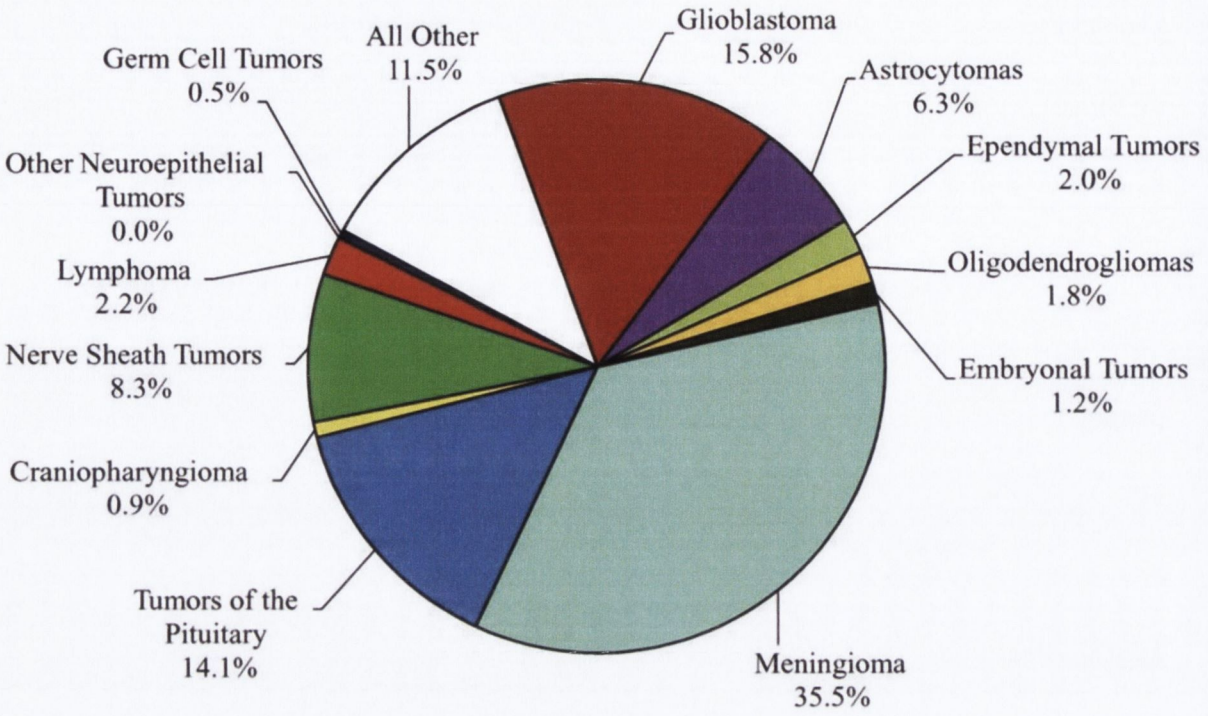

Figure 1.6: Relative incidence of glioblastomas in comparison with other CNS tumour types. *Data presented is the relative frequency of reported tumour types in the US between 2005 and 2009. (Dolecek, Propp et al. 2012)*

One way of classifying CNS tumours is by their grade, as assigned by the World Health Organisation, and where gliomas are concerned there are four grades of increasing severity. Pilocytic astrocytomas constitute grade I tumours, and these growths are benign and rarely require more than periodic monitoring. Grade II diffuse astrocytomas demonstrate a moderately proliferative and invasive phenotype, whereas grade III anaplastic astrocytomas display atypical nuclei and increased mitosis and infiltration in comparison. Finally glioblastoma multiforme constitute grade IV gliomas. These highly proliferative and invasive tumours are histologically similar to grade III anaplastic astrocytomas, but can be identified by the presence of increased necrosis and angiogenesis (Kleihues, Burger et al. 1993). Identification of tumour grade has huge

implications for patient prognosis, with grade I pilocytic astrocytomas displaying a five-year survival rate of 94%, in comparison with less than 5% in the case of grade IV glioblastomas (Dolecek, Propp et al. 2012).

1.2.2 Genetic Mutations in Glioblastomas

Almost every type of tumour occurs as a result of genetic changes introduced by exposure to mutagens such as UV radiation, toxic metabolites or viral insertions into host DNA. Glioblastomas are no exception, with dysregulation of tumour suppressors such as RB and p53 being reported in the vast majority of glioblastomas (Ueki, Ono et al. 1996; McLendon, Friedman et al. 2008). Proteins such as these are key to the manifestation and progression of glioblastomas as they control entry to the cell cycle (Das, Hashimoto et al. 2005), as well as blocking other processes such as angiogenesis (Van Meir, Polverini et al. 1994).

As well as tumour suppressors such as these, which are almost obligatorily mutated in order for a glioblastoma to form, there are also genes whose mutation alters a specific characteristic of a tumour. Invasion of surrounding neural tissue by a glioblastoma, for instance, is mediated by a number of processes. Firstly the adhesion of tumour cells to the extracellular matrix and other cells must be altered, in order to allow the cancerous cells to move from their point of origin. Secondly, motility requires significant modification of the actin cytoskeleton. Finally, extracellular matrix proteins must be broken down by proteases produced by the newly motile cells to enable their progression through the brain (Lefranc, Brotchi et al. 2005). Each of these requirements must be met

by upregulation and downregulation of various genes. One example of this is IIp45, an inhibitor of tumour invasion whose expression is decreased or absent in many glioblastomas (Song, Fuller et al. 2003; Wu, Song et al. 2010). In contrast IGFBP2 is often upregulated in glioblastomas, and functions to enhance the expression of matrix metalloproteinases that break down proteins of the extracellular matrix (Wang, Shen et al. 2003). A further example of a glioblastoma characteristic that can majorly influence prognosis is the resistance of the tumour to chemotherapeutics, with absent promoter methylation of MGMT resulting in a lack of effectiveness of chemotherapeutics (Hegi, Diserens et al. 2005). This occurs because the MGMT protein functions in DNA repair, and demethylation of its promoter results in its increased expression with consequent protection from the DNA-mutating effects of chemotherapeutics such as temozolomide.

1.2.3 The Blood-Tumour Barrier

The introduction of temozolomide as a chemotherapeutic for the treatment of glioblastomas has resulted in an increase in median survival from 12.1 months to 14.6 months, and two year survival on temozolomide in conjunction with radiotherapy is significantly higher than radiotherapy alone, at 26.5% compared to 10.4% (Stupp, Mason et al. 2005). However the fact remains that despite some measure of progress in median survival lengths, glioblastoma multiforme still remains one of the most difficult cancer types to combat. There are a number of factors contributing to this observed difference, such as glioblastomas being situated in an organ that is highly sensitive to damage, making increases in tumour volume, surgical resection, and cytotoxic treatments considerably more hazardous than in many other sites in the body. However possibly the

greatest reason why glioblastomas are so difficult to treat is the presence of the blood-tumour barrier (BTB).

The BTB exhibits a number of significant deficits in BBB characteristics. TJ proteins demonstrate altered expression, with reported decreases in the levels of proteins such as occludin, claudin-1 and claudin-5 in endothelial cells of anaplastic tumours (Liebner, Fischmann et al. 2000; Ishihara, Kubota et al. 2008). There is variation between these studies, however, with one reporting that claudin-3 expression alone was lost in glioblastoma, with expression of other TJ proteins remaining unchanged (Wolburg, Wolburg-Buchholz et al. 2003). Despite the differences between these observations it is certain that significant loss of barrier characteristics occurs, and this is not only manifested by deficiencies in TJ protein expression. Plakoglobin, a protein important for VE-cadherin adhesion in endothelial cells (Nottebaum, Cagna et al. 2008), was found to be absent in the majority of glioblastoma microvessels (Liebner, Fischmann et al. 2000). Absent also were factors such as the basal lamina protein agrin (Rascher, Fischmann et al. 2002), and correctly matured pericytes (Liebner, Fischmann et al. 2000). The source of these observed losses of barrier characteristics originate from signals released by the growing glioblastoma cells. Endothelial cells cocultured with glioblastoma cells displayed downregulation of TJ proteins, as well as increased paracellular permeability. Interestingly neutralising the glioblastoma cell-released factor TGF-β2 has been observed to partially abrogate this effect (Ishihara, Kubota et al. 2008).

These large-scale deficiencies in barrier properties of the BTB seem at odds with the extremely poor results in treating glioblastomas with chemotherapeutic agents. It has

even been found that fluorescein, with a molecular weight of 376 Da and normally excluded from the brain, leaked into brain tumours (Zhang, Price et al. 1992), as does the MRI contrasting agent gadolinium-DTPA (742 Da) (Larsson, Stubgaard et al. 1990). The photodynamic therapeutic agent hypericin (504 Da) is also observed to successfully permeate glioblastomas (Noell, Mayer et al. 2011). Part of the impact of the BTB on increased tumour resistance to chemotherapeutics is that the blood vessels of small tumours and the tumour periphery often display barrier strength equivalent to healthy brain tissue (Zhang, Price et al. 1992). This is especially important considering that tumour cells have been isolated and grown from samples of brain tissue that had been deemed to be entirely tumour free by histological analysis (Silbergeld and Chicoine 1997). This is due to the previously mentioned ability of glioblastoma cells to invade surrounding tissue, where they are protected against systemically delivered chemotherapeutics by a fully intact BBB. This is a large factor in the high recurrence rate of glioblastomas after surgery. In larger brain tumours it has been observed that systemically delivered chemotherapeutics such as paclitaxel and doxorubicin reaches tumorous tissue at a higher rate than the healthy brain, but that this level reaches less than 15% of the level delivered to tumours in peripheral organs. Furthermore the level of chemotherapeutic only reached cytotoxic levels in approximately 10% of the brain tumours studied (Lockman, Mittapalli et al. 2010). In particular regions at the periphery of the tumour experience deficits in delivery (Agarwal, Manchan Da et al. 2013).

1.3 Traumatic Brain Injury

Traumatic brain injury (TBI) is the leading cause of death among young people and the elderly in the developed world, and results mainly from falls, violence and road accidents. Data collected in Ireland indicates two distinct main patient groups, the elderly and 16-24 year old men – men are overall three times more likely than women to acquire a TBI. TBIs affecting the elderly are largely due to falls, while in young men TBIs are heavily associated with alcohol consumption (Society of British Neurological Surgeons, 2010). The relative prevalence of cause varies country to country, with countries in Southern Europe reporting a majority of TBI cases from road accidents, while in Northern Europe alcohol-related falls cause the majority of TBIs (Hukkelhoven, Steyerberg et al. 2002).

Across Europe the incidence of TBI is approximately 235/100,000 (Tagliaferri, Compagnone et al. 2006). While many people recover fully from TBI, many others are left with significant mental, behavioural and motor deficits, and an estimated figure for people living with ongoing effects from a TBI in Europe is over 7 million (Tagliaferri, Compagnone et al. 2006). In the US approximately 1.7 million people suffer a TBI each year, with 275,000 being hospitalised and 52,000 cases resulting in death (Centers for Disease Control and Prevention, 2006).

1.3.1 Traumatic Brain Injury Pathology

Clinically, TBIs are classified as being mild, moderate or severe. These classifications are commonly arrived at by means of the Glasgow Coma Scale (GCS), which measures eye

response (1-4 points), verbal response (1-5 points), and motor response (1-6 points). A combined GCS of greater than 12 indicates a mild TBI, GCS of 9-12 indicates a moderate TBI, and a GCS of less than 9 indicates a severe TBI. Other scales are occasionally used however, including the Abbreviated Injury Scale, Injury Severity Score, and the length of Post-Traumatic Amnesia (Tagliaferri, Compagnone et al. 2006). In Ireland 69% of all TBIs were registered as mild, 10% as moderate, and 20% as severe (Society of British Neurological Surgeons, 2010).

The types of damage acquired in TBI can be separated into primary and secondary effects. Primary effects are acquired nearly instantly in a TBI as a direct result of damage due to contact or acceleration/deceleration, and they can include leaky ion channels, membrane microporation, conformational changes in proteins, and shearing of blood vessels causing haemorrhage (Maas, Stocchetti et al. 2008). These primary effects of TBI are preventable, for example by use of crash helmets in road-accident scenarios, but are largely untreatable. Secondary effects, meanwhile, lie downstream of these primary effects and begin within minutes or hours or the primary insult, and these effects are all targets for potential treatments for TBI. They include mitochondrial and subsequent energy production impairment, immune cell infiltration and activation, cytokine release, oedema formation and resultant increase in intracranial pressure, and apoptosis (Maas, Stocchetti et al. 2008; Clausen, Hanell et al. 2011).

1.3.2 Diffuse Axonal Injury

The most common primary insult sustained across all severities of TBI is diffuse axonal injury (DAI). This type of nerve damage may occur even in the absence of a direct focal, contact impact, but instead is caused by the inertial forces that occur particularly in road-traffic accidents. These inertial forces cause the soft, pliable brain tissue to rotate and twist, which puts a strain on the white matter causing diffuse damage across large regions of the brain. The direction of head acceleration in animal models of impact-free TBI was found to greatly influence the degree of impairment following the application of force. Sagittal head motion resulted in the mildest coma length and level of disability, followed by oblique head movement. Animals subjected to lateral head movement were the most severely affected. In all cases the amount of observable DAI was directly proportional to the duration of coma and the degree of recovery (Gennarelli, Thibault et al. 1982), indicating that DAI was the primary cause of damage. In the case of coma in particular, evidence indicates that this is caused by axonal damage to the brainstem in particular (Smith, Nonaka et al. 2000).

One of the main outcomes of inertial forces on axons is the disruption of axonal transport, which results in the accumulation of organelles and other transport materials at points where axonal transport has been interrupted (Christman, Grady et al. 1994). This occurs within hours of injury, and can been seen under the microscope as periodic swellings along an axon, referred to as axonal varicosities; if this swelling becomes pronounced it can result in complete disconnection of the axon and its withdrawal into a 'retraction ball'. This later disconnection of axons following DAI is known as secondary

axotomy. When transmission electron microscopy was recently employed in an in vitro model of DAI, it was found that periodic mechanical breaks in microtubules would lead to swellings along the axons at the within hours due to accumulation of transport materials at the sites of the breakages. This axonal pathology occurred despite only one third of microtubules being broken, with transport continuing, at least at first, on the unbroken strands (Tang-Schomer, Johnson et al. 2012). Axonal disconnection and disruption of axonal transport eventually led to Wallerian degeneration of the axon distal to the separation from the neuronal cell body, likely due to failure to transport sufficient NMNAT2, an essential axonal protein (Gilley and Coleman 2010).

As well as higher degrees of damage occurring in the white matter than in grey matter (Shaw, MacKinnon et al. 2001), different cell populations in the brain appear to be affected by DAI to different degrees. For instance one week after fluid percussion injury in rats, myelinated axons had returned to control levels of compound action potential – a measure of the degree of neuronal activity – while unmyelinated axons were still significantly depressed (Reeves, Phillips et al. 2005).

DAI is traditionally diagnosed histopathologically by observing retraction balls by means of silver staining. However the procedure is slow and does not enable recognition of DAI prior to axonal retraction. As such many groups have begun to use beta-amyloid precursor protein as a marker for axonal injury, with positive staining being observed in human brain samples that survived for 3 h up to at least 99 days (Blumbergs, Scott et al. 1994; Sherriff, Bridges et al. 1994). In living patients meanwhile, diffusion tensor imaging

has been reported to be successful in detecting axonal swelling in cases of mild TBI (Bazarian, Zhong et al. 2007).

1.3.3 Cardiovascular Dysfunction

Blood-flow problems are another major early feature of TBI pathology. These can result in ischemia in the injured region or in other regions of the brain, which leads to loss of metabolism, lactic acidosis, and necrosis. Cerebral blood flow (CBF) in patients is usually measured through ^{133}Xe clearance, and in humans this type of measurement indicated that CBF was lowest on the day of injury, and then rose in the days afterward. Patients with CBF values greater than 33 ml/100 g/minute on the day of injury (13 patients) were observed to have a favourable neurological outcome at 6 months post-injury of 58.8%, whereas 0% of those with CBF values less than this (7 patients) had a favourable outcome at 6 months (Kelly, Martin et al. 1997). Quantification of CBF in patients at least 3 months after a TBI indicated that blood flow could still be depressed in regions of the brain, and these regions of hypofusion were associated with observations of diffuse injury (most commonly in the posterior cingulated cortices and the thalami) or focal lesions (frontal cortices) (Kim, Whyte et al. 2010). This clinical data indicates how important CBF is in predicting outcome in cases of TBI, and how central it is to TBI pathology even months later well into the chronic stage.

Vasospasm – the spasming of a blood vessel, which leads to vasoconstriction and ischemia – is one event which can cause drops in CBF following TBI. It has been estimated to occur in approximately 40% of cases of severe TBI in studies using both angiography (Macpherson and Graham 1978) and Doppler ultrasonography (Weber, Grolimund et al.

1990). In the latter study evidence of vasospasm began as early as 2 days post-injury and lasted for approximately 2 weeks, reaching a peak between days 5-7. No relationship was found between vasospasm alone and GCS, intracranial pressure (ICP), or functional outcome at 6 months (Weber, Grolimund et al. 1990); however if it was found subsequently that only a subset of vasospasmodic incidents have a depressive effect on CBF, and when these were considered they were found to be an important predictor of poor outcome (Lee, Martin et al. 1997).

Another blood-flow problem that is a significant indicator of negative outcome in TBI pathology is intracranial haemorrhage. One type, subarachnoid haemorrhage, occurs in approximately 60% of TBI cases, and its occurrence doubles the risk of death (Eisenberg, Gary et al. 1990). Together or alone these deficits in the delivery of blood to the brain can result in regions of hypoxia, with multiple studies finding O_2 levels below 14 mmHg to result in ischemia and cell death (Johnston, Steiner et al. 2005; Rose, Neill et al. 2006).

1.3.4 Metabolic Dysfunction

Dysregulation of neurotransmitter, electrolyte and metabolic levels are events which straddle the transition from primary to secondary TBI pathology. In this way they are effects that likely occur to some degree in every type and severity of TBI, but may be amenable to treatment to reverse or ameliorate their effects.

Metabolic changes in brain regions following TBI appear to be biphasic in nature, with hypermetabolism being observed in the hemisphere ipsilateral to the site of injury

immediately after and up to at least 30 mins post-injury, particularly in the cortex and hippocampus (the metabolism in the latter region being up to 90% higher than in controls). Around 6 h post-injury, however, these regions went into a depressed metabolic state, lasting up to 5 days (Yoshino, Hov Da et al. 1991). This finding was repeated in models of single and repeated blast exposures, with significant decreases in neuronal ATP levels at 6 h following the blast (Arun, Abu-Taleb et al. 2013). This metabolic depression can continue into the chronic phase of TBI, with glucose metabolism having been found to be decreased in the brains of TBI patients up to one month post-injury (Bergsneider, Hov Da et al. 2001). A study of a large number of patients found that 6 month outcome was most strongly associated with metabolic prognostic markers, such as cerebral metabolic rate of oxygen, lactate levels and glucose levels shortly after injury, with other factors such as CBF, BBB integrity, GCS and papillary status being less significant (Glenn, Kelly et al. 2003).

As mentioned, neurotransmitter dysregulation is another prominent feature common to TBI pathology, in particular greatly increased levels of extracellular glutamate which can lead to excitotoxic cell death of over-stimulated neurons. Under normal circumstances glutamate is cleared from the synapse and other extracellular regions by excitatory amino-acid transporters, with one such glial-expressed transporter – GLT-1 – being responsible for the majority of glutamate transport. The increased levels of glutamate observed after TBI coincide with an observed decrease in the expression levels of glutamate transporters, such as GLT-1, in the brain region ipsilateral to the injury, and an induced reversal of this dip in transporter expression decreased GFAP expression level – a marker of intracranial lesions (Diaz-Arrastia, Wang et al. 2013) – and post-traumatic seizure duration (Goodrich, Kabakov et al. 2013).

In contrast to glutamate, electrolytes such as Ca^{2+} rapidly increase their uptake into cells following TBI. This has been elucidated clearly in in vitro models of axonal stretching, where Ca^{2+} increases over the course of about 1 h post-injury. This increase does not appear to occur as a result of microporation of the cell membrane, and it can be prevented by blockage of sodium channels, voltage-gated calcium channels, or to a lesser degree Na^{+}-Ca^{2+} exchangers. This points to a situation where early increases in Na^{+} concentrations within the cell – likely a result of mechanical strain on the cell – leads to Ca^{2+} being influxed into the cell in exchange for Na^{+} ions (Wolf, Stys et al. 2001; Iwata, Stys et al. 2004). The net effect of this abnormally-raised intracellular Ca^{2+} level is the activation of enzymes such as phospholipases and calpains as early as 15 mins post-injury; these then act to cleave lipids and structural proteins, resulting in significant neuronal cell death (Castillo and Babson 1998; Buki, Siman et al. 1999). Ca^{2+} influx has also been linked to damage to mitochondrial integrity, leading to cytochome c release, subsequent caspase-3 activation and further cellular damage (Buki, Okonkwo et al. 2000). These negative effects of increased intracellular Ca^{2+} levels are further backed up by findings that inhibitors of Ca^{2+}-activated enzymes, such as calpain (Bartus, Hayward et al. 1994) and calcineurin (Marmarou and Povlishock 2006; Reeves, Phillips et al. 2007) can protect against ischemic brain damage in models of TBI.

1.3.5 Oedema

One of the key features of many TBIs is an increase in ICP, putting pressure on brain regions surrounding the injured region and worsening blood-flow in the injured brain. The

largest contributing factor towards elevated ICP is intracranial oedema – swelling of the brain that, limited by the skull, has limited space into which to expand before pathological increases in pressure occur. Swelling following a controlled cortical impact (CCI) model of TBI was measured to be 14.3%, with brain water content increasing to 82.5% in the injured region, compared with 79.9% in the controlateral hemisphere (Unterberg, Stroop et al. 1997). Previously it had been believed that observed brain swelling was due to engorgement of intracranial blood vessels, but studies measuring the degree of swelling due to water taken on by oedema and blood demonstrated that the contribution by water was far in excess of that by blood (Marmarou, Fatouros et al. 2000).

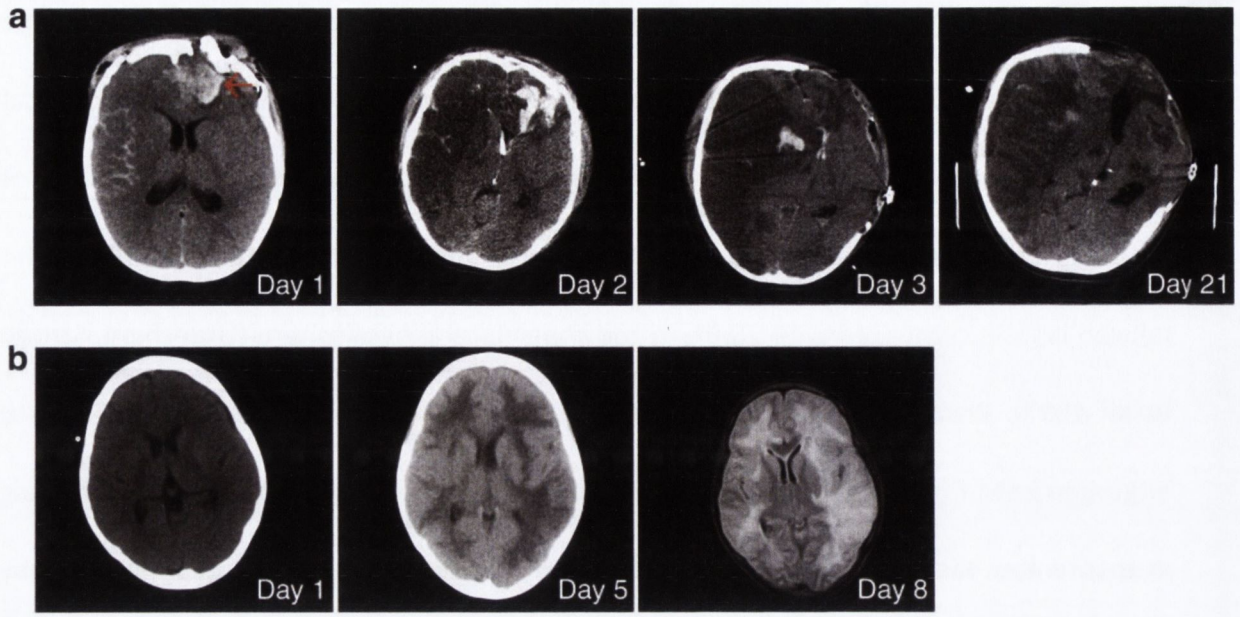

Figure 1.7: Analysis of human cerebral oedema progression. *(a) Serial axial CT scans are shown of a 12 year old boy who suffered a severe TBI while riding an all terrain vehicle. Initial CT shows bilateral injury with a left frontal open depressed skull fracture and underlying haematoma (arrow) and right-sided subarachnoid haemorrhage (panel 1). The follow-up scan 24 h later (panel 2) shows progressive cerebral oedema due to the initial hypoxia and subsequent malignant ICPs resulting in increased right to left brain shift. The patient underwent a left-sided decompressive craniectomy (panel 3) due to refractory ICPs and the follow-up scan 3 weeks later (panel 4) shows persistent oedema despite maximal medical therapy. (b) Three images of a female patient aged 18 years admitted post-cardiac arrest. Left hand Panel: CT scan of the brain less than 24 h after arrest: brain parenchyma appears normal. Middle panel: CT scan day 5, showing massive generalized cerebral oedema as a result of hypoxic ischemic injury. Right hand panel: MRI of the brain at Day 8 showing residual bilateral white matter oedema. (Campbell, Hanrahan et al. 2012)*

Post-TBI oedema can be separated into two main types, vasogenic and cytotoxic oedema. Vasogenic oedema occurs early following TBI primarily at the central core of the injury, where significant numbers of blood vessels are broken and red blood cells and plasma proteins can be observed leaking into the site of injury. This central region can also be enhanced by Gd-DTPA in MRI, indicating opening of the BBB (Katayama and Kawamata 2003). Osmotic brain oedema is similar to vasogenic oedema in that fluid enters the brain from the blood vessels, but rather than large-scale, region-specific breakdown of the BBB oedema is driven by high osmolality within the contused, necrotic core of the TBI. Here osmolality was observed to increase from 311.4 mOsm to 402.8 mOsm at 12 h post-injury, matched by a significant increase in water content. Findings in this study that brain cooling decreased osmolality increases in injured tissue while decapitation did not, indicate that the observed increase in osmotic gradient and water movement was due to metabolism and not blood flow (Kawamata, Mori et al. 2007).

1.3.6 Long-Term Recovery

The pathology discussed up this point involves features of TBI seen in the first few days and weeks following injury. However, TBI is a condition which can affect people for many years afterwards, and two such features of this long term pathology are increased risk of epileptic seizures and neurodegenerative conditions such as Alzheimer's disease. Seizures occur in animal models of TBI in the weeks following injury, and these are used to study effects of anti-convulsive compounds in their amelioration (Guo, Zeng et al. 2013), but TBI patients have been reported to have increased risk of epileptic episodes for at least 10 years following their injury. This risk increases with severity of injury, as well as being

higher in women than in men in the case of mild injuries (Christensen, Pedersen et al. 2009), although this latter finding could potentially be due to gender differences in the type of injuries acquired or under-reporting of mild injuries among men. These chronic stage seizures are the result of alterations in neural circuit organisation due to the loss of many neural and glial cells during the primary and secondary effects of the injury, and regions such as the hippocampus and dentate gyrus have been shown to be particularly involved in the development of post-traumatic epilepsy (Golarai, Greenwood et al. 2001).

Neurodegenerative, dementia-like effects are associated with long-term survival after TBI. This is particularly noticeable in professional sportspeople such as American football players (Guskiewicz, Marshall et al. 2005), and is associated with disturbances of memory, personality, gait, and the onset of Parkinson's-like shaking. These symptoms coincide with shrinkage of brain regions, and upon post-mortem tau-tangles and other cellular abnormalities are found (McKee, Cantu et al. 2009). Family studies have found increased risk of Alzheimer's disease in the years following TBI, with the risk being proportional to severity of injury (Guo, Cupples et al. 2000) and appearing to be higher among males (Fleminger, Oliver et al. 2003). In a pig model of DAI amyloid beta accumulation was observed in all animals (n = 15) between 3 and 10 days after injury (Smith, Chen et al. 1999). This has been seen in the brains of TBI patients also, up to 3 years post-injury, as well as observations of axonal swelling and loss of myelin even at these late timepoints (Chen, Johnson et al. 2009). In both animal and human models this amyloid beta accumulation appears to be a result of the close association of amyloid precursor protein with its processing enzymes presenelin-1 and beta secretase-1 at the sites of transport breakdown and axonal swelling following TBI (Chen, Siman et al. 2004; Uryu, Chen et al.

2007). This demonstrates a clear example of the knock-on effect of TBI pathology, where a primary effect of injury – in this case mechanical breakage of microtubules at the moment of injury – leads in turn to the later effects of TBI, even many years later, and affirms the importance of early intervention in TBI.

1.3.7 Immune Privilege

The immune privileged status of the brain – which shares its status with the eye, the testes and the pregnant uterus – was initially elucidated by studies on tissue transplants to the anterior chamber in the eye. Here the transplanted skin grafts persisted, where in non-immune privileged tissue they were swiftly rejected (Medawar 1948). It has since been found that transplanted tissue grafts in the brain are in fact rejected, but the process takes considerably longer than in the periphery (Finsen, Sorensen et al. 1991). Response to LPS also takes longer, with monocyte recruitment being delayed to 3 days after intracerebral injection of LPS. As well as this a 100-fold quantity of LPS is required for monocytes in the brain to reach the same density as those in the skin following injection there (Andersson, Perry et al. 1992).

These studies indicate that there is a significant barrier to immune activity in the brain, and this is in part a result of the many different layers of membranes and cell types mentioned earlier that must be breached in order to access the brain. This is a complex and multistep process, the first of which is the attachment of leukocytes to the endothelial cells of cerebral blood vessels by means of proteins such as ICAM-1 and -2. A lack of these adhesion molecules results in failure of T cells to transmigrate across

endothelial layers in vitro (Lyck, Reiss et al. 2003). The processes involved in crossing many of the other layers of the BBB have not been fully elucidated, however the matrix metalloproteinase (MMP) enzymes appear to be crucial for penetration of the parenchymal basement membrane by means of dystroglycan cleavage (Agrawal, Anderson et al. 2006). To illustrate the importance of breaching not only the endothelial layer of the BBB – often the only layer considered significant – mice that overexpress the chemotactic factor MCP-1 in the brain accumulate immune cells in the perivascular spaces on the brain side of blood vessels. However, these cells do no damage unless they pass into the parenchyma of the brain, and inhibition of MMP enzyme expression here prevents them from progressing further through the BBB (Toft-Hansen, Buist et al. 2006).

1.3.8 More Than a Barrier

When first discovered immune privilege was believed to be a result of physical separation of the CNS from the systemic immune system by means of the BBB and a lack of lymphatics in the brain preventing systemic immune cell monitoring, and the believed docile phenotype of microglia – macrophages resident in the brain. However, despite the challenges present in crossing the BBB mentioned earlier, the immune system does appear to have access to the brain in certain circumstances. Circulating, inactivated lymphocytes are observed migrating into the CSF at similar concentrations to lymph in the periphery (Seabrook, Johnston et al. 1998), and it has also been found that transgenic T cells that are specific for the myelin protein MBP are found in the brain, completely unresponsive to stimulation, even by antigen in vitro following removal from the brain (Brabb, von Dassow et al. 2000). This means that rather than relying on preventing

immune cells from reaching the CNS alone, other methods must be used to evade or suppress the immune system.

A clue in the evasion of the immune system by the CNS is the fact that viruses often persist long term in neurons, without these cells being discovered and lysed by T cells. In an in vivo study on this cytotoxic T cells injected directly into the brain did not lyse any neurons infected with a virus or cause any damage to the brain. The likely cause of this is the lack of significant MHC expression observed in neuronal cell lines (Joly, Mucke et al. 1991). As MHCs are the proteins that present antigens found within the cell to the immune system, and mark some cells for death due to infection, this would result in cytotoxic T cells being blind, in effect, to neurons. This is particularly important for neurons, as the loss even a small number of neurons can result in the loss of a huge number of axonal connections in the brain, or a patch of blindness in the retina. Due to the lack of regenerative ability in these organs losses such as this are devastating. In contrast to neurons, when the virus had infected leptomeningeal and choroid plexus cells even a greatly reduced number of cytotoxic T cells caused major cell death and tissue damage (Joly, Mucke et al. 1991).

1.3.9 Suppression of Immune Response

To suppress the immune system in the brain a number of different, parallel mechanisms appear to be employed. One such mechanism is the expression of HLA-G in the brain. HLA-G suppresses the activity and cell cycle progression of T-lymphocytes (Ketroussi, Giuliani et al. 2011) and its expression in tumours (Agaugue, Carosella et al. 2011) or skin

grafts (Lazana, Zoudiari et al. 2012) appears to be a method whereby these tissues can escape detection by the immune system via HLA-G-mediated immune suppression. This is similar to the case of the neuropeptide α-MSH, which has been found to greatly reduce the severity of experimental autoimmune encephalomyelitis (EAE) – a model of multiple sclerosis which is defined by high levels of neuroinflammation (Taylor and Kitaichi 2008). α-MSH also increases the population of regulatory T cells, and these cells have an immunosuppressive role by producing IL-9, leading to mast cell activation which results in regional immune dampening (Lu, Lind et al. 2006). The activity of regulatory T cells and mast cells in decreasing the immune response in the brain illustrates how not all immune cell attraction or activation in the brain is necessarily a bad thing, despite the well-studied examples such as EAE where the immune system is the cause of CNA damage. Galectin-1 is another example of a CNS-expressed peptide that is actively upregulated in the case of neuronal damage and which suppresses autoimmunity by increasing the immunosuppressive functioning of regulatory T cells (Toscano, Commodaro et al. 2006; Ishibashi, Kuroiwa et al. 2007). As well as suppressing immune cells directly with neuropeptides, or indirectly via regulatory immune cells, studies indicate that apoptosis may be induced in activated immune cells entering the brain. This is indicated by the presence of the Fas ligand on astrocytes and neurons in rat and human brains. The astrocytes expressing this apoptosis-inducing factor were found in close proximity to blood-vessels (Bechmann, Mor et al. 1999). A further example of astrocyte-induced immunosuppression is their induction of CTLA-4, an inhibitory factor for T-cells (Egen, Kuhns et al. 2002; Gimsa, A et al. 2004). With astrocyte end-feet being the last element of the BBB for infiltrating immune cells to pass, it is appropriate that they are the site of numerous hurdles to immune cell activity in the parenchyma. With all these myriad

mechanisms of blocking, suppressing, or even killing immune cells, the brain is significantly resistant to inflammatory events compared with peripheral organs.

1.4 Clinical Trials in Traumatic Brain Injury

1.4.1 Setbacks

Developing novel, effective treatments for TBI has been fraught with difficulty, with a significant number of clinical failures in recent years. Citicoline, an organic compound hypothesised to improve cognitive outcome, failed a phase III trial in 2012 (NCT00545662). Prostacyclin, a vasodilator and inhibitor of leukocyte adhesion resulted in no significant effect on any measure of outcome at 3 months (Olivecrona, Rodling-Wahlstrom et al. 2009). Similarly, prospective treatments have failed human clinical trials such as dexanabinol, an inhibitor of neuroinflammation (Maas, Murray et al. 2006); darbepoetin alfa, a stimulator of erythropoiesis (NCT01471015); pre-hospital resuscitation with hypertonic saline (Cooper, Myles et al. 2004), and Premarin®, used in hormone replacement therapy (NCT00973674). Many of these had demonstrated quite conclusive results. Premarin® treatment of rats that had received a TBI, for example, resulted in significantly reduced serum glutamate levels, as well as nearly halving the neurological severity score at 24 h (Zlotnik, Leibowitz et al. 2012). As well as this many of these failed studies, which at best produced no positive results, involved hundreds of patients, reflecting a large investment of time and money on top of the years of academic research that had brought the treatment to clinical trial.

Even existing TBI treatments haven't been immune to setbacks. Corticosteroids, for instance, were used for many years to combat TBI, until a series of trials shook the foundations of TBI treatment by calling their use into question. One trial involving 10,008 TBI patients found that the use of corticosteroids actually increased the relative risk of death by nearly 20% (21.1% vs 17.9%) (Roberts, Yates et al. 2004). A meta-review of a series of clinical trials the next year concluded that corticosteroids should no longer be used for TBI (Alderson and Roberts 2005).

The number of different animal models for TBI could be a point of criticism with regard to the difficulty that treatments have encountered at the clinical stage. The majority of studies demonstrate their in vivo results in only one model, and with each model demonstrating marked differences in pathology this is a cause for concern. As well as this the most commonly used animal models – mouse and rat – differ markedly in their brain volumes from humans. Large changes in brain size could fundamentally alter the progression of brain injuries due to the way in which brain tissue compresses, swells, effects of skull thickness and other factors. Other differences between animal and human TBIs could have a serious impact on the results of studies. For instance it has been found that anaesthetics given to animals prior to their receiving a TBI alter TJ protein levels and so modulate BBB permeability (Thal, Luh et al. 2012). This could have a significant effect on drug delivery, immune cell translocation, or oedema formation, all of which would not be present in the case of human TBIs which are received conscious.

Even within a single species significant difference have been observed between background strains in respect to memory and motor functional outcomes following TBI. In

some background strains even sham-operated animals were unable to learn certain tasks (Fox, LeVasseur et al. 1999). In essence a large problem is the homogeneity of current in vivo testing where injuries inflicted are as identical as possible, while in humans TBI is a highly heterogeneous condition. Significant improvements can be made in pre-clinical assessment of prospective therapeutics by widening the range of TBIs that the treatment is assessed with – different injury types, different background strains, and different sized animal models. An approach similar to this was taken in stroke research at a time when the field had experienced a number of setbacks in clinical trials, and a number of recommendations were drawn up in 1999. These recommendations focused on the use of models, as well as assessment of therapeutic index and generation of dosage curves (Loane and Faden 2010).

1.4.2 Ongoing Trials

Despite the setbacks there are a number of potentially highly efficacious treatments being currently trialled for TBI. Many of these deal with specific elements of pathology, as a result of the highly complex, heterogeneous nature of TBI. One phase IV trial which is expected to conclude in December 2013, replaces human growth hormone, which is deficient for many patients following TBI (NCT00957671). Other examples include: a feasibility study for levetiracetam to combat post-TBI epilepsy (Klein, Herr et al. 2012); arginine vasopressin to improve cerebral perfusion pressure in patients (NCT00795366); intravenous delivery of Cerebrolysin, a neurotrophic factor that aids neuronal tissue protection and repair (Masliah and Diez-Tejedor 2012); sodium lactate infusion (NCT01573507) as the brain switches largely from glucose to lactate metabolism

following TBI (Timofeev, Nortje et al. 2013), and using sildenafil (Viagra®) to treat persistent cardiovascular dysfunction following TBI (NCT01762475). A number of studies have already resulted in promising results in humans, such as amantadine hydrochloride, an organic compound already used to treat Parkinson's disease, which improved Disability Rating Scale results significantly among 184 patients (Giacino, Whyte et al. 2012).

Studies such as these are advantageous as due to their focus on a single or small number of specific outcome measures they can be easier to obtain clear evidence of beneficial effect in, rather than multiple outcome measures, or measures which are more difficult to measure objectively and consistently. Despite this, a novel treatment which would treat a large range of post-TBI dysfunctions, by targeting an early or core damage pathway in TBI pathology, would be an exciting development in the field. Oral or intravenous progesterone is a candidate for a drug that could do this, with promising results being reported in animal experiments (Cekic, Johnson et al. 2012). Treatment with this hormone is currently in a number of parallel clinical trials, including a phase IV for mild TBI in athletes (NCT01809639), and a phase III in severe TBI patients due to finish at the end of 2013 (NCT01143064). Results of a number of these trials have already been published, with favourable outcome being reported in patients with DAI at 3 months (Shakeri, Boustani et al. 2013), and a further study reporting that progesterone together with vitamin D is even better than progesterone alone (Aminmansour, Nikbakht et al. 2012). Hypothermia is another treatment for TBI that is showing a lot of promise at treating many outcomes of TBI. Trials on 80 and 136 patients resulted in improvements in ICP, antioxidant enzyme levels, neurological outcome, and mortality (Polderman, Tjong

Tjin Joe et al. 2002; Qiu, Zhang et al. 2007). However there has been some variation in clinical results in respect to hypothermia, with another trial, this time in 392 patients, concluded that no change in outcome or mortality had occurred (Clifton, Miller et al. 2001). Despite this hypothermia still holds much promise for TBI and other neurological conditions, and further trials are underway such as a phase III trial to assess the efficacy of longer term, milder hypothermia of 34-35°C (NCT01886222). Similar to the application of hypothermia to TBI some other strategies also do not consist of the delivery of a standard drug. Hyperbaric oxygen therapy, for instance, has shown promising pre-clinical in vivo results (Lim, Wang et al. 2013) and is currently in a number of human trials (NCT01611194, NCT01847755). The use of autologous bone marrow-derived mononuclear cells is another atypical treatment type, with positive results reducing BBB permeability and improvements in special memory demonstrated in a rat CCI model (Bedi, Walker et al. 2013), and trials for safety and efficacy in humans are ongoing (NCT01575470).

With these in mind it is a very interesting time in the field of TBI research and therapeutic development, but many of the factors involved in this heterogeneous, highly complex injury remain to be elucidated. This is particularly true in the area of neuroinflammation, where evidence points to both beneficial and deleterious effects of immune cell activation following TBI. Until this and other features of TBI are understood more fully problems at the clinical level will likely continue to confound and disappoint.

1.5 Thesis Aims

BRB modulation as described by this lab has been used in the delivery of active compounds to the retina for the treatment of conditions affecting vision. This same RNAi technology has also been used to succesfully to demonstrate a similarly modulated BBB, permeable to low-molecular weight markers, with no evidence to date of deleterious effects (Campbell, Kiang et al. 2008; Campbell, Nguyen et al. 2009; Tam, Kiang et al. 2010; Campbell, Humphries et al. 2013). This work included uninjected, PBS-injected and NT siRNA-injected controls, as well as microarrays looking for off-target effects of the siRNAs in brain tissue. The microarray found 32 genes to be differentially regulated between CL5 siRNA-administered and control brains tissue 48 h after siRNA delivery. None of these genes were reported to be know inflammatory markers, and the very low number of genes compared to the huge number tested indicates that the siRNA has very minimal off-target effects (Campbell, Nguyen et al. 2009).

The core hypothesis of this thesis was that this lab's previously described method for modulating the BBB could be employed in the brain as it had been in the retina, to enable low-molecular weight compounds to pass into the brain. Secondly it was hypothesised that barrier permeability could used in order to move material out of the brain. In order to attempt to test these hypotheses the aim was to firstly demonstrate proficiency with RNAi using CL5 siRNA, and to use this to technology to show that the BBB could be made permeable to low-molecular weight compounds. Following this it was aimed to establish a model of glioblastoma multiforme and to use this to show that active compounds, in this case chemotherapeutic drugs, could gain increased access to the brain and have a larger effect on inhibiting tumour growth. To test the second hypothesis, that material

could be moved out of the brain, it was aimed to establish a model of traumatic brain injury which would demonstrate significant and clearly quantifiable oedema. CL5 suppression would then be used in order to test whether modulation of the BBB could be employed to reduce some of this fluid build-up, and the animals would be assayed for improved cognitive outcome. The final chapter of this thesis takes the form of a small investigation that goes beyond the original two hypotheses. The aim of this investigation was to assay whether treatment of brain injury with CL5 siRNA coincides with alteration in the expression levels of inflammatory cytokines at the site of injury, and following on from this whether inflammation was playing a significant role in either protection or exacerbating damage following TBI.

The investigation of these hypotheses will enable further development of barrier modulation in order to deliver active drugs to the brain, as well as for the first time providing a proof of principal that damaging material can be moved out of the brain.

Chapter 2: Materials and Methods

2.1 Tissue Culture Methods

2.1.1 Maintenance of Cell Stock

Brain Endothelial Cells

bEND cells, sourced from the European Collection of Cell Cultures (ECACC), were grown in T75 filter capped flasks (Sarstedt) in 20 ml Glutamax DMEM (BioWhittaker) supplemented with 50 ml fetal calf serum (PAA Laboratories), and 100 ml sodium pyruvate (2mM, BioWhittaker) per 500 ml bottle. Flasks were stored in a Hepa Class 100 incubator (Thermo Scientific) at 37°C with 5% CO_2. To passage cells the media was pipetted off and cells were washed gently with 5 ml phosphate buffered saline pH 7.2 (PBS) (BioWhittaker). The PBS was then removed and 2 ml of 0.25% Trypsin-EDTA (Gibco) was added to de-adhere cells from the flask. The flask was incubated at 37°C for 5 min with the trypsin, or until the cells were no longer adhered to the flask – some knocking of the flask is usually necessary to dislodge the cells. 10 ml of media was then added to the plate, and the cell suspension was transferred to a universal tube. This was centrifuged at 1,000 rpm for 5 min. The liquid was pipetted out of the tube, being careful to avoid the pellet of cells, and the pellet was resuspended in 1.5 ml DMEM. 500 µl of this cell suspension was added to each of three T75 flasks containing 20 ml of DMEM.

IPSB18

IPSB18 cells (Rooprai, Kyriazis et al. 2007) were maintained and passaged as described for bEND cells with the exception that they were cultured in T175 flasks (Sarstedt) and their medium was Glutamax DMEM supplemented with 10% fetal calf serum, 5 ml MEM NEAA (Gibco) and 5 ml pen/strep per 500 ml bottle.

bGBM

bGBM cells were obtained from a biopsy of a grade 4 glioblastoma multiforme in Beaumont Hospital, Dublin. Culture in the lab was started at p=12.

bGMB cells were maintained and passaged as described for IPSB-18 cells.

GBM270

GBM270 cells were obtained from a grade 4 glioblastoma multiforme from a patient in Duke University Hospital, Durham, North Carolina. In Duke University cells were passed exclusively in mouse flank. On site in Trinity College, GMB270 cells were maintained and passaged as described for IPSB-18 cells, with the exception that media used was Improved MEM Zinc Option containing HEPES buffer at 2.383 g/L, insulin at 5 mg/L, L-glutamine at 584 mg/L, selenium at 5 mg/L, and sodium bicarbonate at 2.2 g/L (Gibco).

2.1.2 Haemocytometer Cell Counting

Cells were trypsinised and spun down at 1,000 rpm for 5 mins (SL16, Thermoscientific).The pellet was resuspended in 5ml of the appropriate medium. 20 µl of the cell suspension was pipetted along the edge of a glass coverslip placed on top of the

haemocytometer (Marienfeld). Cells present within the four corner areas of the marked grid were counted. If too many cells are present to count a further dilution of the spun down cells is made. Each corner is 1 mm x 1 mm x 0.1 mm = 0.1 mm^3 therefore multiplying the average number of cells in one of the four corners by 10^4 gives the number of cells per ml (cm^3).

2.1.3 Growth Curve

80,000 cells were seeded onto each of 8 T25 flasks (Sarstedt) with 5 ml growth medium and left to grow in an incubator at 37°C and 5% CO_2. Every 24 h one of the T25s was taken and the cells were counted using a haemocytometer.

2.1.4 Transfection of siRNA into bEND Cells

6-Well Plate

bEND cells from a T75 flask were counted and $5.5x10^5$ cells were pipetted into 2ml medium in each well of a 6 well plate. The following day the cells were observed to approximately 80% confluent. For each well, 5µl Lipofectamine 2000 (Invitrogen) was mixed with 245 µl Opti-MEM (Gibco-Invitrogen) in a 1.5 ml eppendorf tube. In a separate tube for each well 100 pmol siRNA (targeting or non-targeting) was added to 250 µl Opti-MEM. Each of these siRNA mixtures was added to one of the Lipofectamine, and this was mixed well and incubated at room temperature for 20 min. After this time the contents of each tube was added gently down the sides of one of the wells. The plate was then swirled gently and incubated at 37°C for the required time.

24-Well Plate

5 x 10^5 bEnd.3 cells were plated with 500 µl fetal calf serum-supplemented DMEM in each well of a 24-well plate. The following day cells were observed under light microscope to ensure confirm confluency of approximately 80%. For each well, 1 µl Lipofectamine 2000 (Invitrogen) was mixed with 49 µl Opti-MEM (Gibco-Invitrogen). In a separate tube for each well 20 pmol siRNA was added to 50 µl Opti-MEM I + GlutaMAX I (Gibco). The siRNA mixture is added to the Lipofectamine mixture and this was vortexed briefly, spun down, and incubated at room temperature for 20 min. After this time the resulting transfection mix was added gently down the sides of each the wells. The plate was then swirled gently and incubated at 37°C for the required time.

Due to the small quantities and number of wells involved it is advisable that rather than have separate tubes for each well a master mix is made for each siRNA, unless different concentrations of siRNA are being used.

All eppendorfs, pipette-tips and reagents used in RNA work were nuclease-free (NF). Pipettes were exposed to UV light for 5 mins prior to use.

2.1.5 Immunocytochemistry

A poly-L-lysine (PLL)-coated coverslip was added to each well prior to seeding cells in a 24-well plate. To prepare PLL-coated coverslips, 13 mm coverslips (SLS) were placed in 100% ethanol (Merk) and left overnight with gentle shaking. In the morning the coverslips were given four 10 min washes with sterile H_2O. 2 ml poly-L-lysine solution (Sigma-Aldrich) was added to 100 ml sterile H_2O and mixed well, and the coverslips were added

to this. The coverslips were left in this solution overnight with gentle shaking. The following morning the coverslips were allowed to air-dry on a tissue culture plate in the tissue culture cabinet. To ensure the sterility of the PLL-coated coverslips, one day prior to the addition of cells the coverslips were added to wells of a 24-well plate together with 500 µl DMEM. The coverslips were then left overnight and checked in the morning for bacterial growth.

Once the desired timepoint was reached cells were washed in the wells with ice-cold PBS. PBS was then replaced with ice-cold methanol for 20 mins to fix and this was followed by 2 PBS washes. Wells were then emptied and refilled with 0.05% Triton X-100 and 5% neural goat serum (NGS) (Sigma-Aldrich) in PBS and left for 30 mins. The coverslips were then covered by a 1:100 dilution of rabbit anti-Claudin-5 (Zymed) in 0.05% Triton X-100 and 1% NGS in PBS and were left overnight on a shaker at 4°C.

In the morning the coverslips were given an ice-cold PBS wash for 10 mins with gentle shaking, followed by blocking with 0.05% Triton X-100 and 5% NGS in PBS for 30 mins. A 1:400 dilution of secondary rabbit IgG-Cy3 (Jackson-Immuno-research, Europe) in 0.05% Triton X-100 and 1% NGS in PBS was then added and left at room temperature for 2 h. The coverslips were then given 3 PBS washes followed by a drop of 1:5,000 DAPI for 30 s. Following this the coverslips were carefully picked up using tweezers and transferred onto separate microscope slides, cell side down onto a drop of AquaPoly/Mount mounting medium (Polysciences).

2.1.6 Harvesting Mouse Bone Marrow-Derived Macrophages

The femurs and tibiae were removed from mice and the fat and muscles were cut away to leave clean bones. Both ends of each bone were then cut with a scissors. A 20 ml syringe was filled with DMEM Glutamax (Gibco) medium supplemented with 10% FCS and 1% Pen Strep (Gibco), a 27-guage needle attached, and the bone marrow was flushed through the bones into a sterile petri dish. Bone marrow aggregates were broken up by repeated passage through a 20 ml syringe with a 19-guage needle attached. The cells were then transferred to a 50 ml tube and centrifuged at 1,200 rpm for 5 mins. Cells were re-suspended in media containing 25 ng/ml macrophage colony stimulating-factor and plated into 6 dishes per mouse, with 10 ml of media per mouse. Plates were in an incubator at 37°C with 5% CO_2.

72 h later the cells were fed by adding 10 ml of medium containing 25 ng/ml macrophage colony stimulating-factor per dish. 48 – 72 h later cells were trypsinised, counted and seeded for RT-PCR.

2.1.7 Isolation of Primary Mouse Peripheral Blood Mononuclear Cells

500 µl of blood was taken by terminal bleed from wild-type C57 mice and transferred into EDTA-coated 1.3 ml micro tube (Sarstedt) to prevent blood clotting. The blood was then diluted with an equal volume of PBS. 500 µl of Ficoll Paque Plus (GE Healthcare) was added to two 1.3 ml micro tubes and 500 µl of the blood-PBS mixture was added slowly to each tube. The tubes were centrifuged at 2,000 rpm for 30 mins, with the acceleration and deceleration set to 5 G. After centrifugation, three distinct layers were visible – the

bottom red blood cell layer, the clear Ficoll layer, and the yellow plasma layer. A ring of white blood cells is seen between the plasma and Ficoll layer. This layer was transferred into a new 1.3 ml micro tube by pipette and the volume was adjusted to 1 ml with PBS. This tube was centrifuged at 2,000 rpm for 10 mins, and following this the supernatant was removed and the volume was adjusted to 1 ml once again with PBS. The 10 min centrifugation was repeated, the supernatant was removed and the cell pellet was re-suspended in 1 ml of RPMI 1640 growth medium (Lonza) supplemented with 10% FCS and 1% Pen Strep.

2.1.8 RNA Extraction from Cells

RNA was isolated using reagents and protocol supplied in the RNeasy Mini Kit (Qiagen). Cells were trypsinised and spun down at 1,000 rpm for 5 mins. 350 µl Buffer RLT, to which 1% 2-mercaptoethanol (Sigma Aldrich) had been added, was added to the cell pellet, and cells were homogenised in this buffer by pippetting 50 times. 350 µl of 70% RNase-free ethanol was then added and the mixture was transferred to an RNeasy spin column placed in a 2ml collection tube. This column was centrifuged at 10,000 rpm for 15 s, after which flow-through was discarded. 350 µl Buffer RW1 was then added, and the column was centrifuged at 10,000 rpm for 15 s, with the flow-through being discarded again after centrifugation. 10 µl of DNase I (30U) was added to 70 µl of Buffer RDD, and the mixture was added directly to the column and incubated at 37°C for 1 h. After the incubation 350 µl Buffer RW1 was added and the column was centrifuged at 10,000 rpm for 15 s. Flow-through was once again discarded, and 500 µl Buffer RPE was added to the column and centrifuged at 10,000 rpm for 15 s. This step was then repeated with centrifugation was

extended to 2 mins. After removal of the flow-through, the column was centrifuged again at 13,000 rpm for 1 min. The RNeasy spin column was then placed in a new 1.5 ml collection tube, ensuring that no ethanol is carried over, and 30-50 μl of RNase-free water was added to the spin column membrane. The column was centrifuged at 10,000 rpm for 1 min to elute the RNA. The concentrations of RNA in the samples were measured using a NanoDrop Spectrophotometer ND-1000 (Labtech) and samples were stored at -80°C.

2.2 In Vivo Methods

2.2.1 Animal and Experimental Groups

All studies carried out in the Ocular Genetics Unit in TCD adhere to the ARVO statement for the use of Animals in Ophthalmic and Vision Research. Wild-type C57 (C57BL/6J), Caspase $1^{-/-}$ (B6N.129S2-Casp1^{tm1Flv}/J), IL-1R$^{-/-}$ (B6;129S1-Il1r1^{tm1Roml}/J), IL-18$^{-/-}$ (B6.129P2-Il18^{tm1Aki}/J), NLRP3$^{-/-}$ (B6N.129-Nlrp3^{tm2Hhf}/J), mice were originally sourced from Jackson Laboratories, and Balb/c (BALB/cOlaHsd) mice were sourced from Harlan Laboratories. ASC$^{-/-}$ mice were developed by the laboratory of Vishva Dixit, Department of Physiological Chemistry, Genentech, San Francisco, USA. All mice were bred on-site at the Bioresources Unit in TCD.

2.2.2 Injectable Anaesthetics and Analgesics

0.5 ml of 1 mg/ml medetomidine (Janssen) was added to 0.375 ml of 100 mg/kg ketamine hydrochloride (Pfizer). This was then made up to 4.125 ml with 0.9% NaCl for injection (Braun). The resulting solution was mixed thoroughly and injected, using a 30G needle (BD Microlance) into the peritoneum at a dose of 100 µl/10g. Animals were then placed into a separate cage for 5-10 mins until they were observed to be unconscious. An unconscious state was ensured by firmly pressing a hind paw to test for flinching.

A 1 ml ampule of 0.3 mg/ml buprenorphine (Animalcare) was made up to 6ml with 0.9% NaCl for injection. 100 µl of this solution was injected subcutaneously into the scruff prior to surgical procedures being carried out.

2.2.3 JetPEI Complexing of siRNA

Into two RNAse-free tubes for each animal was added 100 µl 10% glucose solution and 100 µl RNAse-free H2O. 20 µg siRNA was added to one of the tubes, while 6.4 µl in vivo-JetPEI™ (Polyplus Transfection) was added to the other. Both tubes were mixed by inversion and spun down at 1,000 rpm for 5 s, and the contents of the in vivo-JetPEI tube were added to the other tube. This was then once again mixed by inversion and spun down at 1,000 rpm for 5 s, and then left at room temperature for 15 mins and kept on ice afterwards until injection.

2.2.4 Tail Vein Injection of Mice

A mouse was restrained within a plastic tube and a rubber bung with a groove was inserted so the animal's tail remains outside the tube while the rest of the animal is restrained within. If the animal is anaesthetised this restraining is unnecessary.

The solution to be injected is loaded into a 1 ml syringe (Terumo) using an 18 G needle if solution is in a 1.5 ml eppendorf. The 18 G needle is detached and replaced with a 30 G needle. The syringe is held needle-up and tapped until all air bubbles have travelled to the top and the air is excluded prior to injection. In the meantime the animal's tail is warmed using a heat lamp to make veins more visible and swollen. This can be enhanced further by occluding the lateral tail veins with your fingers to stop blood flow out of them. Taking great care the tip of the needle is inserted into one of the lateral tail veins and the plunger is slowly depressed. If the needle is correctly inserted into the vein the plunger will depress easily, if not resistance will be felt and the needle must be removed and insertion must be tried again.

2.2.5 Controlled Cortical Impact Brain Injury

Equipment and protocol provided by Oliviero L. Gobbo (Colgan, Cronin et al. 2010).

Prior to beginning animals were anaesthetised and injected with an anti-analgesic. They were then placed into a stereotactic head-frame (Kopf) with a heat-pad under them to maintain body temperature. A burr-hole was drilled in the skull at coordinates 2 mm caudal and 2 mm right of bregma. The tip of a pneumatically-driven impactor of diameter 3.5 mm was zeroed to the top of the brain through the craniectomy. The piston was

positioned to a depth of 1 mm and a strike of force 128 N was delivered directly to the brain. The animal was then removed from the stereotactic frame, sutured, and anti-anaesthetics.

2.2.6 Cold-Induced Traumatic Brain Injury

C57 mice of at least 3 months of age were injected intraperitoneally (IP) with ketamine and domitor using a 30 G needle and 1 ml syringe. Once the animal barely responded to pressure applied to the paw it was placed into a stereotactic frame, ensuring its head was rigidly in the frame. The skull was exposed using a scalpel and a point 2 mm posterior and 2 mm right of bregma was measured out and marked with a black dot. The end of a metal rod was placed into liquid N_2 for 1 min and then held against the marked point on the skull for 30 s. The scalp was sutured closed and the animal was brought back around with antisedan and kept on a heat pad at body temperature until it recovered.

2.2.7 Dissection of Traumatic Brain Injury Region

Following sacrifice of animal the brain was carefully excised from the skull and placed in a sterile, empty petri dish. The brain was then cut into separate hemispheres using a scalpel. The right side hemisphere that contained the TBI was laid on its side and the front 3 mm of tissue, cut in a straight line, was removed. This was then repeated for the back 2 mm of the brain, and 1 mm of the ventral side was also removed. The remaining piece of tissue was flipped 90° so that 1 mm of the right side of the brain could be removed. What remains at this point is a cube of brain tissue approximately 1.5 mm^3 containing the TBI,

and with only one remaining brain surface – the dorsal surface where the TBI was inflicted.

2.2.9 Terminal Perfusion of Mice

0.5 ml of 1 mg/ml medetomidine (Janssen) was added to 0.375 ml of 100 mg/kg ketamine hydrochloride (Pfizer). This was then made up to 4.125 ml with 0.9% NaCl for injection (Braun). The resulting solution was mixed thoroughly and injected, using a 30 G needle (BD Microlance) into the peritoneum at a dose of 300 µl / 10 g. Once the animal no longer responded to pressure stimulus on the foot it was pinned in each paw on its back. Working quickly the rib-cage was opened and pinned back to expose the heart. A large needle was inserted into the left ventricle and the substance to be perfused was injected at a steady rate.

Figure 2.1: *A successfully perfused brain, absent of visible blood vessels and noticeably lighter in colour.*

On occasion Evans blue (Sigma) was injected intraperitoneally 4 h prior to terminal perfusion at a concentration of 45 mg/kg.

2.2.10 Brain Water Content Quantification

When the desired timepoint was reached the animals are sacrificed and their brains excised. The TBI region and the equivalent controlateral brain region are dissected out of the rest of the brain and placed into separate 1.5 ml eppendorfs which were pre-weighed on a fine balance. The tubes plus brain regions were then weighed using the same fine-balance. The brain regions were speed-vacuumed overnight at 50°C and again weighed on the same fine balance. Water content in the regions can then be calculated.

2.2.11 Brain Tumour Inoculation

0.5 ml of 1 mg/ml medetomidine (Janssen) was added to 0.375 ml of 100 mg/kg ketamine hydrochloride (Pfizer). This was then made up to 4.125 ml with 0.9% NaCl for injection (Braun). The resulting solution was mixed thoroughly and injected, using a 30G needle (BD Microlance) into the peritoneum at a dose of 100 µl / 10 g. Once unresponsive the animal's head was placed into the stereotactic frame as in the case of TBI administration. The skull was exposed and a point 0.5 mm rostral and 2.5 mm right of bregma was measured out and marked with a black dot. A small hole was drilled in the skull at this point, making sure not to damage the brain beneath, and a Hamilton syringe filled with the desired number of tumour cells was slowly lowered to a depth of 3 mm straight downward through the hole. 6 µl of the cell suspension was then injected at a rate of 1

µl/min over a 6 min period using an infusion pump (NANOmite, Harvard Apparatus). The needle was then slowly withdrawn and the scalp sutured closed. Finally the animal was brought back around with antisedan and kept on a heat pad at body temperature until it recovered.

2.2.12 Delivery of Chemotherapeutics

Selected dose of doxorubicin "Ebewe" 2 mg/ml (Ebewe Pharma) was made up for each animal by diluting with PBS up to final a volume of 200 µl per animal. Doxorubicin was delivered by intraperitoneal injection.

One capsule of Temodal 100 mg (MSD) was carefully opened and the powder inside was diluted to the desired dosage using PBS up to final a volume of 200 µl per animal. Temozolomide was delivered by intraperitoneal injection.

Care was used at all times to wear protective clothing, gloves and eyewear when working with chemotherapeutic agents.

2.2.13 Serum Isolation

Directly after sacrificing it a mouse as much blood as possible was removed from the heart and chest cavity using a pipette. This blood was added to a 15 ml red cap tube (Sarstedt) which had previously been swirled with 200 ul EDTA disodium salt solution (Sigma-Aldrich) to prevent coagulation. This was then spun at 1,000 rpm for 10 mins to spin down the blood cells, and then the serum above was pipetted into a 1.5 ml eppendorf.

2.2.14 Capillary Fractionation

During this protocol samples should be kept on ice as much as possible.

Tissue to be fractionated was homogenised in 5 ml DMEM using a dounce homogeniser and homogenate was poured into a 50 ml tube. This was spun at 3,000 rpm for 5 mins. The resulting pellet was transferred to a petri-dish containing 0.005% dispase (Sigma-Aldrich) in DMEM and this was incubated at 37°C for 2 h. The contents of the dish were then spun at 3,000 rpm for 5 mins in a 50 ml tube. The pellet was then resuspended in 12% dextran from Leuconostoc spp. (~70,000Da, Sigma-Aldrich) in PBS with a short amount of vortexing. This was then spun at 3,000 rpm for 10 mins. At this stage a small, mostly red, ring-shaped pellet should be visible at the bottom of the tube. The majority of the tissue should be floating on top of the dense dextran solution. If this is not the case the dextran concentration can be increased and the sample spun down again. The red pellet alone is resuspended in PBS and centrifuged at 2,000 rpm for 5 mins to wash the capillary fraction. Following this the pellet was re-suspended in protein lysis buffer (62.5 mM Tris, 2% SDS, 10 mM Dithiothreitol, 10 µl protease inhibitor cocktail / 100 ml (Sigma Aldrich), centrifuged at 12,000 rpm for 20 min at 4°C and supernatant removed for western blot analysis.

2.2.15 RNA Extraction from Tissue

RNA was isolated using reagents and protocol supplied in the RNeasy Mini Kit (Qiagen). Each brain region was placed in 350 µl Buffer RLT, to which 1% 2-mercaptoethanol (Sigma Aldrich) had been added, and tissue was homogenised in this buffer by dounce

homogeniser. 350 µl of 70% RNase-free ethanol was then added and the mixture was transferred to an RNeasy spin column placed in a 2 ml collection tube. This column was centrifuged at 10,000 rpm for 15 s, after which flow-through was discarded. 350 µl Buffer RW1 was then added, and the column was centrifuged at 10,000 rpm for 15 s, with the flow-through being discarded again after centrifugation. 10 µl of DNase I (30U) was added to 70 µl of Buffer RDD, and the mixture was added directly to the column and incubated at 37°C for 1 h. After the incubation 350 µl Buffer RW1 was added and the column was centrifuged at 10,000 rpm for 15 s. Flow-through was once again discarded, and 500 µl Buffer RPE was added to the column and centrifuged at 10,000 rpm for 15 s. This step was then repeated with centrifugation was extended to 2 minutes. After removal of the flow-through, the column was centrifuged again at 13,000 rpm for 1 min. The RNeasy spin column was then placed in a new 1.5 ml collection tube, ensuring that no ethanol is carried over, and 30-50 µl of RNase-free water was added to the spin column membrane. The column was centrifuged at 10,000 rpm for 1 min to elute the RNA. The concentrations of RNA in the samples were measured using a NanoDrop.

2.2.16 Protein Extraction from Tissue

Lysis buffer was made by adding 0.75 g 62 mM Tris, 2 g 2% SDS and 0.154 g 10 mM dithiothreitol to 100 ml deionised H_2O. A Protease Complete Mini protein inhibitor tablet (Roche) was added to 10 ml of this solution. Tissue sample was homogenised using a dounce homogeniser, and 1 ml of the lysis buffer with protease inhibitor was added. This was pipetted up and down until homogenous and was then transferred to a 1.5 ml eppendorf tube.

2.2.17 Cryosectioning of Tissue Samples

200 ml 4% paraformaldehyde (PFA) was made by first adding 20 ml 10 X PBS to a conical flask. 8 g PFA powder was added to this along with a small volume of deionised H2O (dH2O). Very concentrated NaOH was added dropwise with constant swirling until the PFA powder is fully dissolved in the PBS. pH was then reduced to 7.4 using HCl and the volume was increased to 200 ml with dH2O.

Removed tissues were placed in 4% PFA overnight at 4°C. The next day the PFA was replaced with 10% sucrose in PBS, and this was left at room temperature until the tissues had sunk to the bottom. This was repeated with 20% and finally 30% sucrose. The tissues were then submerged in optimal cutting temperature (OCT) compound (Tissue-Tek) in plastic moulds. These moulds were then frozen using liquid N_2, using isopropanol to slow the cooling, and 12 µm sections were made using a Leica CM1900 cryosectioner.

2.2.18 Immunohistochemistry of Cryosectioned Tissue

Cryosectioned tissue samples on slides were drawn around with a liquid blocker pen (EBSciences) to create an area where the solutions would sit and stay covering the sections.

Sections were first permeabilised by covering with 0.5% Triton X-100 (Sigma) in PBS for 20 mins and then blocked in 0.5% Triton X-100 and 5% NGS (Sigma) in PBS for 20 mins. This was then replaced with 1:100 primary antibody (Invitrogen) in 0.5% Triton X-100 and 1% NGS in PBS, and the slides were left overnight at 4°C in a humidity chamber.

In the morning the slides were given three 10 min PBS washes and were blocked again in 0.5% Triton X-100 and 5% NGS in PBS for 20 mins. Secondary Cy3 antibody (Abcam), at 1:300 dilution in 0.5% Triton X-100 and 1% NGS in PBS, was left on the sections for 3hrs at room temperature. Following this the slides were give 4 PBS washes. The sections were then checked under an Axioplan 2 fluorescent microscope with HBO 100 W ultraviolet bulb, HAL 100 visible spectrum bulb and MC 200 CHIP camera (Zeiss) using analysis^B (Soft Imaging System) imaging software. If background staining was still too high more PBS washes were done. Once the background was low enough 1:5,000 DAPI (Sigma) in PBS was added for 30 s, and then a coverslip was added to each slide with mounting medium.

2.2.19 TUNEL Staining

12 µm cryosections on polylysine slides were washed 3 times with PBS for 5mins each and then the sections were drawn around with a liquid blocker pen. Sections were incubated in 20 µg/ml proteinase K (Sigma Aldrich) in NF H20 at 37°C for 5 mins. Slides were then given 2 PBS washes and then left in 70% ethanol and 30% acetic acid for 5 mins at 4°C. Following another 2 PBS washes sections were given another incubation in 20 µg/ml proteinase K in NF H20 at 37°C for 5 mins. Slides were then given 2 PBS washes and covered with 4% PFA for 5mins at 4°C. After giving all slide 3 further PBS washes the positive control sections alone were covered with 30 U DNase I in 50 mM Tris HCL (pH 7.5) for 10 mins at room temperature and then washed once in PBS. Labelling mix (Roche) (50µl per slide) was added onto negative control slides and onto all other slides a 1:10 dilution of enzyme mix (Roche) in labelling mix and this was left at 37°C for 1 h. After this

incubation time 1:5,000 DAPI was added for 30 s and mounting medium and coverslips were placed onto the slides.

2.2.20 High Resolution T_2-Weighted MRI

Mice were anaesthetized in a sealed chamber with 5% isofluorane (Baxter) in oxygen and placed on an MRI-compatible support cradle, which has a built-in system for maintaining the animal's body temperature at 37°C. Anaesthesia was maintained using 2% isofluorane delivered via a mask, and a probe was placed under the animal to monitor electrocardiogram and respiration. The cradle was then positioned within the MRI scanner. Accurate positioning was ensured by acquiring an initial rapid pilot image, which was then used to ensure correct positioning for all subsequent scans. T_2-weighted images were then acquired (resolution, 0.141 X 0.141 X 5 mm^3; matrix, 128 X 128 X 36; TR/TE, 4,179.3/36 ms; flip angle, 90°; acquisition time, 1 min 6 s).

MRI used was a 7 Tesla BioSpin Animal Scanner (Bruker).

Images produced were analysed using ImageJ or MIPAV software.

2.2.21 Contrast Enhanced T_1-Weighted MRI

Mice were anesthetized with 5% isofluorane in oxygen and placed on an MRI-compatible support cradle, which has a built-in system for maintaining the animal's body temperature at 37 °C. A probe was placed under the animal to monitor electrocardiogram and respiration. The cradle was then positioned within the MRI scanner. Accurate positioning was ensured by acquiring an initial rapid pilot image, which was then used to

ensure correct positioning for all subsequent scans. Extravasation across the BRB or BBB was then visualized in T_1-weighted MRI images (resolution, 0.156 X 0.156 X 5 mm^3; field of view = 20 X 20 X 17.9 mm^3; matrix, 128 X 128 X 30; TR/TE, 500/2.7 ms; flip angle, 30°; number of averages, 3; acquisition time, 2 min 24 s; repetitions, 10). The contrasting agent gadopentetate dimeglumine (Gd-DTPA) (Bayer) was administered at 0.1 mM/L per kg via the tail vein during the scan, directly following the first of the 10 repetitions.

MRI used was a 7 Tesla BioSpin Animal Scanner (Bruker).

Images produced were analysed using ImageJ or MIPAV software.

2.2.22 Arterial Spin Labelling

The ASL MRI sequence consisted of the preparation interval that contained the inversion pulse to magnetically label inflowing arterial blood water in the neck, followed by a variable post-labelling delay and then snapshot fast low angle shot acquisition in the brain. Parameters used were as follows: slice thickness, 2 mm; fast low angle shot TR, 6.938 ms; echo time TE, 2.63 ms; RF flip angle, 30°; FOV, 3.0 × 3.0 cm; image matrix, 128 × 64; receiver bandwidth, 100 kHz. Values for MTT, CTT and rCBV were quantified using a non-compartmental model of cerebral perfusion.

2.2.23 Neurological Severity Score Assessment

A measure of neurological severity was obtained using ten tests for markers of motor and cognitive function, as previously reported (Flierl, Stahel et al. 2009). The tests were as follows:

1. Exit a circle with a diameter of 30 cm within 3 min;
2. Ability to use all four limbs;
3. Initiative and ability to walk straight;
4. Startle reflex;
5. Inquisitive behaviour;
6. Ability to balance on a beam 7 mm wide for 10 s;
7. Cross a 30 cm beam of width 3 cm at a height of 10 cm in 3 min;
8. Cross a 30 cm beam of width 2 cm at a height of 10 cm in 3 min;
9. Cross a 30 cm beam of width 1 cm at a height of 10 cm in 3 min;
10. Ability to perch on a round beam of width 5 mm.

All tests were performed by an individual blinded to the experimental treatment groups.

2.2.24 T-Maze Test

The protocol for spontaneous T-maze alternation was followed as previously established (Deacon and Rawlins 2006).

The animal being tested was first placed at the start position *(Figure 2.2, Start)* and allowed to choose an arm of the T-maze to enter *(Figure 2.2, A or B)*. Once in one of the arms that arm of the maze was isolated using a sliding partition, confining the animal inside for 30 s. After this time the animal was removed and the partition raised again. The animal was then placed at the start position again facing away from the arms and given 2 mins to choose an arm. If the animal chooses the arm it did not choose the first time this

is considered a positive result for alternation; if it chooses the same arm this is a negative result.

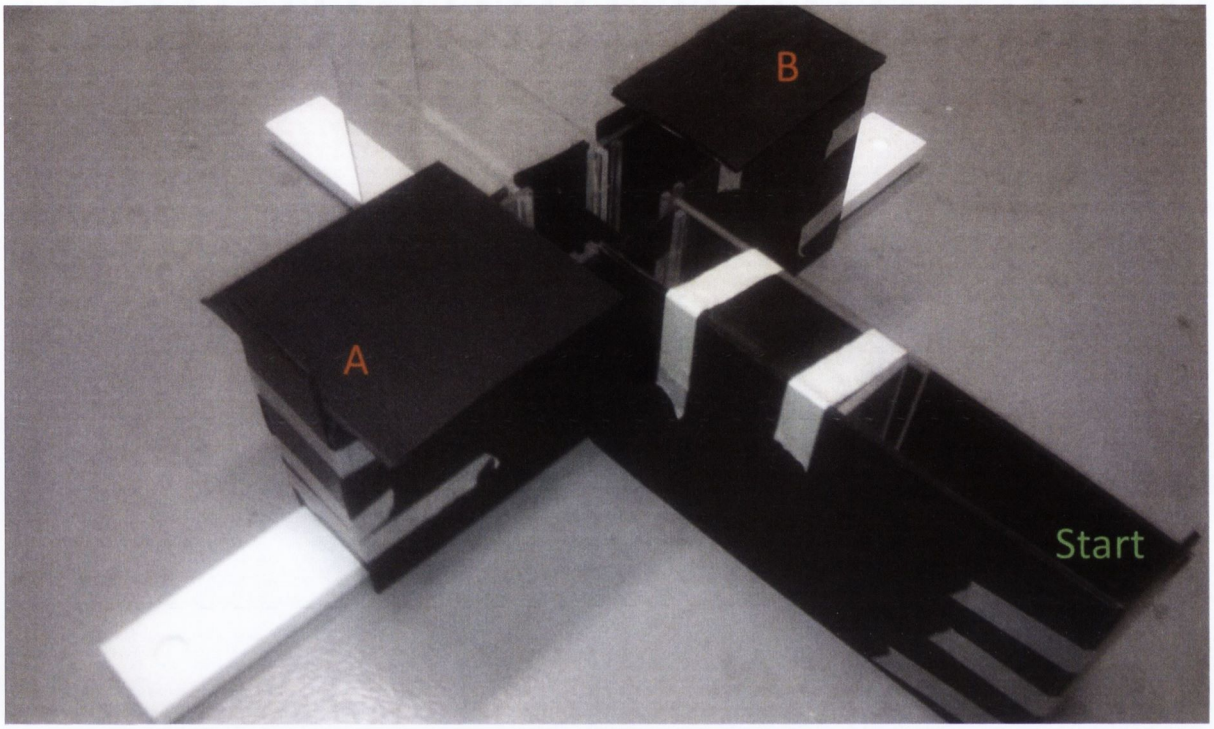

Figure 2.2: T-maze structure.

Mice begin the T-maze where 'Start' (green) is indicated, and they travel up the maze until they reach point 'A' or 'B' (red). Here they are confined for 30 s before being returned to the 'Start' position for their second trial.

All tests were performed by an individual blinded to the experimental treatment groups.

2.3 Analytical Techniques

2.3.1 siRNA Sequences

Sequences of the claudin-5 siRNA used in this study were from Dharmacon and were as follows:

Sense sequence: 5'-CGUUGGAAAUUCUGGGUCUUUdTdT-3'

Antisense sequence: 5'-AGACCCAGAAUUUCCAACGUUdTdT-3'

Non-targeting control siRNA-targeting luciferase was used as a non-targeting control.

Sense sequence: 5'-CUUACGCUGAGUACGUCGAdTdT-3'

Antisense sequence: 5'-UCGAAGUACUCAGCGUAAGdTdT-3'

2'OMe-modified claudin-5 siRNA was synthesized by Dharmacon and were as follows, where 'm' prefixing a nucleotide indicates 2'OMe modification at this residue.

Sense sequence: 5'-CGUmUGGAAAUUCUGmGGUCUUUdTdT-3'

Antisense sequence: 5'-AGACCCAGAAUUUCCAACGUUdTdT-3'

2.3.2 RT-PCR

15 µl of the following master mix was added to each well of a 96-well RT-PCR plate (Nunc) as per *Table 2.1*.

Component	Volume
2 x QuantiTect SYBR Green	510 µl
QuantiTet RT Mix	7.5 µl
Target or β-actin Primer Mix (10pmoles/µl)	51 µl
NF H_2O	200 µl

Table 2.1: Master mix for 96-well RT-PCR.

Added to this was 5 µl of sample RNA (0.4 ng/µl), or H_2O for negative control wells. Samples were plated in triplicate, H_2O controls were plated in duplicates. The 96-well plate was covered with an acetate sheet, briefly spun down and then placed into a 7300 Real Time PCR System (Applied Biosystems). RT-PCR reaction conditions were as follows:

50°C x 20 min

95°C x 15 min

[95°C x 15 s, 60°C x 1 min] X 37 times

A dissociation stage was added consisting of:

95°C x 15 s

60°C x 30 s

95°C x 15 s

Results were analysed using 7300 System Software (Applied Biosystems), and the ΔΔCT method of analysis was employed in Microsoft Excel using the Applied Biosystems protocol.

(http://www3.appliedbiosystems.com/cms/groups/mcb_support/documents/generaldocuments/cms_042380.pdf, pg.52)

Primers were supplied by Sigma-Aldrich and sequences are as follows:

Claudin-5 left: 5'-CTGGACCACAACATCGTGA-3' and right: 5'-CACCGAGTCGTACACTTTGC-3'

β-actin left: 5'-GGGAAATCGTGCGTGACAT-3' and right: 5'-GTGATGACCTGGCCGTCAG-3'

NGF left: 5'-CCGCAGTGAGGTGCATAG-3' and right: 5'-GCTTCAGGGACAGAGTCTCC-3'

IL-1–left: 5'-TCAGGCAGGCAGTATCACTC-3' and right: 5'-AGGATGGGCTCTTCTTCAAA-3'

ICAM-1 left: 5'-CCATCACCGTGTATTCGTTT-3' and right: 5'-GAGGTCCTTGCCTACTTGCT-3'

CINC-1 left: 5'-CCGAAGTCATAGCCACACTC-3' and right: 5'-GTGCCATCAGAGCAGTCTGT-3'

RANTES left: 5'-TCTTGCAGTCGTGTTTGTCA-3' and right: 5'-GGGTCAGAATCAAGAAACCC-3'

2.3.3 BCA Assay

Reagents supplied by the ThermoScientific BCA Protein Assay Kit.

Standards were prepared as follows:

Tube	Deionised H_2O (µl)	Stock BSA (µl)	BSA Conc. (µg/ml)
A	0	40	2,000
B	10	30	1,500
C	20	20	1,000
D	25	15	750
E	30	10	500
F	35	5	250
G	40	0	0

Table 2.2: Bovine serum albumin standards prepared for BSA assay.

Working reagent was prepared by mixing Reagents A and B in a 50:1 ratio.

10 µl of each standard or of a 1:5 dilution of each sample was each added to three wells of a 96-well plate (Nunc). 200 µl working reagent was then added quickly to each well to begin the reaction. The plate was left in a 37°C incubator for 30 min. Following incubation the plate was placed into a spectrometer (BioRad SmartPec 3000) at 595 nm and a standard curve was calculated which allowed for the estimation of protein concentration in the samples.

2.3.4 Western Blot

A 12% resolving gel was made using 6.6 ml deionised H_2O, 5 ml 1.5 M Tris HCl (pH 8.8), 8 ml 30% acryl (Sigma-Aldrich), 0.2 ml 10% SDS (pH 7.2), 0.2 ml 10% APS (Sigma-Aldrich), and 20 µl TEMED (Sigma-Aldrich), and this was poured between two glass plates. Occasionally for larger proteins a 10% resolving gel was used, in which case deionised H_2O

was changed to 7.93 ml and 30% acryl to 6.67 ml, while all other reagent quantities remained the same. On top of this was poured a 4% stacking gel containing: 6.8% deionised H_2O, 1.67 ml 0.5M Tris HCl (pH 6.8), 1.33 30% acryl, 0.1 ml 10% SDS (pH 7.2), 0.1 ml 10% APS and 10 µl TEMED. The stacking gel was poured so that it would extend 1 cm below the comb, which was placed into the stacking gel.

SDS loading buffer was made containing 250 mM Tris HCl, 500 mM dTT, 50% glycerol, 10% SDS, and 0.5% bromophenol blue. 8 µl of this and 2 µl β-*mercaptoethanol* were added to 30 µl aliquots of each protein sample. These mixtures, as well as 10 µl of a prestained protein ladder (New England BioLabs) were boiled at 100°C for 10 min and were then loaded into the wells in amounts determined by BCA assay so that equal quantities of protein were being loaded. 10 X running buffer was made with 30.3 g Tris, 144.2 g glycine and 10 g SDS made up to 1 L with deionised H_2O and a pH of 8.6 was checked. The gel was run at 60 mA for 2 h in 1X running buffer.

SDS-PAGE transfer buffer was made containing 2.9 g glycine, 5.8 g Tris, 0.037 g SDS, and 200 ml methanol made up to 1 L with deionised H_2O. After running the gel was removed for semi-dry transfer and placed over 4 layers of filter and a PVDF membrane (Millipore) which had been dipped in methanol for 30 s. 4 further layer of filter paper were placed on top and all layers were wet with transfer buffer. An electric current of 80 mA was applied for 2 h.

After this time the PVDF membrane was placed into 10 ml Ponceau S Solution (Sigma-Aldrich) to ensure transfer had occurred correctly. 10XTBS was made with 60.5 g Tris and 87.76 g NaCl in 1 L deionised H_2O and a pH of 7.5 was checked. Once protein bands were viewed the membrane was washed in 1X TBS every 10 min for 1 h with gentle agitation. The membrane was then blocked in 5% skimmed milk powder (Marvel) in 1X TBS for 30

mins with gentle agitation. This was poured off and the membrane was washed overnight with a 1:2,000 dilution of polyclonal rabbit primary antibody in 5% skimmed milk powder in 1X TBS at 4°C, covered and with gentle agitation. In the morning the antibody solution was poured off and the membrane was washed with 1X TBS every 10 min for 1 h. A 1:2,000 dilution of horse-radish peroxidase-conjugated anti-rabbit secondary antibody in 5% skimmed milk powder was left on the membrane with gentle agitation for 3 h. The membrane was then washed with 1X TBS every 10 min for 1 h. Primary antibody concentrations were occasionally increased to resolve faint bands or decreased to reduce background.

To develop images of the protein bands the membrane was placed into a 1:1 mixture of ECL Western Blotting Detection Reagents (GE Healthcare) for 1min. Excess liquid was drained off the membrane which was then placed between two acetate sheets. This was then placed in a cassette in a dark room and a piece of x-ray film (Fuji) was placed over the membrane in acetate. The cassette was closed for 5min or longer if required, and after this time the x-ray film was placed into developer solution until an image became visible, then was transferred to H_2O to stop the development and then to fixing solution. The fixing solution was then washed off in water and the film was allowed to dry.

Antibodies used were: polyclonal rabbit anti-mouse claudin-5 primary (Zymed), polyclonal rabbit anti-mouse β-actin primary (Abcam), and goat anti-Rabbit peroxidase secondary antibody (Sigma).

2.3.5 Taqman Assay

Reagents and protocol supplied by Applied Biosystems.

Firstly RNA samples were diluted so they each had the same concentration of RNA/µl. Reverse-transcription to cDNA was then carried out by adding 1-100 ng RNA, diluted to 10 µl with NF H_2O, to 2 µl 10 X Reverse Transcriptase Buffer, 0.8 µl 25 X dNTPs, 2 µl 10 X Random Primers, 1 µl Multiscribe Reverse Transcriptase, and 4.2 µl NF H_2O. Reverse transcriptase reaction was then carried out at the following conditions:

25°C × 10 mins

37°C × 120 mins

85°C x 5 mins

4°C hold

4 µl cDNA was then added to 5 µl Fast Taqman Mix, 0.5 µl target primer, and 0.5 µl β-actin primer. Transcriptional changes were measured in a StepOne Plus machine, using Taqman Gene with reaction conditions as follows:

50°C × 2 mins

95°C × 20 s

[95°C × 1 s, 60°C × 20 s] × 40

Target gene used a FAM reporter. Transcript levels were standardized using β-actin with a VIC reporter in the same well, and analysed using StepOne Software v2.2.2 using the ΔΔCT method.

Target gene used was IP-10 (Mm00445235_m1).

2.3.6 Proteome Profiler Array

Reagents and protocol supplied by RnD Systems, Catalogue # ARY006.

Cytokine array membranes were blocked in 2 ml Array Buffer 7 for 1 h at room temperature. Tissue protein samples were prepared by adding up to 1ml of each sample to 0.5 ml of Array Buffer 4. 15 μl Detection Antibody Cocktail was added to each sample and left to incubate at room temperature for 1 h. Array Buffer 7 was then removed from the membranes and the sample/antibody mixtures were added to the membranes. The membranes were incubated overnight at 4°C on a rocking platform shaker. The following day, membranes were washed 3 X 10 mins with 20 ml of Wash Buffer. Diluted Streptavidin-HRP was then added to the membranes and incubated for 30 mins at room temperature. The 3 X 10 min washes were repeated. Membranes were then covered with Chemi Reagent Mix for 1 min and placed between 2 acetate sheets with excess reagent drained off. The membranes were covered with X-ray film in a film cassette and exposed for approximately 5 mins. The X-ray film was subsequently developed until the signal was observed. The film was then rinsed with water and fixed.

The data was anaylsed using ImageJ. The average pixel density of the pair of duplicate spots for positive signals and reference spots were determined. An average background

signal was subtracted from each spot. The positive signal pixel densities were then divided by the corresponding reference spot pixel densities. Corresponding signals on the different membranes were then compared to determine relative change in angiogenesis/cytokine-related proteins between samples.

2.3.7 Data Analysis

Statistical analysis was performed using Student's *t*-test, with significance represented by a *P*-value of ≤0.05. For multiple comparisons, ANOVA was used with a Tukey-Kramer post test and significance represented by a *P*-value of ≤0.05. For arterial spin labelling analyses, ANOVA followed by a Bonferroni post test for multiple comparisons was used with *P*≤0.05 representing significance. All analyses were carried out using GraphPad Prism® version 5.02.

Chapter 3: Claudin-5 siRNA Efficacy

3.1 Abstract

Treatment of many conditions of the eye and brain are made very difficult by the presence of the BRB and BBB, which prevent the transport of molecules from the blood into these organs. Due to these physiological barriers a drug that is developed for use in the eye or brain must be directly injected intraocularly or stereotactically, or use another route to bypass the BRB or BBB. This lab has in the past demonstrated that low-molecular weight compounds can cross from the blood via the paracellular route following the suppression of a TJ protein, CL5, by means if RNAi. This technology has been used to deliver compounds to treat conditions of the retina, and has also shown permeability of the brain to molecular markers and active compounds. This chapter demonstrates my ability to use this technology to suppress CL5 in the brain, with resulting permeability of the BBB, with siRNA being delivered to cells by means of a PEI carrier agent. Following this a small investigation is supplied demonstrating that delivery of CL5 siRNA complexed with PEI does not stimulate an IFN-α response in vitro or in vivo. This chapter establishes the techniques and evidence that provide the basis for much of the work carried out in later chapters.

3.2 Introduction

The severe constriction of the paracellular spaces between endothelial cells of the BBB is a major barrier to drug delivery to the brain (Pardridge 2005). As discussed previously, this is due to structures called tight junctions (TJs), which are positioned on the apical end of the plasma membrane and pair with a TJ on the neighbouring endothelial cell to constrict the paracellular pore. Suppression of these tight junction proteins, in particular the claudin protein claudin-5 (CL5), has been shown to increase permeability of the BBB, enabling low-molecular weight compounds to pass into the brain (Campbell, Humphries et al. 2011).

3.2.1 Targeting Claudin-5 by RNAi

CL5 is highly enriched in endothelial cells of CNS vasculature (Morita, Sasaki et al. 1999), and is required for facilitating BBB size-selectivity (Ohtsuki, Sato et al. 2007). Much of the focus on CL5 as being key to BBB integrity comes from the generation of CL5 knockout mice (Nitta, Hata et al. 2003). These mice are born alive, but similar to claudin-1-deficient mice (Furuse, Hata et al. 2002) they die within 1 day of birth. No morphological abnormalities were reported, however injection of a 443 Da molecular weight tracer into the bloodstream of the mice demonstrated impairment of the BBB. Interestingly, when molecules of sizes of 1.9 kDa (microperoxidase) or greater were perfused, no observation of diffusion across the BBB of CL5-deficient mice. Moreover, the BBB of these mice was also shown to exclude other large molecules, such as serum albumin (~68 kDa) and tetramethylrhodamine-conjugated dextran (~10k Da), while Hoechst stain H 33258 (562

Da) was found to be the largest molecule that successfully diffused across the BBB of CL5$^{-/-}$ mice (Nitta, Hata et al. 2003). The observation of the size selectivity of the BBB when CL5 was deleted led to the possibility that targeting CL5 could be a means to selectively modulate the BBB, while potentially still excluding anaphylatoxins, bacteria, viruses or other dangerous material access to the CNS. While the mice in this study died in their first day after birth, no evidence of bleeding or cerebral oedema were observed (Nitta, Hata et al. 2003). It was thus hypothesized that short-term and reversible modulation of the BBB would not compromise the long-term health of the animal, similar to how a temporary down regulation of TJ transcripts, for instance upon exposure to alcohol (Simet, Wyatt et al. 2012), should not affect the CNS once the down-regulation is not permanent. The observation of size-selective BBB opening gave the idea that RNA interference (RNAi) could be used to downregulate CL5 levels in a wild-type mouse and potentially a patient with similar results, with the BBB returning to normal permeability again following treatment.

RNAi works by delivering small, double-stranded, ~21 nucleotide (nt) RNA molecules into cells. These double-stranded RNAs were first discovered in 2001 and were found to effectively and temporarily decrease gene expression initially in mammalian cell lines (Elbashir, Harborth et al. 2001), and *Drosophila melanogaster* embryonic lysates (Elbashir, Martinez et al. 2001). This interference was found to be highly sequence specific – the sequence of the small interfering RNA (siRNA) needing to be complementary to the mRNA of the target gene, and alterations of this sequence abolishing or greatly mitigating its suppressive effect Elbashir, Martinez et al. 2001). RNAi interference works by taking advantage of an endogenous system of interference by small RNAs, predominantly micro

RNAs (miRNA). This was first discovered in *Caenorhabditis elegans* where the gene lin14 was found to be post-transcriptionally downregulated by the miRNA lin4 (Lee, Feinbaum et al. 1993; Wightman, Ha et al. 1993). This endogenous RNAi process was discovered to be mediated a series of large proteins and protein complexes. Following transcription the first of these, Drosha, processes the transcribed RNA into a ~70 nt pre-miRNA duplexed with itself and containing a stem-loop structure (Lee, Ahn et al. 2003). This pre-miRNA is then transported into the cytoplasm and here it is processed by the enzyme Dicer into a double-stranded miRNA duplex containing 2 nt 3' overhang (Hutvagner, McLachlan et al. 2001). Following this final processing step the mature miRNA duplex unwinds and is bound by RISC, a multi-protein complex that prevents translation of the target sequence of the miRNA (Caudy, Myers et al. 2002; Hutvagner and Zamore 2002) (*Figure 3.1*).

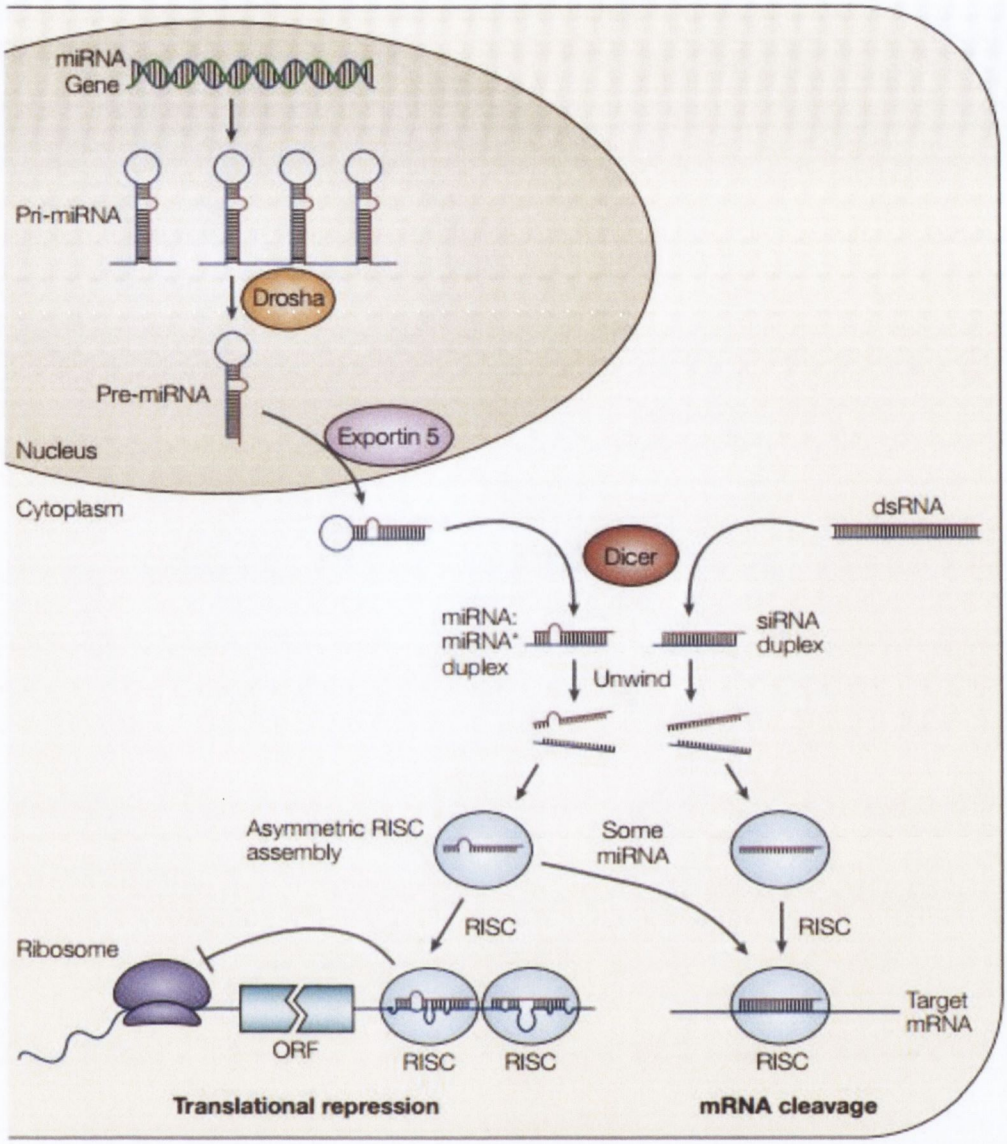

Figure 3.1: Process of post-transcriptional suppression mediated by endogenous miRNA and introduced siRNA. *Pre-miRNA (left) is transcribed from DNA, processed into its hairpin structure by Drosha, and then exported from the nucleus by Exportin 5. In the cytoplasm pre-miRNAs or introduced dsRNAs are processed by the protein Dicer into miRNA or siRNA duplexes respectively. From here the two strands unwind and are bound by the multi-protein complex RISC. This complex then binds the target mRNA and prevents translation. (He and Hannon 2004)*

Exogenously introduced dsRNAs are also processed by Dicer to produce a mature siRNA duplex (Ketting, Fischer et al. 2001). Also as in the case of miRNAs this siRNA duplex then unwinds and is bound by the RISC complex which then prevents translation of the sequence in a target-specific manner. In contrast to miRNAs, however, RISC-mediated silencing using siRNAs involves cleavage of the target mRNA, rather than inhibition of translation (Martinez, Patkaniowska et al. 2002) (*Figure 3.1*).

RNAi mediated by introduced siRNA is a powerful tool, and is most commonly developed to suppress the translation of harmful mutant proteins, for instance mutant IMPDH which causes the RP10 form of retinitis pigmentosa (Tam, Kiang et al. 2008). However there are also applications for using RNAi in order to downregulate normal, functioning genes for instance in the RNAi targeting of the antiapoptotic Bcl-2 gene in studies on the treatment of cancer (Klasa, Gillum et al. 2002). RNAi has been successfully used to reduce the levels of claudins in the septate junctions of C. elegans, and this was shown to have the effect of temporarily opening septate junctions (Asano, Asano et al. 2003). This finding was repeated in this lab in mice, with suppression of CL5 expression occurring at the BBB after 24 and 48 h after siRNA administration, and with levels of expression returning to normal after 72 h and remaining normal 1 week later (Campbell, Kiang et al. 2008).

3.2.2 Demonstration of Barrier Modulation by MRI and Other Methods

In order to show that the BBB, suppressed for CL5, was amenable to increased transport of low-molecular weight material, MRI In a MRI study the individual or material being studied is exposed to a strong magnetic field, in the case of the purpose-built animal

scanner used during the course of this thesis – 7 Tesla (Bruker). This magnetic field is then oscillated at particular intensities and frequencies, and inside the field hydrogen atoms are excited and release a radio frequency signal that is detected. Molecules containing the highest proportion of excited hydrogen atoms will generate the greatest amount of signal, and in tissue these molecules are water, and to a lesser extent fat. Regions of high concentration of water (or fat) will show up in an MRI scan as an area of high intensity – white – signal. (McRobbie 2007). As well as this exogenous MRI contrasting agents that generate large amount of signal can be introduced. One such agent is gadolinium-diethylene triamine pentaacetic acid (Gd-DTPA), which has a molecular weight of 742 Da. This molecular weight puts it in the same size-range as many low-molecular weight drugs of interest for delivery to the brain, and for this reason Gd-DTPA is used regularly during this project to demonstrate successful BBB modulation. The permeation of Gd-DTPA across the BBB with or without CL5 suppression is shown in *Figure 3.2*.

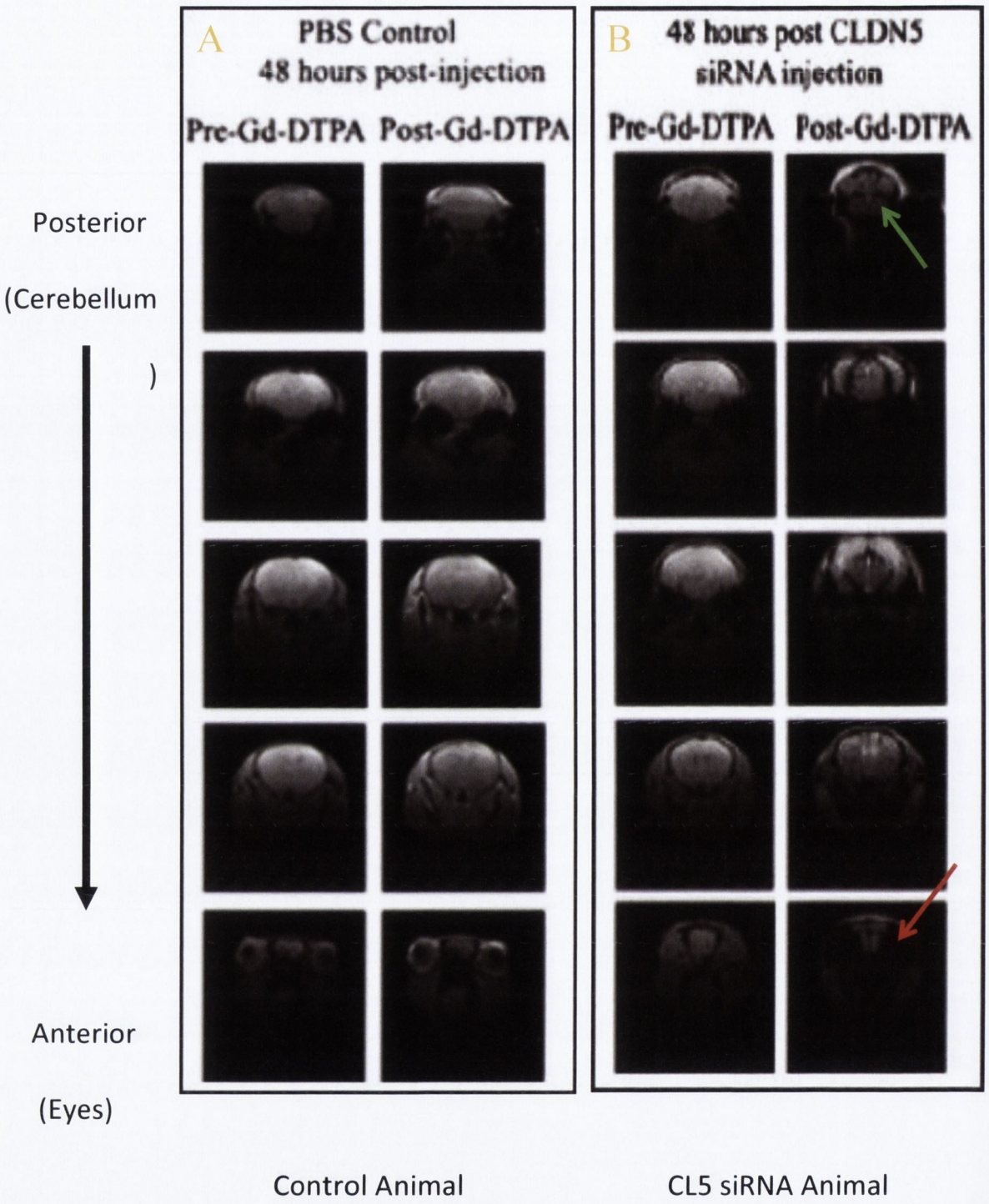

Figure 3.2: MRI images of the brains and eyes of mice injected with CL5 siRNA or PBS before and after Gd-DTPA. *(A, Left) The first column shows a posterior-anterior sequence of images from a PBS-injected negative control mouse before injection with Gd-DTPA; the second column shows this same animal after injection with Gd-DTPA. (B, Right) The next column shows a CL5 siRNA-injected mouse before and injection with Gd-DTPA; the final*

column shows this same animal after injection with Gd-DTPA. Gd-DTPA diffusion into the brain (green arrow) and the eye (red arrow) is clearly observable as patches of black under MRI. (Campbell, Kiang et al. 2008)

In this Figure Gd-DTPA can be seen within the brains and eyes of mice with CL5 suppression (*Figure 3.2, B, Post-Gd-DTPA*), whereas no change is observed in control mice injected with PBS pre- and post-Gd-DTPA injection (*Figure 3.2, A*). Once again size-selectivity was demonstrated, with a molecule of 4.4 kDa still being excluded from the brain and eyes of CL5 siRNA-injected mice (Campbell, Kiang et al. 2008). Interestingly, this size selectivity was found to return gradually with time, with EZ-link TM sulfo-NHS-biotin extravasation from the vasculature still occurring at 72 h after CL5 siRNA injection while Hoechst H33342 was excluded at this time point, meaning that barrier integrity could now exclude a molecule of 562 Da but not 443 Da (Campbell, Kiang et al. 2008). One week post siRNA injection, none of the molecules used could passively diffuse across the barrier.

This technique was first used to modulate the inner BRB and deliver drugs in two animal models of retinopathies, and in so doing demonstrate the great potential of this approach. In one treatment scenario, it was shown that guanosine triphosphate (GTP) could be delivered to the retinas of IMPDH1$^{-/-}$ mice (Campbell, Nguyen et al. 2009). IMPDH is the rate-limiting enzyme in the de novo production of GTP, which is central to visual phototransduction. Mice lacking the IMPDH1 enzyme exhibit gradual and age dependent degeneration of their retinal outer segments concomitant with diminished electroretinography (ERG) readouts. Following CL5 suppression and subsequent systemic

injection of GTP – a molecule with a molecular weight of 523 Da and which normally is prevented from crossing the inner BRB – ERG results showed an increase in rod-isolated b-wave activity compared with non-targeting siRNA injected or un-treated control mice. Modulation of the inner BRB in the absence of GTP was demonstrated to have no effect on ERG, indicating that modulation of the barrier itself had no effect on ERG results (Campbell, Nguyen et al. 2009).

In the second animal model delivery of the calpain inhibitor ALLM (402 Da) to the retina was enhanced in albino BalB/c mice exposed to high intensity light. This exposure to strong light in BalB/c mice results in massive photoreceptor apoptosis, and this process is mediated by activation of calpains. ALLM was administered systemically 48 h after systemic injection of CL5 or non-targeting siRNA, and this was shown to significantly decrease the number of apoptotic cells in the ONL retinas 12 and 24 h after light ablation in the CL5 suppressed animals (Campbell, Nguyen et al. 2009).

The BRB is similar in characteristics and TJ protein make up to the BBB, and this technique was then extended to include delivery of therapeutic compounds across the CL5-suppressed BBB. Here a low molecular-weight neuroprotective agent, thyrotropin-releasing hormone (360 Da), was delivered to the brains of mice. A significant increase in the behavioural readout of animals was observed when the BBB was modulated prior to systemic injection of the hormone (Campbell, Kiang et al. 2008), indicating that enhanced delivery had been achieved.

3.2.3 siRNA Delivery Methods

In the study on thyrotropin-releasing hormone, delivery of siRNA to endothelial cells of the BBB was enabled by means of hydrodynamic injection. According to this method siRNA was rapidly injected in a bolus of a volume of PBS equal to 10% of the animal's body weight (Campbell, Kiang et al. 2008). This injection protocol would pose a significant hurdle to translation into human application, with 10% of an adult patient's body-weight being in the litres. Delivery of a shRNA vector that suppresses CL5 by means of AAV has also been demonstrated (Campbell, Humphries et al. 2011). This approach has the benefit of resulting in a stable, inducible source of BBB modulation which would be highly beneficial to longer term, chronic conditions. However pan-brain delivery of AAV would be extremely difficult, and use of viral vectors is still a significant barrier to clinical progression.

Due to these issues in the current study it was decided to use a polyethylenimine (PEI) delivery method. Initially used to aid in the transfection of cells with DNA, this compound acts by complexing with nucleic acids an cancelling out their net anionic charge by the presence of multiple cationic amino groups (Tang and Szoka 1997). These reduced charge complexes are taken up into cells by caveolae- and clathrin-coated pits, with only the latter route leading to transfection of the cell, at least in the case of DNA (Rejman, Bragonzi et al. 2005). Since its discovery PEI has been used to effectively deliver RNA to in vitro neuronal cells (Sridharan, Patel et al. 2013), breast tumours (Navarro, Sawant et al. 2012; Shen, Sun et al. 2013), liver tissue (Kang, Tachibana et al. 2010; Park, Hong et al. 2011) and many other cell types. Of particular relevance to this study PEI has been

reported also to enable transfection of endothelial cells in vivo following systemic delivery (Kim, Yockman et al. 2006; Li, Yang et al. 2012).

These findings demonstrate effective transfection of cells using low-volume, systemic delivery of nucleic acid/PEI complexes. Further support comes in the form of several ongoing clinical trials in which PEI is used, such as NCT00595088 in which DNA is non-virally delivered to bladder cancer. Together these reports led to its use in the current study, in order to move beyond the short-comings of hydrodynamic and AAV-based delivery.

One final concern is the possibility that exogenously introduced siRNA could result in an interferon (IFN) response in animals. This would be extremely damaging for the study as the consequent inflammation would interfere greatly with measuring of outcomes, and would make impossible any later transition to clinically relevant studies. There is published data also that IFN responses can occur in response to siRNAs, which result from dsRNA or single-stranded siRNA detection by TLR7 or TLR3 (Kariko, Bhuyan et al. 2004; Hornung, Guenthner-Biller et al. 2005; Judge, Sood et al. 2005; Sioud 2005). These reports have observed that these responses occur in a sequence-specific manner and appears to occur in response to RNA molecules that are longer than those used in the present study (Reynolds, Anderson et al. 2006). As well as this however it has been reported that siRNAs, of the length used in the course of this thesis, can have a profound effect on angiogenesis (Kleinman, Yamada et al. 2008; Cho, Albuquerque et al. 2009), and even lead to degeneration of healthy tissue in the retina (Yang, Stratton et al. 2008; Kleinman, Kaneko et al. 2012) regardless of sequence.

To answer some of these concerns, extensive work has been carried out previously by this lab in order to demonstrate that the siRNAs used in this thesis, both targeting and non-targeting, do not exhibit unintended effects such as inflammatory responses. This work has also concentrated on demonstrating that NT siRNA is an effective control for CL5 siRNA. The previous work by this lab studying the effects of CL5 siRNA on the BBB and iBRB used uninjected controls, PBS-injected controls, as well as NT siRNA-injected controls. At no point in any of the findings was there any observed difference between any of the controls in terms of CL5 expression level, CL5 continuity at the BBB, or the extravasation of any compounds into the brain (Campbell, Kiang et al. 2008; Campbell, Nguyen et al. 2009). Neither was there any observed damage to tissue in a histopathological screen of CL5 siRNA that was carried out (Campbell, Hanrahan et al. 2012), or in toxicology testing in African green monkeys carried out for both CL5 and NT siRNA by this lab (as of yet unpublished). Further to this, the 2009 PNAS paper published by this lab included microarray data comparing gene expression data in brain samples of mice that had been systemically injected with CL5, NT, or no siRNA. The data from Affymetrix GeneChips, which contain >28,000 coding transcripts and >7,000 non-coding transcripts and was generated by 5 replicates, looked for off-target effects of the siRNAs in brain tissue. The microarray found 32 genes to be differentially regulated between CL5 siRNA and control brains, and 22 genes to be differentially regulated between CL5 and NT siRNA-administered mouse brain tissue 48 h after siRNA delivery. None of these genes were reported to be know inflammatory markers, and the very low number of genes compared to the huge number tested indicates that these siRNAs have very minimal off-target effects (Campbell, Nguyen et al. 2009). Finally, the particular NT siRNA used during the course of this project, targeting the luciferase gene and with the target sequence 5'-

CTTACGCTGAGTACTTCGA-3', has been used effectively as a non-targeting siRNA in a number of previous studies (Tam, Kiang et al. 2008; Valli, Oliveros et al. 2011; Cho, Chang et al. 2012).

The comprehensive past testing of CL5 siRNA in comparison to various controls by this lab, as well as the microarray data, have all indicated that NT siRNA in isolation is an effective control for CL5 siRNA in continuing to study its effects on BBB modulation. Ideally it would be desirable to use uninjected, PBS-injected, as well as NT siRNA-injected controls for all experiments. However in consideration of the high amount of animal experiments in this thesis, and the evidence presented previously for the effectiveness of NT siRNA as a control for CL5 siRNA, it was decided to limit controls to the NT siRNA group only. The addition of extra control cohorts can mean considerable increases in numbers of animals sacrificed as well as time taken to carry out certain experiments. In MRI experiments, for instance, each animal may take up to an hour each to prepare and scan; here the addition of even one more control group can make it impossible to carry out an experiment in one day, resulting in the necessity to split experimental groups between two different days – a step which risks increasing variation as experimental protocols are carried out seperately to one another. It is for these reasons that NT siNA was often used in isolation as a control for CL5 siRNA during the course of this thesis.

3.2.4 Chapter Aims

In this course of this chapter I aimed to become proficient in the siRNA technologies of this lab, and to demonstrate succesful suppression of CL5 at the transcript and protein level. This suppression would be the first in this lab using the jetPEI siRNA delivery system,

and I aimed to use this delivery method to replicate the detailed observations reported previously by this lab where CL5 was succesfully suppressed in the brain and the retina following hydrodynamic injection (Campbell, Kiang et al. 2008; Campbell, Nguyen et al. 2009). Following this I aimed to use this jetPEI-delivered CL5 suppression to enable an MRI contrasting agent, Gd-DTPA, to extravasate into the brain where it will not normally reach. This also is a replication of work carried out previously by this lab in both the brain and the retina (Campbell, Kiang et al. 2008; Campbell, Nguyen et al. 2009). Finally, a small scale investigation of CL5 siRNA in comparison to a 2' OMe modified siRNA targeting CL5 was carried out to investigate if IFN-α levels are elevated following NT siRNA delivery. This was in response to a reviewer's comments during the course of our publishing a paper using CL5 siRNA (Campbell, Hanrahan et al. 2012), and it provides a small amount of data to indicate that CL5 siRNA does not result in an IFN-α response in vitro or in vivo.

3.3 Results

3.3.1 In Vitro Suppression

CL5 siRNA was assessed for its effectiveness at down-regulating CL5 mRNA transcript in vitro using bEnd.3 cells. This line of mouse brain microvascular endothelial cells is the closest in vitro model of the mouse BBB, are used extensively in its study, and express CL5 protein at high levels (Thal, Luh et al. 2012). 5 x 10^5 bEnd.3 cells were plated with 500ul fetal calf serum-supplemented DMEM in each well of a 24-well plate. The following day these cells were transfected with 20 pmol CL5 or NT siRNA was complexed with Lipofectamine 2000. Transcript down-regulation was measured by RT-PCR from 24 h after transfection up until 1 week post-transfection (*Figure 3.3*).

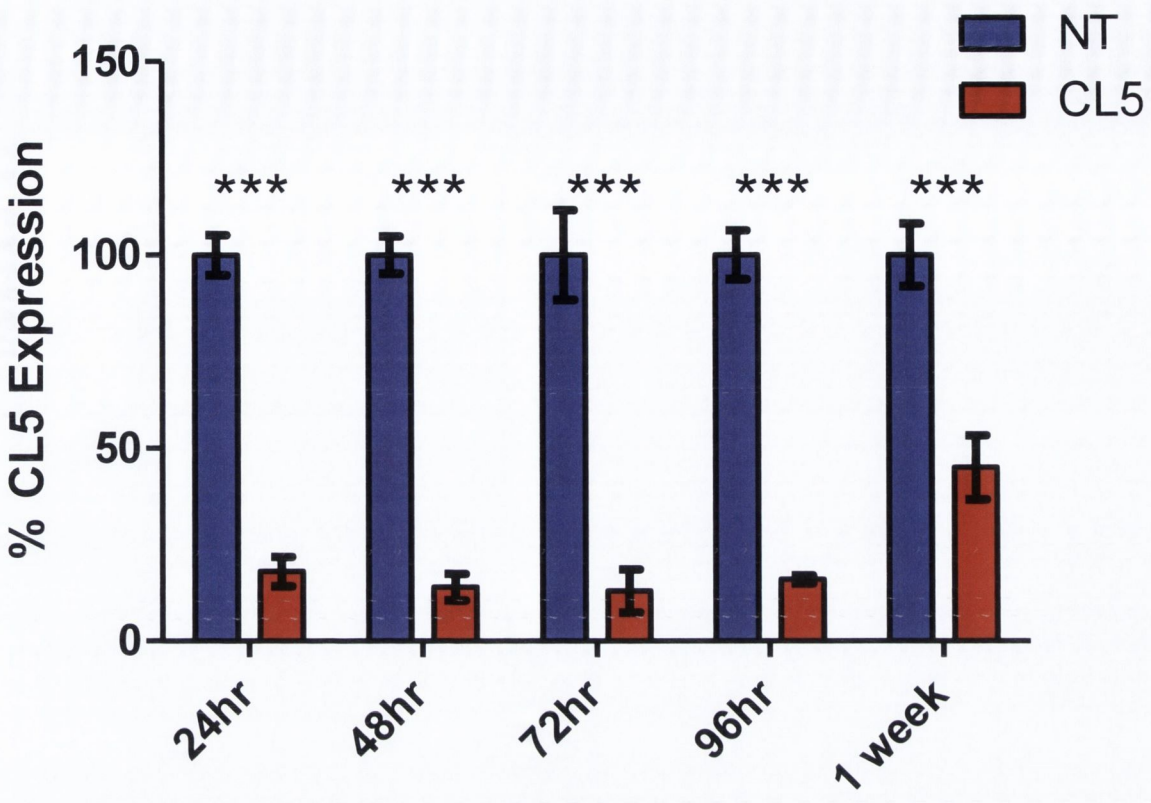

Figure 3.3: RT-PCR of CL5 mRNA following CL5 or NT siRNA transfection of mouse bEnd.3 cells. *CL5 transcript levels were significantly decreased as early as 24 h after transfection and until at least 1 week post-transfection in vitro. For each timepoint CL5 levels in NT siRNA-treated samples were set at 100%. (***P≤0.001, ANOVA with Tukey's post test. NT siRNA, n=3, CL5 siRNA, n=3. Data are means and s.e.m.)*

Data reproduced with permission of James Keaney, Trinity College Dublin.

The RT-PCR data illustrated in *Figure 3.3* shows that endothelial cells treated in vitro with 20 pmol CL5 siRNA have their CL5 mRNA level decreased by approximately 80% compared to NT siRNA-transfected cells at 24 h. This degree of effect persists for at least four days. One week following transfection the CL5 mRNA level had risen to approximately 50% of the post NT siRNA-transfected level.

Next the protein expression level was observed in bEnd.3 cells transfected with CL5 or NT siRNA, this time scaling up to 6-well plate format (*Figure 3.4*). Protein was isolated from cells 48 h following transfection with siRNA as this has previously been shown to be the peak of CL5 protein suppression following CL5 siRNA.

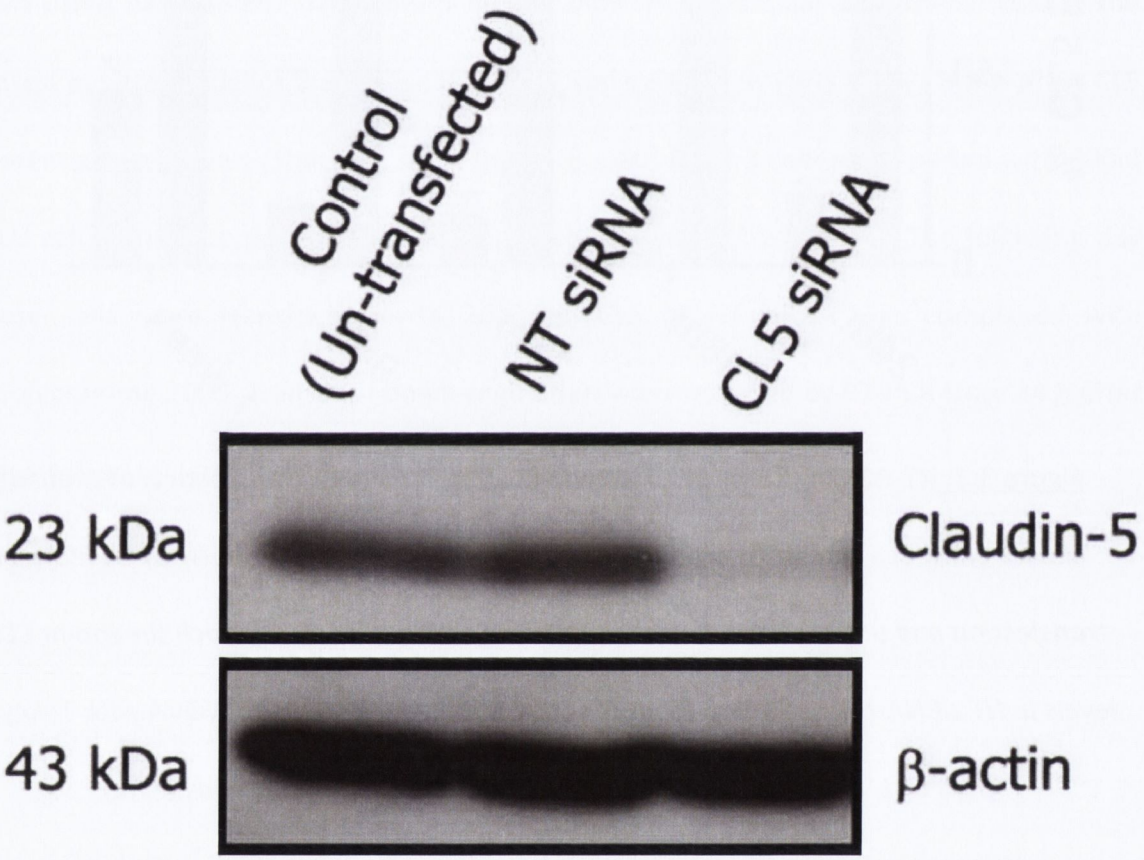

Figure 3.4: Western blot for CL5 protein following CL5 or NT siRNA transfection in vitro.

Western blot for CL5 (23 kDa) and β-actin (43 kDa) on bEnd.3 cells was carried out 48 h after transfection with NT or CL5 siRNA. Image representative of 3 separate repetitions.

The level of CL5 protein, appearing at approximately 23 kDa, appeared to be approximately equal in cells transfected with NT siRNA as in cells that were un-

transfected. CL5 siRNA-transfected cells, on the other hand, showed a markedly decreased level of CL5 protein. B-actin levels were equivalent across the three treatment groups (*Figure 3.4*). This blot is representative of equivalent finding that have been consistently found by Matthew Campbell, James Keaney, Ema Ozaki and others, as well as myself, in the lab. One such blot is shown in *Figure 3.5.*

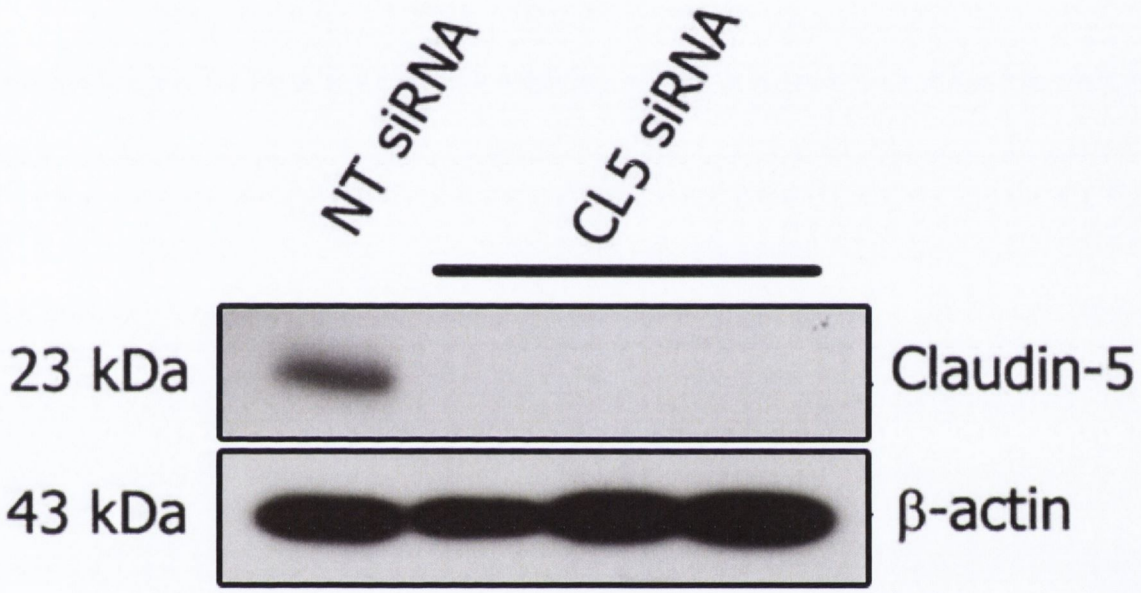

Figure 3.5: Western blot for CL5 protein.

Western blot for CL5 (23 kDa) and β-actin (43 kDa) on bEnd.3 cells was carried out by James Keaney after transfection with NT or CL5 (n=3) siRNA.

As can be seen the suppression observed by James Keaney in vitro in bEnd.3 cells (*Figure 3.5*) was comparable to that observed in *Figure 3.3.*

3.3.2 In Vivo Suppression

The effectiveness of the siRNA at decreasing CL5 levels was next tested in vivo. To do this 20 ng NT or CL5 siRNA was diluted in 200 ul of a 5% glucose solution, as was 6.4 µl in vivo-jetPEI™. After being briefly mixed, the in vivo-jetPEI™ solution was added to the siRNA solution, and the resulting solution was vortexed and briefly centrifuged. Following room temperature incubation for 15 mins, to allow complexes to form, the mixture was injected into the tail veins of 3 month old C57/Bl6 mice. After 48 h the animals were sacrificed, and their brains removed. One hemisphere from each brain was homogenised using a dounce homogeniser, and then capillary fractionated using high molecular weight dextrans (>70,000 Da). These sugar molecules bind to endothelial cells, but not to neural tissue, in the brain homogenates and this characteristic is used to spin down and separate the brain microvascular compartment. Protein was isolated from the resulting red pellet of vascular cells, and a western blot for CL5 performed (*Figure 3.6*).

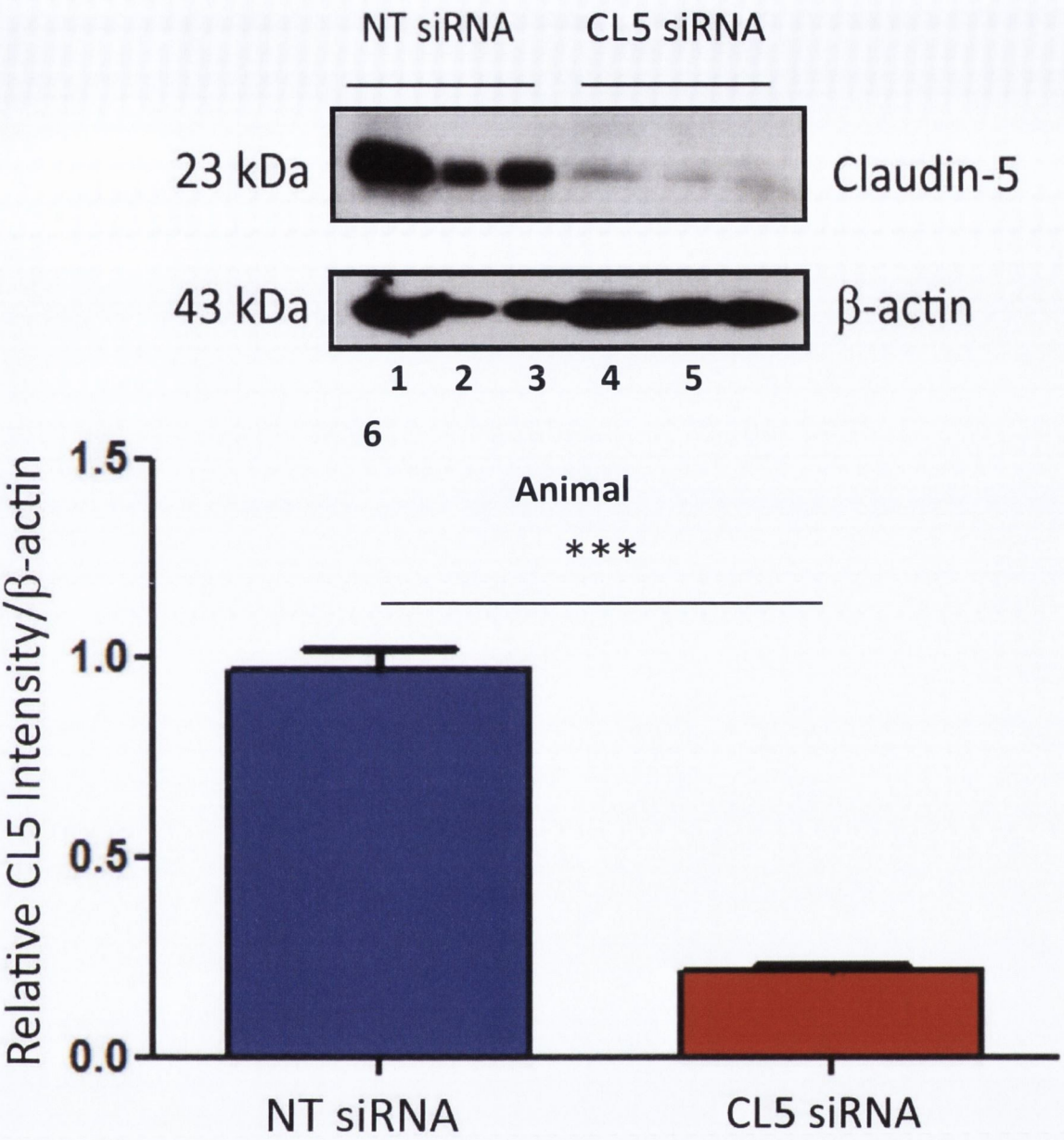

Figure 3.6: Western blot for CL5 protein in brain microvasculature 48 h CL5 or NT siRNA administration in mice. *Top: Western blot for CL5 (23 kDa) and β-actin (43 kDa) on brain capillary fractionations 48 h after tail vein administration of NT or CL5 siRNA. Bottom: graph of the relative pixel intensity of the CL5 bands in NT and CL5 siRNA-administered animals, controlled for β-actin levels. Levels of CL5 were significantly decreased in capillary fractions of mouse brains 48 h post-injection. (***P≤0.001, Students t-test. NT siRNA, n=3; CL5 siRNA, n=3. Data are means and s.e.m.)*

Here CL5 protein levels can clearly be observed, in the raw western blot image, to have dropped significantly 48 h after systemic CL5 siRNA delivery compared to NT siRNA (*Figure 3.6*). When quantified it observed that over 75% of the expression level of CL5 has been abolished, as measured by relative pixel intensity of the bands in the raw image.

Figure 3.6 uses NT siRNA as a control for CL5 siRNA in the absence of other controls. As mentioned in the introduction to this chapter experiments showing CL5 suppression that employed multiple controls have been published previously by this lab. These controls were uninjected, PBS-injected, and NT siRNA injected animals, and none of the suppression studies found any difference between any of these controls (Campbell, Kiang et al. 2008; Campbell, Nguyen et al. 2009).

The other brain hemisphere was taken for immunohistochemical staining in order to visualise CL5 levels in situ following siRNA administration. The tissue was sliced into 12 µm sections in a cryostat, which were then stained overnight using a rabbit anti-CL5 antibody at 4°C, and for 2 h using a secondary rabbit IgG-Cy3 antibody at 37°C. Sections were then stained with a 1:5,000 solution of DAPI in PBS for 30 s and mounted (*Figure 3.7*).

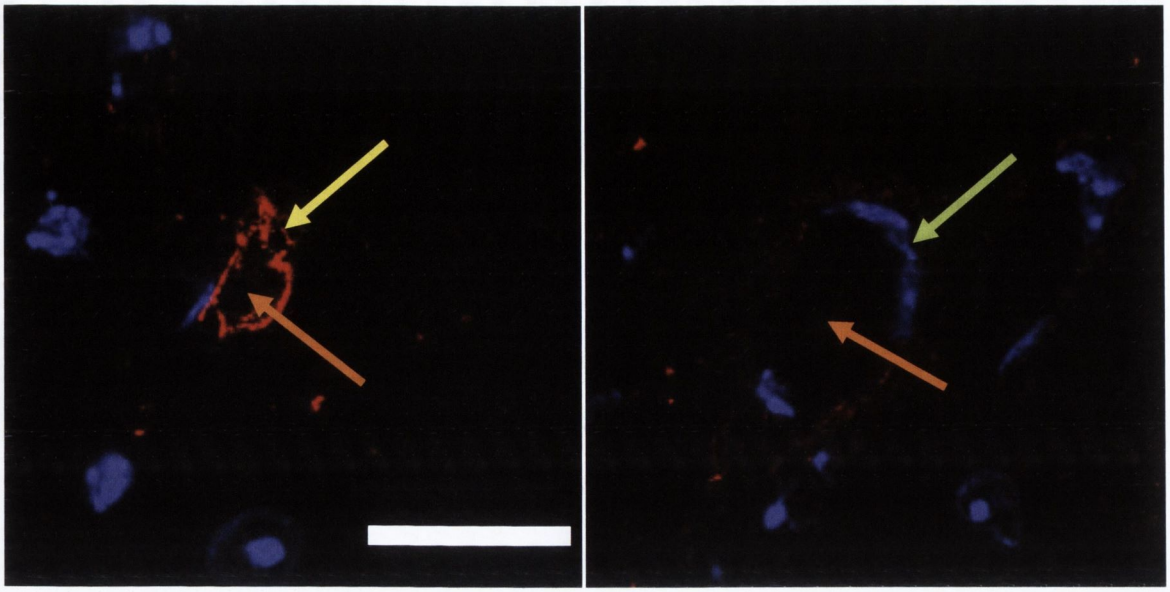

Figure 3.7: Immunohistochemical staining of CL5 protein in brain sections following siRNA delivery. *At left is a brain section from a NT siRNA animal 48 h after siRNA delivery; at right a CL5 animal at the same timepoint. The lumen of a blood vessel can be seen in each image (orange arrow). Surrounding the blood vessel in the NT animal can be seen strong, continuous CL5 staining (yellow arrow). In the CL5 siRNA-administered animal the nucleus of an endothelial cell can clearly be seen (green arrow), but the CL5 staining here is fragmented and reduced in intensity compared with the NT animal. (Red = CL5 staining; blue = DAPI. Scale bar = 100 μm.)*

The staining observed in brain sections (*Figure 3.7*) backs up in situ the result in western blot (*Figure 3.4*) that a high level of suppression of CL5 at the protein level is achieved in vivo 48 h following tail vein delivery of siRNA targeting the transcript. In the right panel of *Figure 3.7* the blood vessel is identified by the characteristically flattened nuclei of endothelial cells as well as patchy CL5 staining. The presence of a complementary stain for another endothelial cell marker, such as the TJ protein ZO-1, would however provide greater confidence that the image in the right panel is a blood vessel. This imaging of

blood vessels for CL5 suppression have been carried out extensively by this lab in both the brain (Campbell, Kiang et al. 2008) and the retina (Campbell, Nguyen et al. 2009). In the brain these stains were carried out using PBS-injected and uninjected controls, as well as NT siRNA animals. In these experiments comparable CL5 staining was observed in all three controls, with only CL5 siRNA-administered animals showing reduced, patchy CL5 staining as in *Figure 3.7* (Campbell, Kiang et al. 2008).

3.3.3 Blood-Brain Barrier Modulation

The next step was to analyse whether the CL5 suppression achieved in vivo at this timepoint would result in modulation of the BBB. This can be tested by attempting to deliver a compound across the barrier into the brain, where said compound would normally not be capable of reaching. For this purpose gadolinium (III) - diethyltriaminepentaacetic acid (Gd-DTPA) was used.

48 h after systemic injection of 20 µg siRNA via the tail vein C57 animals were transported to a dedicated animal MRI. After a high resolution, T_2-weighted scan to ensure that no abnormalities were present, animals were cannulated by their tail veins and a T_1-weighted set of 12 scans, lasting 20 mins in total, was started. Directly after the first of the 12 scans was finished 100 µl of a 1:3 Gd-DTPA solution was injected via the tail vein cannula, and the resulting enhancement in the brain was observed (*Figure 3.8*).

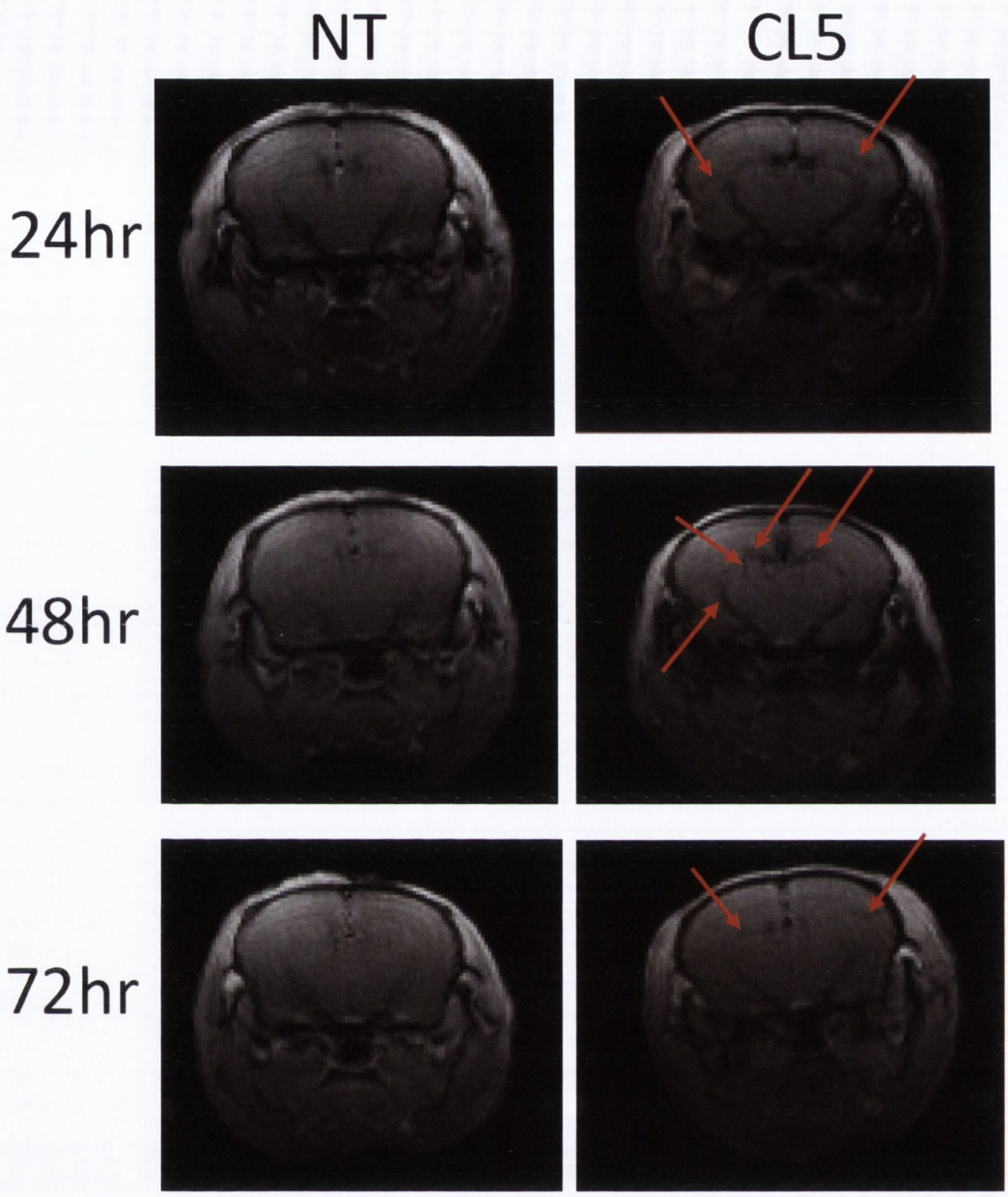

Figure 3.8: Enhanced Gd-DTPA delivery to the brain following CL5 siRNA. *Left: T_1-weighted contrast enhanced MRI image of mouse brain at 24, 48 and 72 h after systemic injection of 20 μg NT siRNA. Gd-DTPA enhancement (dark areas) is restricted to blood vessels in the brain following systemic injection of the contrast agent during the scan. Right: Brain of a CL5 siRNA-injected mouse at 24, 48 and 72 h. Enhanced Gd-DTPA concentration surrounding blood vessels in the brain, as well as increased contrasting throughout the brain, is present at 48 h. Prominent regions Gd-DTPA extravasation are*

highlighted with red arrows. This extravasation appears to be present to a lesser extent at 24 and 72 h than at 48 h.

The difference between the Gd-DTPA contrasting in NT and CL5 animals was subtle at 24 and 72 h, but was readily observable at 48 h as lower pixel intensity surrounding blood vessels and an increased 'mottled' appearance of the cortex in CL5 animals (*Figure 3.8*). Experiments showing Gd-DTPA extravasation into the brain after CL5 suppression that employed multiple controls have been published previously by this lab. These controls were uninjected, PBS-injected, and NT siRNA injected animals, and none of the suppression studies found any difference between any of these controls, with no observed increase in contrasting agent entering the brain (Campbell, Kiang et al. 2008).

The contrast-enhanced T_1-weighted MRI scan used here is made up of 12 repetitions, with Gd-DTPA being injected after the first of these. As such the effect of this systemic Gd-DTPA can be quantified by selecting a number of 9 voxel (0.178 mm^2) areas in different areas of the brain, away from visibly contrasted blood vessels, and measuring the average pixel intensity within the area for each scan. With these values the kinetics of Gd-DTPA as it passed through the brain can be quantified, and compared between NT and CL5 siRNA animals (*Figure 3.9*).

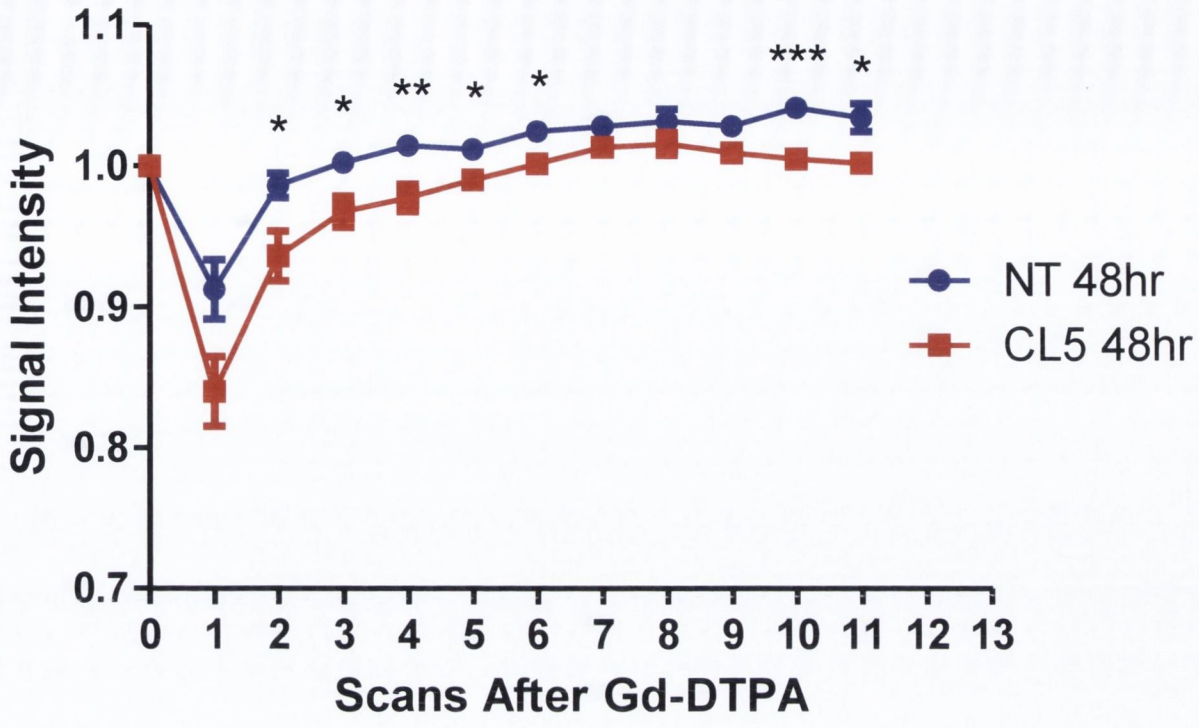

Figure 3.9: Quantification of Gd-DTPA contrasting in mouse brain cortex after CL5 and NT siRNA. *48 h after tail vein injection of Gd-DTPA, bolus chase analysis of the contrast agent in T_1-weighted MRI of a cortical region of the mouse brain showed a slower clearance rate of Gd-DTPA in the CL5 siRNA group compared with the NT siRNA group. Quantification was obtained by measuring pixel intensity in the same area of brain tissue in each animal, in the scan before and each of the 11 scans after systemic Gd-DTPA injection. (P≥0.05; Student's t-test. NT 48 h, n=6; CL5 48 h, n=8.)*

In this figure scan 0 represents the baseline signal intensity of the brain before Gd-DTPA injection, with scan 1 representing the large alteration in signal intensity as the contrasting agent enters the brain parenchyma. Over the following 20 min, during which the next 10 scans were carried out, Gd-DTPA saturated the available tissue into which it

could enter, and was subsequently cleared from the brain. The significantly altered pixel intensity in mice given CL5 siRNA 48 h previously indicates that higher quantities of Gd-DTPA were detectable within the brains of these animals, and that this higher quantity of Gd-DTPA took longer to clear compared with NT control mice (*Figure 3.9*). This data shows that 48 h following systemic injection of CL5 siRNA with jetPEI the BBB has been modulated to the extent that a molecule of at least 742 Da will extravasate across into the neuronal space. Gd-DTPA contrasting in the brain has been previously shown by this lab, where greater quantities of Gd-DTPA were measured crossing the BBB into the parenchyma in animals that had been given CL5 siRNA. In those experiments uninjected, PBS-injected and NT siRNA-injected controls were used, none of which showed any significant change in Gd-DTPA extravasation (Campbell, Kiang et al. 2008).

3.3.4 Inflammatory Response to siRNA

Given the data available that siRNAs can induce TLR-mediated inflammatory responses in vitro and in vivo (Kanasty, Whitehead et al. 2012), it was decided to test the CL5 siRNA, with an without in vivo-jetPEI, for these responses.

An siRNA with 2 modifications in the sense strand was designed as follows: 5'-CGUmUGGAAAUUCUGmGGUCUUUdTdT-3'. 20 µg of this modified siRNA was complexed with in vivo-jetPEI and injected into the tail veins of C57/Bl6 mice. Effective suppression of CL5 was observed in the capillary isolations prepared from the brain samples 48 h post-injection (*Figure 3.10*).

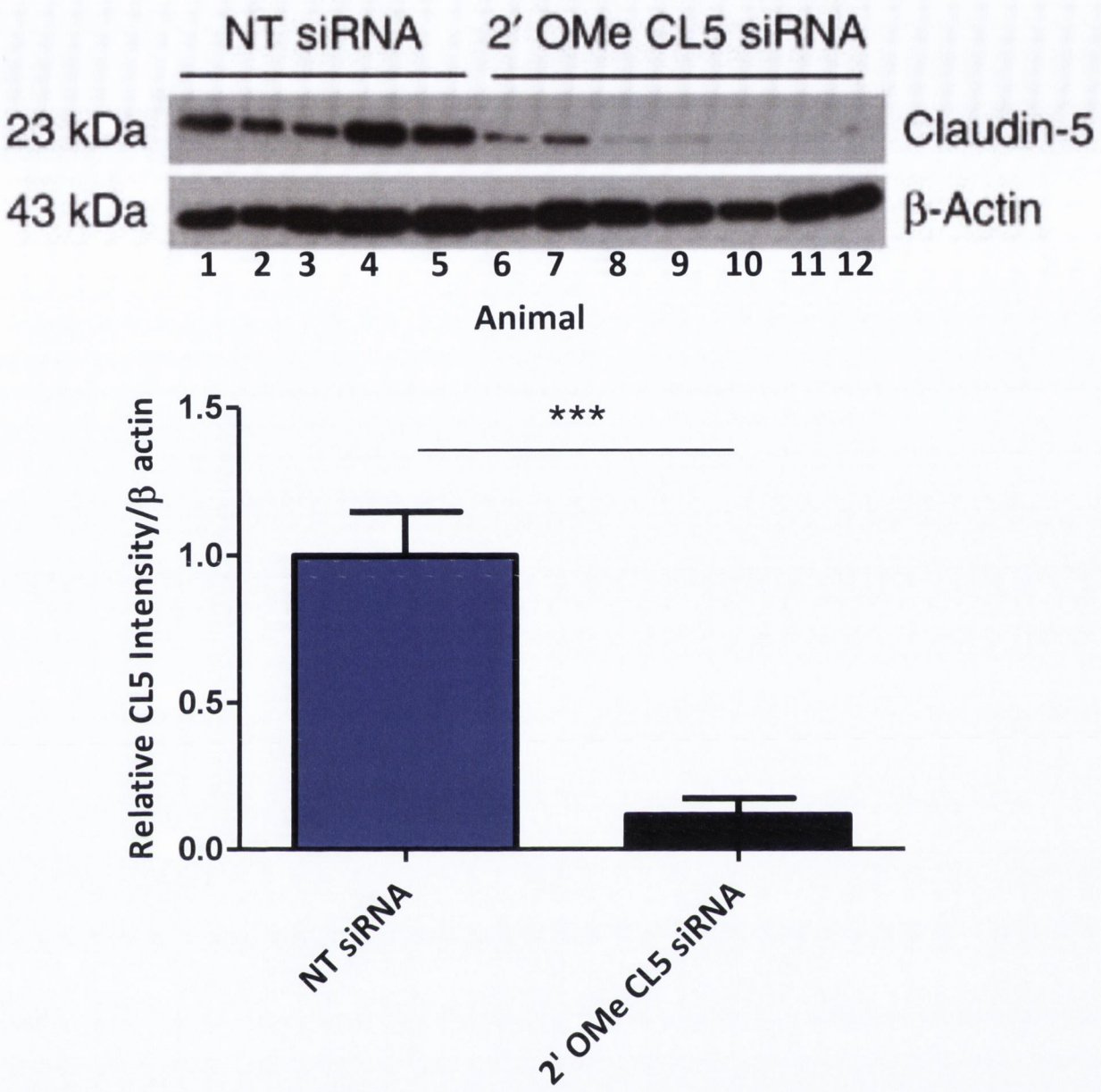

Figure 3.10: Suppression efficacy of 2'OMe-modified CL5 siRNA. Top: *Western blot for CL5 (23 kDa) and β-actin (43 kDa) on brain capillary fractionations 48 h after tail vein administration of 20 μg NT or 2'OMe CL5 siRNA.*

*Bottom: Graph of the relative pixel intensity of the CL5 bands in NT and CL5 siRNA-administered animals, controlled for β-actin levels. Levels of CL5 were significantly decreased in capillary fractions of mouse brains 48 h post-injection. (***P≤0.001, Students t-test. NT siRNA, n=5; 2' OMe CL5 siRNA, n=7. Data are means and s.e.m.)*

As can be seen, the suppression observed using the 2'OMe-modified CL5 siRNA (*Figure 3.10*) is comparable to that observed with the normal CL5 siRNA (*Figure 3.4*). With suppression demonstrated the two siRNAs were assessed on their inflammatory profile.

Bone-marrow derived macrophages (BMDMs) from WT C57/Bl6 mice were isolated and grown. These cells were treated with 20 pmole NT, CL5 or 2'OMe CL5 siRNA, with or without in vivo-jetPEI^{TM}, for 24 h, and transcript levels of IFN-α were subsequently analysed (*Figure 3.11*).

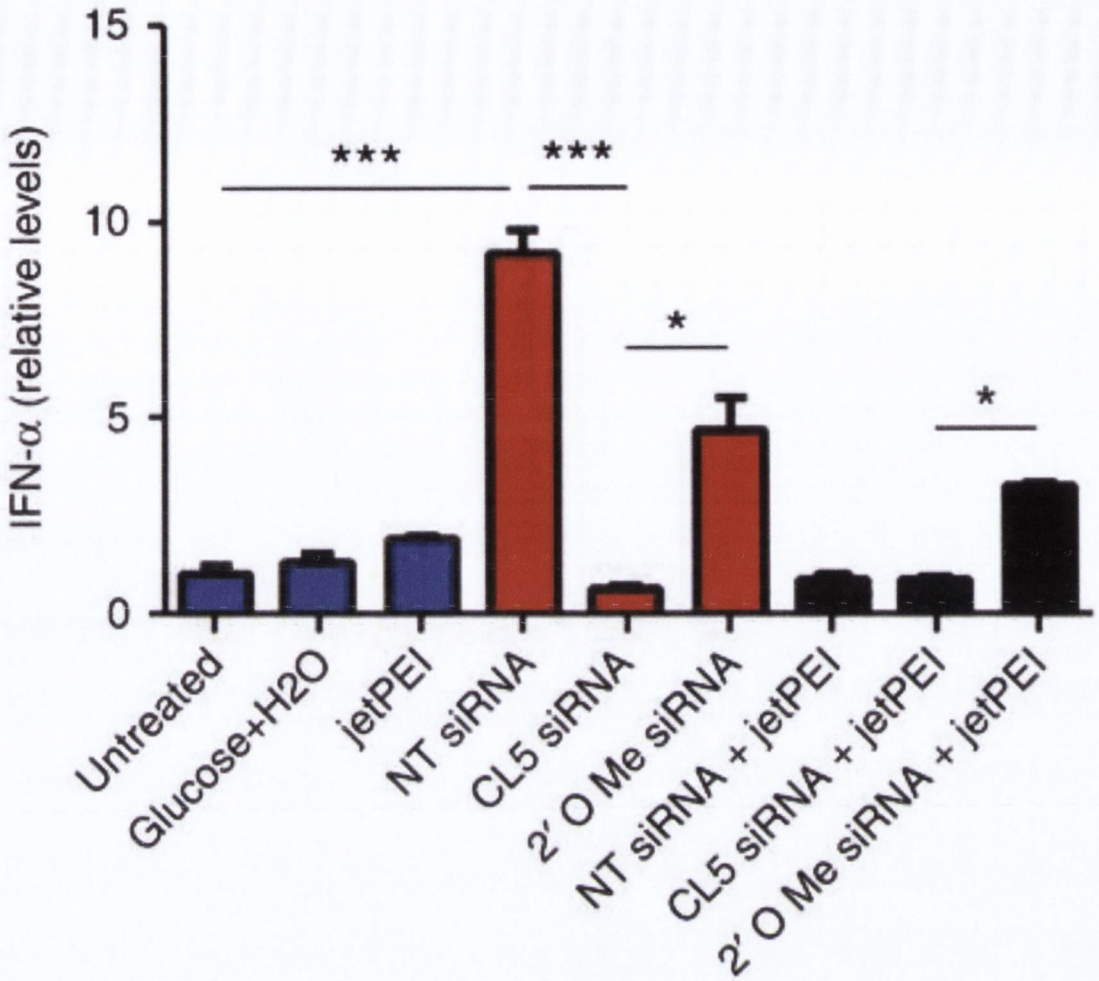

Figure 3.11: RT-PCR analysis of IFN-α in BMDMs following exposure to siRNAs. *In BMDMs treated with NT siRNA, a significant up-regulation of IFN-α was observed compared with untreated, glucose-treated or in vivo-jetPEI™ treated cells. Levels were also significantly increased in NT siRNA treated cells when compared with CL5 siRNA. 2'OMe-modified CL5 siRNA-treated cells expressed significantly higher IFN- when compared with un-modified CL5 siRNA. siRNAs complexed with in vivo-jetPEI™ produced an overall decreased level of IFN- expression, but this was significantly higher with 2'OMe-modified CL5 siRNA and in vivo-jetPEI™. All compounds being studied were applied to BMDM cells for a period of 24 h. (*P≤0.05, ***P≤0.001, ANOVA with Tukey's post test. Untreated, n=3; Glucose+H20, n=3; jetPEI, n=3; NT siRNA, n=3; CL5 siRNA, n=2; 2'OMe CL5*

siRNA, n=3; CL5 siRNA, n=2; 2'OMe CL5 siRNA + jetPEI, n=3; NT siRNA + jetPEI, n=3; CL5 siRNA + jetPEI, n=3)

The level of IFN-α transcript in BMDM's exposed to a 5% glucose in H_2O dilution mix, or in vivo-jetPEI in 5% glucose, was not significantly above that of the baseline, untreated level. IFN-α production was significantly increased in NT siRNA-treated cells compared with untreated cells. This level was significantly decreased in the 2'OMe-modified siRNA-treated cells, affirming previous findings that 2'OMe-modified siRNAs elicit a weaker inflammatory response (Robbins, Judge et al. 2007). However application of CL5 siRNA to BMDMs did not result in a similar increase as was observed for NT siRNA, and instead the level of IFN-α transcript after exposure to CL5 siRNA was unchanged from that of untreated cells (*Figure 3.11*).

Furthermore we also isolated peripheral leukocytes from the blood of mice 24 h post-injection of the three siRNAs (NT, CL5 and 2'OMe-modified CL5) and found no detectable IFN-α expression (*Figure 3.12*).

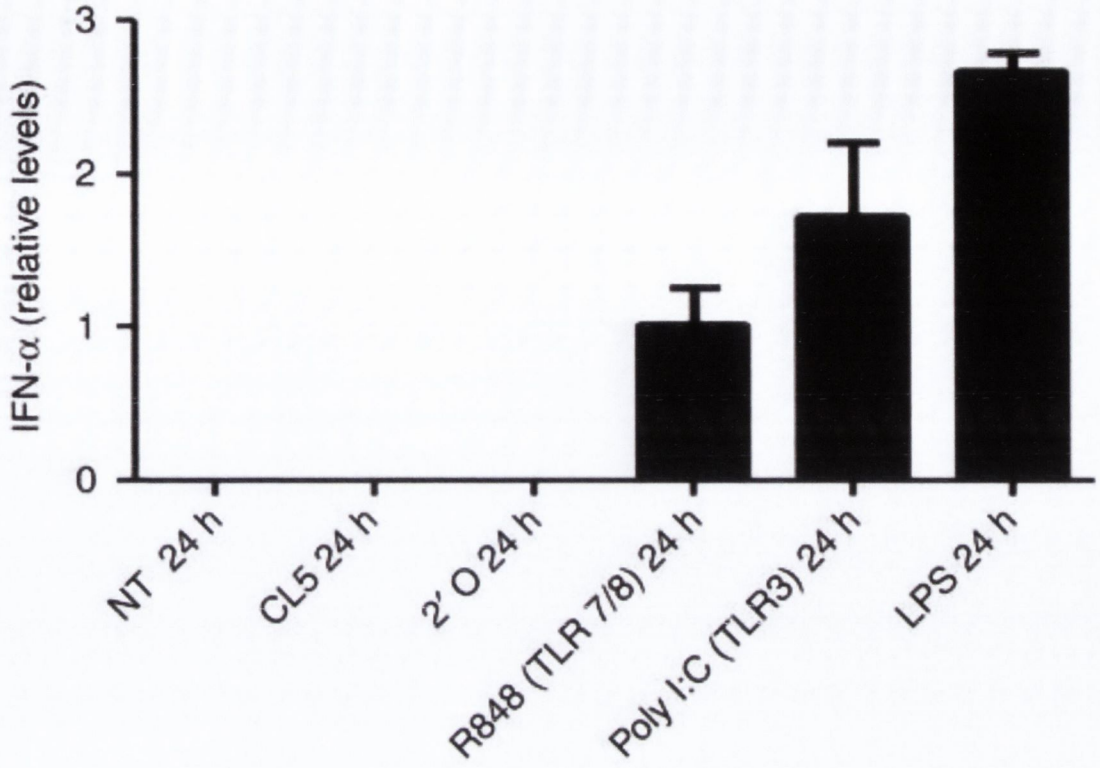

Figure 3.12: RT-PCR analysis of in vivo IFN-α production in response to siRNA or positive controls. *Peripheral blood mononuclear cells were isolated from terminally-bled C57 mice 24 h after systemic, tail vein injection of 20 ng siRNA complexed with 6.4 µl in vivo-jetPEI. RNA was isolated from these cells, as well as cells exposed in vitro to positive controls for TLR activation for 2 h, and RT-PCR was carried out. IFN-α could not be detected in the blood of any of the animals exposed to siRNA and in vivo-jetPEI. (P=n/a. NT, n=4; CL5, n=4; 2'OMe, n=4; R848, n=3; Poly I:C, n=3; LPS, n=3)*

Tail vein administration of NT siRNA, CL5 siRNA or 2'OMe-modified CL5 siRNA showed no significant increases in IFN-α expression when compared with positive controls (poly I:C-TLR3, R848-TLR7 and LPS-TLR4) (Figure 3.12).

When taken together these data indicate that 2'OMe-modified CL5 siRNA proves highly effective at suppressing CL5 at the protein level, but it does not result in any improvement in the observed safety profile compared with the unmodified CL5 siRNA, which does not appear to result in an IFN-α response at least at the transcript level. It is still possible that by post-transcriptional modification IFN-α levels are increased in response to unmodified Cl5 siRNA, though assaying for alterations in IFN-α levels in response to inflammatory signals at the transcript level alone has been shown previously to be an effective method (Pau, Cheung et al. 2012).

3.4 Discussion

Despite the aforementioned previous use of the CL5 siRNA by this lab the assessment of the in vitro and in vivo efficacy of this approach was of crucial importance. The first reason for this is that previously the majority of barrier modulation work using the CL5 siRNA has been carried out in the retina, not the brain (Campbell, Nguyen et al. 2009)(Tam, Kiang et al. 2010; Campbell, Humphries et al. 2013). Despite the close similarity of the inner BRB and the BBB, a change as large as disease model or target organ – or both as in this case – are large enough to warrant a revaluation of protocols. Many unknown factors could be different moving from the retina to the brain, and changes in dosing, delivery mechanism or strain of mouse could be required. A further consideration here is that this study was led by an individual not previously versed in the use of siRNA. Discovery of potential errors at the start could prevent great difficulty in tracking down the source of problems at a later stage of this study.

Secondly, the work that was previously carried out targeting low molecular weight compounds to the brain carried out by this laboratory thus far carried out delivery by means of hydrodynamic injection or by AAV-mediated delivery of a shRNA-expressing vector (Campbell, Kiang et al. 2008; Campbell, Humphries et al. 2011). Changing from this method to the use of PEI necessitate changes in protocol which require appropriate testing, as well as carrying the chance of failing to demonstrate efficacy in suppressing CL5 and modulating BBB strength at all.

Finally, in this study it was decided to delve further and to elucidate whether the PEI-siRNA complexes were causing detectable inflammatory responses in healthy animals or isolated immune cells. If responses of this type were observed it could represent a major barrier to progression of the study as the chances for translation into human studies would be greatly damaged. In the least alterations to complexing reagent or siRNA sequence would have to be made.

In vitro suppression at the transcript level was observed to strongly occur following transfection of bEnd.3 cells (*Figure 3.3*). These levels had begun to return at 1 week following transfection, but were still significantly depressed compared to NT siRNA-transfected cells. This suppression was also found at the protein level 48 h following transfection (*Figure 3.4*).

This 48 h timepoint was used in vitro as well as for quantitative demonstration of CL5 suppression in vivo (*Figure 3.6* and *Figure 3.8*). The reason for this was because while it has previously been shown that protein levels decrease rapidly after siRNA administration, and take a number of days to return to baseline levels, maximal suppression is observed at 48 – 72 h (You, Lee et al. 2010). This agrees with numerous

previous observations by this lab that CL5 is most efficiently suppressed at 48 h in vivo enabling delivery of low-molecular weight compounds (Campbell, Kiang et al. 2008; Campbell, Nguyen et al. 2009).

In this study brain capillary fractionations were carried out on brains from animals that had received siRNA prior to western blots being begun. The reason for this is that endothelial cells make up only a small percentage of cells in the brain, and so it is desirable to enrich for this cell fraction before assaying for CL5 levels.

Together these data from RT-PCR and western blot in vitro, and western blot and immunohistochemistry in vivo, demonstrate that the CL5 protein is effectively and markedly suppressed following CL5 siRNA.

MRI is used throughout the course of this study as a means to assess the permeability of the BBB and BTB to low molecular weight compounds. The advantage of using MRI in this case rather than staining compounds such as biotin, is that this approach observes the movement of a compound across the BBB over time in situ. This means that one does not need to take a number of separate animals for separate timepoints following injection of the compound, all of which could potentially demonstrate differing penetration of the BBB. Instead one can observe all desired timepoints post-injection of the contrasting agent within the same animal. This has the effect of reducing error as well as animal numbers.

Also, as the animal does not need to be sacrificed in order to observe the results, the same animal can be used for behavioural or other testing. This further reduces the number of animals required, which is always something to strive for. Furthermore carrying out multiple studies on a single cohort of animals means that the results you

observe later in this study in, for example NSS testing, are generated from the same animals in which lesion volumes are measured. In more traditional methods of measuring BBB strength that involve sacrifice, greater variation is introduced by use of different animals for different experiments.

Throughout the course of this study Gd-DTPA is used as MRI contrast agent. Gd-DTPA has the advantage over many other contrast agents by achieving maximum extra-vascular enhancement 5 – 6 mins after systemic injection, with relatively rapid return to baseline (Ross, Delamarter et al. 1989). This means that a number of animals can be scanned within one session, as well as reducing the risk that the animal will die due to reduction in body heat while under longer-term anaesthesia. Finally, with a molecular weight of 742 Da, extravasation into the brain parenchyma by Gd-DTPA (*Figure 3.8* and *Figure 3.9*) demonstrate a proof of principal for the enhanced delivery of many low molecular weight compounds to the brain, for instance the chemotherapeutic compounds doxorubicin (544 Da) and temozolomide (194 Da).

It has been reported that 2'OMe backbone modifications in even 2 residues of a siRNA reduce inflammatory responses (Robbins, Judge et al. 2007). The exact mechanism whereby this occurs has not been established, but it has been suggested that due to a difference in the number of modified nucleotides in mammals and in bacteria. Mammalian RNA contains a high level of nucleotide modifications and these sequences do not activate TLRs, whereas bacterial and mitochondrial RNA is largely unmodified and do activate TLRs (Kariko, Buckstein et al. 2005). Interestingly though, 2'OMe-modified RNA has been reported to block the activity of TLR7 even when not incorporated into a

siRNA. Instead simply the presence of 2'OMe-modified RNA abrogated the TLR7 response not just against siRNAs, but also against a small-molecule TLR7 agonist, loxoribine (Robbins, Judge et al. 2007). This result suggests that rather than altering the recognition of the siRNA by TLR7, 2'OMe modifications are antagonistic to the activity of the receptor. 2'OMe CL5 siRNA was shown in this study to also effectively suppress CL5 at the protein level (*Figure 3.10*). The suppression observed here appears to be similar to that observed for unmodified CL5 siRNA mentioned earlier (*Figure 3.6*), although with the two transfections and western blots being carried out on different days they cannot be directly compared by relative pixel densitometry. There are issues in making historical comparisons such as this, as experimental protocols carried out on different days may vary greatly due to either error or else fluctuations in experimental conditions. This has the effect of increasing variation between experiments carried out on different days, with samples assayed on the same day being the most desirable for comparative purposes.

With respect to gauging the inflammatory responses to NT, unmodified CL5 and 2'OMe CL5 siRNA these were separately added to BMDMs for 24 h before IFN-α expression was quantified. These nucleic acids were added to BMDMs with or without having been complexed with PEI. The reason for observing responses with and without PEI was that while PEI was used in all animal delivery of siRNA during the course of this study, it cannot be guaranteed that none of the siRNA remains uncomplexed.

PEI-based delivery polymers have previously been reported in a number of in vivo studies to be safe to use. PEI-coated nanoparticles, for instance, have been reported not to cause inflammation when used in the cornea, even for 7 concurrent days (Sharma, Tandon et al. 2011), with an equal lack of immune activity reported following cochlear delivery of PEI-complexed nucleic acids (Tan, Foong et al. 2008). In one comprehensive study the levels

of liver enzymes as well as numerous cytokines including TNF-α, IFN-γ, IL-6, and IL-1β were assessed in mouse serum following injection of PEI-complexed siRNA. None of the factors investigated displayed increased expression (Bonnet, Erbacher et al. 2008).

In contrast, however, it has also been reported that a greater level of immune stimulation occurs when siRNAs are encapsulated in siRNA delivery agents, than siRNA or delivery agent alone (Judge, Sood et al. 2005). This may occur due to an increase in the amount of siRNA reaching the endosomal compartment inside cells, which is required for immune activation by siRNA and where TLR7 and TLR8 are located (Sioud 2005). One of the delivery agents used in the Judge et al. study was PEI, the same as was used during the course of this study to aid delivery of siRNA in vivo. Due to the marked difference in findings between these two studies neither one could be relied upon. As such it was important to test the IFN-α response to in vivo-jetPEI™-complexed siRNA during the course of this work, with IFN-α being chosen as it has been reported to be the major inflammatory response factor to TLR7-activation, the major TLR that responds to the presence of siRNAs (Kim, Longo et al. 2004; Hornung, Guenthner-Biller et al. 2005; Kim, Choung et al. 2007; Yan, Regalado-Magdos et al. 2010).

It was found that the transcription of IFN-α in response to NT siRNA decreased significantly when complexed with in vivo-jetPEI™, and CL5 siRNA remained at its basal level. The level of IFN-α produced by BMDMs in response to 2'OMe siRNA was still significantly higher than CL5 siRNA when they were both complexed with in vivo-jetPEI (*Figure 3.11*).

siRNA recognition by TLR7 is sequence-dependent, and so the specific sequence of the CL5 siRNA could be responsible for the difference in response. It has been reported that uridine (U) and guanosine (G)-rich sequences, particularly UG dinucleotides, correlate

with increased TLR7 activation (Heil, Hemmi et al. 2004), however the combined number of UG dinucleotides on the two strands of each siRNA is equal. Other teams have found the number of U residues to be the significant determinant for immune-activation – with more U's increasing TLR7 recognition (Goodchild, Nopper et al. 2009) – however the CL5 siRNA in fact contains more U residues than the NT siRNA (14 vs 8 respectively). In fact this same study determined that 'CG clamps' – CG dinucleotides with a corresponding CG on the other strand with which to bind – are correlate with lower TLR7 activation, however the NT siRNA contains two CG clamps while the CL5 siRNA contains none (Goodchild, Nopper et al. 2009). However other groups have found the relative positioning of significant nucleotides along an RNA strand to be important (Gantier, Tong et al. 2008), so it is likely that the particular combination of nucleotides on the strands of the unmodified CL5 siRNA, or a feature of its tertiary structure, allows it to evade TLR7 recognition.

Finally, as the previously described experiment had been carried out in vitro using isolated BMDMs a further assay was carried out, this time in vivo. Here peripheral blood mononuclear cells were isolated and RNA extracted 24 h after injection with NT, unmodified CL5 or 2'OMe CL5 siRNA complexed with PEI. Positive controls were supplied by exposing peripheral blood mononuclear cells to potent activators of TLRs (R848 for TLR7, poly I:C for TLR3, and LPS for TLR4) for 2 h. Statistical analysis could not be carried out for these samples due to a failure to detect any measurable IFN-α in any of the samples from animals given siRNA and PEI (*Figure 3.12*), however it is clear from these combined findings (*Figure 3.11* and *Figure 3.12*) that no inflammatory risk due to induction of IFN-α could be detected for CL5 siRNA. This finding does not exclude the chance that other interferons or cytokines may be upregulated in response to CL5 or

other siRNAs, however the previously mentioned microarray data reported by this lab demonstrates that there is no alteration in regulation of inflammatory genes, at least at the transcript level (Campbell, Nguyen et al. 2009), as well as no findings to indicate inflammation in histopathological screening of organs (Campbell, Hanrahan et al. 2012) or toxicological analysis of African green monkeys.

Together the results in this chapter demonstrate that CL5 siRNA, when complexed with PEI, is effective at suppressing CL5 in vitro and in vivo, that this suppression leads to BBB permeability up to at least 742 Da. Furthermore it has been demonstrated, once again in vitro and in vivo, that CL5 siRNA complexed with PEI does not lead to an inflammatory IFN-α response.

3.5 Future Directions

The majority of the work in this chapter functioned to repeat the findings that have been repeatedly found and reported by this lab concerning the ability of CL5 siRNA to suppress CL5 in vitro and in vivo, and that this suppression results in permeability of the BBB to low-molecular weight compounds (Campbell, Kiang et al. 2008; Campbell, Nguyen et al. 2009; Tam, Kiang et al. 2010; Campbell, Humphries et al. 2013). This work was important to repeat, however, in order to demonstrate that another individual could carry out these techniques accurately, and in this should be continued when new researchers use barrier modulation techniques in order to reduce the chance of error.

The in vitro and in vivo assessment of siRNAs should be extended to include more factors than IFN-α alone. This would be particularly interesting as some of the siRNAs assayed in this study did appear to elicit an IFN-α response in vitro. No such response is observed in response to CL5 siRNA, and as previously mentioned microarray data available for CL5 and NT siRNA in the brain showed no off-target expression of inflammatory genes (Campbell, Nguyen et al. 2009), as well as histopathological data in mouse (Campbell, Hanrahan et al. 2012) and African green monkey toxicology trials (as of yet unpublished) demonstrated no adverse effects. Nonetheless, even if confined to NT siRNA findings of an inflammatory response would be quite serious and so further exploration into this should be carried out.

Chapter 4: Chemotherapeutic Delivery in a Model of Glioblastoma multiforme

4.1 Abstract

Glioblastoma multiforme has a survival rate lower than the majority of other tumours. This is in part due to the difficulty in treating tumours within the brain with chemotherapeutics, leading to a reliance on resection and radiotherapy which proves insufficient in the majority of cases. Previous work by this lab has focused on delivery of low-molecular weight compounds to treat condtions of the retina. This chapter aimed to extend this work to the brain, using barrier-modulation by means of CL5 siRNA to enable greater access for chemotherapeutics to a model of glioblastoma. In order to accomplish this protocols were developed to inoculate nude mice with two different glioblastoma cell lines, which developed into tumours that grew until animals had to be put down. The jetPEI-delivered CL5 siRNA method described in Chapter 3 was then applied to this model, which resulted in increased permeability of the tumour periphery to a low-molecular weight MRI contrasting agent similar in size to currently used chemotherapeutics. Following this a small scale survival study was carried out using two chemotherapeutics in conjunction with CL5 suppression. Results obtained here trended towards increased median survival of animals given chemotherapy following BBB modulation, but fell short of providing convincing evidence for efficacious treatment.

4.2 Introduction

4.2.1 Crossing the Blood-Tumour Barrier

It has been previously found that AAV vectors injected into the middle carotid artery of a dog with benign intracranial meningioma were able to transduce a high percentage of tumour cells after only one injection (Chauvet, Kesava et al. 1998). With the viral size being measured in kilodaltons, and many chemotherapeutic compounds being less than 1kDa, one would expect that delivery to brain tumours would be equivalent to delivery to peripheral tumours. However the relative ease of delivery in this case is due to excessive fenestration and leakiness of meningioma tumour capillaries, which facilitate permeability to viral vectors, or other large molecules.

Within most forms of primary brain tumour delivery patterns such as that observed in meningioma are not possible. As mentioned previously there is evidence of a loss of BBB characteristics in blood vessels within tumours, but normal BBB expression patterns persist in peri-tumoural areas at the expanding edges of the tumour (Zhang and Olsson 1997) (*Figure 4.1)*.

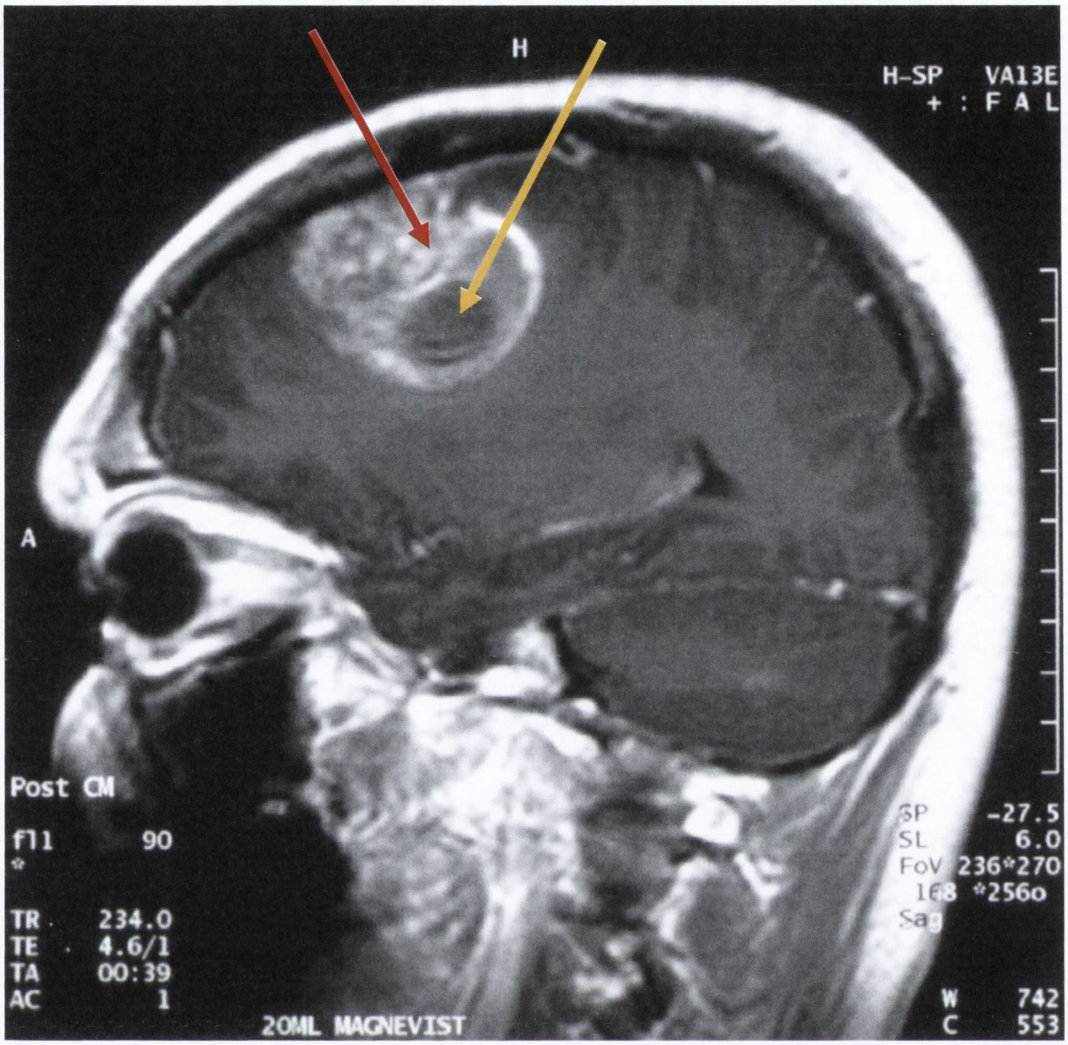

Figure 4.1: Human glioblastoma showing characteristic BTB. *This image shows a contrast enhanced magnetic resonance image of a glioblastoma multiforme. Visible are area of the tumour which are highly permeable (red arrow) to Gd-DTPA (here under the trade-name Magnevist), and regions of the tumour in which Gd-DTPA extravasation cannot occur (orange arrow). Image is credited to the NIH and is in the public domain.*

Regions of altered expression of BBB markers coincide with changes in access to the brain parenchyma, with tumour blood vessels being permeable to, for instance, methotrexate (454 Da), while peri-tumoural and normal brain regions are not (Kroll, Pagel et al. 1994). This altered barrier present in tumours is referred to as the BTB. While the relative

permeability at the core of tumours (*Figure 4.1*) means that increased concentrations of chemotherapeutics at these sites are observed, the relative strength of the BTB at peri-tumoural regions renders chemotherapy ineffective in the treatment of brain tumours beyond small increases in survival length.

Bypassing the BRB to enable delivery of some drugs to the retina or other parts of the eye is already possible. Intraocular injections are used to deliver drugs such as bevacizumab (Avastin) and ranibizumab (Lucentis) for choroidal neovascularisation (Fine, Zhitomirsky et al. 2009), the antisense nucleotide formivirsen for cytomegalovirus (Perry and Balfour 1999), and carbachol for postoperative intraocular pressure (Stuhr, Miller et al. 1998). However, despite these treatments being impressive breakthroughs and delivering relief to patients from previously untreatable conditions, and the fact that the retinal barrier and BBB are highly similar in form and function, the brain is far less accessible than the retina to injection.

Nonetheless bypassing of the BBB and BTB by injection has been attempted in the form of stereotactic injections under surgical conditions through a small bore-hole and into the brain, and a number of clinical trials have been carried out employing this delivery method (Colombo, Zanusso et al. 1997; Wakabayashi, Yoshi Da et al. 2001; Takahashi, Yamaguchi et al. 2005). Delivery of chemotherapeutics or oncolytic vectors throughout a tumour is a problem for a single injection, and it is likely the reason why many groups reported very promising results in rodents which have not been equalled in human patients is due to the larger size of human brain tumours (Rainov and Kramm 2001). To counter this some groups have employed multiple needle placement to access the whole

of the tumour mass (Qureshi, Bankiewicz et al. 2000) while some employ solvent facilitated perfusion, whereby the drug – for instance a chemotherapeutic such as BCNU – is stereotactically injected in a water-miscible organic solvent, such as ethanol. This solvent can easily travel through aqueous environments inside and between cells and also through the hydrophobic cell membranes, and so travel further through the tumour (Hamstra, Moffat et al. 2005).

A major limitation of this delivery method is the fact that it is a surgical procedure, and as such would likely exclude or at least greatly limit its use for chronic conditions and longer term cancer treatments that require repeated doses of a drug. This is a problem shared by intraocular injections into the eye. Avastin and Lucentis are injected every 2-4 weeks (Rosenfeld, Heier et al. 2006) and formivirsen every week (Perry and Balfour 1999). Each injection carries a risk of infection and other complications including damage to neuronal tissue (Ness, Feltgen et al. 2010), and while the chances may be low for each dose, repeated injections mean that occurrences of these adverse effects will take their toll on the patient population. Added to this is the drain on hospital facilities and the considerable discomfort to patients, many of whom are very elderly, to undergo repeated surgical procedures. Also, as mentioned a major drawback of stereotactic injection of drugs into the brain is that diffusion of the injected substance is limited to only a few millimetres from the site of injection (Rainov and Kramm 2001). This would necessitate too many separate injections to make pan-brain delivery practical. As such, for treatment of the vast majority of conditions of the CNS to be possible the blood-neuronal barriers must be altered or bypassed.

4.1.2 Methods of Traversing the Blood-Brain and Blood-Tumour Barriers

A large number of methods of modulating the BBB and BTB have been attempted, with varying levels of success and clinical potentials. These have included exposure to electromagnetic fields (Nittby, Grafstrom et al. 2008), substances such as Freund's adjuvant (Huber, Witt et al. 2001), histamine, free radicals (Ballabh, Braun et al. 2004), VEGF-A (Argaw, Gurfein et al. 2009) and IFN-γ (Masocha, Rottenberg et al. 2007). However, many of these are damaging, such as free radicals, or exhibit unwanted side effects, for instance uncontrolled barrier leakage. Ca2+ deficiency (Klingler, Kniesel et al. 2000), loss of astrocytes (Willis, Leach et al. 2004), and hypoxia (Koto, Takubo et al. 2007) are among other barrier-weakening factors unlikely to have clinical applications, but which alter the barrier strength in a range of CNS disorders.

Hyperosmotic mannitol involves the infusion into ceratoid artery in the neck of a concentrated solution of the sugar mannitol. This hyperosmotic solution causes shrinkage of the endothelial cells of the BBB or BTB (Balint, Krizbai et al. 2007) and causes β-catenin – a constituent of cadherin which forms adherens junctions – to become phosphorylated and dissociate away from the adherens junction (Farkas, Szatmari et al. 2005). One or both of these events results in a decrease in TER to 100-300 Ωcm^2 within 5mins (Butt, Jones et al. 1990) and paracellular pore-opening of 200nm compared with a normal poor size of 6-7nm (Rapoport 2000), although larger pores must be present also as herpes virus (600 nm) and adenovirus (350 nm) have been reported to be delivered to the brain following hyperosmotic mannitol treatment (Muldoon, Nilaver et al. 1995). This technique has been used clinically to aid the delivery of chemotherapeutics to brain

tumours for over 20 years, with significant increases in patient survival times observed (Neuwelt, Goldman et al. 1991; Gumerlock, Belshe et al. 1992), and has also been used in animal models to deliver drugs such as anti-seizure drugs (Marchi, Betto et al. 2009) and novel anticancer neutron capture therapeutics (Barth, Yang et al. 2002; Hsieh, Chen et al. 2005).

Bradykinin, or rather its more stable artificial counterpart RMP-7, is a 9 amino acid peptide that binds the bradykinin B_2 receptor on endothelial cells and leads to rapid (within 15 mins) BBB permeability as well as its just as rapid reversal, with the barrier returning to normal by 30-60mins after RMP-7 administration (Borlongan and Emerich 2003). RMP-7 has been used in a number of studies where it has been effective in aiding the delivery of drugs to the brain, for instance the delivery of the 477 Da analgesic loperamide (Emerich, Snodgrass et al. 1998). Another drug successfully delivered to brain tissue using RMP-7 was cyclosporin-A (1,202 Da) which on its own can be used in the treatment of animal models of Parkinson's disease and stroke, but only at a high dose which has nephrotoxic and hepatotoxic side effects. In the study low doses ($1/10^{th}$ the normal dose) of cyclosporine-A was delivered to the brains of rats with a model of Parkinson's disease using RMP-7-mediated BBB modulation, and this exerted a neuroprotective effect equivalent to the regular dose (Borlongan, Emerich et al. 2002). This method was also used to increase delivery of the chemotherapeutic carboplatin to rat gliomas and the tissue surrounding them (Elliott, Hayward et al. 1996), however in human phase II trials this approach, while having a positive trend, did not result in significant increases in patient survival (Prados, Schold et al. 2003).

One final strategy, employed by van Helden et al., is the inhibition of the P-glycoprotein efflux pump using a drug called tariquidar. This enables drugs such as oximes – which are antidotes to nerve agents but are substrates for the P-glycoprotein transporter– to persist in brain tissue and have an effect without being effluxed back across the BBB. In this study tariquidar and oximes protected rats from seizures and convulsions caused by the nerve agent soman (Joosen, van der Schans et al. 2011). Inhibition of efflux pumps is an interesting approach, and appears to be quite effective, however it is limited to transport of a specific and narrow pool of drugs. Despite these limitations there is potential for a combinatorial approach between efflux pump inhibitors together with improved methods of delivery across the BTB.

While many of these approaches have exhibited some success, an alternative approach being pursued here is the suppression of the BBB and BTB TJ protein CL5 in order to mediate increase paracellular transport of molecules into, or out of, healthy and tumourous brain tissue brain. In this section I present the work to date in a project to deliver chemotherapeutic agents to a murine model of glioblastoma multiforme (GBM).

4.2.3 Chapter Aims

In this course of this chapter I aimed to choose a cell line and succesfully establish a mouse model of glioblastoma multiforme by direct stereotactical inoculation into the brain. Following this I aimed to use the jetPEI-delivered CL5 siRNA method described in Chapter 3 to modulate the BTB and surrounding intact BBB to enable a low-molecular weight compound, of a similar size to currently used chemotherapeutics, increased access

to the tumour and surrounding tumour periphery. Lastly, the chemotherapeutics doxorubicine and temozolomide would be systemically delivered following BTB and BBB modulation with CL5 siRNA. This would function as a small pilot study to investigate whether the improved access to low-molecular weight compounds increase survival times.

4.3 Results

4.3.1 Growth Curves of IPSB18 and bGBM Cells

To compare the tumour formation potential of two available brain tumour cell types, IPSB18 and bGBM cells, growth curves were set up. This was carried out by seeding eight T-25 cell culture flasks with 80,000 cells (3,200 cells/cm^2) in 5ml of media each on day 0 and left to grow at 37°C and 5% CO_2. Cell numbers were then counted each day for eight days (*Figure 4.2*).

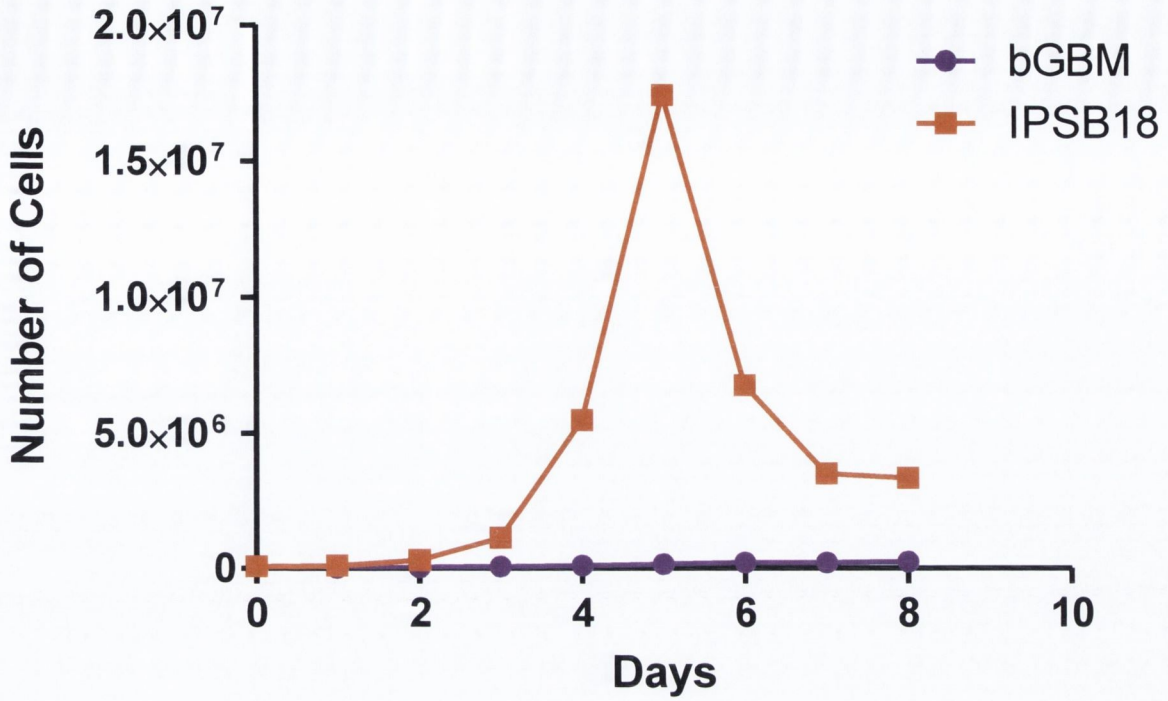

Figure 4.2: Growth curves of bGBM and IPSB18 cells. *Graph illustrates the growth of bGBM (blue) and IPSB18 (red) cells over 8 days following seeding at a density of 3,200 cells/cm^2. The cell density for IPSB18 cells rapidly reached a peak of 696,000 cells/cm^2 on day 5 and then rapidly fell back to a plateau of approximately 140,000 cells/cm^2. bGBM cells on the other hand initially dipped in number, falling to 1,160 cells/cm^2 on day 2, before climbing steadily to reach a peak of 9,800 cells/cm^2 on day 8. (bGBM and IPSB cells were seeded at p=16 and p=17 respectively; no media change was undertaken.)*

bGBM cells, after a slow start, increased by 50-100% each day – a rate which would be an impressive growth rate under normal circumstances but which paled in comparison to the IPSB cells. The latter grew at an extremely aggressive rate, more than tripling each day at peak growth, before cell numbers decreased again after day five (*Figure 4.2*).

4.3.2 Imaging of IPSB and bGBM Brain Tumours

The far more aggressive growth of IPSB18 cells in vitro did not necessarily mean that they were the better candidate for the generation of tumours in vivo, as their impressive growth rate might not have been reflective of their ability to grow in the brain. Alternatively, it was possible that IPSB18 cells would grow too fast in vivo, and would necessitate the ending of animals' lives before useful data could be acquired. As such, following growth assessment a small number of nude (Foxn1) mice were inoculated with IPSB18 or bGBM cells.

Tumours were inoculated in the brains of nude mice by stereotactic injection of 60,000 IPSB18 cells at a point 2.5 mm right and 0.5 mm rostral from bregma, and 2 mm deep. Tumours were clearly visible in MRI as soon as day 5 following injection. Tumours then grew to a considerable size over the following eleven days, taking up much of the hemisphere into which they were implanted (*Figure 4.3*). The condition of the animal necessitated euthanasia at day 21.

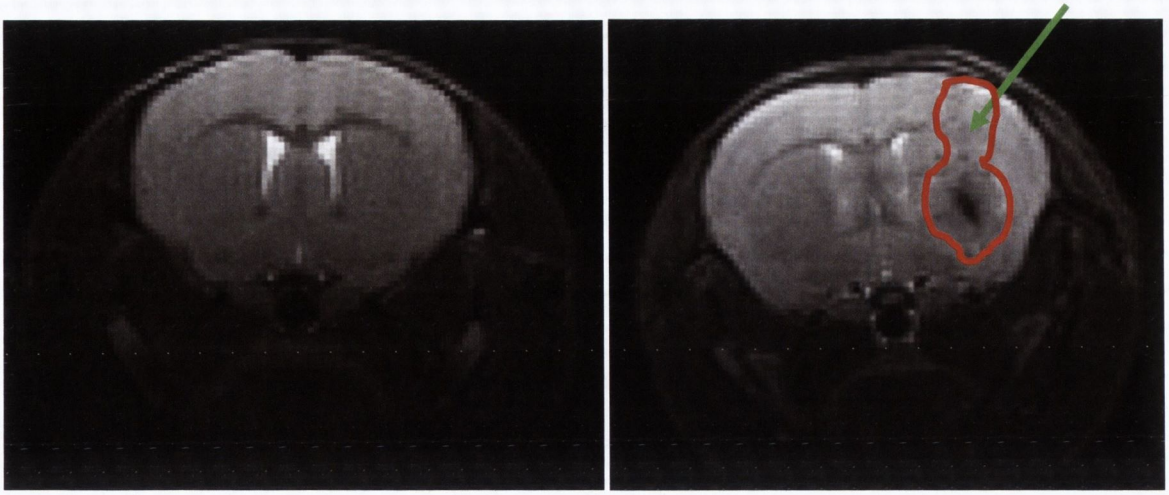

Figure 4.3: T_2-weighted image of an IPSB18 tumour in comparison with a control brain.

The tumour (outlined in red) is positioned in the right hemisphere of a nude mouse brain (right panel). The tumour is identifiable by the site of injection (black), with mottled high and low intensity signal expanding out from this point of tumour inoculation. Also visible is the disruption of the line formed by the lateral ventricle (green arrow) when compared to the controlateral hemisphere. In comparison the control brain (left panel) demonstrates symmetrical hemispheres without the mottled pattern of contrasting. Image was taken 16 days following inoculation with 60,000 IPSB cells. Image representative of 12 tumours scanned originating from this cell type.

In this T_2-weighted, high resolution imagine observed in *Figure 4.3* the tumour appears as a mottled area of increased and decreased signal, with a large area of decreased contrasting at the site of injection of the cells. Markedly decreased signalling such as this is often indicative of either pooled blood as a result of the injection, or of cell death at the centre of the tumour. At this point both options were possible, and neither was expected to impact the study.

Next a T_1-weighted contrast-enhance MRI scan was carried out on each animal, during which the contrast agent Gd-DTPA was injected via canulation of the tail vein (*Figure 4.4*).

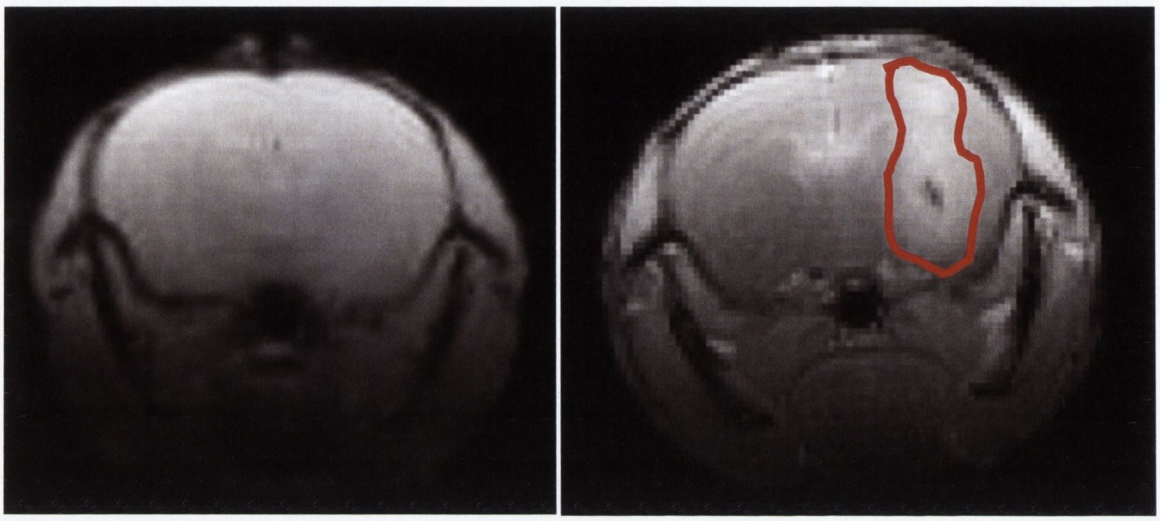

Figure 4.4: T_1-weighted contrast-enhanced MRI image of an IPSB18 tumour. *Caudal brain slice of a control mouse (left panel), and a brain 16 days following inoculation with 60,000 IPSB cells (right panel). Gd-DTPA is observed in the right hemisphere of a nude mouse. This contrasting appears as high intensity, white colouring (within red shape). Image on right representative of 12 tumours scanned originating from this cell-type.*

The contrasting observed here under MRI (*Figure 4.4*) is due to the relative permeability of the BTB in areas of reduced CL5 expression. This indicates the presence of a tumour of considerable size following IPSB18 cell inoculation.

Having observed the lower growth rate in bGBM cells compared with IPSB18 cells in vitro (*Figure 4.1*), it was hypothesised that they would likely develop slower in vivo also. As in the case of IPSB18-injected mice, bGBM animals were scanned by MRI 16 days following stereotactic tumour cell injection (*Figure 4.5*).

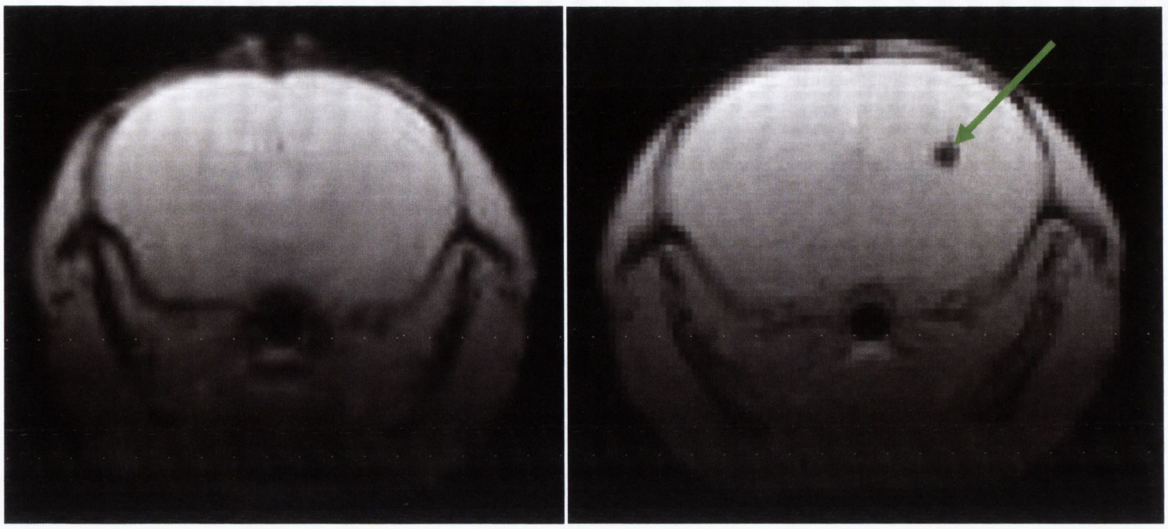

Figure 4.5: T_1-weighted contrast-enhanced MRI image of a bGBM tumour. *Shown is a caudal brain section of a control mouse brain (left panel), and a brain into which 60,000 bGBM tumour cells were injected into the right hemisphere 16 days previously (right panel). No Gd-DTPA contrasting is observed, all that remains is the site of injection, appearing as black hypocontrasting (green arrow). Image on right representative of 6 tumours scanned originating from this cell-type.*

As can be seen in the T_1-weighted scan above (*Figure 4.5*) there is a marked difference from the IPSB18 tumour scan at the same timepoint (*Figure 4.4*). There is no Gd-DTPA contrasting visible in the bGBM scan, indicating impermeability of the BBB to the molecule and therefore the lack of a BTB. This is a strong sign that bGBM cell inoculation failed to result in tumour growth, or at least of a tumour of sufficient size to be clearly visible under MRI. One alternative is that a tumour of bGBM cell-origin did grow but which had a BTB of sufficient strength to exclude GD-DTPA. If this were the case the lack of permeability to Gd-DTPA would be a sign of a lack of glioblastoma characteristics.

4.3.3 Cell Death in IPSB18 Tumours

Next sectioning was carried out in order to determine the origin of the area of extreme hypocontrasting at the centre of the IPSB18 tumours (*Figures 4.2* and *4.3*). As mentioned, necrotic cell death and bleeding were hypothesised as being two possible origins for this signal. Sections were made of brains that had been stereotactically injected with 60,000 IPSB cells 8 and 16 days previously. No obvious haemorrhaging was visible in sections through the tumours, and necrosis has been reported previously in many brain tumours and does appear as a dark area in MRI (Seidel, Dorner et al. 2011), so sections were TUNEL stained to assay for cell death (*Figure 4.6*).

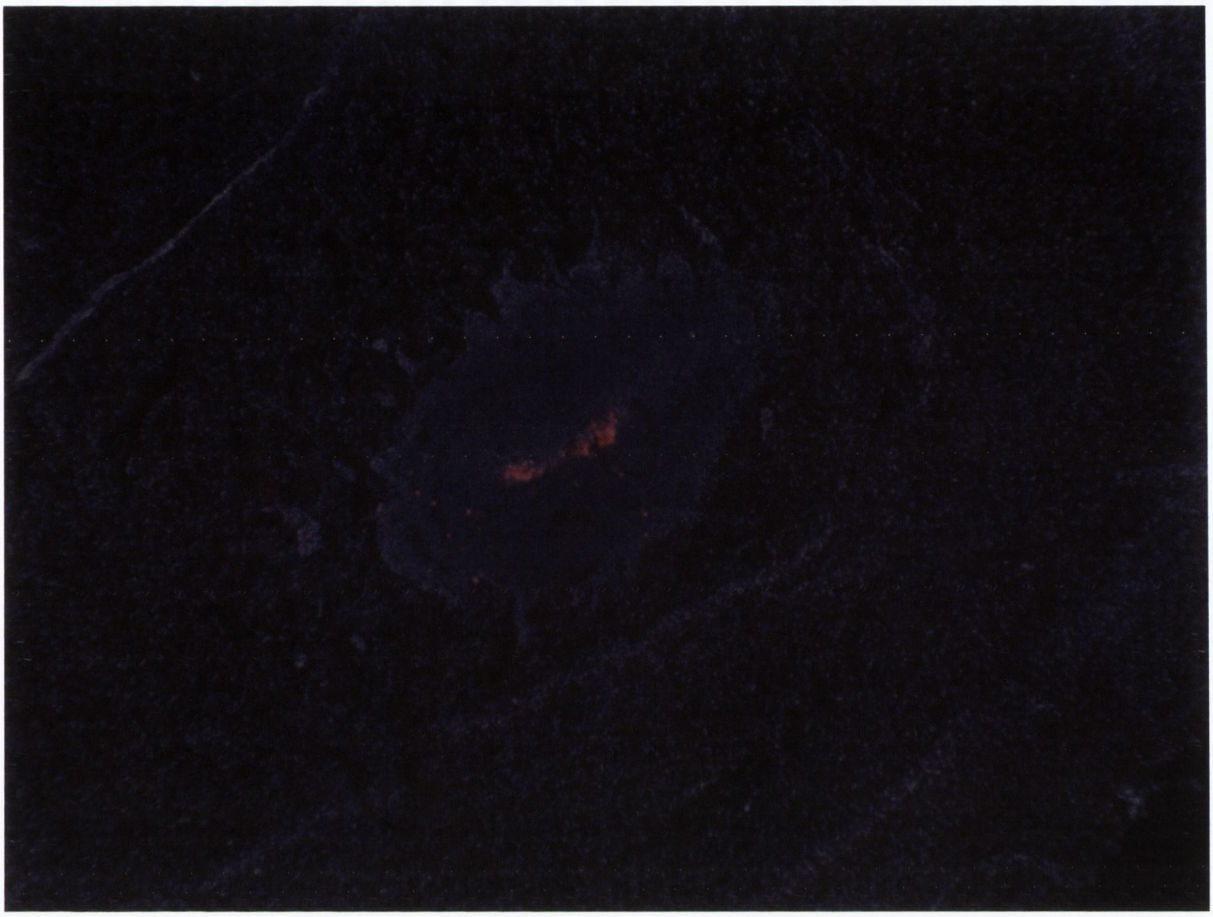

Figure 4.6: TUNEL staining of day 8 tumour. *DAPI (blue) and TUNEL (red) staining of tumorous growth 8 days after inoculation with IPSB cells.*

As seen in *Figure 4.6* clear TUNEL-positive staining occurs at the centre of this tumour, indicating significant central, and to a lesser extent scattered, cell death.

Figure 4.7: TUNEL staining of day 16 tumour. *DAPI (blue) and TUNEL (red) staining of tumorous growth 16 days after inoculation with IPSB cells.*

By 16 days post-tumour inoculation cell death at the centre of the tumour mass is once again clearly visible by TUNEL staining, only this time to a far greater degree (*Figure 4.7*). These findings support the hypothesis that cell death was responsible for the significant areas of decreased signalling in MR imaging of IPSB18 tumours (*Figures 4.2* and *4.3*), although TUNEL staining shown in *Figure 4.6* and *Figure 4.7* were only carried out in single animals at the timepoints shown, in order to obtain qualitative images.

4.3.4 Improved Permeability of Brain Tumour Region

Once the IPSB brain tumour model was established with confidence, experiments were undertaken to test the hypothesis that CL5 siRNA would improve tumour permeability to Gd-DTPA. This would provide the first step in a proof-of-principal exercise to demonstrate that pre-treatment with CL5 siRNA could improve low-molecular weight compound, particularly chemotherapeutic, delivery to a greater portion of the tumour mass, including the leading edge where growth occurs and where the BTB is still quite impermeable.

The tumour mass was observed to be permeable to the Gd-DTPA tracer prior to CL5 siRNA delivery (*Figure 4.8*, centre left, bottom left pseudocolour). 48 h after CL5 siRNA-injection scans were repeated and this time Gd-DTPA was observed to permeate a far larger area surrounding the central mass of the tumour into the peri-tumoural border region (*Figure 4.8*, centre right, bottom right pseudocolour).

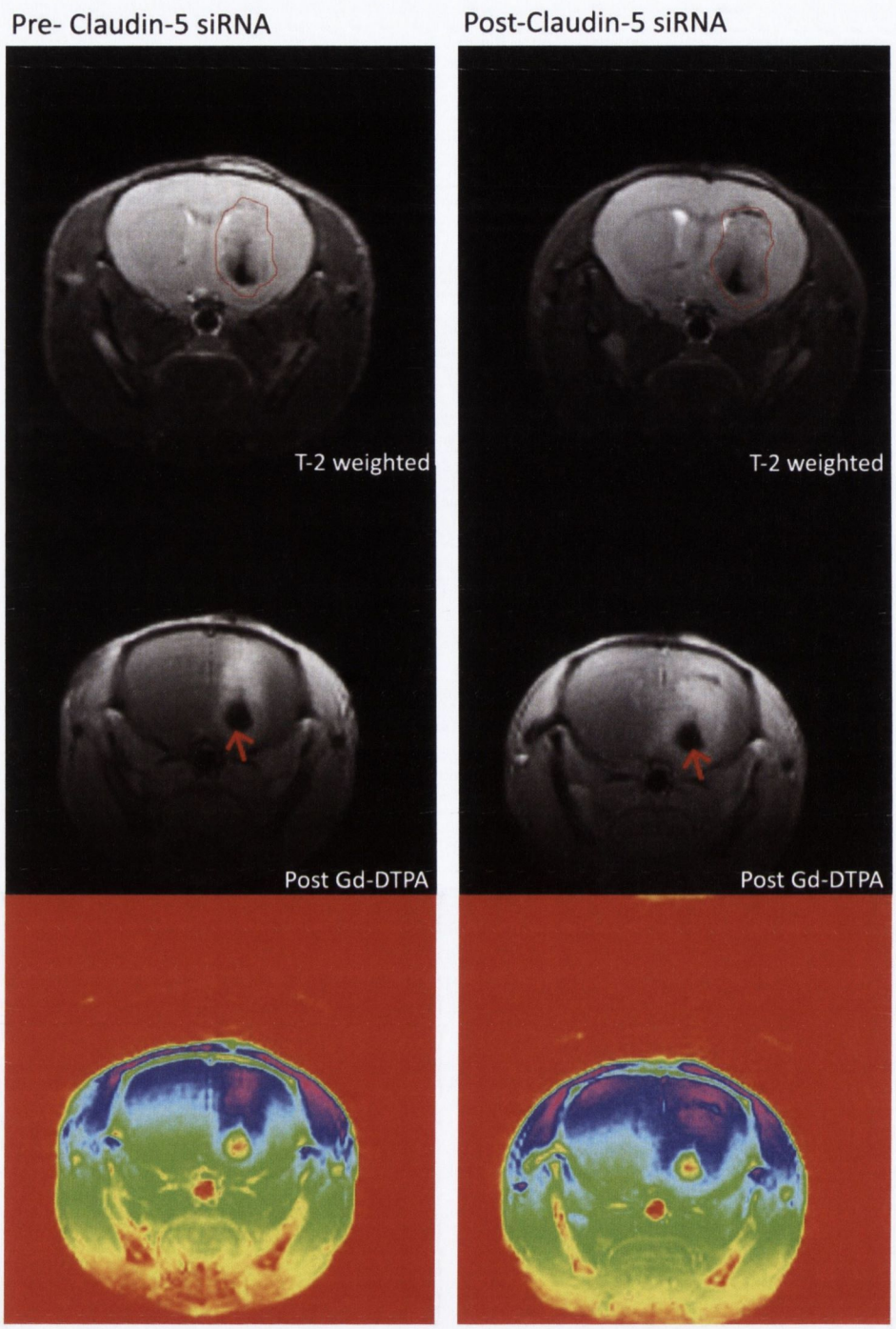

Figure 4.8: Improved delivery of Gd-DTPA to tumour region. *Top: high-res T-2 weighted images without tracer molecule with the tumour visible in the right hemisphere (red outline). Images on right are take 48 h after CL5 siRNA systemic delivery via the tail vein. Central: T-1 weighted scan following Gd-DTPA administration. Arrows point to the necrotic tumour core. Bottom: Pseudocolour image of post-Gd-DTPA scan.*

While 2 days had passed since the previous scan new tumour growth is highly unlikely to account for the scale of the increase in extravasation, particularly as the size of the tumour on the high-res scan is not noticeably larger after the 48 h (*Figure 4.8*, top right vs left).

Following the demonstration of enhanced low-molecular weight compound delivery to brain tumours by means of CL5 suppression, it was decided to carry out a pilot study on the administration of the chemotherapeutic doxorubicin in conjunction with CL5 siRNA. For this study 11 nude mice were inoculated with 100,000 IPSB18 cells, and were then administered CL5 siRNA on day 5 and 100 mg/kg doxorubicin on each of days 5-8. Tumours were then visualised on day 11 by means of T_2-weighted MRI, and volumes were measured blind to treatment group (*Figure 4.9*).

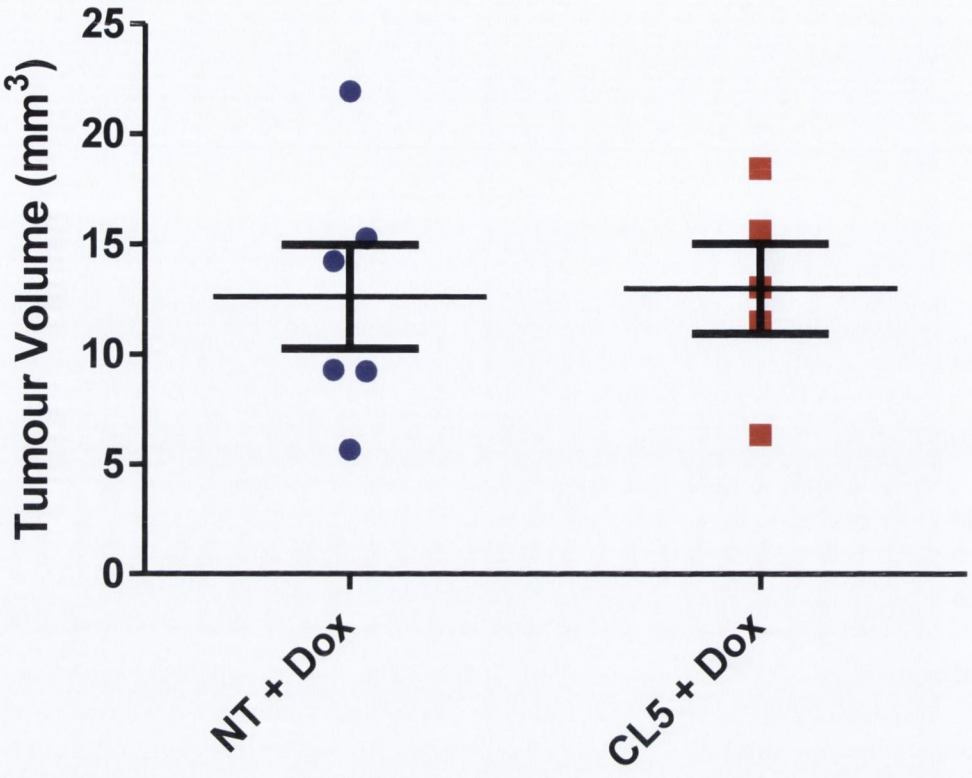

Figure 4.9: Volume of IPSB18 tumours following siRNA and doxorubicin. *CL5 or NT siRNA was delivered systemically via the tail-vein on day 5, with doxorubicin (100mg/kg) being administered via intraperitoneal injection on days 5, 6, 7, and 8. Volumes of tumours were measured by visible extent in T_2-weighted MRI on day 11. (NT + Dox, n=6; CL5 + Dox, n=5)*

As can be observed in *Figure 4.9* there was no significant difference in the volumes of IPSB18 tumours following an intensive course of chemotherapy with BBB modulation.

As mentioned in the introduction to Chapter 3, experiments demonstrating the effectiveness of NT siRNA as a control for CL5 siRNA have been previously published by this lab. These include no observed differences between uninjected, PBS-injected, and NT siRNA injected animals in terms of CL5 expression, or in movement of low-molecular weight compounds into the brain (Campbell, Kiang et al. 2008; Campbell, Nguyen et al.

2009). This data also included microarray data showing that gene expression effects of NT siRNA on the mouse brain are minimal, if present at all (Campbell, Nguyen et al. 2009). Together it was believed that this data provided enough justification to reduce the use of animals and time, and to use only NT siRNA as a control for CL5 siRNA in these experiments.

4.3.5 Treatment of GBM270 Tumours

At this stage in the project a collaboration was established with a research team in Duke University, North Carolina headed by Dr. Gerald Grant, to work on the enhanced delivery of chemotherapeutics to brain tumours by means of CL5 suppression. This group had an established model of human 270 glioblastoma cells derived from an adult patient at Duke University Hospital and passaged in the mouse flank only. These cells grew consistently in the brain, and resulted in animal death after about 21 days when untreated. Similar to the improved Gd-DTPA delivery observed in IPSB18 cells (*Figure 4.8*), Gd-DTPA permeated a far wider area of the tumour when administered systemically 48 h following CL5 siRNA injection (*Figure 4.10*).

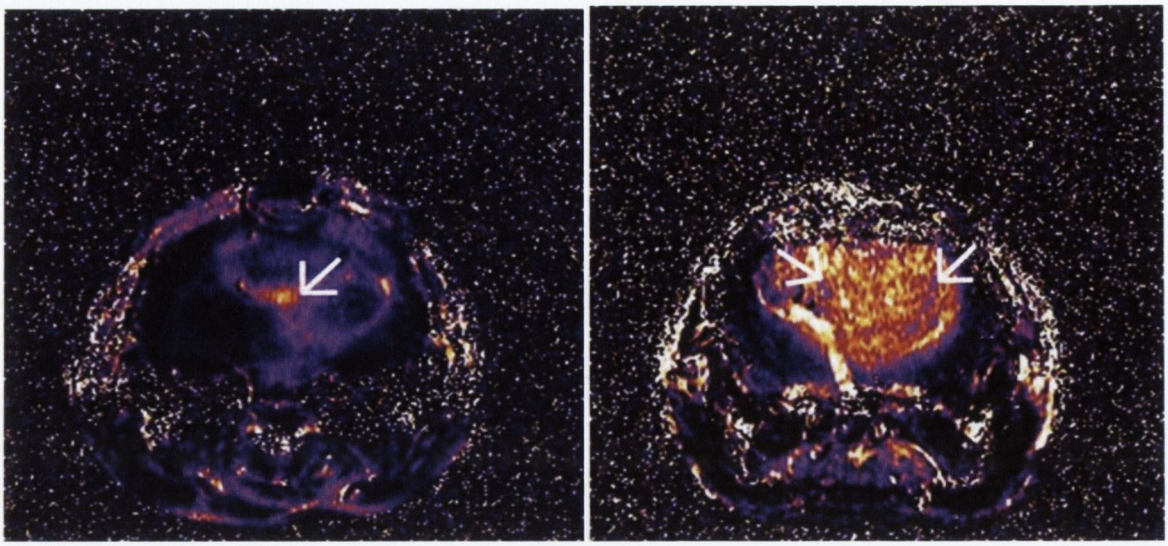

Figure 4.10: Improved delivery profile in a GBM270 tumour using CL5 siRNA. *Left: Pseudocolour MRI of Gd-DTPA permeation in a tumour generated using GBM270 cells in the brain of a mouse in the absence of CL5 siRNA. Right: Gd-DTPA permeating into a far greater extent of the tumour 48 h following systemic CL5 siRNA administration. Reproduced with permission of Dr. Gerald Grant, Duke University.*

With these GBM270 cells having been consistently used with confidence by our collaborators in Duke University for some time, it was decided to begin using this cell line also.

Glioblastoma were inoculated stereotactically with 600,000 GBM270 cells – a higher cell number being used to better ensure tumour establishment. Animals were administered with 20 µg NT or CL5 siRNA on day 3, 7, 11, 15 and 19 via the tail vein, and 48 h after each of these siRNA injections 6 mg/kg doxorubicin diluted in PBS was intraperitoneally injected. After the last doxorubicin injection on day 21 the mice were left until they died due to the tumour or euthanasia was necessary due to signs of discomfort (arching of

back, lack of movement, weight loss, low body temperature). Illustrated in *Figure 4.11* is the comparative size of a GBM270 tumour removed from an animal that died due to its growth.

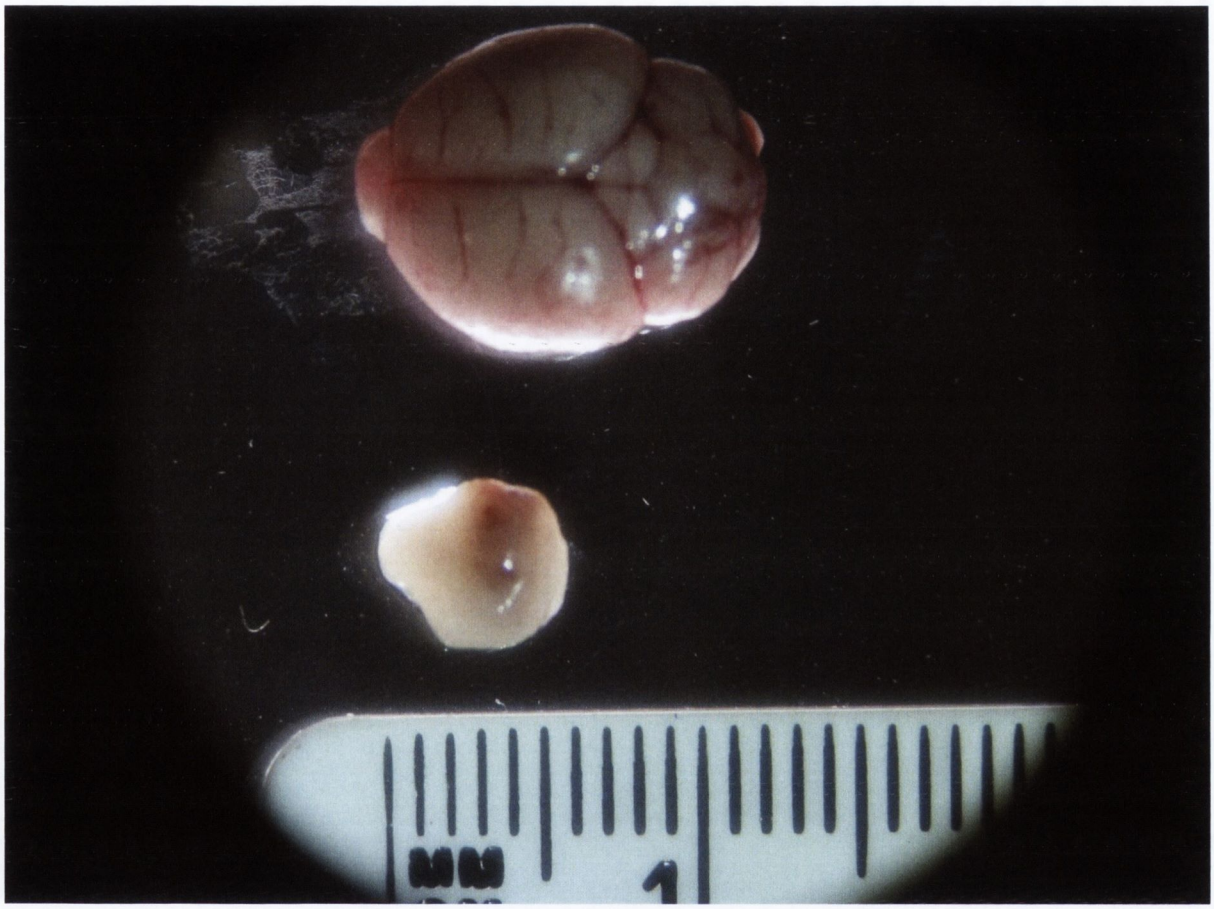

Figure 4.11: GBM270-derived tumour size at death. *Tumour was excised from the brain upon animal death due to the tumour. Normal Foxn1 brain is positioned above for scale.*

As can be seen, the size of these end stage tumours is significant (*Figure 4.11*), taking up nearly a quarter of the volume of the entire mouse brain.

The weights of tumours were found to be rather uniform at the point of death, regardless of when the animal passed away (*Figure 4.12*).

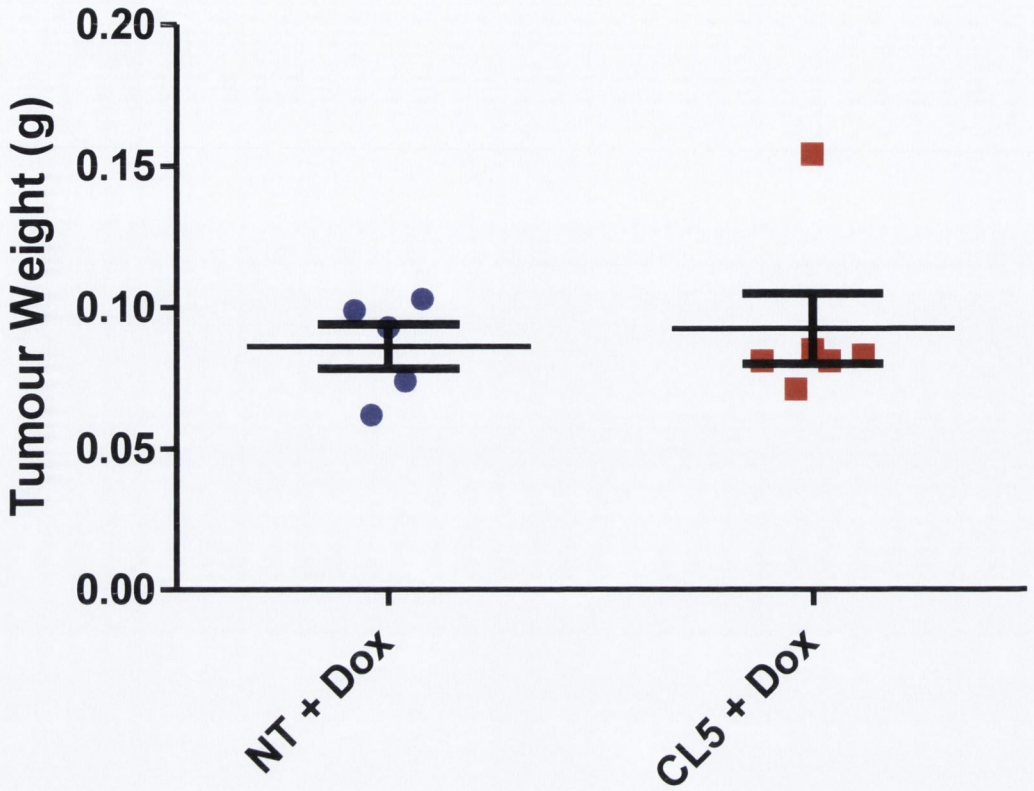

Figure 4.12: Weight of GBM270 tumours upon animal death. *Tumours from animals treated with NT or CL5 siRNA and doxorubicin were excised and weighed as soon as animal was discovered to have died or was euthanized. (NT + Dox, n=5; CL5 + Dox, n=6)*

This indicates that the mice tend to die when their tumours reach a particular size – approximately just under 0.1 g (*Figure 4.12*) – pointing to tumour size being the likely primary cause of death. This is to be expected as the growing glioblastoma exert pressure on surrounding healthy brain tissue in proportion to their size, causing haemorrhages and interfering with normal brain function.

The length of survival of each animal given doxorubicin and CL5 or NT siRNA was recorded (*Figure 4.13*).

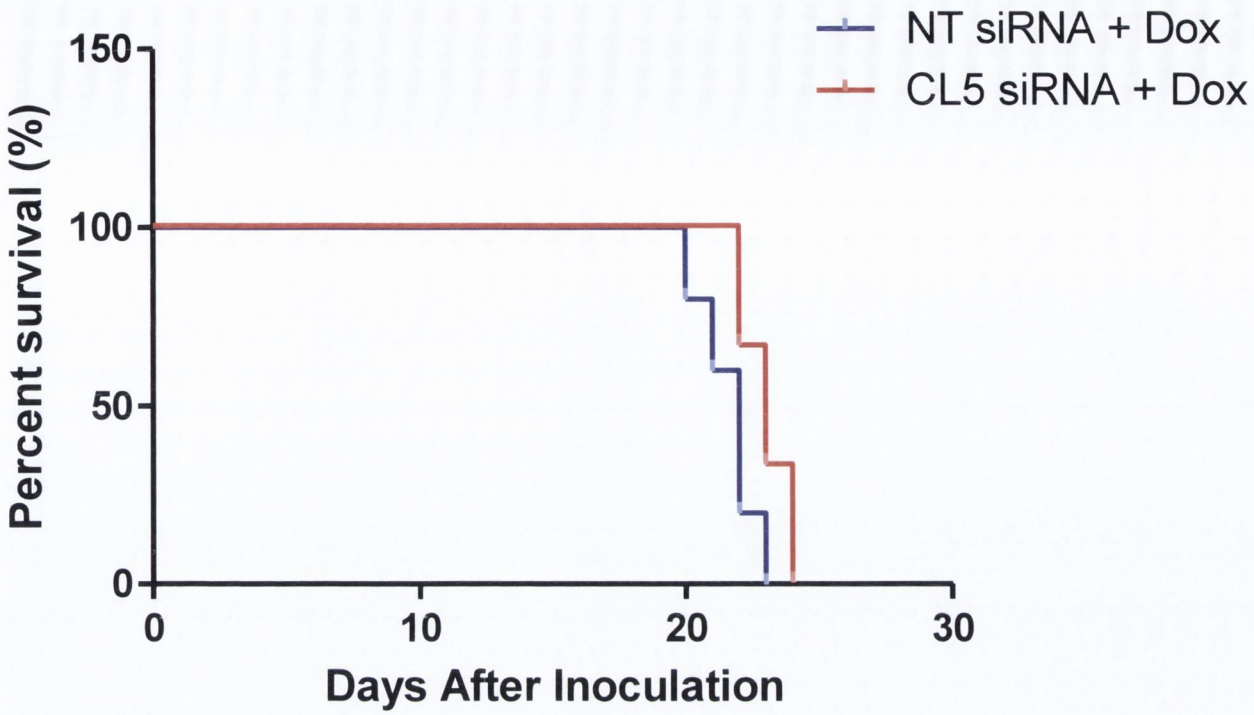

Figure 4.13: Survival of GBM270-inoculated mice following siRNA and doxorubicin.

Median survival: NT, 22 days; CL5, 23 days. Statistical analysis of survival curve fell short of significance by a very slight margin, with the Log-rank (Mantel-Cox) Test resulting in a p-value of 0.0509. (NT n=5, CL5 n=6)

While the median survival increased by only one day, it can be seen in Figure 4.13 that this was not due to a single animal holding out for a day longer, but instead both the onset of animal deaths as well as the end of the survival course were later in the BBB-modulated animals. The observed p-value of 0.0509 is a strong indication that the addition of CL5 siRNA to a doxorubicin treatment regimen increased survival length of animals with glioblastoma.

Survival experiments were repeated once more using GBM270 cells, with tumours being inoculated using 60,000 cells. As well as supplying a different number of cells to inoculate

the tumour, two different chemotherapeutics were used – doxorubicin and temozolomide (195 Da), both of which are used in the clinic to treat glioblastoma. Both drugs were used at a dose of 6 mg/kg. The dosing regimen was altered to a single dose of NT or CL5 siRNA on day 5 after tumour inoculation and chemotherapeutic for 5 days running from day 5-9. The survival course of this experiment is shown in *Figure 4.14*.

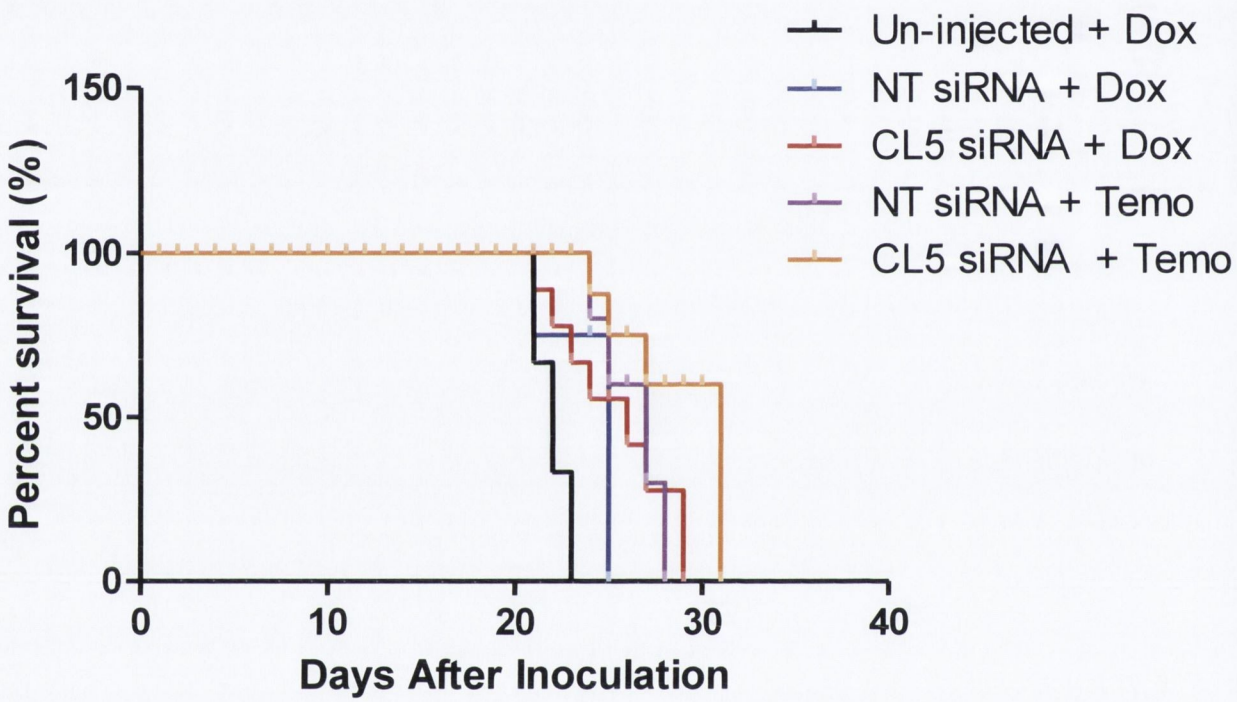

Figure 4.14: Survival of GBM270-inoculated Foxn1 mice with siRNA and single-dose chemotherapy. *Median survival: Un-injected + Dox, 23 days; NT siRNA + Dox, 25 days; CL5 siRNA + Dox, 28 days; NT siRNA + Temo, 29 days; CL5 + Temo, 31 days. (Un-injected + Dox, n=3; NT siRNA + Dox, n=5; CL5 siRNA + Dox, n=7; NT siRNA + Temo, n=4; CL5 + Temo, n=4)*

As can be seen in *Figure 4.14*, medium survival is extended from the baseline set by untreated control animals in all combinations of chemotherapeutic and siRNA. NT siRNA with doxorubicine provides the least benefit, while NT siRNA in conjunction with

temozolomide is the second least effective treatment in terms of latest survival among the cohorts. CL5 siRNA with doxorubicine was observed to increase median survival over NT siRNA with doxorubicine. Finally, CL5 siRNA together with temozolomide provided the longest median survival in this limited, low animal number study.

4.3 Discussion

Initially a number of cell lines were assessed for their suitability to generate a GBM. Two cells types were compared. The first was a primary isolation of cells from a GBM in a patient at Beaumont Hospital, Dublin. This cell line shall be referred to as Beaumont GBM, or bGBM. The second cell type was the anaplastic human astrocytoma cell line IPSB18.

IPSB18 cells were first isolated in King's College Hospital, London, from a patient with a grade III malignant astrocytoma (Knott, Edwards et al. 1990). Despite being of glioma, rather than glioblastoma, origin, IPSB18 cells have been reported to have a very high growth rate (Knott, Edwards et al. 1990), and have been used in a number of in vitro studies in recent years on tumour signalling (Van Meter, Broaddus et al. 2004) and chemotherapeutic efficacy (Rooprai, Kyriazis et al. 2007; Higgins and Pilkington 2010; Kinsella, Clynes et al. 2011).

These two brain tumour cell types – bGBM and IPSB18 – were assessed in vitro and in vivo for their tumourgenic potential, and in order to conduct a proof-of-principal study on the efficacy of chemotherapeutic delivery in conjunction with BBB modulation mediated by suppression of CL5 using siRNA.

IPSB18 far outstripped bGBM cells in their performance in the in vitro growth curve (*Figure 4.2*). IPSB18 cells did however undergo a crash in cell numbers following day 5 of the 8 day-long growth curve, losing over half their viable cell density between day 5 and 6. This fall was most likely due to depletion of the media's nutrients, or a build up of toxic by-products of metabolism, a hypothesis which was supported by the observation of large amounts of cell debris in IPSB18 flasks towards the end of the growth curve experiment.

Nude mice, used in this study as the mouse strain into which tumours were inoculated, are so called due to a mutation in the transcription factor Foxn1(nu), which results in hair follicles that are structurally weak and often break off at the surface (Mecklenburg, Paus et al. 2004). This results in largely hairless, thus nude, animals. Another effect of the lack of functioning Foxn1 transcription factor, however, is a failure to differentiate and grow thymic epithelial cells, which in turn results in a failure to develop and select T-cells (Ma, Wang et al. 2012). As far back as the 1970s it was recognised that nude mice – due to their lack of T-cells – would not reject foreign, transplanted tissue, such as skin grafts (Krueger, Manning et al. 1975). This has resulted in the animal's use as a model for the growth of tumours of human origin. Human tumour cells, such as from biopsy or established cell line, can be taken and transplanted into a nude mouse, resulting in a growing human tumour.

Due to its leaky barrier Gd-DTPA permeates the majority of the tumour, which is clearly visible in the right hemisphere under MRI (*Figure 4.4*). It is likely, however, that there are areas on the peripheral, leading edge of the tumour which are not visible in *Figure 4.4*. Here leaky angiogenic vessels may not yet have grown and barrier strength could be maintained. These areas of the tumour could effectively be invisible to MRI scanning and

this is one reason why brain tumours can be so challenging to surgically resect completely.

In this image (*Figure 4.4*) Gd-DTPA extravasation into the brain is indicated by increased pixel intensity, however it is worth noting that in the experimental demonstration of increased permeability to Gd-DTPA following CL5 siRNA in the previous chapter it was marked by decreased pixel intensity. This can be explained by the unintuitive relationship between Gd-DTPA concentration and signal intensity that has been reported previously. It was observed that Gd-DTPA demonstrated a positive relationship between concentration and signal intensity at lower concentrations, however once the concentration of the contrasting agent passed a certain point signal intensity would then decrease with increase concentration (Shahbazi-Gahrouei, Williams et al. 2001).

There was a noticeable region of bleeding or necrosis at the point of the stereotactic injection (*Figure 4.3*, *Figure 4.4* and *Figure 4.5*), however this is likely to be caused by the injection itself. One alternative to this is that initial growth of a tumour of bGBM origin terminated after a number of days followed by necrosis or apoptosis of the tumour. This would likely leave an area of low signal intensity such as was observed in these day 16 scans. One further possibility that should be recognised is that bGBM tumours did form, perhaps slowly, but that the BTB of these cell masses was sufficiently strong to prevent Gd-DTPA traversal. In this case bGBM tumours could potentially not be clearly visible on MRI, particularly if small.

A number of weeks later these bGBM animals were still alive and appeared healthy while the IPSB animals had all died or were euthanized by 4 weeks following stereotactic injection of cells. This meant that the growth of IPSB tumours could be qualitatively assessed by visible mass volume in MRI, and by survival time of the animals. Neither of

these criteria could be met by bGBM cell-injected animals. For these reasons IPSB cells were selected to develop the human GBM model in nude mice.

TUNEL staining, used to assess the central region of IPSB18 cell-derived tumours, is normally used to label cells specifically undergoing apoptosis, where DNA is cut in many places to expose 3' termini. These termini are the element detected and labelled by the terminal deoxynucleotidyl transferase active in the TUNEL assay. Large scale DNA damage of the kind that occurs during necrosis may also be detectable by TUNEL stain (Grasl-Kraupp, Ruttkay-Nedecky et al. 1995), and both necrosis and apoptosis have been reported to occur in tumours. One group describes a 300-400 μm zone of central cell death, with apoptosis mainly occurring following necrosis, and being situated on the outskirts of the central necrotic region (Bell, Whittle et al. 2001). Necrosis in glioblastoma has been hypothesised to be caused by the observed accumulation of extracellular glutamate which leads to AKT pathway activation resulting in nutrient overconsumption (Noch and Khalili 2009).

Whichever form of cell death that these central tumour cells underwent they were readily detected by TUNEL staining in large numbers at the core of the IPSB18 tumours at day 8 and day 16 following tumour inoculation (*Figure 4.6* and *Figure 4.7*). This provided support to cell death at the centre of the tumour as being the cause of the observed low MRI signal intensity in this region (*Figure 4.3* and *Figure 4.4*). This cell death could be due to this being the site of injection, with the force applied while injecting causing cells to die. Alternatively the observed cell death could be a result of increased pressure at the centre of the tumour due to unchecked cell proliferation, a lack of adequate blood supply

to the tumour core, toxic cell product accumulation, nutrient depletion, or by a combination of these factors.

With doxorubicin having a similar molecular weight to Gd-DTPA (544 Da vs 742 Da respectively) it was hoped that improved peri-tumoural permeation to the contrasting agent would reflect a greater access for the chemotherapeutic to the tumour. The observed increase in the area of Gd-DTPA contrasting in the tumour (*Figure 4.8*) represents a qualitative demonstration of the potential of CL5 siRNA to aid in chemotherapeutic delivery in the expanding tumour periphery. In this region the BTB is more intact and various agents including doxorubicin have been reported to be excluded, despite their permeation into the central tumour mass (Lockman, Mittapalli et al. 2010).

There was a relatively short duration of IPSB18 tumour growth, of approximately 3 weeks, before animals' conditions became terminal. Because of this the mice in this study were receiving a very high dose of doxorubicin, at 100 mg/kg, with the hypothesis being that this provided the best chance to obtain an indication of successful retardation of growth. However the mice in this experiment rapidly lost weight and grew weak. In fact shortly following the MRI scans the experiment had to be abandoned and the animals euthanized due to concerns about their condition. No significant difference in tumour volume was observed by T_2-weighted MRI (*Figure 4.9*), and due to doxorubicin toxicity the survival length of these treated animals could not be measured.

Despite the lack of results demonstrating effective treatment of IPSB tumours the experiment had been successful in establishing a protocol for inoculating a glioblastoma-like tumour, as well as providing data supporting the hypothesis of an increased region of

chemotherapeutic delivery by suppression of CL5 in the leading edge of the tumour (*Figure 4.8*).

Following the successful establishment of protocols and proof of principal, the cell type being used was changed to GBM270 cells acquired from our collaborators in Duke University, North Carolina. These cells had the advantage over IPSB18 cells of not having being passed in vitro for large amounts of time, with passage having been carried out in the mouse flank only. IPSB18 cells, despite their aggressive growth (*Figure 4.2*) and successful recapitulation of a brain tumour with the leaky vessels of a characteristic BTB (*Figure 4.4*), these cells were originally isolated from a grade III malignant astrocytoma (Knott, Edwards et al. 1990), rather than a grade IV glioblastoma as was the aim of this study. For these reasons, as well as their more recent isolation from a patient, GBM270 cells would likely result in an improved tumour phenotype, closer to that of endogenous glioblastomas.

Data from the team in Duke University illustrated an improved zone of Gd-DTPA extravasation in GBM270-cell tumours (*Figure 4.10*), similar to that observed in the experiments using IPSB18 cells (*Figure 4.4*). GBM270 cells were inoculated into nude mice and tumours grew successfully. These animals were given repeated doses of NT or CL5 siRNA every 4 days, and 48 h after each tail vein siRNA injection 6 mg/kg doxorubicin was injected intraperitoneally. This reduced dose of doxorubicin was chosen to enable animals to reach end stage of tumour progression so that it could be evaluated whether treatment was increasing survival length. This dose has also been used a number of times in the past (Rahman, Carmichael et al. 1986; Hong, Huang et al. 1999; Anders, Adamo et al. 2013).

As can be seen in *Figure 4.11* the tumours formed by GBM270 cells grew to occupy a large portion of the mouse brain. The tumour mass is simple to identify within the brain of the deceased animal, recognisable by its solid, dense texture, its slightly different colour, and by the presence of multiple haemorrhages on its surface. These haemorrhages are likely due to leaky, angiogenic vessel growth, or by pressure exerted by the tumour on surrounding tissue. The compact, dense character of these tumours is such that they can be lifted out from the rest of the brain with a pair of tweezers without any cutting.

In the subsequent survival plot of these animals there was a small increase in survival times of mice given CL5 siRNA in conjunction with 6 mg/kg doxorubicin, in comparison with those given NT siRNA (*Figure 4.13*). The observed median survival increase of 1 day in mice, where the entire time course is three weeks, could have the potential to increase survival in humans by weeks at least. Another interesting point is that with the average tumour weight being nearly identical in the two groups of animals (*Figure 4.12*), despite the slightly extended survival, would indicate that the enhanced doxorubicin delivery was retarding the growth of the tumour, rather than extending survival by a different mechanism. However, as mentioned this survival course failed to attain significance, despite being close ($p=0.0509$). Therefore further demonstration of increased survival would certainly be necessary before there could be confidence that CL5 siRNA was resulting in improved chemotherapeutic delivery and increased survival lengths in this model.

The team that was collaborated with on this project from Duke University reported to us success in establishing tumours using as few as 10,000 GBM270 cells. It was hypothesised

that using a lower number of cells in further survival studies might enable more time for the tumour to end the animal's life, and that this extension of baseline survival could enable CL5 treatment to have a greater effect. Therefore when the survival timecourse was repeated using GBM270 cells 60,000 cells were used, rather than 600,000 for the previous survival experiment.

A single, early delivery of doxorubicin or temozolomide was used in order to strongly target tumours when they are smaller in size and likely to have a stronger BTB. A stronger barrier should improve the observed difference between NT and CL5 treatments, and effective delivery of chemotherapy at an early stage of tumour development is likely to have a greater effect on delaying its growth. As well as this, restricting chemotherapy to early after inoculation will limit the amount of interference with animals at later stages when they are becoming weak, and will reduce chemotherapy toxicity effects at these later, more vulnerable timepoints.

Chemotherapy was given for 5 days starting on the day of siRNA injection, and the reason for this – rather than a single dose at the 48 h timepoint – was that as demonstrated previously in *Figure 3.2,* CL5 suppression is not isolated to a single dip 2 days after injection, but instead involves a number of days of suppressed mRNA levels. This was supported by MRI data indicating Gd-DTPA extravasation into the brain parenchyma at 24 and 72 h post CL5 siRNA injection, although to a lesser extent than that observed at 48 h (*Figure 3.8*). Maintaining a constant level of chemotherapeutic in the body during this period would have the effect of maximising the total quantity of chemotherapeutic available to cross the modulated BTB and BBB. It is also the case, even with CL5 suppression, that the periphery of the body acts as a major sink for systemically delivered drugs targeting the CNS. So it was hypothesised that already having chemotherapeutic in

non-CNS portions of the body at the time of maximal CL5 suppression would lessen this drug-sink effect.

Treatment of this mouse model of glioblastoma with doxorubicine in combination with barrier modulation gave indications of an increase in median survival in two separate experiments, however neither of these survival courses reached statistical significance (*Figure 4.13* and *Figure 4.14*). Temozolomide also gave indications of increased median survival, and to a greater extent than that observed for doxorubicine (*Figure 4.14*), although the lack of statistical significance and low animal numbers, as well as the lack of a temozolomide control lacking any siRNA at all means that this finding is less dependable again.

4.4 Future Directions

The experiments presented in this chapter provide a small pilot study on chemotherapeutic delivery in glioblastoma. Glioblastomas were successfully reconstituted and imaged using two different cell types, and their permeability to low molecular weight compounds appeared to be increased following suppression of CL5siRNA. The slight improvement in median survival times of animals given chemotherapy combined with BBB modulation is promising, but falls short of convincing evidence for the application of CL5 siRNA to enable improved chemotherapeutic delivery to glioblastomas.

Moving on from here focus should be on demonstrating that increased levels of chemotherapeutic drugs reach reconstituted glioblastomas. This could be done by using

techniques such as mass spectrometry or HPLC to quantify increases in the concentration of drugs such as doxorubicine or temozolomide, as in (Rousselle, Clair et al. 2000). Alternatively, doxorubicine is autofluorescent (Mohan and Rapoport 2010), so alternatively this could be used to measure increased delivery to the tumour site. These experiments would have the advantage of directly demonstrating chemotherapeutic delivery to glioblastoma following CL5 suppression, rather than relying on indirect evidence of Gd-DTPA extravasation into tumours. While Gd-DTPA is of a similar size to doxorubicine there are mechanisms other than BBB strength that could mean that doxorubicine might still be excluded, such as drug efflux transporters (Schinkel and Jonker 2003).

Another approach that could be taken would be to establish a stably-expressing glioblastoma cell line that would express a GFP vector under the control of a doxycycline-inducible promoter. These vectors are available in the Humphries lab. With these cells a glioblastoma model could be established that would be GFP-positive where reached by doxycycline, which is a similar molecular weight to Gd-DTPA and doxorubicine. This model would enable direct visualisation of the amount of tumour reached by low-molecular compounds following NT or CL5 siRNA-administration and systemic doxycycline delivery. The number of tumour cells reached could also be quantified by FACS-sorting. Systemic delivery of doxycycline in conjunction with a chemotherapeutic agent would make it possible to quantify by FACS the number of surviving tumour cells following sacrifice at pre-determined time-points.

Experiments such as these suggested would provide an increased body of evidence that the glioblastomas are being reached by the systemically delivered chemotherapeutics. This would mean that if animals are not showing increased survival then it is an issue of

timing and dosage of chemotherapeutics, or of over-aggressivity of the tumours not giving time for amelioration, or of another mechanism whereby improved delivery is not directly resulting in increased survival.

Chapter 5: Relief of Oedema in a Model of TBI

5.1 Abstract

Water build-up in the brain following cases of TBI result in swelling of the affected region and a consequent increase in ICP. This rise in pressure is one of the major causes of disability and morbidity following TBI, and treatments are generally limited to hyperosmotic mannitol infusion and craniectomy. Modulation of the BBB has thus far been used by this lab to enable compounds to enter the brain where they otherwise wouldn't. The aim of this chapter was to apply the technique of BBB modulation by means of CL5 suppression to instead enable fluid to move out of the brain in a modal of oedema, and by this to attempt to improve outcome following TBI. To do this a model of cold-induced TBI was established in which brain water content was readily observed and quantified. CL5 siRNA was systemically delivered following administration of these TBIs, and changes in water content in the injured region was observed to decrease. This decrease in oedema coincided with an increase in opening of the BBB to low-molecular weight compounds at the periphery of the site of injury, and improved blood-flow. Finally, motor and behavioural outcome – as measured by neurological severity score and T-maze - were observed to significantly improve in mice treated with CL5 siRNA following TBI.

5.2 Introduction

5.2.1 Pathology of Traumatic Brain Injury

Early effects of TBI that occur as a direct result of the impact/force include leaky ion channels, membrane microporation, conformational changes in proteins and shearing of blood vessels causing haemorrhage (Maas, Stocchetti et al. 2008). Secondary effects begin within minutes or hours and include mitochondrial and subsequent energy production impairment, immune cell infiltration and activation, cytokine release, apoptosis, and oedema formation (Maas, Stocchetti et al. 2008; Clausen, Hanell et al. 2011). As discussed earlier one of these secondary effects, oedema formation, results in swelling of the brain which increases pressure throughout the cranium, particularly at sites proximal to the injury.

Despite BBB opening appearing to be an important cause of vasogenic oedema in early and central oedema following TBI, later oedema and oedema in the periphery of the injury are caused by another form of oedema (Kawamata, Katayama et al. 2000). These findings are largely based on MRI measurements of the apparent diffusion coefficient (ADC) of brain tissue, which when raised indicates the occurrence of vasogenic oedema. This was observed to increase in animal models in the first 60 mins after injury together with brain water content, however at this point ADC values began to fall once more whereas brain water content continued to rise during the first 24 h (Barzo, Marmarou et al. 1997), indicating that another form of oedema had taken over. A similar result is seen

in human patients, where low ADC values are reported in regions of high water content (Marmarou, Signoretti et al. 2006).

Vasogenic oedema occurs early following TBI primarily at the central core of the injury, where significant numbers of blood vessels are broken and red blood cells and plasma proteins can be observed leaking into the site of injury. This central region can also be enhanced by Gd-DTPA in MRI, indicating opening of the BBB (Katayama and Kawamata 2003). Another form of brain oedema, osmotic oedema is similar to vasogenic oedema in that fluid enters the brain from the blood vessels, but rather than large-scale, region-specific breakdown of the BBB oedema is driven by high osmolality within the contused, necrotic core of the TBI. Here osmolality was observed to increase from 311.4 mOsm to 402.8 mOsm at 12 h post-injury, matched by a significant increase in water content. Findings in this study that brain cooling decreased osmolality increases in injured tissue while decapitation did not, indicate that the observed increase in osmotic gradient and water movement was due to metabolism and not blood-flow (Kawamata, Mori et al. 2007).

The type of oedema that predominates after the early stage is cytotoxic oedema, and is marked by intracellular fluid accumulation and cell swelling. This cellular water uptake is driven by ion dysfunction, resulting in hyperosmotic cytoplasm and an osmotic gradient across the cell membrane, and which correlates with increased ICP (Stiefel, Tomita et al. 2005). One of the potential causes of this ionic dysfunction is glutamate uptake. As mentioned previously, early stage TBI pathology is marked by high extracellular glutamate concentrations, and despite decreased glutamate transporter expression (Goodrich, Kabakov et al. 2013) glutamate uptake into cells in the injured region still continues and

this uptake requires the co-transport of three Na^+ ions for each molecule of glutamate. This transport can occur despite strong ionic gradients, resulting in water being drawn into the cell by osmosis (Zerangue and Kavanaugh 1996). To illustrate this glutamate-mediated cell swelling, a cell size increase of 10% was reported 2 h after addition of glutamate addition to glial cells in vitro (Staub, Peters et al. 1997). This swelling by osmosis is likely compounded by the previously mentioned increases in Na^+ and Ca^{2+} ion uptake early after TBI (Wolf, Stys et al. 2001; Iwata, Stys et al. 2004). Finally, cellular swelling of brain cells could be caused by lactic acidosis as a result of a decrease in glucose utilisation and a switch to anaerobic lactate utilisation (Timofeev, Nortje et al. 2013). Lactic acidosis producing a pH of 5.0 in vitro led to a cell volume increase of nearly 40% in glial cells (Staub, Peters et al. 1997). A table outlining the main characteristics and differences between the different forms of cerebral oedema observed following TBI is provided (*Table 5.1*).

Type of Oedema	Initiating Factor	Characteristic Features
Vasogenic	Broken blood vessels / damage to BBB	Serum proteins in brain (Matsumoto, Lo et al. 1995; Murakami, Kawase et al. 1998)
Osmotic	Necrotic cell debris	Water movement regardless of blood-flow (Kawamata, Mori et al. 2007)
Cytotoxic	Ion dysfunction; hyperosmotic cytoplasm	Cell swelling (Staub, Peters et al. 1997)

Table 5.1: Origin and distinguishing characteristics of the different forms of oedema observed in TBI.

It is often assumed that the oedema observed following TBI is a result of BBB opening, however a number of studies indicate that this is not necessarily the case. In one study for instance, oedema was measured in high numbers of rats given differing types of TBI and BBB integrity was estimates using the tracers Evans blue and gadolinium-DTPA. In one of the TBI models BBB opening was observed in both hemispheres, however while an increase in water content of 1.5% was observed in the injured hemisphere, the water content of the uninjured hemisphere remained constant at 78.25%. In another TBI model BBB permeability was reversed 4 h after injury whereas oedema increased over 24 h (Beaumont, Marmarou et al. 2000; Beaumont, Fatouros et al. 2006). This demonstrates that BBB permeability is not sufficient to cause oedema, and this is further backed up by the lack of any observable oedema formation in studies by this lab utilising suppression of TJ proteins in the BBB (Campbell, Kiang et al. 2008), and also by studies on the biphasic nature of BBB permeability following TBI. Here it was observed that the first opening of the BBB does correlate with the formation of oedema, however the second opening of the BBB in fact coincides with the decrease in oedema recorded between 48 and 72 h (Baskaya, Rao et al. 1997). It is feasible here in fact that the second opening of the BBB could facilitative to relieving excess water build up in the injured tissue. Also, opening of the BBB by mannitol infusion has been shown to diminish oedema after TBI in rats (Bareyre, Wahl et al. 1997).

A potential further cause of oedema that has emerged in recent years is aquaporin-4 (AQ-4). AQ-4 is expressed on astrocytic end-feet present at the BBB and this protein plays a major part in water transport into and out of the brain and has been implicated in forms

of oedema other than TBI. In brain tumours for instance increased AQ-4 expression was found to correlate with increased peri-tumoural oedema (Dua, Devi et al. 2010). Recently a number of studies were carried out on AQ-4 in models of cerebral ischemia, which results in cerebral oedema. It was found in one study that successful treatment of animals to reduce oedema coincided with a reduction in AQ-4 expression (Hoshi, Yamamoto et al. 2011), and more directly it has been shown that inhibition of AQ-4 significantly reduces oedema as a result of ischemia (Igarashi, Huber et al. 2011). Also, mice lacking the protein altogether experienced a 35% decrease in brain swelling in an acute water intoxication model of cerebral oedema, as well as showing markedly decreased swelling of foot processes on astrocytes surrounding capillaries (Manley, Fujimura et al. 2000)). The oedema caused by cerebral ischemia, however, is largely cytotoxic oedema, and the opposite result was observed with AQ-4 expression and vasogenic oedema, with AQ-4 deletion aggravating the oedema (Papadopoulos and Verkman 2007). With cytotoxic oedema playing the major role in brain swelling in TBI after the early phase, a role for AQ-4 water transport is feasible in TBI. This hypothesis is supported by the finding that in the first 35 mins oedema forms equally in mice with mislocalised AQ-4 and control animals, but later was significantly reduced (Vajda, Pedersen et al. 2002). It has also been reported that administration of anti-AQ-4 antibody after TBI in rats significantly decreased oedema despite no change in BBB permeabilisation (Higashida, Kreipke et al. 2011), as well as similar findings for the role of another aquaporin in TBI oedema, aquaporin-1 (Tran, Kim et al. 2010).

A further factor that could explain the large increase in water uptake in the brain is the observation of increases in nitric oxide concentration in cerebral ischemia (Malinski,

Bailey et al. 1993). In mice lacking nNOS, the enzyme responsible for producing this potent vasodilator in nervous tissue, regions of oedema were found to be smaller in a model of ischemia than in wild-type mice (Huang, Huang et al. 1994; Hara, Huang et al. 1996). Similar to the case of AQ-4, the effect of nitric oxide on oedema is not straight forward, with findings showing an opposite effect to that of nNOS removal for eNOS. When this endothelial-expressed nitric oxide producing enzyme is missing infarct volumes are over 20% larger in the same mouse model of ischemia (Huang, Huang et al. 1996), indicating that endothelial-produced nitric oxide is protective here.

These findings are likely caused by the ability of nitric oxide to alter TJ expression in glomerular endothelial cells in vitro (Bevan, Slater et al. 2011), an effect which is reversible using the NOS inhibitors L-NMMA and L-NAME, and its effect is dependent on VEGF activation and the PI3-kinase/Akt pathway (Mayhan 1999; Handa, Stephen et al. 2008). VEGF activation leads to nitric oxide production by eNOS through phosphorylation on Ser177 of the enzyme (Feliers, Chen et al. 2005), however phosphorylation of some other sites on eNOS result in inhibition of enzyme activity. Thr497 is one of these sites, and interestingly phosphorylated of this residue is sufficient to prevent endothelial permeability (Oubaha and Gratton 2009). These findings, including the previously mentioned data on larger regions of oedema in eNOS knockouts, suggest that increasing endothelial permeability in cases of cerebral oedema could reduce lesion volumes. Considering finally that inhaled nitric oxide has been found to be protective in TBI (Terpolilli, Kim et al. 2013), it was decided to establish a model of TBI oedema and to test the ability of CL5 to improve oedema volume and other outcome measures.

5.2.2 Preclinical Models

For studies on TBI selection of an appropriate model greatly effects the successful acquisition of results, as well as for the clinical relevance of findings. These issues are of critical importance, particularly in the light of the failure of a significant number of clinical trials in the field. One issue is that TBIs themselves are highly heterogeneous, and can be likened to a collection of different conditions all occurring in parallel, with many affecting each other as they progress. This diversity of effects, as well as the many different ways in which a human TBI can be acquired, is reflected in the wide array of different TBI animal models.

Diffuse Axonal Injury

DAI can be modelled on its own in an impact-free model, which involves acceleration of the head in one of three directions – sagittal, oblique or lateral, or a combination of these. In this way the model simulates the damage sustained in non-ejection vehicle accidents where rapid deceleration shakes and rotates the head, or in some assault cases such as shaken baby syndrome. Animals subjected to this model commonly suffer comas, with coma length being proportional to the force of head movement. Lateral head movement was also observed to result in the most severe pathology, indicating that the brain is less pliable under rotational forces along this axis (Gennarelli, Thibault et al. 1982). Factors such as the degree of rotation, rotation speed, and acceleration can all be varied to deliver a broad spectrum of DAI severities. Axonal damage occurs mostly in the absence of vascular disruption (Smith, Chen et al. 1997), resulting in a model where DAI

can be studied in isolation from the wide range of pathological characteristics present in impact models of TBI.

Weight-drop

This model of TBI is performed by allowing an object to fall freely through a guide-tube onto the skull of the anaesthetised animal. The weight of the object and height from which it falls can both be altered to give injuries of different grades, and if desired the incidence of skull fracture can be reduced by gluing a steel disc onto the skull (Marmarou, Fo Da et al. 1994). This latter precaution can be useful as skull fractures can reduce ICP, which is an important aspect of post-TBI pathology. The pathology of this model is broad as one would expect from a non-specific injury such as this, with features such as DAI, brain stem haemorrhage, oedema, limb deficits, respiratory problems, convulsion and death being reported during the development of the technique (Fo Da and Marmarou 1994; Marmarou, Fo Da et al. 1994). This model has enabled the discovery of other pathological features of TBI, such as angiogenesis of permeable blood vessels in the vicinity of the injury, mediated by VEGF production by astrocytes and immune cells (Skold, von Gertten et al. 2005).

Controlled Cortical Impact

CCI produces a similar type of injury to that acquired in weight-drop TBI, but with the CCI insult being administered by striking the dura of the exposed brain using a pneumatic cylinder (Dixon, Clifton et al. 1991). Different regions of the brain can be impacted in this way, producing differing injury pathologies due to the brain regions in the direct vicinity of the impact being the most severely affected. CCI is the most commonly used TBI

model, due in large part to the many pathological features which arise including DAI, BBB disruption, neuroinflammation, and subdural and intraperenchymal hematomas. At later timepoints later pathological features of TBI arise, such as oedema, alterations in CBF, as well as chronic phase inflammation. One of the main advantages of this model of TBI is the multitude of aspects that arise in human TBIs, which are almost by nature extremely heterogeneous, complex injuries.

Fluid-Percussion Injury

In this model rather than impacting the brain or skull being impacted with a solid object, the force is a rapid increase in pressure delivered by means of water or saline. The fluid is injected onto the dura, exposed by craniectomy, in a fully enclosed system by striking the injector with a hammer on a pendulum, which enables alterations of hammer weight, drop height and angle for variable injury strengths. Due to the injection of fluid into the enclosed system ICP rises rapidly, displacing and deforming brain tissue. Because the injury is administered by means of an increase in pressure the brain region which comes in contact with the fluid is not necessarily the most injured region, in fact studies have shown that the brainstem is most vulnerable to the rapid increase in ICP (Thibault, Meaney et al. 1992). Damage does occur elsewhere however, and the fluid injection site does have a significant effect on the level of cell death in various brain regions. For instance rostral application of fluid pressure results in higher cortical than hippocampal cell death, while caudal, medial or lateral fluid injection resulted in the opposite damage profile as well as higher levels of reactive astrocytes (Floyd, Golden et al. 2002). Other

features of fluid-percussion pathology include haemorrhages, oedema, brain atrophy and cavitation, and memory deficits (Dixon, Lighthall et al. 1988; Iwamoto, Yamaki et al. 1997; Floyd, Golden et al. 2002).

Blast Injury

Blast injuries have risen to prominence in recent years due to conflicts around the world, as has the field of research into traumatic brain injuries caused by blasts. As well as the risk of shrapnel causing significant damage to the brain, overpressure waves emanating from an explosion travel through the bodies of individuals nearby applying strong kinetic forces which distort and place high strain onto their brains. Soldiers and civilians who are caught in the vicinity of one or a number of blasts can appear wholly unharmed externally, but can suffer from headaches, concussion, brain swelling, post-traumatic stress disorder, chronic pain and an increased risk of Alzheimer's disease (Rosenfeld, McFarlane et al. 2013; Veitch, Friedl et al. 2013). In fact in one study illustrating the prevalence and long-term mental health impact of TBI in war zones, nearly a third of veterans of the recent Iraq and Afghanistan conflicts surveyed reported suffering more than one type of head injury, and in that group individuals were six-fold as likely to have suffered from -traumatic stress disorder, four-fold as likely to have depression, and twice as likely to experience alcoholism (Maguen, Madden et al. 2012).

To model these injuries in animals by means of a reproducible, repeatable technique the most common method is to use a shock tube – a long, cylindrical tube containing two chambers separated by a membrane. Compressed air or helium is pumped into the first chamber, the compression chamber, until the membrane bursts or until the desired

pressure is met in which case the membrane is burst by a blade within the shock tube. The animal, restrained at the end of the second chamber, the expansion chamber, receives the blast overpressure waves, with the restraint preventing tertiary blast injuries caused by being thrown against objects by the blast wave (Reneer, Hisel et al. 2011). In this model animals can either be exposed to a single blast, or multiple minor blasts, with the intensity of each blast being variable by alteration of the pressure in the compression chamber or distance of the animal from the membrane. Animals exposed to these blasts exhibit neuronal swelling, oxidative stress, immune cell infiltration, caspase-3 cleavage and apoptosis, amyloid precursor protein accumulation, losses of consciousness, haemorrhages on the surface of the brain and within the cortex, and cognitive deficits (Cernak, Wang et al. 2001; Cernak, Wang et al. 2001; Ahlers, Vasserman-Stokes et al. 2012; Tompkins, Tesiram et al. 2013).

Cold-Induced Injury

This is another model of impact-free brain injury, and similar to the model of DAI is designed to more closely study a lower number of pathological factors of TBI. Cold-induced injuries are carried out by holding a liquid nitrogen-cooled metal probe of 3mm diameter against the exposed skull of anaesthetised mice, or other animal, for 30 seconds. This produces a highly reproducible model of vasogenic oedema when blood vessels at the injury site necrose and spill their contents. This region of oedema has low heterogeneity and is clearly demarcated allowing clear quantification by MRI or other methods (Houkin, Abe et al. 1996; Campbell, Hanrahan et al. 2012), which is why it is chosen in many studies aimed at understanding or attempting to reduce cerebral oedema following TBI (Oury, Piantadosi et al. 1993; Murakami, Kondo et al. 1999; Kawai,

Kawanishi et al. 2003; Campbell, Hanrahan et al. 2012). The model does demonstrate other features of TBI however, with widespread cell death in the injured region, significant changes in CBF, marked release of inflammatory cytokines, and motor and memory deficits (Campbell, Hanrahan et al. 2012). One disadvantage of this model is that it does not recapitulate all the features of TBI that occur in humans; however for specific studies such as the one presented here it is highly advantageous.

5.2.3 Claudin-5 Suppression to Relieve Cerebral Oedema

It was decided to apply the BBB-modulating effect of CL5 siRNA observed in Chapter 3 (*Figure 3.8*) and Chapter 4 (*Figure 4.8*) to this selected model of vascular oedema in TBI. Rather than transiently enabling drugs to pass into the brain, it was hypothesised that increased permeability inside and surrounding the TBI would enable increased flow of water out of the brain and back into the blood, as is illustrated in *Figure 5.1*.

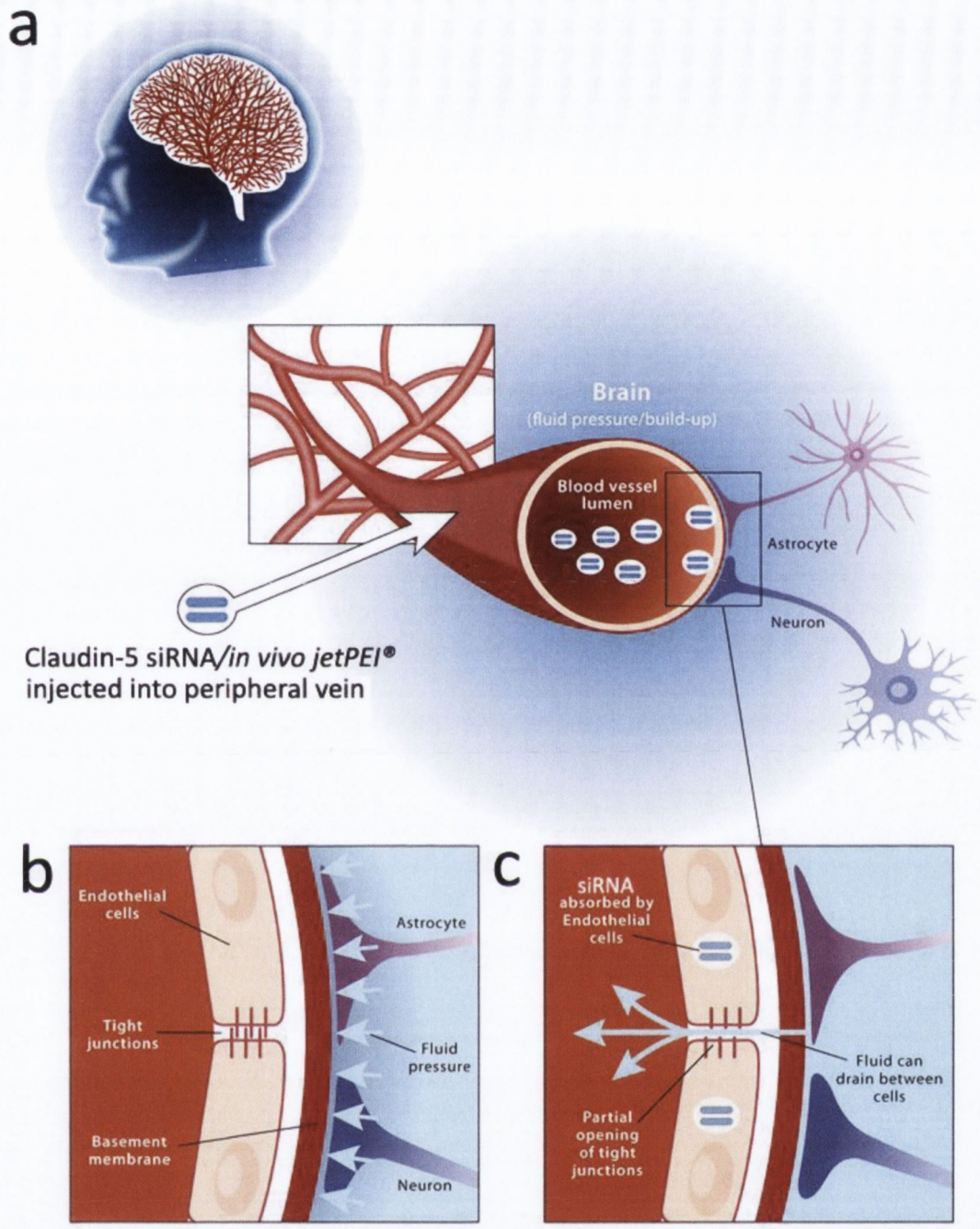

Figure 5.1: Schematic of barrier modulation in cerebral oedema. *a) CL5 siRNA, with PEI delivery agent, reaches the vasculature of the brain following systemic injection. b) Fluid pressure and water build-up associated with vasogenic oedema exerts immense pressure on the surrounding neural environment. c) Suppression of CL5 by means of the CL5 siRNA allows for enhanced movement of water from the extra-neural environment to the vasculature.*

Transient opening of the BBB by mannitol infusion has been shown to diminish oedema after TBI in rats (Bareyre, Wahl et al. 1997), and this treatment is commonly used in humans currently. It was hypothesised that BBB modulation by means of CL5 suppression could be similarly beneficial in cases of TBI by enabling oedema to be relieved via the otherwise blocked paracellular pathway (*Figure 5.1*). It is this approach that we endeavoured to investigate in this chapter.

5.2.4 Chapter Aims

The aim of this chapter was to use the effect of jetPEI-delivered CL5 siRNA to modulate the BBB, as described in Chapter 3, to relieve fluid build up in a model of brain oedema. This is the first time that this lab has used CL5 siRNA to enable the movement of material out of the brain or retina, rather than into it. To do this it was aimed to first establish a model TBI in which oedema could be readily observed, and to establish protocols to measure brain fluid content. Following this it was aimed to use CL5 suppression to enable fluid to move out of the brain by means of MRI and direct brain water content quantification. MRI would also be used to observe changes in BBB integrity around the injured region, in order to show if CL5 suppression was enabling improved access for material to flux across the BBB. be used to To demonstrate improvement by measures other than the extent of TBI oedema it was aimed to use MRI water-labelling to detect blood-flow changes at the site of injury, which would provide evidence of an improvement in access to the injured region. Finally it was investigated if changes in oedema volume coincide with an improvement in motor and behavioural outcome.

5.3 Results

5.3.1 Establishment of a Model of Vasogenic Oedema

In this chapter an impact-free model of TBI was used - cold-induced vasogenic oedema. This approach involves holding a liquid N_2-cooled metal rod against a stereotactically measured point on the skull 2 mm right and 2 mm caudal to bregma for 30 s. This causes rapid accumulation of water at the site of the injury, easily visible on MRI (*Figure 5.2*).

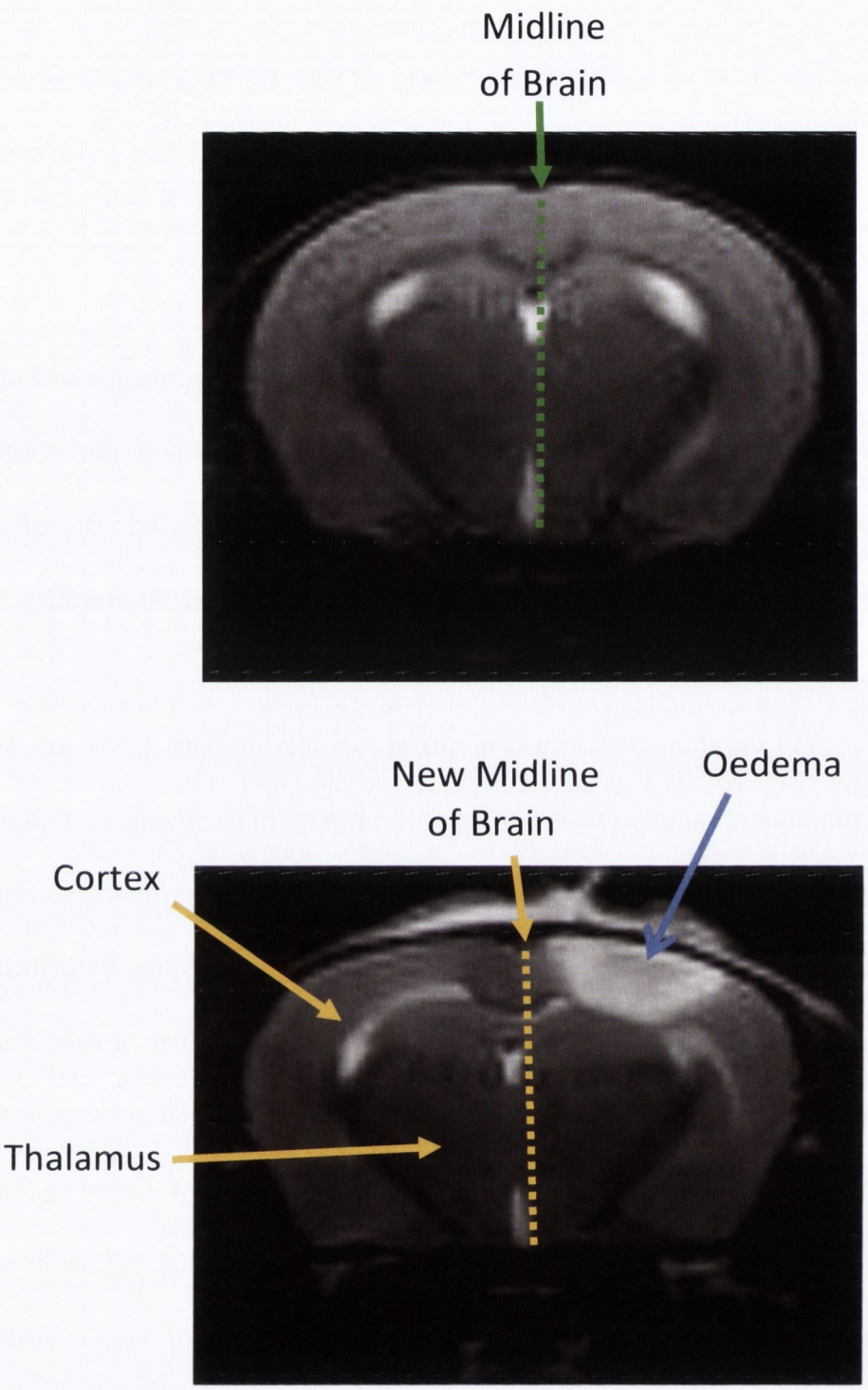

Figure 5.2: MRI image of a cold-induced vasogenic oedema compared with uninjured brain. *High water concentration (blue arrow) manifests in the right hemisphere within the cortex as high intensity signalling on T_2-weighted MRI. The resulting increase in brain volume has shifted the midline of the brain towards the left (orange line). This can be compared with the original midline shown above in an uninjured brain (green line).*

The 'lesion' in these images (*Figure 5.2*) is an area of hyper-intense MRI signal which results from high water content, and therefore shows the area of oedema that coincides with and surrounds the cold-induced injury. This region is clearly observable when compared with the same brain region in an uninjured brain. The oedematous region swells to such an extent that the midline of the brain is shifted away from the injury into the left half of the brain (*Figure 5.2, orange line)* when compared to the midline in an uninjured brain (*Figure 5.2, green line*).

This is not the case in many other models of TBI, and as can been seen in *Figure 5.3* impact models such as CCI produce complex, heterogeneous injuries.

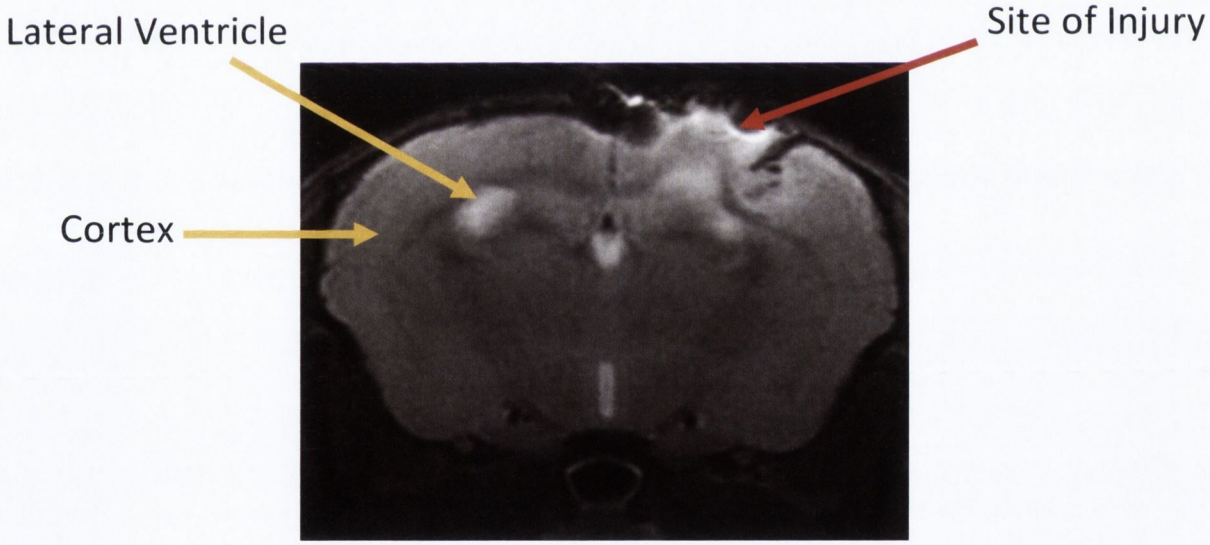

Figure 5.3: T_2-weighted MRI image of an oedema caused by CCI. *High water concentration (high intensity, white) is visible amidst significant tissue disruption in the right hemisphere within the cortex.*

The injury, and particularly the extend and severity of oedema, observed here (*Figure 5.3*) was more difficult to measure and to reproduce with confidence.

The onset of oedema observed in *Figure 5.2* is rapid, within hours of the injury, and the swelling from this vasogenic oedema is accompanied by a midline shift away from the injured hemisphere. The initial injury, as well as secondary damage caused by swelling, results in a region of cell death visible around and beneath the injury site (*Figure 5.4*).

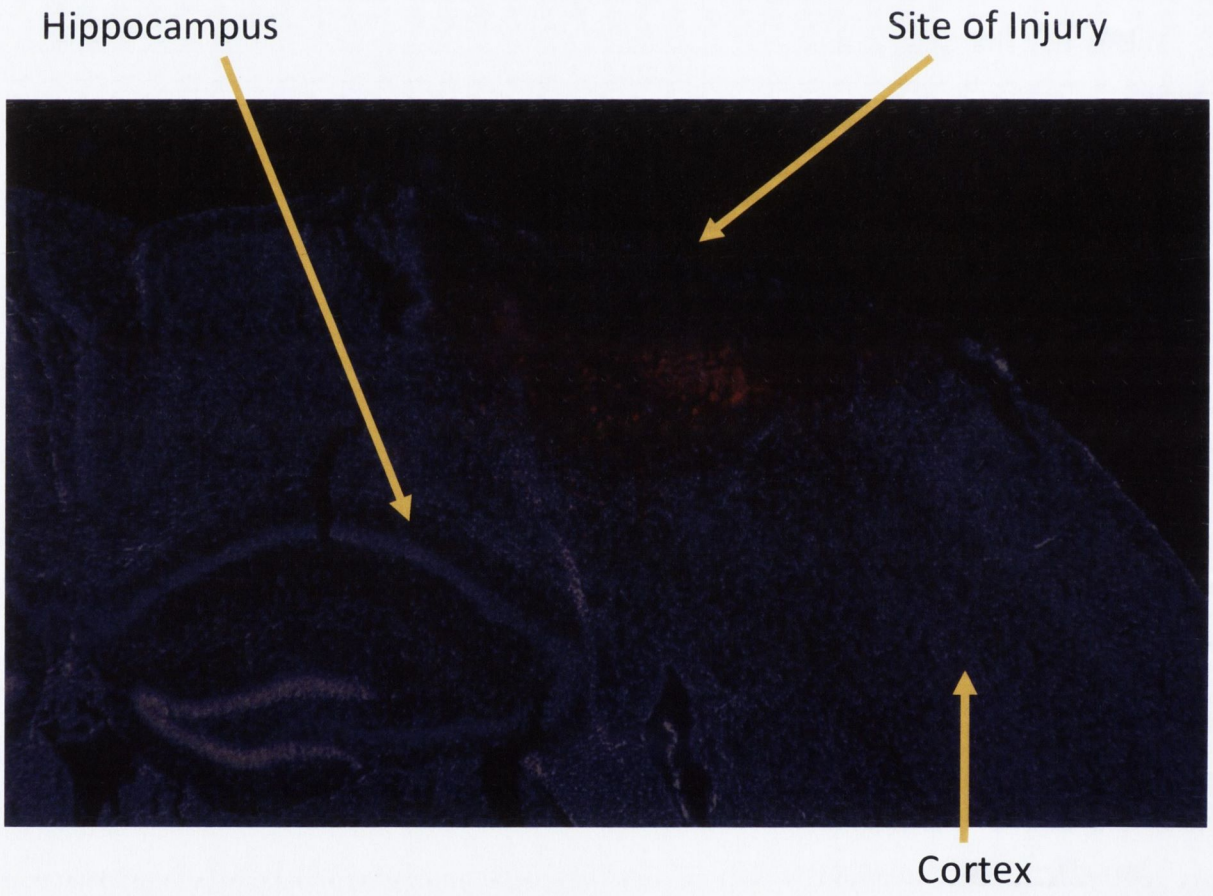

Figure 5.4: Cell death following TBI. *Overlaid TUNEL (red) and DAPI (blue) staining of a cold-induced TBI 24 h after injury. A region of TUNEL$^+$ cells is clearly visible directly beneath the site of injury where the cooled probe was held against the skull. This region extends downward to the outer extent of the hippocampus.*

It can clearly be seen that 1 day following cold-induced TBI a large region of cell death, as detected by TUNEL staining, has formed directly under the site of injury (*Figure 5.4*). The extent of this zone of cell death extends to the edge of the hippocampus.

Accompanying this cell death is a loss of tissue integrity, with many blood vessels in the region rupturing, spilling their contents and no longer providing circulation through the injured region. This is observable in *Figure 5.5* where TBI-affected animals have been injected intraperitoneally with 45 mg/kg Evans blue. After 3hrs animals were perfused with 20ml PBS, resulting in clearance of Evans blue from all areas with functioning circulation.

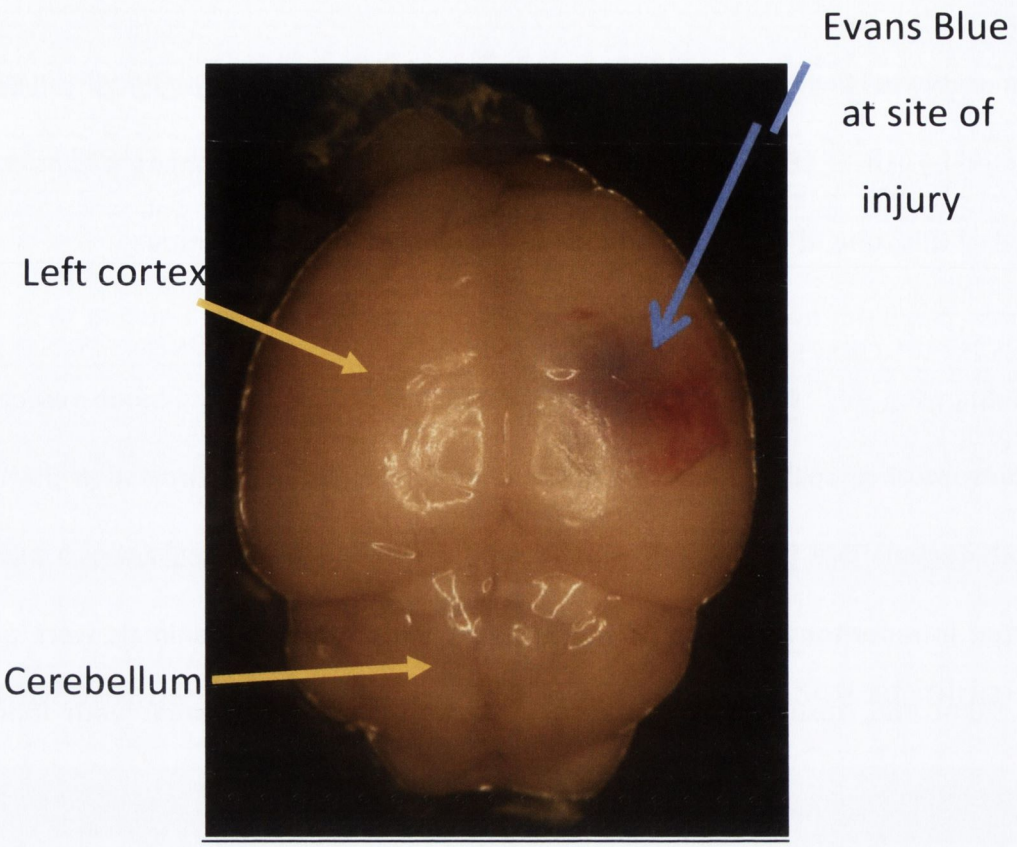

Figure 5.5: Mouse brain following successful perfusion of an Evans blue-injected animal with a TBI. *Evans blue is observed at the site of injury on the right cortex (blue arrow), as well as some surface haemorrhaging. The rest of the brain is clear, free from observable blood vessels or Evans blue. This figure is representative of 5 animals that were systemically injected with Evans blue following TBI.*

Figure 5.5 illustrates that blood vessels in the injured region have burst and terminate here following TBI. This allows Evans blue to accumulate at the injury site but fail to be cleared by circulating PBS.

Much of the central injured area in *Figure 5.4* is ablated when the TBI is first acquired, and this loss is unlikely to be preventable. However the area that can hypothetically be saved is the penumbral region just under the initially ablated region, around the top of

the hippocampus. This region is lost later, around 48-72 h following injury and is believed to be lost due to secondary damage caused largely by oedema. The hypothesis was that modulation of the BBB by means of CL5-suppression could enable the fluid that builds up due to vasogenic oedema to be relieved back into the circulatory system, thus relieving pressure on surrounding tissue and potentially reducing this secondary tissue loss.

5.3.2 Measurement of TBI Oedema Reduction

To measure this hypothesised reduction in water build-up in TBI high-resolution T_2-weighted scans were carried out over a range of timepoints on wild-type, gender matched, three month old C57 mice that had been administered TBIs. Representative pseudocolour scans of a NT and a CL5-siRNA administered animal are shown in *Figure 5.6*.

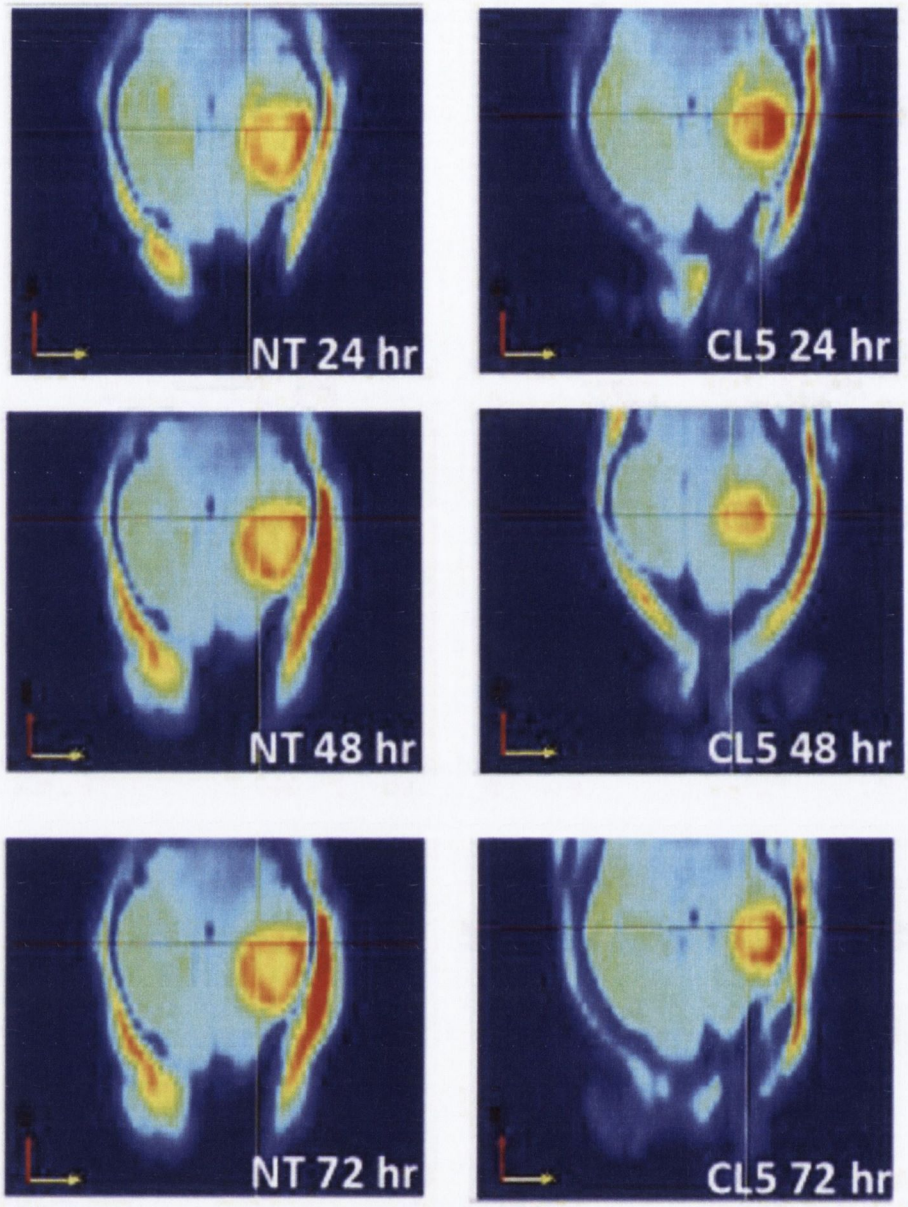

Figure 5.6: Shrinkage of TBI oedema following CL5 siRNA. *Pseudocolour T_2-weighted images of TBI oedematous regions 24 and 72 h. The extent of oedema in the animal given NT siRNA (left column) does not reduce to the same extent as those give CL5 siRNA. siRNA was injected systemically via tail vein injection within 2 h of TBI administration.*

The CL5 siRNA-administered animal in *Figure 5.6* does appear to show a noticeably reduced oedematous lesion, particularly at the 48 and 72 h timepoint. However choosing

representative images such as these is problematic as there are questions such as which horizontal brain sections to choose. As such the three-dimensional volumes of these lesions across 24, 48 and 72 h were measured using MIPAV software and the quantification of these in 20 animals is shown in *Figure 5.7*.

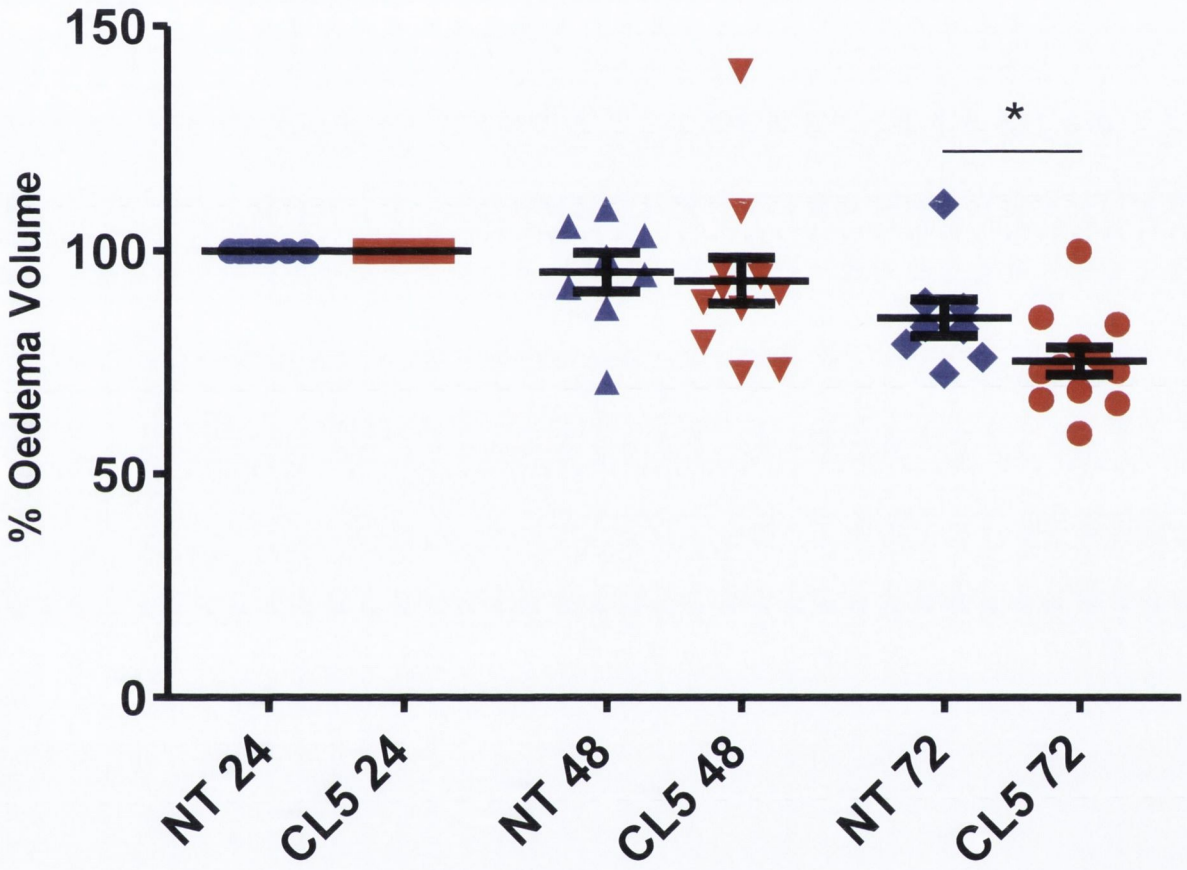

Figure 5.7: Quantification of TBI lesion shrinkage between 24 and 72 h. *Volumetric analyses of oedematous regions were carried out from T_2-weighted MRI images using an automatic MIPAV tool, while being blind to the treatment groups. Volumes at 24 h were set to 100%, with later timepoints being compared to this first timepoint. (*P≤0.05, Student's t-test. CL5, n=12; NT, n=8. Data are mean ± s.e.m.)*

As is observed in *Figure 5.7*, a significant decrease in TBI lesion volume is observed between 24 and 72 h in mice given CL5 siRNA after the injury but not in those given NT siRNA. There was no significant difference observed in the raw volume figures at 24 h so it is not the case that CL5 siRNA-treated animals were worse at the 24 h timepoint and simply improved from there.

For this and other figures measuring TBI oedema volume baseline volumes were set for each animal at 24 h, and in this form of analysis the measure of success is a reduction in oedema volume, using each animal as its own control. TBI is a progressive condition with a high amount of heterogeneity between animals, as there are between patients. Because of this the approach was taken to treat each animal as its own control in order to address some of these problems associated with TBIs. For each of the experiments analysed in this way the starting volume of lesions at 24 h was analysed to ensure that these values were not different between groups at this timepoint. The raw 24 h volumes of animals from *Figure 5.7* are laid out in *Table 5.2*.

CL5	NT
9.3142	10.476
11.8751	38.389
9.6108	8.798
6.3578	11.8158
12.4783	22.9246
7.7964	6.5407
10.5897	6.1501
17.259	8.192
5.987	
6.1798	
10.3326	
27.824	
Average = 11.30	**Average = 14.12**

Table 5.2: TBI oedema volumes at 24 h after TBI and siRNA. *As can be seen there is significant variation between animals in terms of starting TBI lesion volume. No significant difference is present between the two groups. (P>0.05, Student's t-test. CL5, n=12; NT, n=8.)*

If baseline TBI volumes were different between groups at 24 h this would have a knock-on effect, skewing results obtained at later timepoints. However no significant difference was observed at the 24 h timepoint between groups in any TBI volume analysis experiment.

5.3.3 Direct Quantification TBI Water Content

In order to assess oedema reduction directly, injured brain regions from animals given TBI and 20 µg NT or CL5 siRNA were dissected out from recently sacrificed animals and weighed before and after drying out the tissue using vacuum and heat. Quantification of this is displayed in *Figure 5.8*.

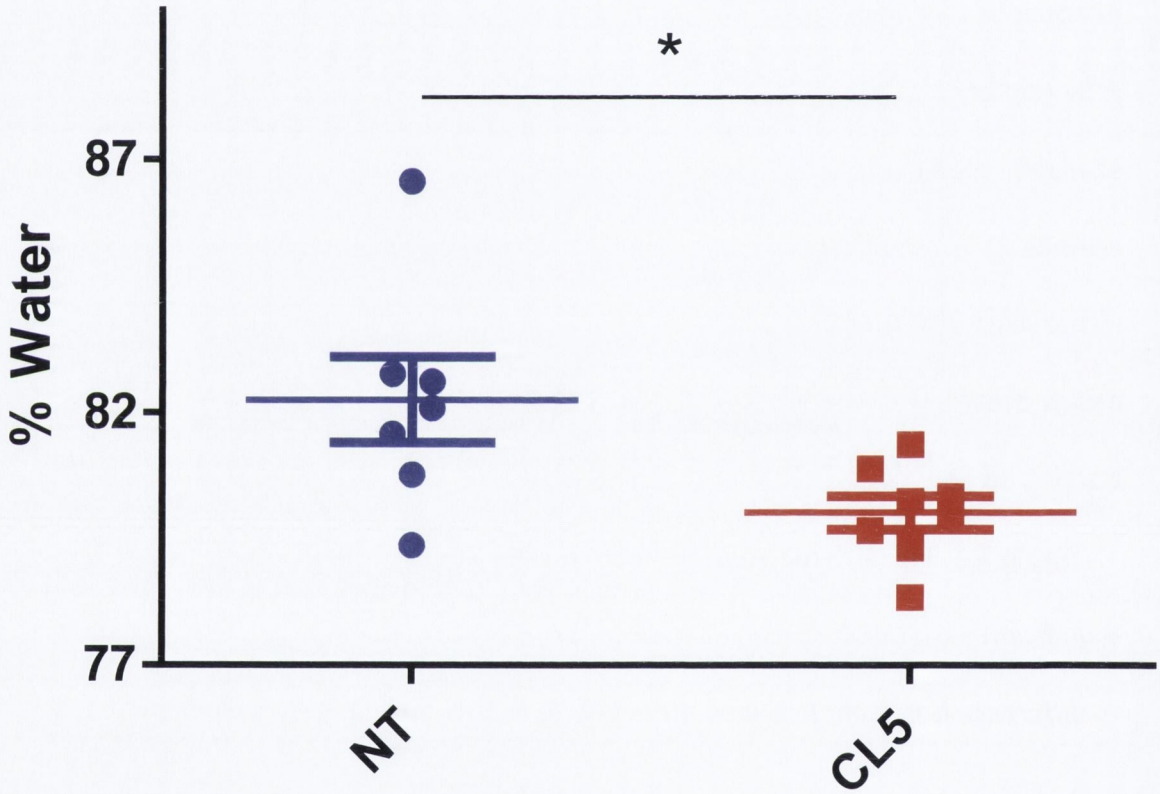

Figure 5.8: TBI region water content. *Water content of the dissected brain region was measured by weighing the tissue before and after tissue desiccation by vacuum drying at 50°C. The TBI regions from animals given 20 µg CL5 siRNA following injury demonstrated significantly lower water content than those given NT 20 µg siRNA. Assessment was carried out 24 h after TBI and siRNA. (*P≤0.05, Student's t-test. NT, n=7; CL5, n=8. Data are mean ± s.e.m.)*

Normal brain water content in rodents changes with age, with levels decreasing after birth. In all these in vivo experiments animals were age matched to as close to three months of age as possible, and healthy brain water content at this age is reported as being approximately 78% (Beaumont, Marmarou et al. 2000; Beaumont, Fatouros et al. 2006; Li, Gao et al. 2013). As can be seen in *Figure 5.8* no animals in either the NT or CL5 siRNA treatment groups are at or below this level. However the average water content or 80.013% in the CL5 group was found to be significantly lower than that in the NT group, which averages at 82.248%. This data support previously discussed findings in MRI scanning showing a reduced water-enriched region (*Figure 5.6*), and together these results make a strong case for the oedema-relieving potential of CL5 siRNA following TBI.

5.3.4 Alterations in siRNA Delivery Dosage and Timing

The timepoint for siRNA administration of 2 h following TBI administration was chosen as a reasonable timecourse in an emergency clinical setting. Along these lines it was desirable also to establish an effective minimum effective dose for CL5 siRNA, and so the amount of CL5 siRNA administered was halved in the next experiment to 10 μg and TBI volume change was once again measured (*Figure 5.9*).

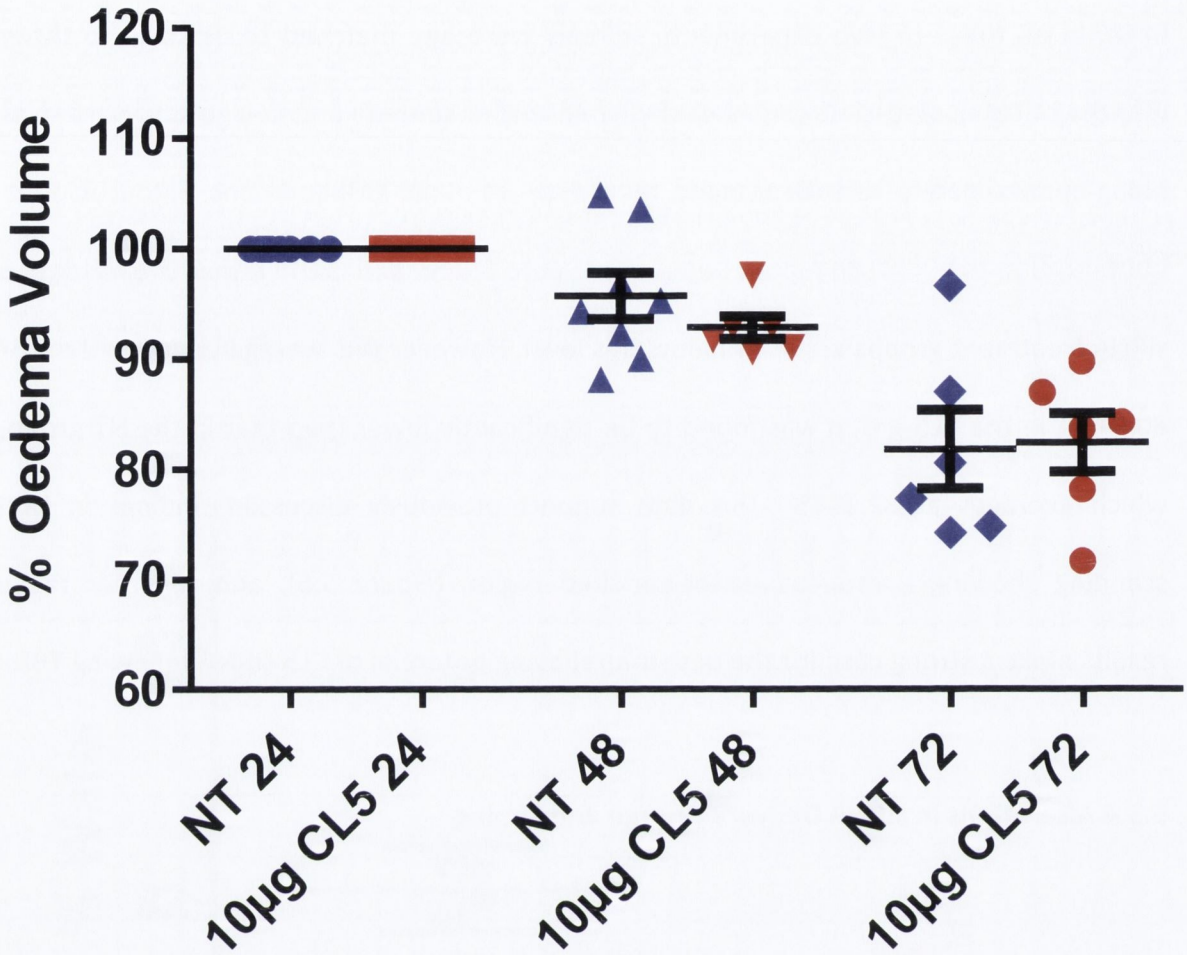

Figure 5.9: Quantification of TBI lesion shrinkage with half dose of CL5 siRNA. *20 µg NT siRNA was administered as normal, whereas the dose of CL5 siRNA given following injury was halved to 10 µg. Volumetric analyses of oedematous regions were carried out from T_2-weighted MRI images using an automatic MIPAV tool, while being blind to the treatment groups. Volumes at 24 h were set to 100%, with later timepoints being compared to this first timepoint. (P≥0.05, Student's t-test. CL5, n=12; NT, n=8. Data are mean ± s.e.m.)*

No significant difference was observed between TBI volumes in animals receiving 10μg CL5 siRNA and those receiving 20 μg NT siRNA (*Figure 5.9*). This indicates that the minimum dose for CL5 siRNA to effectively reduce oedematous volume between 24 and 27hrs post-injury lies between 10 and 20 μg. It was decided in this experiment to maintain the quantity of NT siRNA at 20 μg, rather than halve this also to 10 μg. This was done in order to maintain this control cohort as close as possible to the parameters used in controls for each other experiment in this study, which enables better comparison of results between experiments.

The next step undertaken in evaluating the conditions for CL5 effectiveness was to delay siRNA delivery in order to evaluate the window of time in which treatment could theoretically be administered in a clinical setting (*Figure 5.10*).

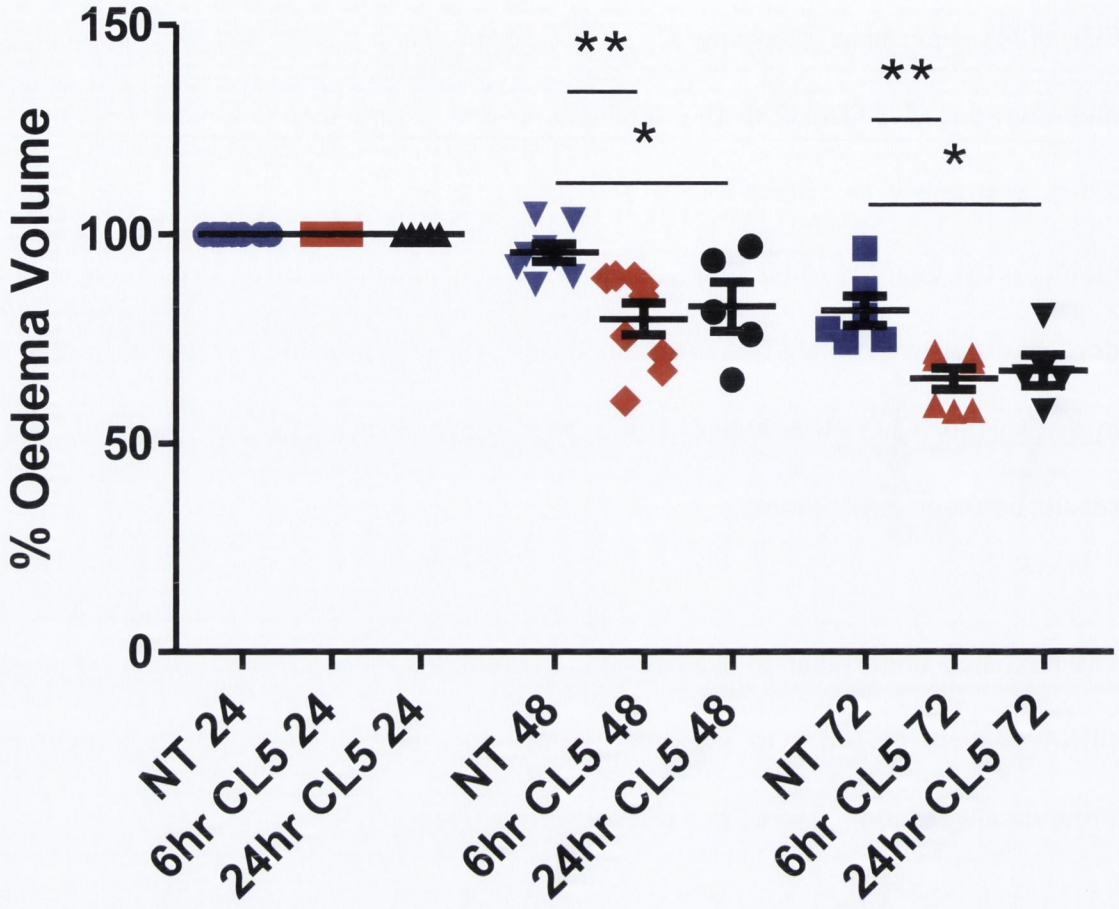

Figure 5.10: Effectiveness of delayed CL5 siRNA in reducing TBI oedema volume. *20 μg NT siRNA was administered to animals within 2 h of injury as in other experiments; however administration of 20 μg CL5 siRNA was delayed until 6 h in one cohort of animals, and 24 h in another cohort. Volumetric analyses of oedematous regions were carried out from T_2-weighted MRI images using an automatic MIPAV tool, while being blind to the treatment groups. Volumes at 24 h were set to 100%, with later timepoints being compared to this first timepoint. (**P≤0.01 and *P≤0.05 for 6 h and 24 h injections, respectively; ANOVA with Tukey's post test. NT siRNA at 24 and 48 h, n=8; NT siRNA at 72 h, n=6; CL5 siRNA 6 h at 24 and 48 h, n=9; CL5 siRNA at 72 h, n=7; CL5 siRNA 24 h at all timepoints, n=5. Data are mean ± s.e.m.)*

Somewhat surprisingly CL5 siRNA remained effective when administered both 6 h and 24 h after TBI (*Figure 5.10*). The average reduction in lesion volume was greater when siRNA was delivered 6 h following TBI instead of 24 h later, at 79.863% and 82.811% respectively 48 h after TBI and 65.520% and 67.473% at 72 h. However there was no significant difference between the two delivery timepoints. Once again in this experiment the protocol for administering NT siRNA remained unchanged in order to have a constant control cohort between different experiments.

5.3.5 Effect of Claudin-5 siRNA on Barrier Strength Following Traumatic Brain Injury

In order to assess where in the TBI and surrounding region the CL5 siRNA was acting, a series of T_1-weighted MRI scans were carried out to assess the extravasation of Gd-DTPA with and without BBB modulation. Seen in *Figure 5.11* is the pattern of Gd-DTPA permeation into the brain in three animals given NT siRNA.

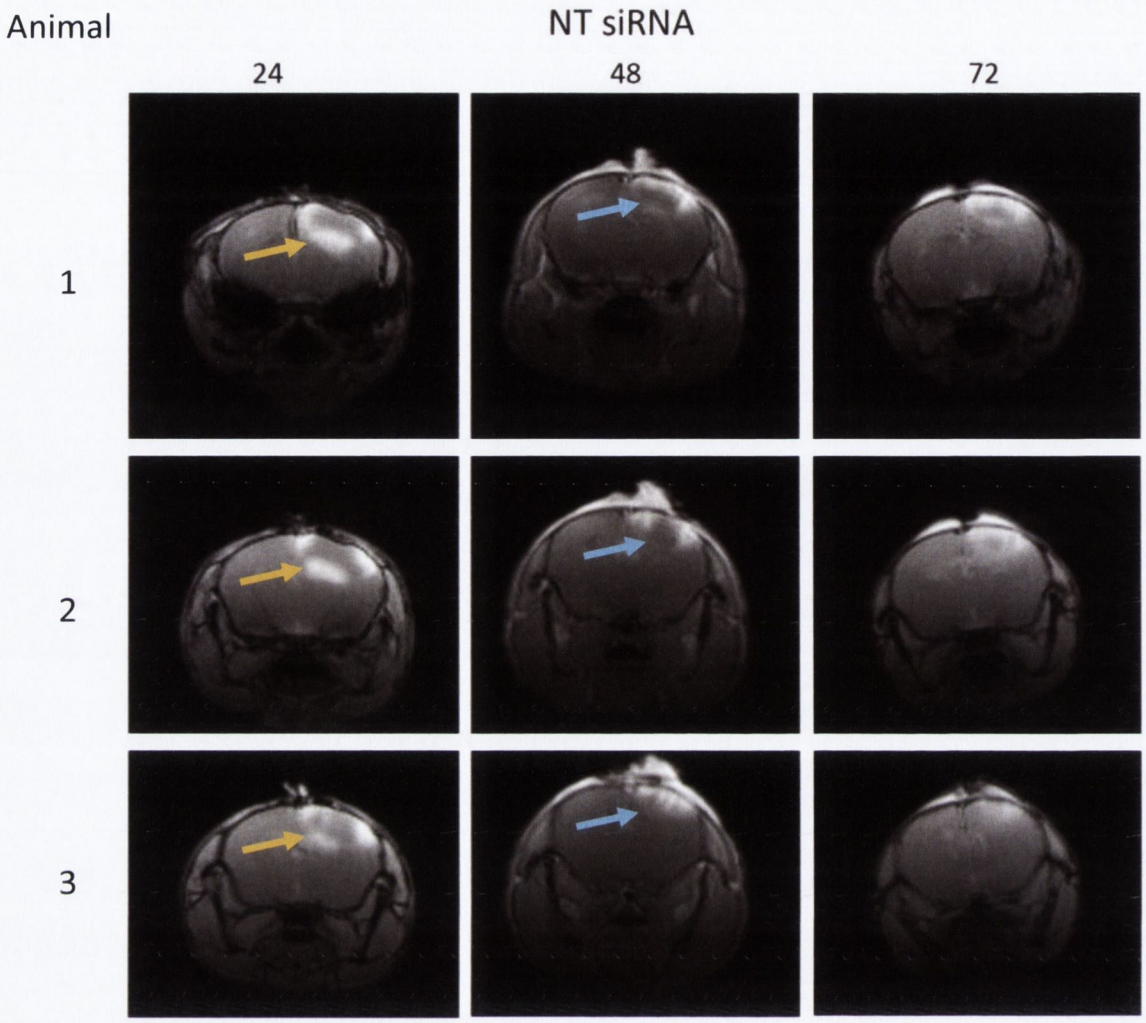
Animal
NT siRNA
24
48
72
1
2
3

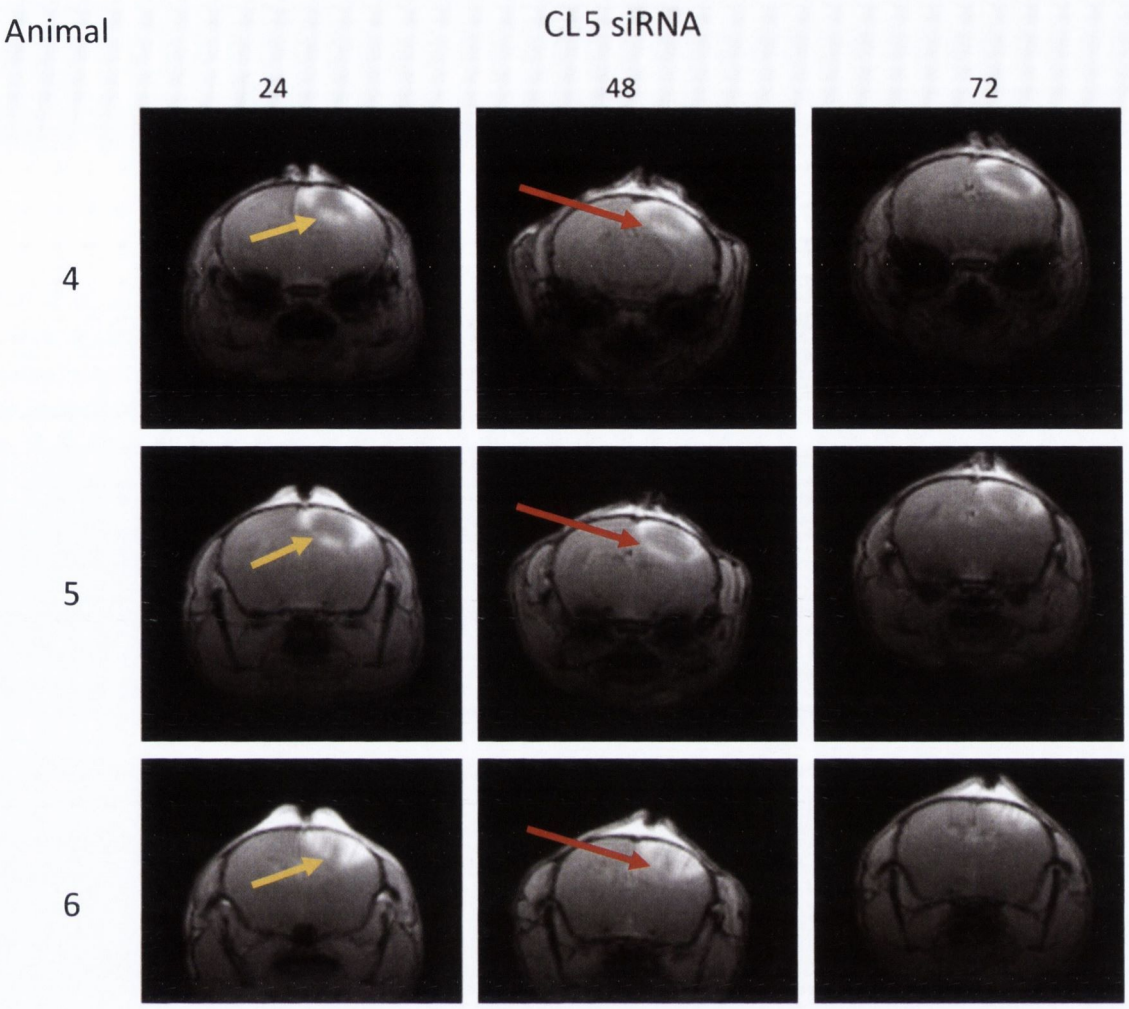

Figure 5.11: Pattern of Gd-DTPA extravasation around a TBI in NT and CL5 animals. *A coronal brain slice through the centre of the injured region is shown at three timepoints in each of 6 different animals. The 6 C57 mice were given a TBI followed by 20 µg NT siRNA (animals 1, 2 and 3) or 20 µg CL5 siRNA (animals 4, 5 and 6). 24 h (left), 48 h (middle) and 72 h (right) T_1-weighted MRI scans were performed during which Gd-DTPA was systemically infused. At 24 h Gd-DTPA is seen extravasating (high contrast, white) at the penumbra of the injured region in all 6 animals (yellow arrows). At 48 h this extravasation is observed to be greatly reduced in NT mice (1, 2 and 3; blue arrows) but is maintained in CL5 animals (4, 5 and 6; red arrows). The 3 animals shown here for each group are representative of n=6 for both CL5 and NT siRNA-administered animals.*

Figure 5.11 illustrates a biphasic pattern of Gd-DTPA extravasation in mice given NT siRNA (animals 1, 2 and 3), where the contrasting agent permeates into the brain in the regions surrounding the injury at 24 h and 72 h, while contrasting in the penumbra beneath the TBI disappears at 48 h. In animals given CL5 siRNA (animals 4, 5 and 6) on the other hand the patterns of extravasation is markedly altered. Here at 48 h after injury and CL5 siRNA delivery, a strong ring of permeability to Gd-DTPA is maintained as in the other timepoints (*Figure 5.11*).

5.2.6 Arterial Spin Labelling Following Traumatic Brain Injury

In one experiment, a significant difference in the relative cerebral blood volume (rCBV) was detected between NT and CL5 animals (*Figure 5.12*); CBV is a measure of the amount of blood passing through a region of interest.

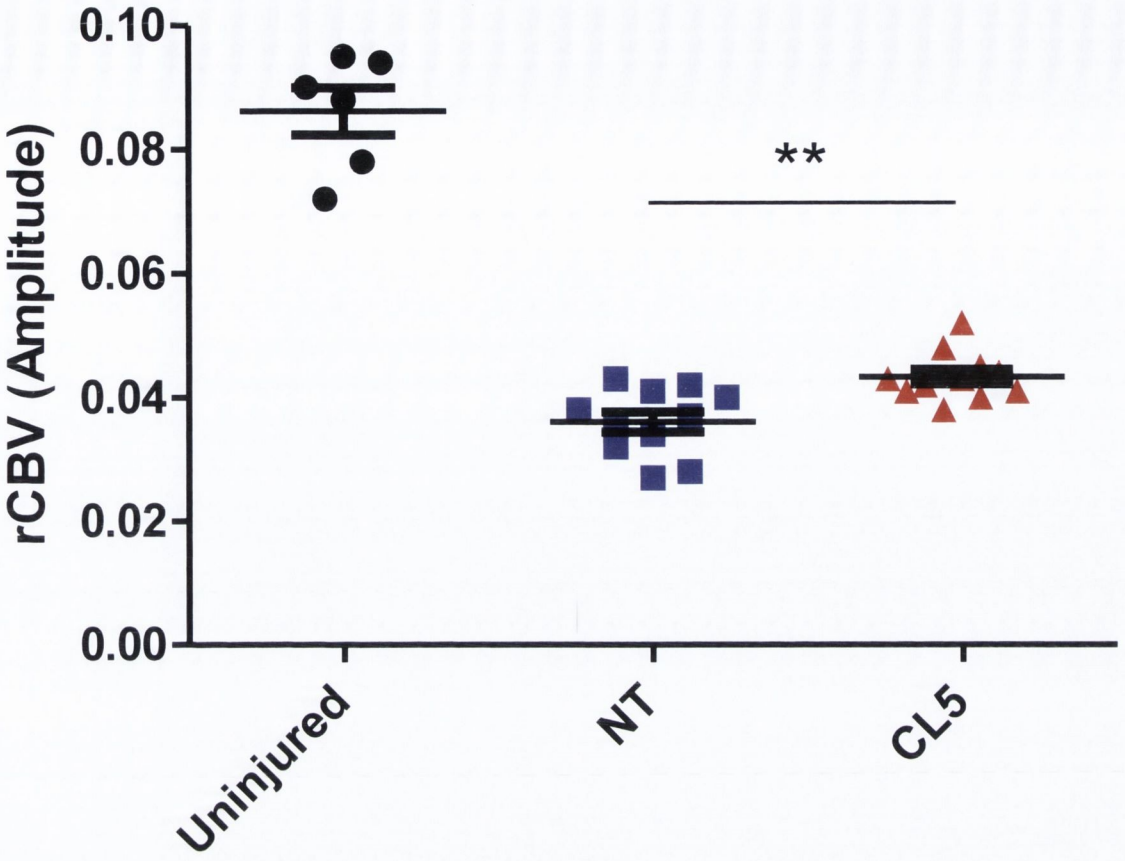

Figure 5.12: rCBV recovery in CL5 animals. *rCBV measurements from the TBI region are greatly reduced in both NT and CL5 animals compared with corresponding control, uninjured brain regions. However a significant increase is observed in CL5 animals compared with NT animals. (**p<0.01, One-way ANOVA, Bonferroni post test for multiple comparisons. Uninjured, n=6; NT, n=11; CL5, n=11. Data are mean ± s.e.m. Parameters used were as follows: slice thickness = 2 mm, fast low angle shot TR = 6.938 ms, echo time TE = 2.63 ms, RF flip angle = 30° FOV = 3.0×3.0 cm, image matrix = 128×64, receiver bandwidth = 100 kHz.)*

Reproduced with permission of Dr. Michael Kelly, FMRIB Centre, Nuffield Department of Clinical Neurosciences, University of Oxford.

Mice injected with CL5 siRNA had a significant increase in rCBV that trended towards a control, uninjured brain region rCBV (*Figure 5.12*). This finding suggests a partial recovery of blood flow through the TBI of mice receiving CL5 siRNA.

To assess the rates of exchange of water in the tissue, capillary transit time was also assessed. This is a measure of the time taken for labelled arterial water to cross the TBI region. CTT was observed to be significantly higher in the injured region of mice receiving CL5 siRNA than in NT or control mice (*Figure 5.13*).

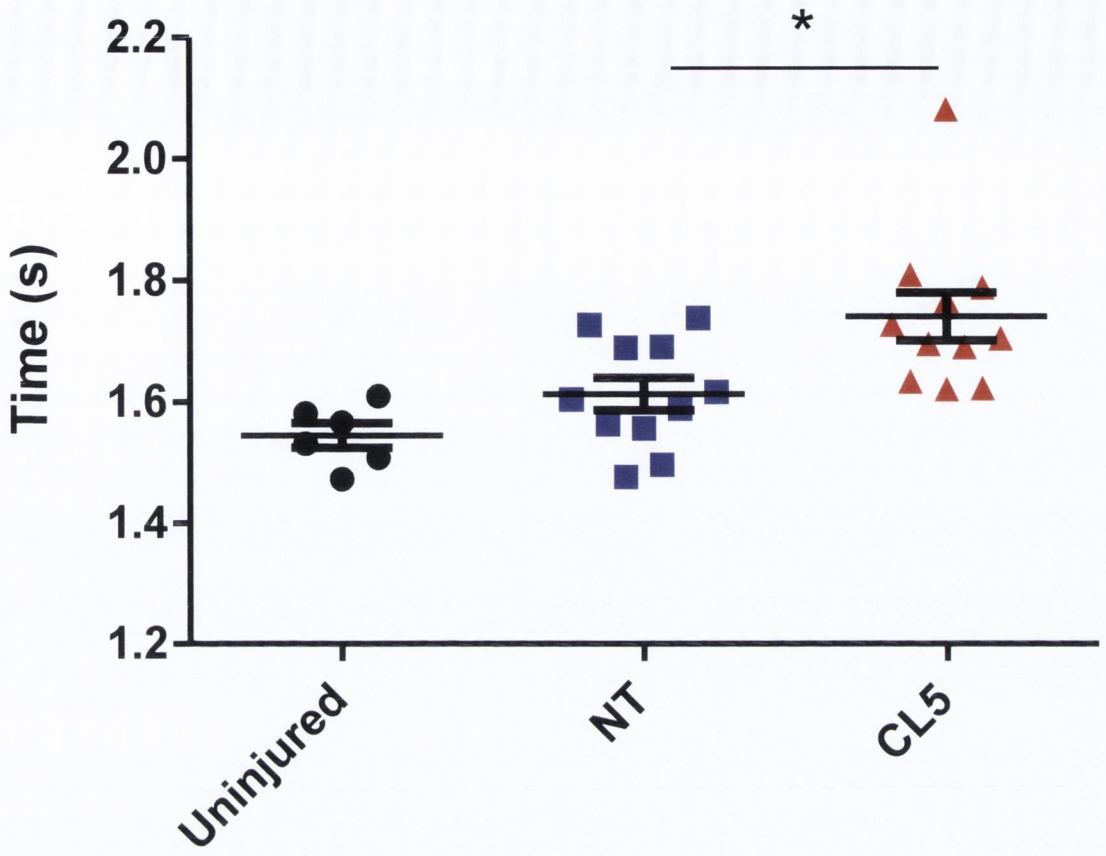

Figure 5.13: Increase in CTT in CL5 animals. CTT *measurements from the TBI region are significantly increased in animals given CL5 siRNA compared with NT animals and corresponding control, uninjured brain regions. (*p<0.05, One-way ANOVA, Bonferroni post test for multiple comparisons. Uninjured, n=6; NT, n=11; CL5, n=11. Data are mean ± s.e.m. Parameters used were as follows: slice thickness = 2 mm, fast low angle shot TR = 6.938 ms, echo time TE = 2.63 ms, RF flip angle = 30° FOV = 3.0×3.0 cm, image matrix = 128×64, receiver bandwidth = 100 kHz.)*

Reproduced with permission of Dr. Michael Kelly, FMRIB Centre, Nuffield Department of Clinical Neurosciences, University of Oxford.

Longer transit time for blood-borne water crossing the TBI region in CL5 animals than in NT or control brain regions (*Figure 5.13*) is indicative of increased paracellular flux of water. This increased exchange would result in labelled water remaining in the injured region for longer as the TBI region is traversed, increasing CTT.

No significant differences in rCBV or CTT in brain regions controlateral to TBI regions were observed between treatment groups, indicating that CL5 siRNA had no effect on these characteristics of blood flow in the healthy brain.

5.3.7 Motor and Cognitive Outcome

After observing a decrease in lesion size (*Figure 5.7*), and an improvement in blood flow in the injured region (*Figures 5.14* and *5.15*), our next step was to see if this would have any effect on behaviour or functional ability.

The first method employed to test this was the neurological severity score (NSS). NSS consists of ten tests on a range of behaviour and motor function of animals. Tests include crossing beams of varying width in a limited amount of time, ability to perch with all four legs and the presence of seeking behaviour. NSS is used in a range of models of brain damage to assess neurological damage, and it has been used previously to measure the difference in damage caused by different severities of TBI (Flierl, Stahel et al. 2009).

Normal, wild-type C57 mice received a perfect score of 0 fails. The NSS score for an animal given anaesthetic and sham surgery but no TBI was found to be 8 at 1 h after

surgery, with this returning to 0 by 8 h post-surgery (*Figure 5.14*). This result gives an estimate of when the effects of the anaesthetic can be discounted from contributing to NSS results.

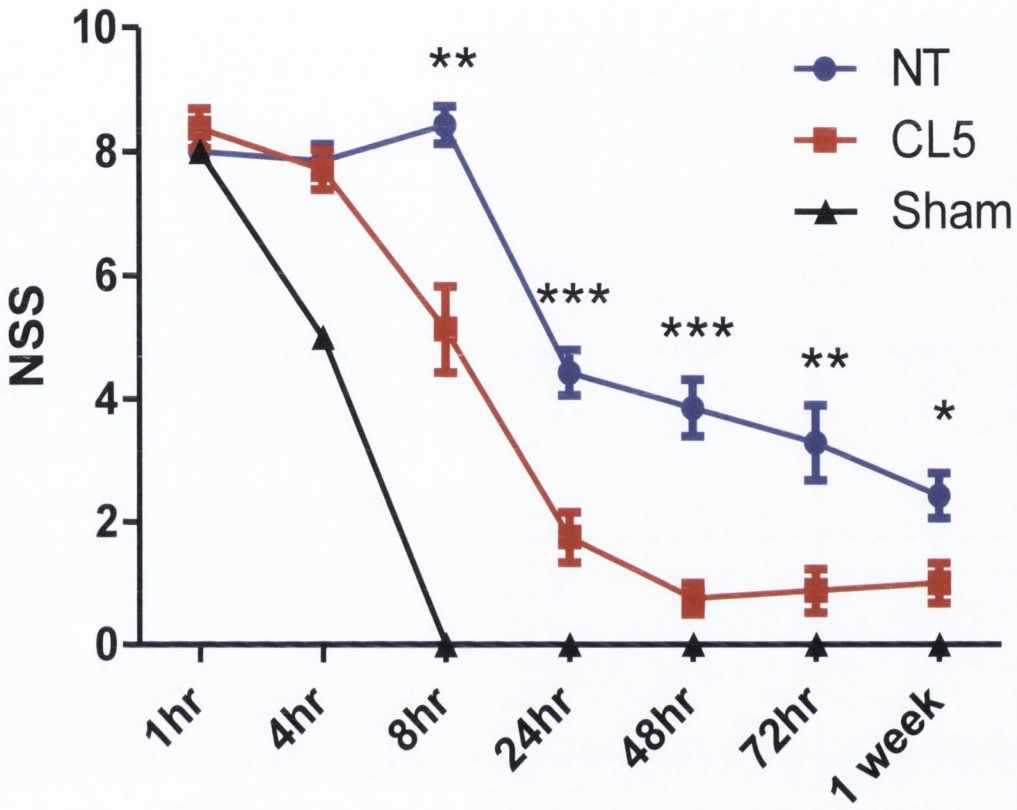

Figure 5.14: NSS results for animals given TBI and NT or CL5 siRNA. *Significantly improved NSS performance was observed in CL5 compared with NT animals from 8 h up to 1 week post-injury and siRNA delivery. NSS tests were carried out blind to treatment group throughout the timepoints to prevent bias. (***P≤0.001 at 24 and 48 h, **P≤0.01 at 8 and 72 h, *P≤0.05 at 1 week; Student's t-test. NT siRNA, n=8; CL5 siRNA, n=8; Sham, n=1. Data are mean ± s.e.m.)*

As illustrated in *Figure 5.14* from 8 h after injury animals treated with CL5 siRNA scored significantly lower on the NSS scale at every timepoint up to 1 week when the experiment

was ended. It is noted that the scores of NT animals actually get worse between 4 and 8 h; this is likely due to the wearing off of analgesic effects of the sedatives. A similar deterioration at this same timepoint was previously reported in a model of severe TBI, whereas a less severe model did not demonstrate this increase in score (Flierl, Stahel et al. 2009).

A breakdown of the tests passed and failed in animals at the 1 week timepoint is shown in *Table 5.3*. These tests are:

A. Exit a circle with a diameter of 30 cm within 3 min;
B. Ability to use all four limbs;
C. Initiative and ability to walk straight;
D. Startle reflex;
E. Inquisitive behaviour;
F. Ability to balance on a beam 7 mm wide for 10 s;
G. Cross a 30 cm beam of width 3 cm at a height of 10 cm in 3 min;
H. Cross a 30 cm beam of width 2 cm at a height of 10 cm in 3 min;
I. Cross a 30 cm beam of width 1 cm at a height of 10 cm in 3 min;
J. Ability to perch on a round beam of width 5 mm.

	A	B	C	D	E	F	G	H	I	J
CL5-1	O	O	O	O	O	O	O	X	O	O
CL5-2	O	O	O	O	O	O	O	O	O	O
CL5-3	O	O	O	O	O	O	O	X	X	O
CL5-4	O	O	X	O	O	O	O	O	X	O
CL5-5	O	O	O	O	O	O	O	O	O	O
CL5-6	O	O	X	O	O	O	O	O	X	O
CL5-7	O	O	O	O	O	O	O	O	O	O
CL5-8	O	O	O	O	O	O	O	O	X	O
NT-1	O	O	X	O	O	O	O	O	X	O
NT-2	O	O	X	O	O	O	O	O	O	O
NT-3	O	O	O	O	O	O	O	X	X	O
NT-4	O	O	X	O	O	O	X	X	X	O
NT-5	O	O	O	O	O	O	O	X	X	O
NT-6	O	O	X	O	O	O	O	X	X	O
NT-7	O	O	X	O	O	O	O	X	X	O
Sham	O	O	O	O	O	O	O	O	O	O

Table 5.3: Breakdown of results by individual tests in all animals at end-point of NSS.

Animals tested were 8 mice given CL5 siRNA following TBI, 7 given NT siRNA, and one shame operated animal.

As can be seen in *Table 5.3* the sham operated mouse as well as 3 CL5 animals recorded perfect score results at this end-point of the experiment, while none of the NT siRNA-administrated animals succeeded in passing every test. The only tests failed by any animals at this timepoint were the ability to walk straight, as well as crossing beams of varying widths.

Figure 5.14 uses NT siRNA as a control for CL5 siRNA in the absence of other controls for animals that were administered TBIs. As mentioned in the introduction to this chapter experiments showing CL5 suppression that employed multiple controls have been

published previously by this lab. These controls were uninjected, PBS-injected, and NT siRNA injected animals, and none of the suppression studies found any difference between any of these controls in terms of suppression efficiency or detected any deleterious effects of siRNAs used in this study (Campbell, Kiang et al. 2008; Campbell, Nguyen et al. 2009; Campbell, Hanrahan et al. 2012). This includes findings by this lab is safety assessment in African green monkeys of no negative histopathological or toxicological impact of siRNAs used in this study (as yet unpublished).

In addition to NSS tests, T-maze tests were carried out. This test of hippocampal memory involves the animal being tested exploring a T-shaped maze and choosing between two identical paths. The animal is then replaced back at the start of the maze to choose again (T-maze set-up shown in *Figure 2.2*. Memory of having been down one path combined with natural inquisitiveness should lead the mouse to choose the path it did not initially choose. As observed in *Figure 5.15* the rate of alternation, i.e. choosing a different path the second time, in control animals given sham surgery but not TBI was approximately 75% - the spontaneous alternation rate previously reported for wild-type mice (Deacon and Rawlins 2006). For animals given NT siRNA following TBI the alternation rate had dropped to below 50%, whereas in animals given TBI and CL5 siRNA the rate was partially rescued to just over 60%.

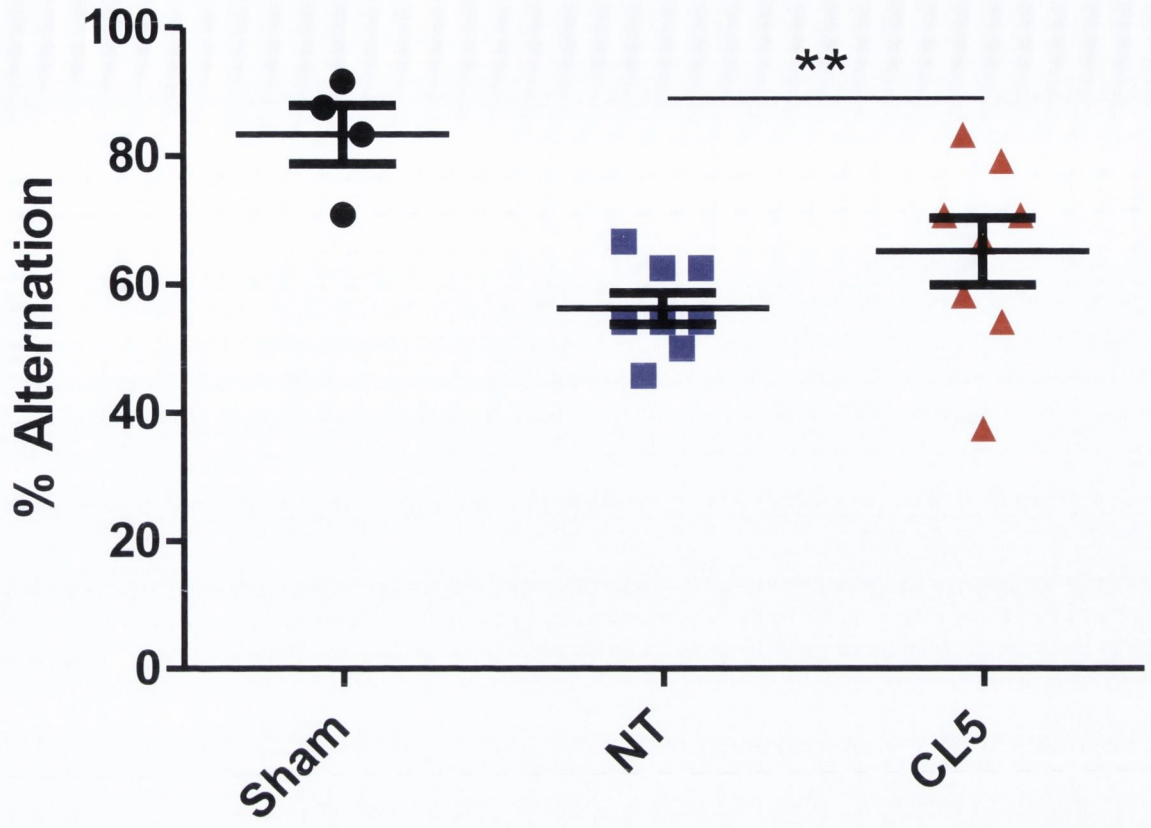

Figure 5.15: T-maze results following TBI and siRNA. *T-maze test was administered over the course of one week, three weeks following TBI and siRNA administration. (**P≤0.01, Student's t-test. NT siRNA, n=8; CL5 siRNA, n=8; Sham, n=4. Data are mean ± s.e.m.)*

This result, with significant animal numbers, is another major piece of evidence supporting the beneficial effect of transient CL5-suppression in the treatment of TBI, with improvement in the T-maze test (*Figure 5.15*) indicating preservation of tissue in the hippocampus – the main brain region involved in spontaneous alternation.

5.4 Discussion

The aim of this project was to apply a treatment to animals following TBI that would have the effect of reducing cerebral oedema and therefore mitigate the downstream deleterious effects of brain swelling. As such it was believed that starting with a model which excluded certain other features of a complex, impact-induced TBI such as DAI and impact haemorrhages would be advantageous. A model of cold-induced TBI was selected after a brief comparison with CCI (*Figure 5.2* versus *Figure 5.3*). This choice was primarily due to the uniform shape of the oedematous region (*Figure 5.2*), with clearly defined borders. TBI lesions such as this are straight forward to quantify using imaging software such as ImageJ or MIPAV. In addition to the clearly defined borders as viewed by MRI, imaging software packages such as these have tools that can be employed to automatically select and measure regions of high signal intensity. These tools easily pick out the TBI region from the surrounding tissue, reducing error, variation and bias.

As can be seen in *Figure 5.4* at 24 h the most heavily injured region closest to the surface no longer stains positive for DAPI, indicating that cells here have become so heavily damaged that their DNA has lost integrity to such an extent that staining of the AT-rich regions normally bound by DAPI is no longer possible. TUNEL staining is visible in a wider region of the site of injury, but also is not present directly at the surface of the cortex. This appears to indicate that in this area cells are most heavily damaged or have been necrotic for the longest period, resulting in either degradation to the extent that the terminal deoxynucleotidyl transferase enzyme active in the TUNEL stain encounters insufficient contiguous DNA or clearance of fragmented DNA by elements of the immune

system. Below this region there is an area of cell death detectable by TUNEL staining that is still within the area unstained by DAPI, and then below this is a further region stained by both DAPI and TUNEL where cell death is more recent or less severe. Together this indicates that loss of DAPI staining is a marker of cell death following cold-induced TBI, however TUNEL staining reveals a larger region of dying cells.

Next animals given cold-induced TBI were injected systemically with Evans blue and terminally perfused with PBS in order to flush the dye from systemic circulation. Evans blue dye has a high affinity for serum albumin, and due to the large size of this protein it is excluded from the brain under normal circumstances by the BBB (Hawkins and Egleton 2006). Following TBI, however, Evans blue was observed to have extravasated into the brain (*Figure 5.5*). This is an indication of significant damage to blood vessels in the injured region, with broken vessels dead-ending and releasing their contents into the core injured region. This means that besides Evans blue all other blood constituents, such as erythrocytes and serum proteins, are also being spilled from blood vessels which have lost their integrity. This material accumulates and contributes to vasogenic oedema.

At this stage of experiments in this chapter attempts were made to measure a decrease in CL5 levels following TBI and siRNA delivery. This was attempted by means of RT-PCR, Western blot, and immunohistochemistry, however this proved more difficult to carry out than expected. RT-PCRs that were carried out in TBI regions suffered from low quality RNA, likely due to the presence of large amounts of cells in various states of death and molecular disintegration in the region, and for CL5 this meant a failure to acquire data fit for analysis. Western blots carried out for CL5 were also unsuccessful, likely due to the

same reason, and after a number of failed attempts it was decided that the large amount of indirect evidence for CL5 suppression was sufficient. These data include increased Gd-DTPA extravasation (*Figure 5.6*), reduced oedema volume (*Figure 5.7*), and direct quantification of decreased TBI water content (*Figure 5.8*). As well as this there are many examples of decreased CL5 expression in the brain following CL5 siRNA or shRNA that have been reported by this lab (Campbell, Kiang et al. 2008; Campbell, Humphries et al. 2011). Damage to cerebral blood vessels in the TBI region is unlikely to interfere with CL5 siRNA access or activity in TBI blood vessels due to the observation that Evans blue dye is successfully delivered to the TBI (*Figure 5.5*). However if CL5 siRNA efficiency was impaired in the central injured region this would potentially not be a barrier to effective reduction in oedema. The reason for this is that the tissue hypothesised as being the most likely to be saved by decreases in oedema is the penumbral edge of the injury, particularly where the TBI borders the hippocampus. Here tissue perfusion is expected to still be largely intact and so CL5 siRNA would be expected not to encounter significant barriers to delivery. It was felt that in the face of significant amounts of data indicating that CL5 was suppressed, as well as previously published results of CL5 siRNA in the brain (Campbell, Kiang et al. 2008; Campbell, Humphries et al. 2011), the use of further animal numbers in order to reattempt direct quantification of CL5 levels could not be justified.

As is qualitatively illustrated in *Figure 5.6*, and quantified in *Figure 5.7*, CL5 was effective at reducing oedema following cold-induced TBI. In both figures animals given NT siRNA in the first 2 h after injury were observed to show limited shrinkage of oedema volume by 72 h. CL5 siRNA, by contrast, induced marked decreases in the fluid-enriched region. The speed at which this effect is observed is apparent by the quantification of water content

in TBI regions at only 24 h following TBI and siRNA administration (*Figure 5.8*). This is the most direct measure of oedema, and the significant reduction observed here demonstrates the speed at which the CL5 siRNA acts in the TBI region to release water build up or prevent it accumulating in the first place. Compounding this is the fact that even with the significantly lower starting water percentage at 24 h shown here, lesion volumes still shrink at a faster rate in CL5 siRNA-treated animals (*Figure 5.7*).

The finding that oedema-reduction following CL5 siRNA occurs within the first 24 h following injury was an important result with respect to the clinical potential of this treatment. This is because due to the secondary injuries acquired as a result of oedema rapid reduction in ICP is key to positive patient outcome (Taylor, Butt et al. 2001). If significant oedema reduction had not been observed until a much later timepoint, perhaps following repeated injections of CL5 siRNA, expectations of improvements in cognitive outcome would have been lower.

With highly encouraging results having been found using the initially attempted CL5 siRNA doses and timepoints of delivery, it was decided to alter these in order to observe which elements of the protocol were crucial for this effect. Firstly the quantity of CL5 siRNA systemically delivered in injured animals was halved from 20 to 10 µg per animal. This reduction was found to completely abolish the significant effect of CL5 siRNA in reducing cerebral oedema following TBI (*Figure 5.9*). Throughout the course of this study on the effect of CL5 siRNA following TBI this was the only time that no positive effect of the siRNA was observed. It was decided in this experiment to maintain the quantity of NT siRNA at 20 µg, rather than halve this also to 10 µg. This was done in order to maintain this control cohort as close as possible to the parameters used in controls for each other

experiment in this study, which enables better comparison of results between experiments.

Increasing the delay between TBI and siRNA delivery (from 2 h post-injury to 6 and 24 h post-injury), by contrast, did not negate the reduction in oedema found in animals given CL5 siRNA (*Figure 5.10*). This is even the case for the 48 h MRI scan which takes place only 24 h after the delayed 24 h CL5 siRNA injection. *Figure 3.2* indicates that at the transcript level CL5 is suppressed after only 24 h following CL5 siRNA, however the half-life of the CL5 protein will mean that protein levels are still likely to not yet be optimally suppressed. *Figure 3.8*, however, does appear to show modulation of the BBB in vivo at the 24 h timepoint, visualised by hypocontrasted regions where Gd-DTPA has permeated out of blood vessels and into the brain.

Next the strength of the BBB in the brains of animals given TBI and NT or CL5 siRNA was assayed by contrast-enhanced T_1-weighted MRI using Gd-DTPA. It has been previously been reported that the BBB following TBI undergoes two separate periods of opening, which coincide with alterations in oedema (Baskaya, Rao et al. 1997). This coincides with observations made in the current study that NT animals undergo a biphasic opening of the BBB following TBI. The first opening of the barrier is noted at 24 h, with significant Gd-DTPA extravasation being visible surrounding the site of injury, with the second similarly patterned opening being seen at 72 h (*Figure 5.11*).The second opening of the BBB in fact coincides with the decrease in oedema recorded between 48 and 72 h (Baskaya, Rao et al. 1997). It is feasible here in fact that the second opening of the BBB could facilitative to relieving excess water build up in the injured tissue in response to high pressure inside the cranium. Between these timepoints at 48 h, however, Gd-DTPA is observed not to

extravasate around the TBI to the same extent, in particular in the lower penumbra of the injury, above where the hippocampus is situated. Another possible explanation observed for the lack of Gd-DTPA extravasation at this 48 h timepoint is that a temporary loss of blood flow to the penumbra prevents delivery of the contrast-agent. However particularly in the light of previous studies on biphasic BBB opening following TBI this is the more likely explanation.

In the CL5 siRNA-treated animals this biphasic pattern of barrier opening is replaced by consistent opening of the BBB to Gd-DTPA extravasation surrounding the TBI at all timepoints (*Figure 5.11*). This indicates that the penumbra is accessible to systemic circulation throughout the first 72 h, which would enable fluid build up – and consequent increases in pressure – to be released in CL5 animals. In NT animals on the other hand, fluid could not be released via the paracellular pathway at this timepoint, leading to increased lesion volume and increased ICP in the penumbra.

In order to further explore the effect of CL5 siRNA in the TBI region arterial spin labelling (ASL) was employed with the aid of a collaborator, Dr. Michael Kelly of the FMRIB Centre, University of Oxford. T_1 and T_2 MRI scans employed thus far use magnetic gradients to cause protons – in particular hydrogen atoms – to align themselves in the magnetic field. This results in the detection of water in particular, and to a lesser extent fat. ASL on the other hand magnetically labels the water in blood upstream of the region of interest, which then flows through the region being detected as it does so. This allows for a number of blood flow analyses.

The increase in the quantity of blood in the TBI region (rCBV) in CL5 animals (*Figure 5.12*) points to an improvement in the function of blood vessels in the TBI region. This could

hypothetically represent increased vascular integrity; decreased pressure in this region could result in less resistance to blood flow, or a combination of effects. The rCBV value is observe to more closely approach that of the same brain region in uninjured control animals, which is a positive finding for CL5 animals.

The time taken for blood to cross the TBI region (CTT) in injured mice given CL5 siRNA has in contrast moved significantly away from CTT results observed in uninjured brain regions (*Figure 5.13*). This increased CTT is indicative of labelled blood-borne water remaining in the injured region for a longer period of time as it traverses it. The key hypothesis here is that if labelled water can enter tissue then oedematous water within tissue can also enter the blood, and in regions of water build-up and high pressure this will result in net loss of water from brain tissue. Consequently it is believed that this result is a further indication of increased water flux within the TBI following CL5 siRNA delivery, resulting in a reduction in oedema.

Results observed in NSS (*Figure 5.14*) and T-maze (*Figure 5.15*) point to the ability of CL5-suppression to have an effect not only on the visible lesion characteristics such as volume and blood flow, but on functional ability, indicating the preservation of neurological tissue that is lost in NT animals. One curious finding is how early the benefit in NSS becomes apparent – 8 h (*Figure 5.14*). In the absence of detailed staining experiments being carried out to observe the kinetics of CL5 at the TJ directly following TBI in the presence or absence of CL5 siRNA, the strongest hypothesis is that early downregulation of CL5 transcript leading to a lack of CL5 replacement at the TJ results in slight changes in protein levels at early timepoints. This effect could be compounded by cycling of TJ proteins to and from the paracellular cleft directly following TBI, and the TJ protein phosphorylation

that accompanies this shuttling. With water being such a miniscule molecule, 18 Da in size, compared to the potential BBB modulation of approximately 1,000Da, even a very slight decrease in CL5 levels would likely have an effect on water flux in and around the injured region. This hypothesis is supported by the previous finding that the water content within CL5 TBIs had already fallen significantly lower than those observed in NT TBIs at 24 h after injury and siRNA delivery (*Figure 5.8*).

Regions central to the site of injury are likely to be rapidly ablated and irrecoverable, while brain regions more distal to the site of injury are unlikely to have enough damage as to be a good measure for improvement following treatment. The hippocampus on the other hand, lies within the maximum extent of cell death following TBI (*Figure 5.4*), as well as bordering the region in which BBB opening was previously shown to be maintained by CL5 siRNA (*Figure 5.13*). This hypothesis appears to have been correct, as animals that received CL5 siRNA demonstrate markedly improved performance in T-maze 3 weeks after TBI (*Figure 5.15*).

5.5 Future Directions

The findings presented in this chapter include the succesful establishment of a model of oedema in the form of a cold-induced TBI mouse model, in which the hypothesis that water movement out of the brain would be aided by CL5 suppression was tested. Results presented indicate that this hypothesis was correct, with significant shrinkage of oedematous TBI lesions together with improvements in motor and behavioural

performance. From here however a number of experiments could be carried out in order to expand and improve on this work.

Firstly suppression of CL5 in animals that had been given TBIs was not succesfully demonstrated. These attempts failed most likely due to interference from the highly necrotic mass of tissue at the core of the tissue, however further attempts should be made this time concentrating on the penumbra of the injured region where prospective staining or other analyses may be more succesful. Although there is data presented here which is indicative of CL5 being suppressed in the brains of these animals, such as permeability of the penumbra region to Gd-DTPA only in CL5 siRNA-administered animals, a conclusive demonstration of CL5 suppression would be important when moving on with this project.

Next it would be a positive step to show in an in vitro model of the BBB that CL5 suppression increases water flux across the barrier. This would be possible using cell culture vessel that are seperated in two by a monolayer of bEnd.3 cells. These cells would be transfected with CL5 siRNA, NT siRNA, or would be untransfected, and after 48 h tritiated water would be introduced into one side of the cell culture vessel. At various timepoints after this an aliquot of media would be removed from the opposite side of the vessel, on the other side of the endothelial monolayer, and presence of the tritiated water in these samples would be measured by liquid scintillation. As in the case of CL5 suppression there are a number of strong indications presented here that water build up is being relieved by means of CL5 siRNA delivery, such as the increase in MTT of blood as it crosses the injured region, but a direct observation of the ability for CL5 suppression to increase water movoment across a barrier would a strong addition to this.

Together these experiments would help to answer some remaining questions, as well as the possibility that a mechanism other than CL5 suppression and barrier modulation are the primary effectors of improvement in this experimental model. Finally, the work presented in this chapter to relieve fluid build up in the brain could be extended to a further model of TBI, such as CCI or fluid percussion injury, as well as a different model of increased ICP such as stroke.

Chapter 6: Inflammation in TBI Regions

6.1 Abstract

Inflammation is a significant feature of TBI, and provides a large hurdle to positive outcome when it extends into the chronic phase of post-TBI recovery. Meanwhile other studies have found that inflammation can be beneficial in cases of TBI, and some treatments aimed at reducing neuroinflammation can worsen outcome. With inflammation being a major feature of TBI pathology, it was decided as part of our investigation into the amelioration of TBI oedema by means of CL5 suppression to carry out a small investigation into the expression levels of inflammatory markers in treated and untreated mice. When these experiments returned increased levels of a number of factors in mice given TBIs in conjunction with barrier modulation it was decided to explore whether the this increase in inflammation at the acute timepoints observed was likely to be a positive or negative feature of treatment with CL5 siRNA. To this end a number of murine knockouts for key inflammatory components were chosen, and these animals were given TBIs and assayed for TBI volume over 72 h as well as motor and behavioural outcome at 3 weeks. The findings were that the key inflammatory scaffolding protein ASC, but not the NLRP3 inflammasome that it is a part of, plays a significant protective role following TBI, with its absence resulting in reduced TBI oedema shrinkage and impaired cognitive recovery. These results provide an interesting and potentially novel role for ASC in neuroinflammation, independent of the NLRP3 inflammasome.

6.2 Introduction

6.2.1 Neuroinflammation

Despite the demanding requirements of immune cell translocation to and activation in the brain, neuroinflammation is still a highly significant feature of many diseases and injuries of the brain, with immune cells playing important roles in both short and long-term TBI pathology. Wallerian axonal degeneration, seen in DAI for instance, has been shown to induce monocyte infiltration into the ipsilateral hemisphere 24 h post-injury (Bechmann, Goldmann et al. 2005). A possible reason for this post-lesion influx of immune cells might be due to the chemokine SDF-1. This protein is a chemotactic agent for T cells and monocytes, and is constitutively expressed at low levels in the brain. As such any trauma to the brain would expose SDF-1 to the circulating immune system, whereas under normal conditions it is sequestered away behind the BBB. In fact not only is it exposed after brain injury, but its expression is actively altered which attracts immune cells to the injured region specifically, with SDF-1 levels increasing in the penumbra of lesioned brain regions following focal ischemia, and decreasing in uninjured regions. This change in expression coincided with the influx of immune cells that expressed the SDF-1 receptor (Stumm, Rummel et al. 2002). Another mechanism which encourages immune cell infiltration into the brain is the response of endothelial cells to pro-inflammatory cytokines. When exposed to factors such as TNF and IFN-γ, endothelial cells show actin-cytoskeleton restructuring coinciding with fragmentation of ZO-1 staining at the cell periphery. This restructuring of TJs led to a concomitant decrease in

transepithelial resistance by 50% (Blum, Toninelli et al. 1997). Similarly, application of activated leukocytes onto endothelial cell monolayers led to aberrant adherens junction localisation, associated with actin cytoskeleton restructuring and phosphorylation of adherens junction proteins. These changes led to intercellular gap formation and albumin diffusion across the monolayer (Tinsley, Wu et al. 1999). It is clear that in order to counter the immune privilege conferred by the BBB, the immune system, as well as resident cells, employ counter-mechanisms in order to facilitate leukocyte penetration in cases of neuroinflammation.

6.2.2 Dendritic Cells

As well as monocytes and various T cells mentioned previously, a wide range of immune cells play active roles in the brain. One of these is dendritic cells, an antigen-presenting cell that plays an early role in many injuries and infections. This cell-type is normally detected only in the choroid plexus and the meninges in the uninjured brain (Matyszak and Perry 1996), but following TBI, dendritic cells, which likely differentiate from activated monocytes crossing the barrier, are found in increasing quantities infiltrating injured regions of the brain (Israelsson, Bengtsson et al. 2008). Neutrophils also have been observed to enter the CSF in significant numbers following injection into the subarachnoid space of IL-1β (Quagliarello, Wispelwey et al. 1991), a pro-inflammatory cytokine that plays an important role in post-TBI inflammation. Once in the brain, or during their transmigration into it, neutrophils may play a role in weakening the BBB and thus enabling further immune cell invasion (Tinsley, Wu et al. 1999), and certainly IL-1β-mediated recruitment of neutrophils is often associated with negative consequences,

such as increased water content in ischemic brain damage (Yamasaki, Matsuura et al. 1995).

6.2.3 Astrocytes

While not normally being considered immune cells, astrocytes play a large role in detecting and – as has previously been illustrated – modulating responses to damage or infection in the brain. Astrocytes express high levels of TLR3, as well as lower levels of TLRs 1, 4, 5 and 9, and produce cytokines such as IL-6, IP-10 and IFN-β in response to their ligation (Jack, Arbour et al. 2005). TLRs were first recognised for their ability to detect pathogen-associated molecular patterns (PAMPs), and these astrocyte-expressed TLRs are capable of detecting a wide range of pathogenic markers such as dsDNA, LPS and flagellin. However TLRs, including TLR3 and 4, are also capable of detecting danger-associated molecular patterns (DAMPS), endogenous molecules which are normally sequestered within the cell membrane of a cell, and whose presentation to TLRs indicates cell death such as that which occurs following TBI. Complicating the role of astrocytes and these TLRs in inflammatory scenarios, TLR3 activation can result in protective cytokine release such as IL-9, -10 and -11, and together TLR3-induced factors were found to improve neuronal survival in ex-vivo human brain slice cultures (Bsibsi, Persoon-Deen et al. 2006).

6.2.4 Microglia

The final cell type to be discussed, and probably the most significant post-TBI immune cell, are microglia. This monocytic cell lineage are the brain's resident macrophage, although under normal circumstances they express low or undetectable levels of macrophage phenotypic markers such as MHC I and II, CR3, FcR, CD68, LCA and CD4, which are then upregulated upon activation (Galea, Bechmann et al. 2007). It is significant to note that as the only immune cell type that is always observed in the brain under normal, non-inflammatory conditions, microglia can be activated by pathogens or tissue damage without any alteration in the BBB or other factors compromising the immune privilege of the brain. Microglia survey the brain microenvironment by means of highly motile filopodia, which, following BBB disruption or TBI, rapidly extend and converge upon the site of injury without movement of the cell body. This chemotaxis appears to be directly in response to extracellular ATP, such as that which would be spilled from cells upon TBI, and in fact this chemotaxis can be stimulated by the injection of ATP into the brain parenchyma. Once at the site of injury the microglial protrusions appear to shield healthy tissue from damaged tissue, and activate microglia and other immune cells (Davalos, Grutzendler et al. 2005; Nimmerjahn, Kirchhoff et al. 2005). Similar to astrocytes, microglia express TLRs, and induction of TLR signalling by sensing PAMPs or DAMPs in the brain microenvironment results in microglial activation and subsequent release of proinflammatory cytokines (Jack, Arbour et al. 2005), as seen in the activation of microglia via their filopodia.

Through these sensory mechanisms microglia function as the brain's watchdogs, alert for signs of damage and jumping into action sectioning off injured areas and recruiting further immune cells upon activation. As part of this role microglia also convey inflammatory signals received from the periphery throughout the brain priming it for response. Systemic LPS induces TNF-α within the exposed circumventricular organs, and this TNF-α expression increase spreads across microglia of the brain parenchyma, even though these areas have not been exposed to LPS directly. Interestingly this LPS-induced microglial activation is not on its own damaging to the CNS, but if the inhibitory activity of glucocorticoids within the brain is blocked (Nadeau and Rivest 2003). This indicates that upon receiving external danger signals microglia actively produce proinflammatory cytokines, but do not enter a fully neuroinflammatory phenotype due to inhibitory signals in the brain. This is significant because in models such as EAE, unchecked inflammation in the brain, even in the absence of other non-autonomous mediators of damage, can be hugely damaging to the brain. As mentioned in the previous section systemic immune cells encounter many barriers to entry, activation and even survival in the brain. However microglia have already overcome many significant hurdles by being already present and viable in the brain, and can activate via their sensory extensions and TLRs. Accordingly many inhibitory interactions exist between microglia and endogenous brain cells. Astrocytes, for instance, inhibit LPS-stimulated microglial production of IL-12 and other cytokines when in co-culture (Aloisi, Penna et al. 1997). Neurons also play an important role in microglial suppression, through mechanisms such as axon-terminus release of CD22 which engage microglial CD45 inhibiting TNF-α production (Mott, Ait-Ghezala et al. 2004). In an animal model illustrating neuronal inhibition, mice lacking CD200 on neurons demonstrate an increased microglial response to damage and a more severe onset of EAE

(Hoek, Ruuls et al. 2000). These endogenous mechanisms of microglial suppression are vital for brain integrity, but the safeguards can and do break down. After TBI the danger of neuroinflammatory damage is most significant when inflammation stretches into the chronic phase, and active microglia and macrophages can be detected in brain tissue years after injury (Chen, Johnson et al. 2009).

As well as proinflammatory activity of microglia, which can result in exacerbation of neuronal damage, these cells have important roles in mediating immune suppression and tissue repair themselves. In the case of the former microglia have been found to express HLA-G, the previously mentioned T-cell-inhibitory factor, particularly in areas affected by neuroinflammation, possibly in an attempt to decrease T-cell-mediated inflammation (Wiendl, Feger et al. 2005). Microglia have even been observed fully engulfing infiltrating neutrophils in the brain, and blockage of this process results in higher levels of neuronal damage (Neumann, Sauerzweig et al. 2008).

Microglial mediation of tissue protection and repair other than by suppressing immune responses takes a number of forms. Neuronal synapses can be actively moved and protected from damage (Trapp, Wujek et al. 2007), protecting the delicate network of neural of connections. It was mentioned earlier that glutamate excitotoxicity is a significant danger to neurons in the early stages post-TBI. Interesting microglia upregulate glutamate transporters within 4 h after trauma, with their expression being most pronounced closest to the site of injury (van Landeghem, Stover et al. 2001). This correlation of glutamate transporter expression levels with levels of glutamate accumulation indicates that this upregulation is a protective response by microglia to the

danger posed by build-up of the neurotransmitter after TBI. As well as these, more typical immune activity by microglia, such as antigen presentation and pro-inflammatory cytokine production, for example IL-1β, has been found in models to have neuroprotective results, with abrogation of these responses having deleterious outcomes (Mason, Suzuki et al. 2001; Byram, Carson et al. 2004).

The significant active contribution of neuronal, glial and CNS-resident microglial cells in immune responses and regulation shakes apart the previously held view that damaging immune activity in the brain was a product of BBB breakdown and exposure of the delicate CNS to the systemic immune system. Instead a dynamic system is being revealed, where all the different cell types of the brain play a role in either excluding and suppressing systemic immune cells in some circumstance, or attracting and activating them in others. This raises the notion that inappropriate immune activation in the brain could be as much a product of a dysfunction of the brain itself, than of the immune system.

6.2.5 Adaptive or Maladaptive?

This is a prime example of the oft-mentioned 'double-edged sword' of neuroinflammation, whereby in many situations and models, large amounts of damage are caused by activation of the immune system following CNS insult, while at different timepoints or in different models inflammation can be protective and its inhibition harmful. In further examples of this latter protective component to neuroinflammation, mice lacking IL-1β that undergo demyelination following loss of oligodendrocytes fail to

remyelinate or repopulate oligodendrocyte populations to the same extent as wild-type mice (Mason, Suzuki et al. 2001). Another pro-inflammatory cytokine that sees prominent expression following TBI is TNF-α, and this too is found to promote the expansion of oligodendrocyte precursor cells as well as remyelination (Arnett, Mason et al. 2001).

Clearly the complexity involved in neuroinflammatory processes remains to be fully worked out, whether in TBI or other conditions with an inflammatory component, but what is certain is that it is a mistake to dismiss neuroinflammation as a solely negative, damaging process. Instead there is a delicate balancing act in the CNS between the need to have immune cells that can fight infections that breach the CNS, as well as phagocytose dead and dying cells before they damage other cells around them, and the need for inflammation to be as low as possible in the delicate, non-regenerative neural tissue. Allowing these cells to be inappropriately activated has well documented disastrous results such as multiple sclerosis, but preventing immune cells from activating in cases of infection, cell death or toxin accumulation can be equally deleterious.

6.2.6 Chapter Aims

The aim of this chapter was firstly to investigate whether there was any difference in the expression levels of several key inflammatory cytokines in animals given NT or CL5 siRNA following TBI. Once this had resulted in the discovery of a number of prospective altered inflammatory markers it we had the aim to determine whether inflammation was playing a significant role in either protection or exacerbating damage following TBI. To accomplish this a number of inflammatory knockout mouse lines were chosen and these

were studied as to their recovery following TBI. It was hypothesised that in the case that application of CL5 siRNA in this model of TBI was resulting in higher neuroinflammation this would uncover the result of that this increase was having.

6.3 Results

6.3.1 Inflammatory Cytokine Regulation Following Treatment with siRNA

During the course of evaluating CL5 siRNA as a potential treatment for TBI, a series of RT-PCRs were carried out on NT and CL5 siRNA-treated TBI regions measuring the expression levels of 5 inflammatory markers and growth factors. These were: CINC-1 (*Figure 6.1*), ICAM-1 (*Figure 6.2*), RANTES (*Figure 6.3*), IL-1-β (*Figure 6.4*) and NGF (*Figure 6.5*). The aim of these analyses was to elucidate if there was any significant difference between treatment groups, and so begin to discover if any of these factors might contribute to the observed improvement or if they cause negative effects in the barrier modulated animals. The choice was made to carry out these investigations at the transcript level, despite the possibility that increases at the mRNA level would not reflect increases at the protein level, as RT-PCR enabled us greater throughput in order to generate more data to arrive at an understanding of some of the broad inflammatory changes involved in these cohorts of animals. In each of these cases mRNA levels in animals given an injury and siRNA were compared with those levels in control brain regions that had not been injured or given siRNA.

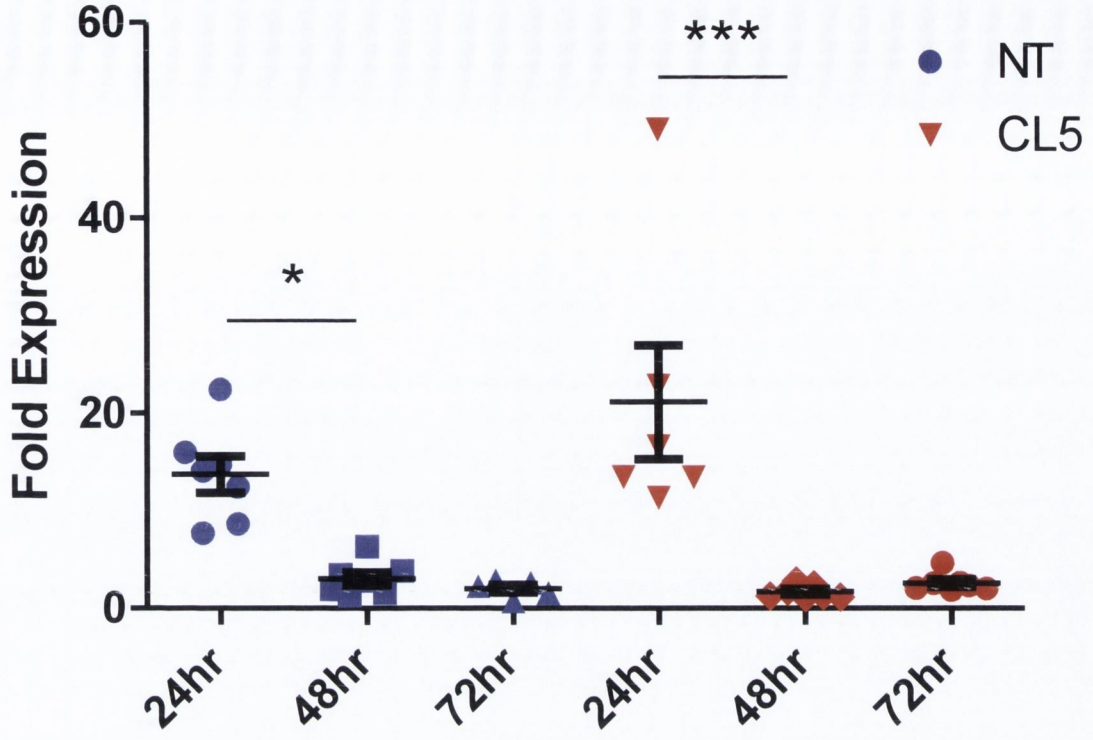

Figure 6.1: RT-PCR of CINC-1 transcript levels after TBI. *CINC-1 mRNA increases 24 h following TBI administration in both CL5 and NT animals. This level then falls significantly at 48 h in both groups, and observes no further significant change between 48 and 72 h. No significant difference is observed between CL5 and NT animals at any timepoint. All data is expressed as fold expression compared to equivalent control brain regions from two uninjured, uninjected C57 mice. (*P≤0.05, ***P≤0.001, ANOVA with Tukey's post test. NT siRNA, 24 and 48 h, n=7; NT siRNA, 72 h, n=5; CL5 siRNA, 24 h, n=6; CL5 siRNA, 48 and 72 h, n=7. Data are means and s.e.m.)*

CINC-1 transcript expression was similar in pattern between NT and CL5 siRNA-treated TBI regions, with strong increases at 24 h followed by rapid decreases at 48 h back to baseline levels observed in control animals (*Figure 6.1*). In CL5 animals the increase at 24 h was significantly greater than those in NT animals.

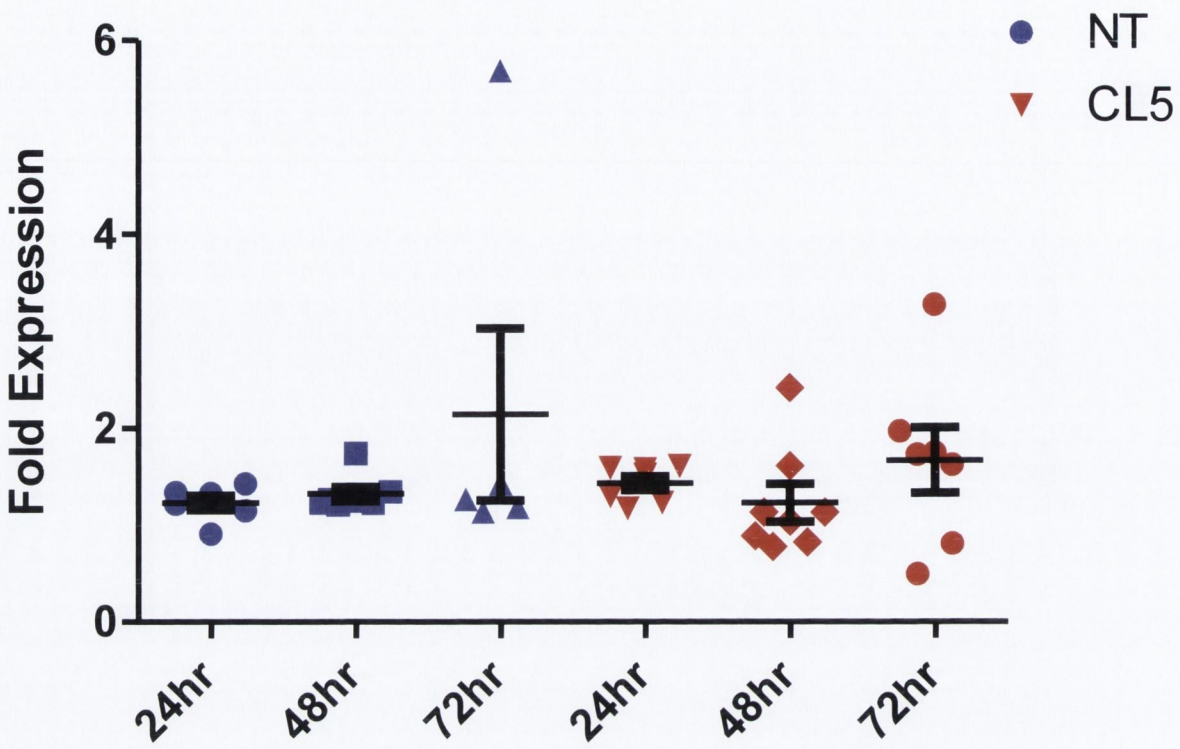

Figure 6.2: RT-PCR of ICAM-1 transcript levels after TBI. *No significant changes are observed between timepoints or between CL5 and NT groups. All data is expressed as fold expression compared to equivalent control brain regions from two uninjured, uninjected C57 mice. (P≥0.05, ANOVA with Tukey's post test. NT siRNA, 24 h, n=6; NT siRNA, 48 h, n=7; NT siRNA, 72 h, n=5; CL5 siRNA, 24 and 72 h, n=7; CL5 siRNA, 48 h, n=8. Data are means and s.e.m.)*

ICAM-1 mRNA levels, in contrast to CINC-1, did not exhibit any differences between any timepoints or treatments (*Figure 6.2*). One potentially notable result was that when 72 h CL5 measurements are compared directly to those of the uninjured, uninjected control brain tissue the 1.668-fold increase in expression is significant (*P≤0.05, Student's t-test). Therefore there may be a trending increase in ICAM-1 levels.

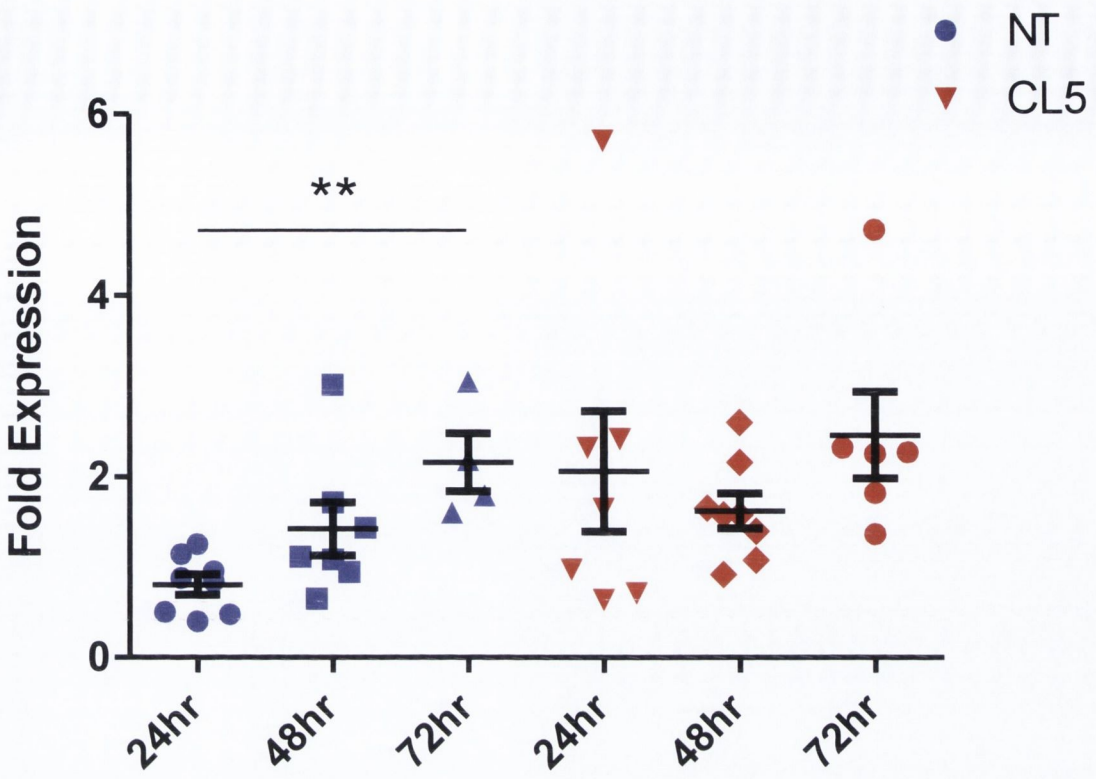

Figure 6.3: RT-PCR of RANTES transcript levels after TBI. *No significant increases occur between the three timepoints in CL5 animals, whereas in NT animals a significant increase is observed between 24 and 72 h. All data is expressed as fold expression compared to equivalent control brain regions from two uninjured, uninjected C57 mice. (**P≤0.001, ANOVA with Tukey's post test. NT siRNA, 24 h, n=8; NT siRNA, 48 h, n=7; NT siRNA, 72 h, n=4; CL5 siRNA, 24 h, n=7; CL5 siRNA, 48 h, n=8; CL5 siRNA, 72 h, n=6. Data are means and s.e.m.)*

RANTES expression does not significantly differ between NT and CL5 groups, however NT animals experience a significant increase in mRNA levels between 24 and 72 h. With levels at 72 h being similar – 2.163-fold in the NT group, 2.460-fold in the CL5 group – with no significant difference between them (*Figure 6.3*). Thus it appears that the CL5 animals reach this higher level sooner, while the NT animals reach this level more gradually from a

lower base at 24 h. In fact over this timecourse CL5 animals experience a 2.063-fold increase over controls, versus a 0.8097-fold increase in NT animals.

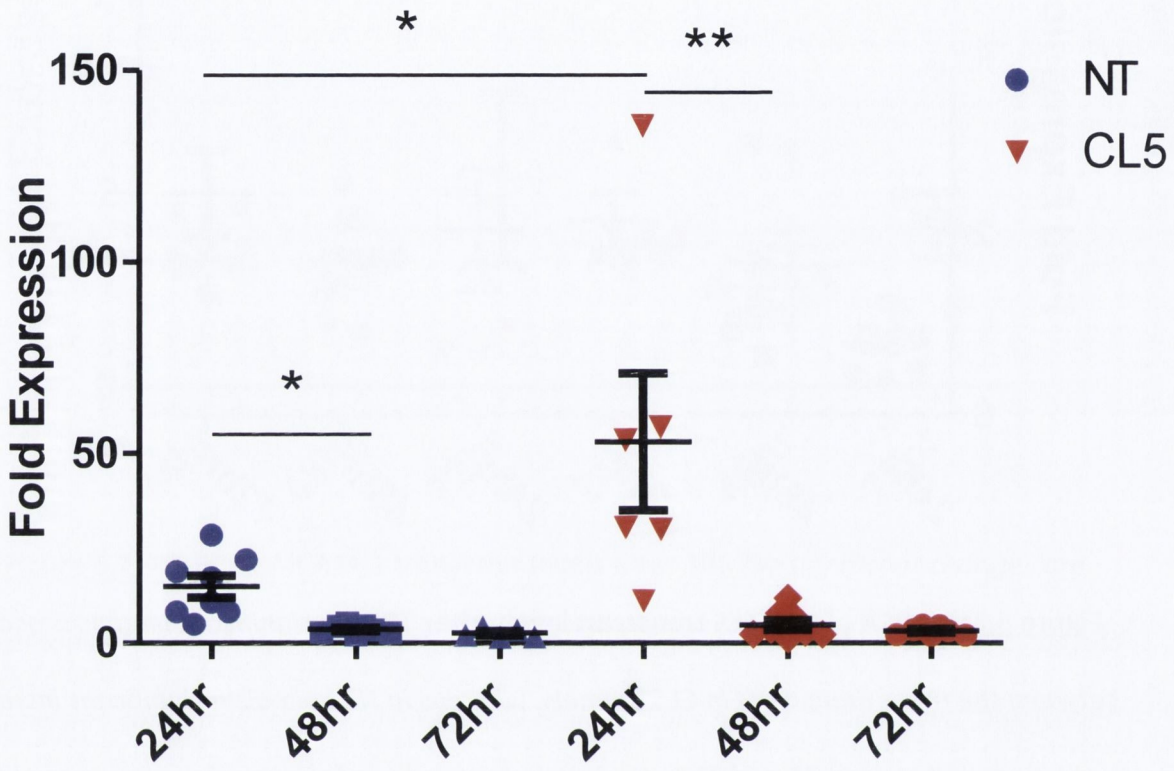

Figure 6.4: RT-PCR of IL-1β transcript levels after TBI. *IL-1-β mRNA levels are increased after 24 h, followed by a significant drop at 48 h in both CL5 and NT groups. The transcript level then remains similarly low at 72 h. The increase in the CL5 group at 24 h is significantly higher than that of the NT group, but after the reduction in expression observed at 48 and 72 h there is no longer any significant difference between them. All data is expressed as fold expression compared to equivalent control brain regions from two uninjured, uninjected C57 mice. (*P≤0.05, **P≤0.001, ANOVA with Tukey's post test. NT siRNA, 24 h, n=8; NT siRNA, 48 h, n=7; NT siRNA, 72 h, n=5; CL5 siRNA, 24 h, n=6; CL5 siRNA, 48 h, n=8; CL5 siRNA, 72 h, n=7. Data are means and s.e.m.)*

IL-1β shares a similar expression pattern following TBI to CINC-1, with marked increases in transcript levels at 24 h in both CL5 and NT groups, which then significantly fall back at 48 – 72 h (*Figure 6.4*). In the case of IL-1β the relative increase is very large, with the average 52.991-fold expression level rise in CL5 animals far outstripping the 14.920-fold increase in NT animals.

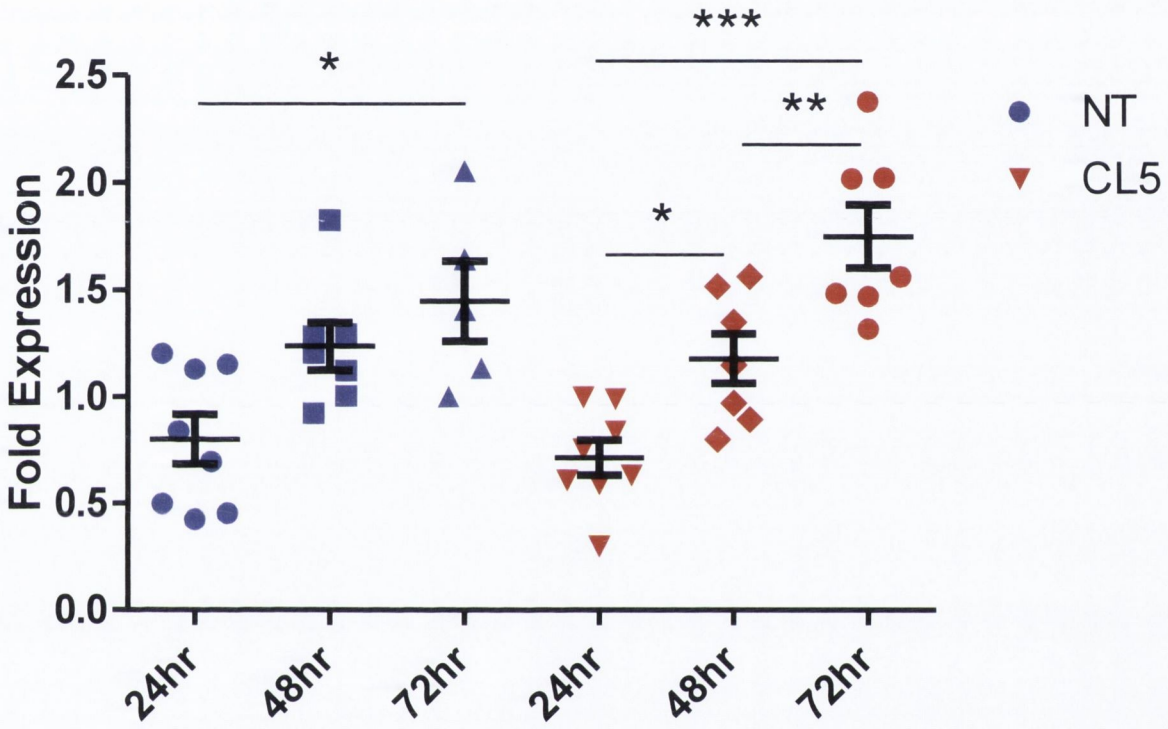

Figure 6.5: RT-PCR of NGF transcript levels after TBI. *In NT animals a significant increase in NGF mRNA level was observed from 24 – 72 h, while increases between 24 and 48 h and 48 and 72 h individually were not significant. In the CL5 group a significant increase was observed from 24 – 48 h and from 48 – 72 h, as well as a significant overall increase between 24 and 72 h. No significant increase is observed between NT and CL5 cohorts. All data is expressed as fold expression compared to equivalent control brain regions from two uninjured, uninjected C57 mice. (*P≤0.05, **P≤0.01, *** P≤0.001, ANOVA with Tukey's post test. NT siRNA, 24 h, n=8; NT siRNA, 48 h, n=7; NT siRNA, 72 h, n=5; CL5 siRNA, 24 h, n=6; CL5 siRNA, 48 h, n=8; CL5 siRNA, 72 h, n=7. Data are means and s.e.m.)*

NGF stands out from the other factors assayed in this series of experiments as it is a protective growth factor and lies downstream of inflammatory events, rather than being directly involved in inflammatory event by attracting, translocating or activating immune cells. NGF was observed to uniformly increase at each timepoint in both NT and CL5 groups, with both of these total increases being significant. There were subtle differences in the pattern of these increases however, with CL5 experiencing significant increases at both 24 – 48 h, and 48 – 72 h. This was due to NGF undergoing a greater overall increase in CL5 animals equal to 1.035-fold the level in control animals' brains, versus an increase of 0.6489-fold in the NT group (*Figure 6.5*). However no significant difference was observed between NT and CL5 cohorts.

6.3.2 Cytokine Proteome Array

The preliminary study using RT-PCR to elucidate the expression levels of certain cytokines had revealed significant differences between animals given NT and CL5 siRNA following TBI. This was then extended to assay a much wider group of cytokines by means of cytokine proteome arrays. In this experiment a small piece of membrane, in which antibodies against 40 different cytokines are embedded, was exposed to whole-tissue protein from a series of TBI timepoints and siRNA treatments. A table outlining the position of each duplicate of antibodies targeting cytokines is provided in *Table 6.1*.

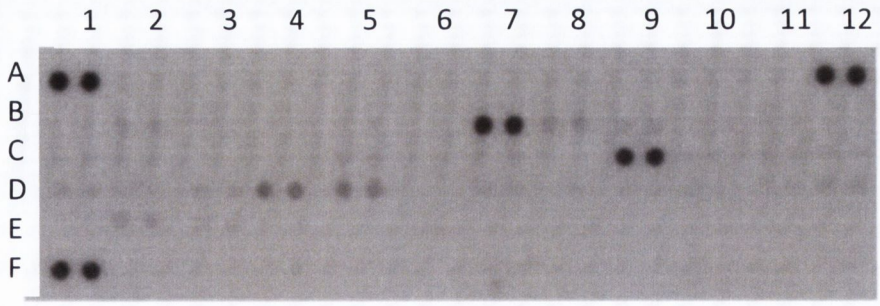

Location	Target	Location	Target
A1	Positive Control	C8	IL-12p70
A2	Blank	C9	IL-16
A3	Blank	C10	IL-17
A4	Blank	C11	IL-23
A5	Blank	C12	IL-27
A6	Blank	D1	IP-10/CXCL10
A7	Blank	D2	I-TAC/CXCL11
A8	Blank	D3	KC
A9	Blank	D4	M-CSF
A10	Blank	D5	JE/MCP-1/CCL2
A11	Blank	D6	MCP-5/CCL12
A12	Positive Control	D7	MIG/CXCL9
B1	BLC/BCA-1/CXCL13	D8	MIP-1 α/CCL3
B2	C5a	D9	MIP-1 β/CCL4
B3	G-CSF	D10	MIP-2
B4	GM-CSF	D11	RANTES/CCL5
B5	I-309/CCL1	D12	SDF-1/CXCL12
B6	Eotaxin/CCL11	E1	TARC/CCL17
B7	ICAM-1	E2	TIMP-1
B8	IFN-γ	E3	TNF-α
B9	IL-1α	E4	TREM-1
B10	IL-1β	E5	Blank
B11	IL-1ra	E6	Blank
B12	IL-2	E7	Blank
C1	IL-3	E8	Blank
C2	IL-4	E9	Blank
C3	IL-5	E10	Blank
C4	IL-6	E11	Blank
C5	IL-7	E12	Blank
C6	IL-10	F1	Positive Control
C7	IL-13		

Table 6.1: Position and target of each pair of antibodies. *Each antibody targeting a cytoking is present as a duplicate of two dots. Staining shown is purely an example.*

The comparison of cytokine protein expression in the TBI region of a C57 mouse 24 h after injury, and the same brain region in an uninjured C57 is shown in *Figure 6.6*.

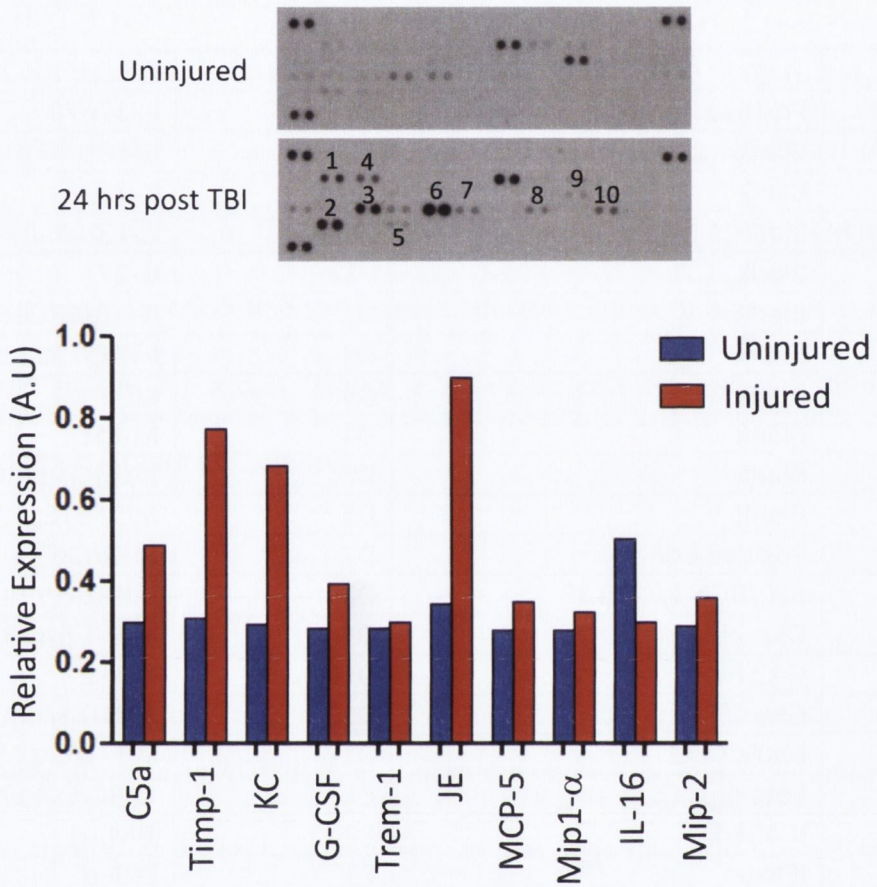

Figure 6.6: Cytokine proteome array of uninjured and injured brain tissue. *Cytokine proteome array was generated from the injured region of a C57 mouse 24 h after TBI, and from the equivalent brain region from an uninjured animal. Profiling identified the following proteins upregulated at the injury site, 1: C5a; 2: Timp-1; 3: KC; 4: G-CSF; 5: Trem-1; 6: JE; 7: MCP-5; 8: Mip1-α; 9: IL-16; 10: Mip-2 (cytokine proteome array image at top). Quantification of the expression levels was performed by measuring pixel intensity (graph above; A.U = arbitrary units of relative pixel intensity.)*

As can be seen in *Figure 6.6* (top) there were at least 10 cytokines on the proteome array that appear noticeably different. Because these arrays were carried out on protein extracted from single mice no statistical analysis could be performed, however pixel intensity from these 10 noticeably altered cytokines are also shown in *Figure 6.6* (bottom).

Following this a series of cytokine proteome arrays were carried out at a range of timepoints following TBI and NT or CL5 siRNA delivery. Findings from the 24 h timepoint are illustrated in *Figure 6.7*.

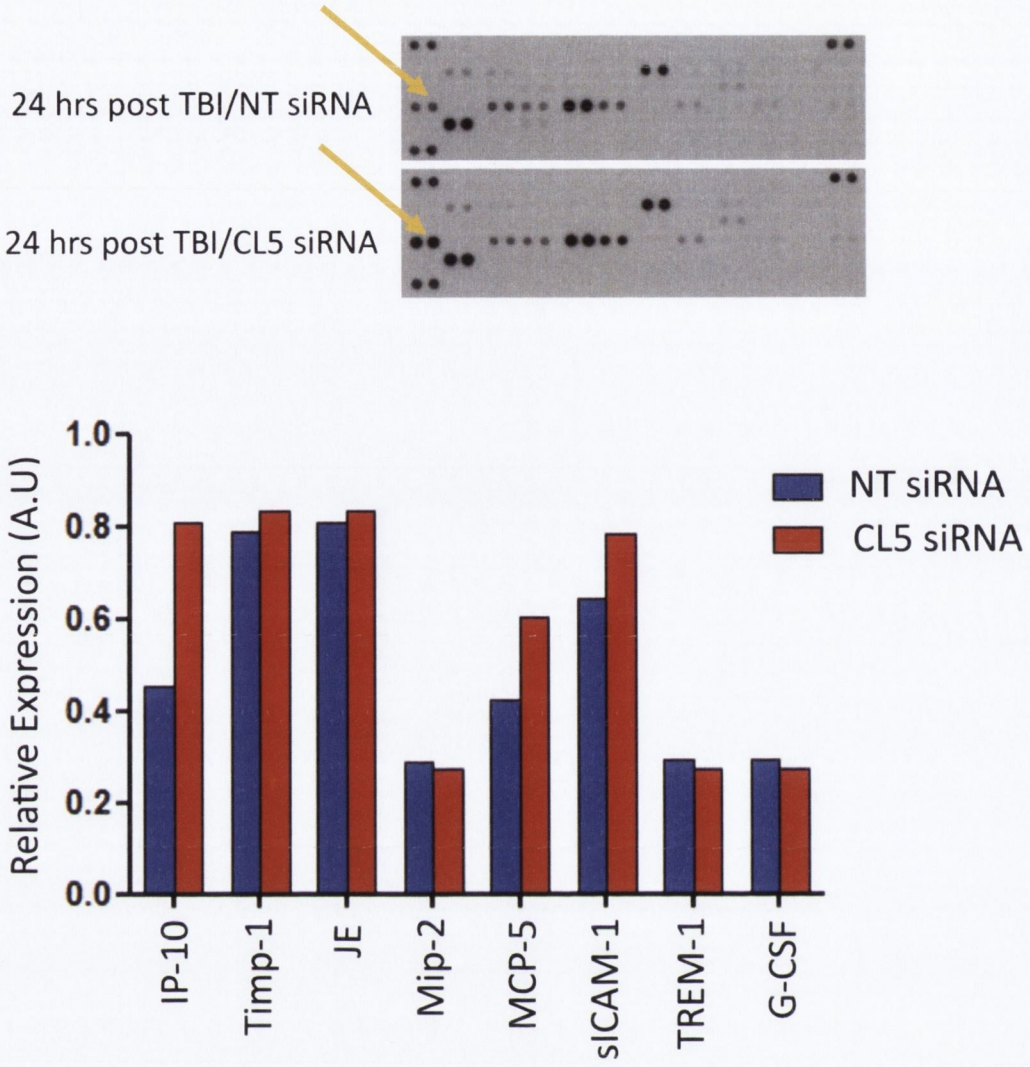

Figure 6.7: Cytokine proteome array of NT and CL5 brain tissue 24 h after TBI. *IP-10 (arrow) was increased approximately 60% in the region 24 h post-CL5 siRNA compared with NT siRNA. Levels of MCP-5 and sICAM-1 were also increased by approximately 30% (cytokine proteome array image at top). Quantification of the expression levels was performed by measuring pixel intensity (graph above; A.U = arbitrary units of relative pixel intensity.)*

In the first timepoint comparing CL5 and NT siRNA-treated TBI regions we see fewer differences than between injured and uninjured animals, but nonetheless a number of

factors that were identified in *Figure 6.6* appear to be differentially regulated in *Figure 6.7*. Most notably of these MCP-5 is upregulated by approximately 30% in the CL5 sample, as well as slight increases of Timp-1 and JE, and marginal decreases in Mip-2, TREM-1 and G-CSF. These latter, lesser observed differences in pixel intensity are too close between CL5 and NT animals to be able to hypothesise that a real difference would exist if animal numbers were higher. Two new factors, that did not demonstrate expression level differences between injured and uninjured animals, are markedly different in *Figure 6.7*. One of these, sICAM-1 is a soluble version of ICAM-1, assayed by RT-PCR in *Figure 6.2*, which did not show clear differences between groups. Finally, the strongest observed difference between the CL5 and NT TBI in this experiment was the greatly increased expression level of IP-10 (CXCL-10).

This increased IP-10 expression persisted at 48 h, although the relative increase in the CL5 sample over NT decreased at this timepoint (*Figure 6.8*) compared to 24 h (*Figure 6.7*).

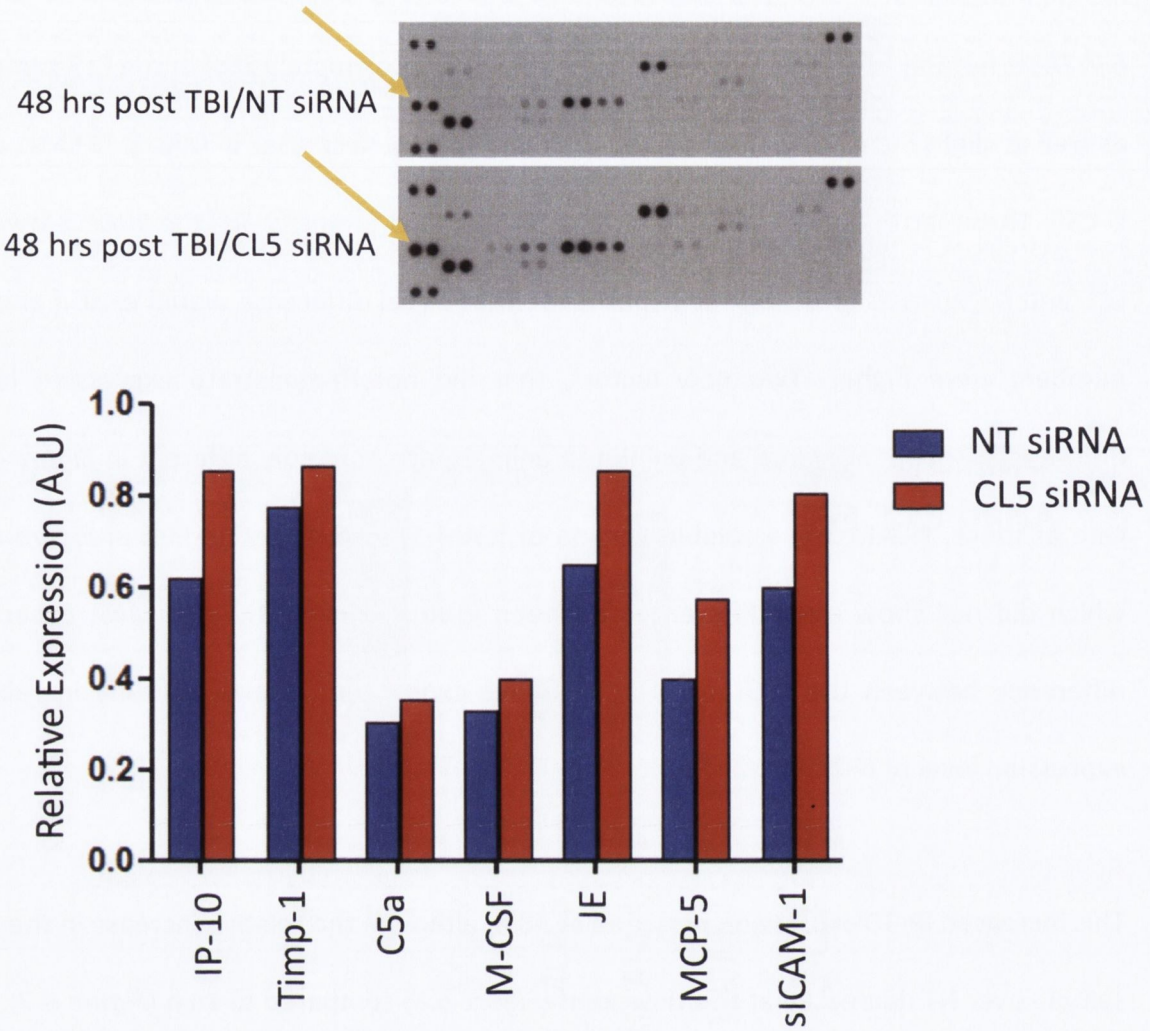

Figure 6.8: Cytokine proteome array of NT and CL5 brain tissue 48 h after TBI. *IP-10 (arrow in cytokine proteome array image at top), JE, MCP-5, and sICAM-1 were all higher in CL5 siRNA-injected mice at 48 h. Timp-1, C5a, and M-CSF were also increased to a lesser degree. Quantification of the expression levels was performed by measuring pixel intensity (graph above; A.U = arbitrary units of relative pixel intensity.)*

At this timepoint the marginal increases in levels of Mip-2, Trem-1, and G-CSF observed in the NT animal at 24 h (*Figure 6.7*) had disappeared. All other differences in cytokine levels at 24 h persisted to 48 h however, with those of JE becoming greater in relative terms in

the CL5 sample and Timp-1, MCP-5, and sICAM-1 remaining approximately equal in comparative terms to levels observed in the CL5 and NT mice at 24 h. Differences in two new factors appeared at this timepoint. C5a had been found to be expressed at a higher level in the injured brain compared to an uninjured one (*Figure 6.6*), and at 48 h post-injury the level of this factor was measured to be higher in the CL5 siRNA-treated TBI than the NT TBI (*Figure 6.8*), although to a lesser degree than in injured versus uninjured. The other differentially regulated cytokine was M-CSF, a macrophage- and microglia-proliferating factor (Smith, Gibbons et al. 2013), which had not been reported to vary in any of the previously mentioned cytokine proteome arrays. M-CSF was slightly increased in the CL5 sample relative to NT (*Figure 6.8*).

At 72 h many of the observed differences in expression had disappeared (*Figure 6.9*).

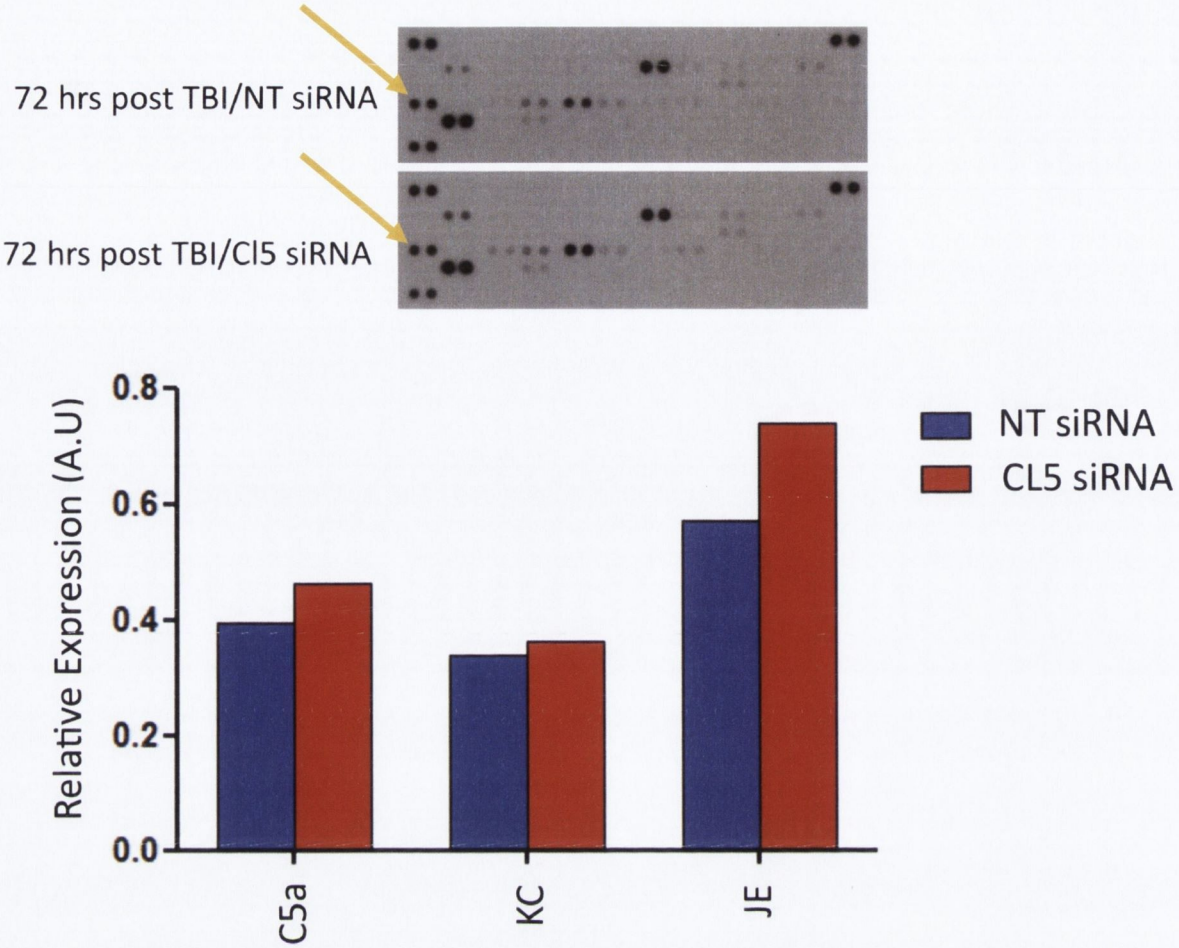

Figure 6.9: Cytokine proteome array of NT and CL5 brain tissue 72 h after TBI. *C5a and KC levels are observed to be marginally higher in the CL5 animal at 72 h, while the difference in JE expression is noticeably greater, with the CL5 animal also showing increased expression relative to NT. No difference in IP-10 expression level is observable at this timepoint (arrow cytokine proteome array image at top). Quantification of the expression levels was performed by measuring pixel intensity (graph above; A.U = arbitrary units of relative pixel intensity.)*

At this timepoint the difference observed at 48 h in C5a expression (*Figure 6.8*)) persisted, with CL5 siRNA resulting in higher expression than NT siRNA, as did the increase in JE protein levels, although to a lesser extent (*Figure 6.9*). The cytokine KC appeared to be at

a higher expression level in the CL5 mouse at 72 h, which had not been observed at 24 or 48 h (*Figure 6.7*, *Figure 6.8*). This difference is marginal however, and as in the case of Mip-2, Trem-1 and G-CSF at 24 h (*Figure 6.7*) may likely fall within the margin of error or sample to sample variation. Notably, the marked increase of IP-10 that was strikingly observed at 24 h, and to a slightly reduced degree at 48 h, is completely absent at 72 h (*Figure 6.9*).

6.3.3 Taqman Assay for IP-10 Expression

In the cytokine proteome arrays there were a series of cytokines that were observed to be differentially regulated in the mouse given CL5 siRNA following TBI versus NT siRNA. Out of these IP-10 stood out as being the most markedly increased factor (*Figure 6.7*), arrow). Together with the failure to observe any difference in the expression in IP-10 between uninjured and injured brains (*Figure 6.6*), it was decided to look further into the expression pattern of IP-10 by carrying out Taqman reverse transcription assay on the 24 and 48 h timepoints (*Figure 6.10*).

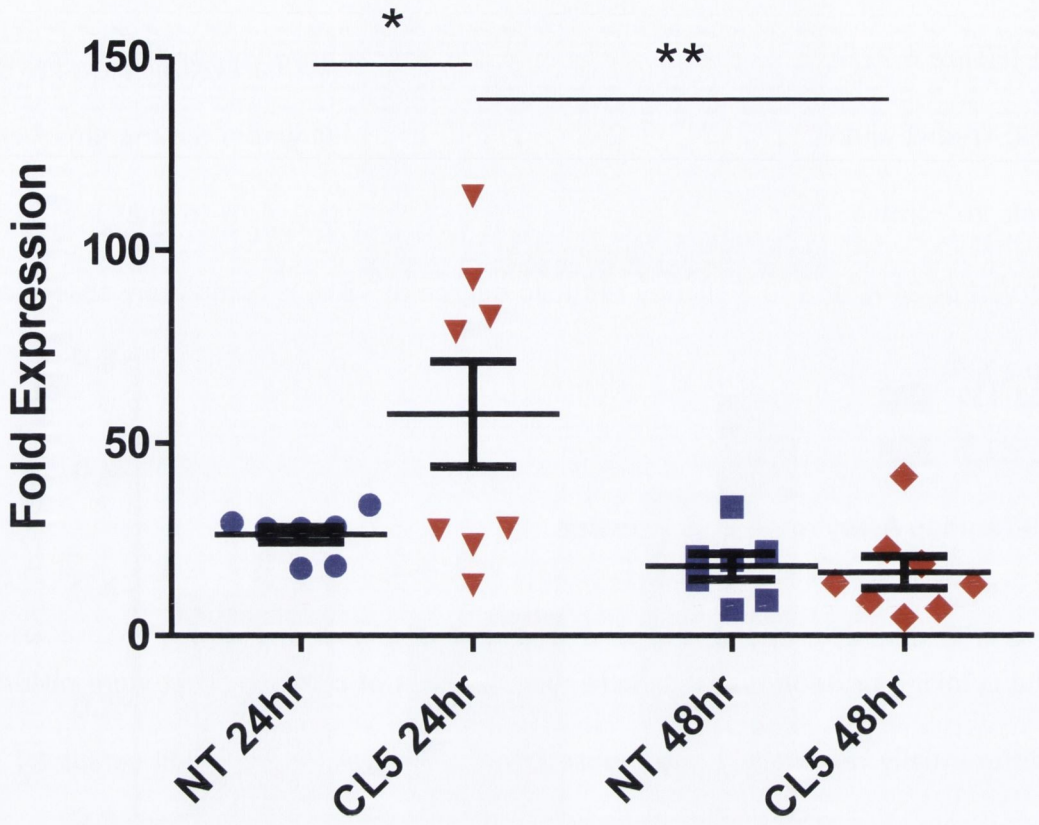

Figure 6.10: Taqman assay of IP-10 transcript levels in TBI regions. *IP-10 mRNA is significantly upregulated in CL5 animals compared to NT animals. This markedly higher IP-10 levels fell significantly to match that those in NT mice at 48 h. All data is expressed as fold expression compared to equivalent control brain regions from two uninjured, uninjected C57 mice. (*P≤0.05, **P≤0.01, ANOVA with Tukey's post test. NT siRNA, 24 h, n=8; NT siRNA, 48 h, n=7; CL5 siRNA, 24 and 48 h, n=8. Data are means and s.e.m.)*

These timepoints were chosen to match the timepoints at which IP-10 protein levels appeared to be increased (*Figure 6.7*, *Figure 6.8*). IP-10 transcript levels were found to be significantly higher in CL5 animals compared to NT animals at 24 h (*Figure 6.10*), which corresponds to the increased protein levels previously observed. At 48 h the transcript level had fallen back in CL5 animals to closely match that of NT animals, in contrast to

protein levels, which were still observed to be higher in the CL5 TBI (*Figure 6.8*). However a delay between decreased mRNA levels and corresponding changes in protein levels is a common occurrence, due to the inherent lag between protein production and its degradation. Therefore these data provide statistical significance to there being increased IP-10 expression in the TBI region at early timepoints – up to 24 h at the transcript level and 48 h at the protein level – following treatment with CL5 siRNA, and hypothetically support the other findings of the cytokine proteome arrays.

6.3.4 Traumatic Brain Injury in Caspase-1 Knockout

After a number of significant findings of differentially regulated cytokine and growth factor regulation following TBI and CL5 siRNA, most of which were increases in expression, it was still not known how these changes impact on TBI treatment with CL5 siRNA. Neuroinflammation could result in CNS damage after TBI, in which case the increases observed are deleterious but insufficient to counteract the net positive effect of CL5 siRNA. Alternatively they may have a positive benefit in the context of this model and they contribute to the observed improvement in animals following treatment. A final possibility is that neuroinflammatory events have a complex role to play following the TBI model employed here, with some factors causing damage while others are protective and promote repair, without a significant overall effect on the particular outcome measures employed in the study on TBI oedema reduction (lesion volume: *Figure 5.7*; cognitive improvement: *Figure 5.14* and *Figure 5.15*).

In order to understand the broad effects of inflammatory activation following TBI murine knockouts of key inflammatory components were used. These knockout animals would be unable to activate certain inflammatory pathways, which would result in large scale downstream effects, such as failure to produce immune maturation, proliferation and activation factors, and failure to attract immune cells to the injured region. Thus if these animals demonstrated improved or impaired recovery following TBI, measured by the same outcome measures of lesion volume and performance used for CL5 suppression, then it could be concluded that neuroinflammation is deleterious or beneficial in the context of this model of TBI.

The first knockout model chosen was the Caspase-$1^{-/-}$ mouse. Because Caspase-1 is a core component of all inflammasomes and is involved in the activation of many inflammatory responses, animals lacking the enzyme should exhibit large scale inflammatory deficiencies. Matching the hypothesis that this would have an effect after TBI, the knockouts exhibited very large differences in their lesion sizes compared with Balb/c control mice (*Figure 6.11*). Despite not being the background strain for Caspase-1 knockout animals, Balb/c controls were chosen for this study in order to enable blind assessment of their recovery, particularly in physiological and memory assays, as Caspase-$1^{-/-}$ mice are white in colour.

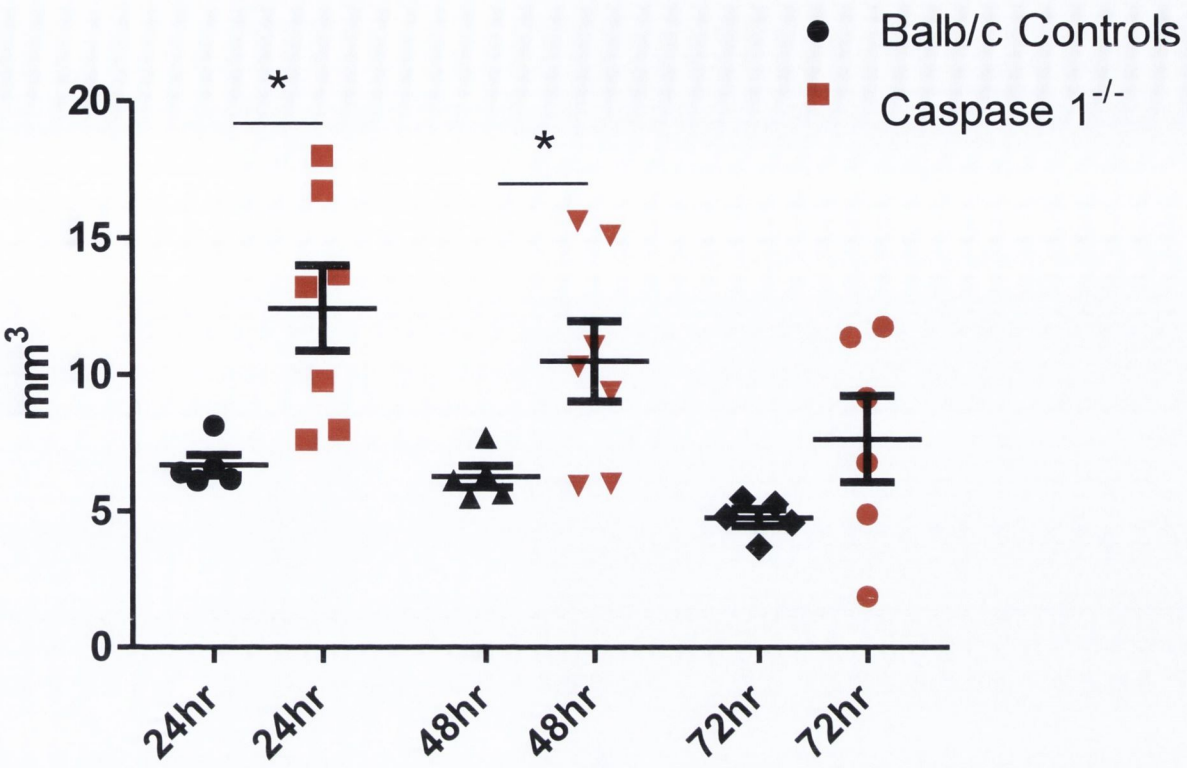

Figure 6.11: Quantification of total TBI lesion size in Caspase-$1^{-/-}$ mice and Balb/c controls. *Volumetric analyses of oedematous regions were carried out from T_2-weighted MRI images using an automatic MIPAV tool, while being blind to the treatment groups. Significant differences were found between lesion absolute lesion sizes in the two groups at 24 and 48 h. (*P≤0.05, Student's t-test. Balb/c controls, 24, 48 and 72 h, n=5; Caspase-$1^{-/-}$, 24 and 48 h, n=7; Caspase-$1^{-/-}$, 72 h, n=6. Data are mean ± s.e.m.)*

The volume of TBIs in Caspase-$1^{-/-}$ animals were so great (*Figure 6.11*) that remaining blind to treatment groups when measuring their extent was nearly impossible. This increased size was significant at 24 and 48 h, although at 72 h no significance was observed. This change at 72 h was due to an increased rate of lesion shrinkage in Caspase-$1^{-/-}$ mice.

In this chapter, in contrast to Chapter 5 (eg. *Figure 5.7*), these studies on TBI lesion volume do not use each animal's volume as its own control. This is because we are no longer purely assessing TBI outcome, but instead the absolute values for lesion volume are of interest as they may differ between mice of different genetics backgrounds from the offset. This was hypothesised to be unlikely in the case of siRNA-treated animals used previously due to their identical genetic background and evidence that the barrier-modulating effect of CL5 siRNA is strongest at timepoints later than 24 h (Campbell, Kiang et al. 2008; Campbell, Nguyen et al. 2009).

Because of the disappearance of this significant size difference it was not clear if longer term outcome measures would demonstrate sustained deleterious effects of Caspase-1 absence. It was possible that acutely increased oedema volume could hypothetically be replaced by improved recovery in the medium and long term, and so assays for later physiological recovery were undertaken, starting with NSS (*Figure 6.12*).

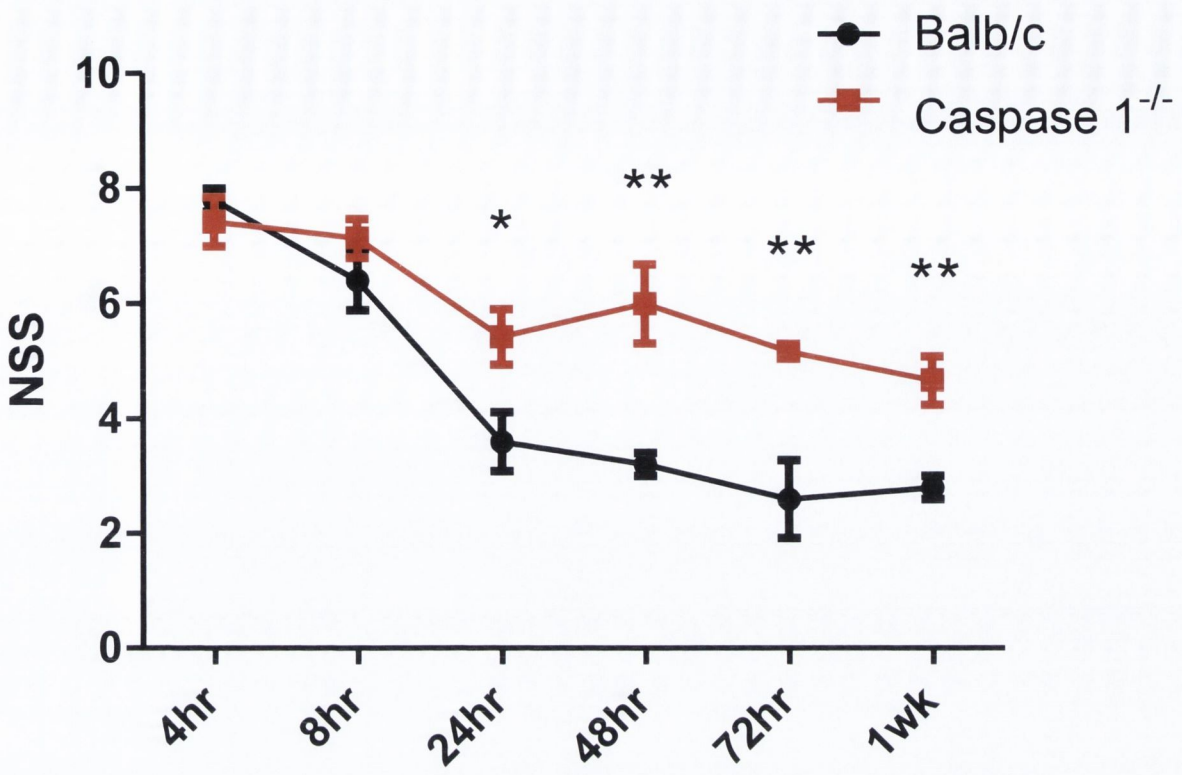

Figure 6.12: **NSS results for Caspase-1$^{-/-}$ mice and Balb/c controls after TBI.** *Significantly impaired NSS performance was observed in Caspase-1$^{-/-}$ animals compared with Balb/c controls from 24 h up to 1 week post-injury. NSS tests were carried out blind to treatment group throughout the timepoints to prevent bias. (*P≤0.05 at 24 h, **P≤0.01 at 48 h – 1 week; Student's t-test. Balb/c controls, n=5; Caspase-1$^{-/-}$, 4 – 48 h , n=7; Caspase-1$^{-/-}$, 72 h and 1 week, n=6. Data are mean ± s.e.m.)*

NSS results shown above (*Figure 6.12*) support the previous finding of worse outcome following TBI in Caspase-1$^{-/-}$ animals (*Figure 6.11*). In this test of motor and behavioural responses Caspase-1$^{-/-}$ mice demonstrated impaired performance from 24 h up to the end of the assay at 1 week post-injury. This appeared to indicate that the initially far worse oedema volumes in knockout animals were sufficient to cause sustained impairments up to at least 1 week following TBI, despite an increased rate of recovery of this TBI

characteristic in comparison with Balb/c controls. This was further backed up by deaths in the Caspase-$1^{-/-}$ group, which lost 3 out of 7 animals during the course of the 23 days in which they were studied, during which no Balb/c control mice died.

A further test of recovery following TBI that was used on these cohorts of animals was the T-maze test of short-term memory (*Figure 5.15*). In this test uninjured animals were used in order to ensure that there were no significant differences in the performances of healthy Caspase-$1^{-/-}$ and wild-type Balb/c mice (*Figure 6.13*).

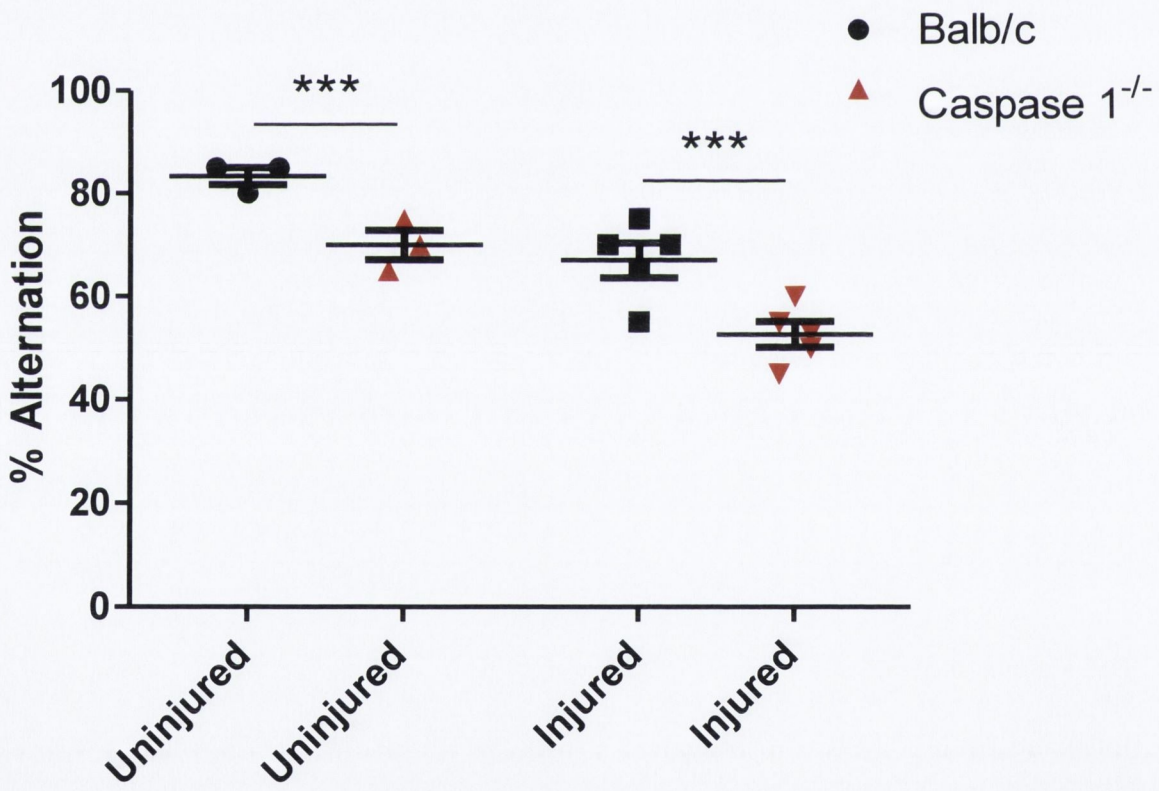

Figure 6.13: T-maze results for Caspase-$1^{-/-}$ mice and Balb/c controls after TBI. *T-maze test was administered over the course of one week, three weeks following TBI administration. (***P≤0.001, Student's t-test. Uninjured Balb/c, n=3; Uninjured Caspase-$1^{-/-}$, n=3; Injured Balb/c, n=5; Injured Caspase-$1^{-/-}$, n=5. Data are mean ± s.e.m.)*

As can be seen in Figure 6.13, Caspase-$1^{-/-}$ mice three weeks after TBI perform significantly worse on T-maze than Balb/c mice with TBI. In fact, with an alternation rate of 52.588%, mice lacking Caspase-1 are barely above the random alternation rate of 50% that would indicate complete lack of short term special memory. However, the uninjured control and knockout mice performed noticeably and significantly differently, with control Balb/c animals alternating at a rate 16.333% higher than the Caspase-$1^{-/-}$ group, which was almost identical to the difference observed between injured cohorts of 17.412%.

This result means that the Balb/c control was the incorrect strain to use as a control for Caspase-$1^{-/-}$ animals. This invalidates the findings gathered in these experiments (Figure 6.11, Figure 6.12, Figure 6.13), and the coat colour difference between Caspase-1 knockout animals and their original C57 background strain makes the strain as a whole unreliable for this analysis.

6.3.5 Traumatic Brain Injury in IL-1R Knockout

From here on the only strains selected for use in these assays in inflammatory involvement in TBI recovery were knockout models on C57 background strains, with the characteristic dark brown coat colour of wild-type C57 mice. This ensured that controls between all groups were from the same strain, making comparisons between the performance of different knockouts of inflammatory components in relation to wild-type C57 animals possible.

The first of these to be investigated was IL-1R, the receptor for IL-1α and IL-1β (*Figure 6.14*).

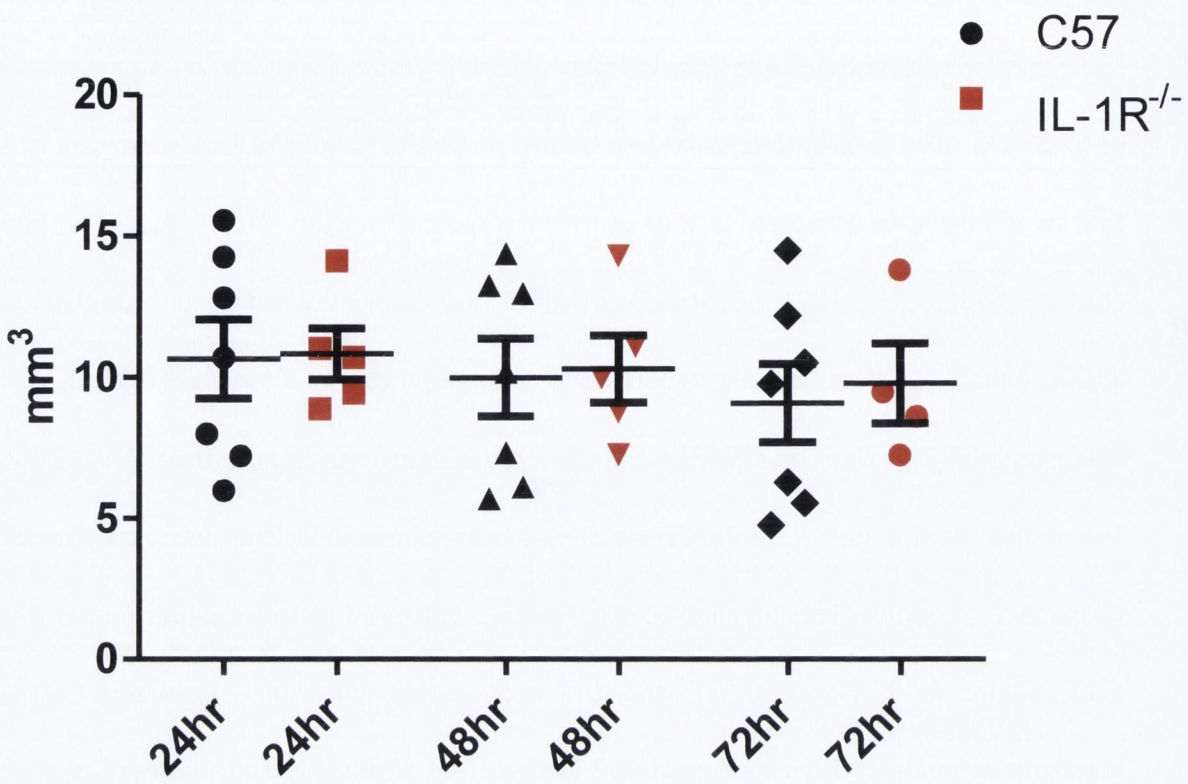

Figure 6.14: Quantification of total TBI lesion size in IL-1R$^{-/-}$ mice and C57 controls.

Volumetric analyses of oedematous regions were carried out from T_2-weighted MRI images using an automatic MIPAV tool, while being blind to the treatment groups. No significant differences in lesion size were observed at any timepoint. ($P \geq 0.05$, Student's t-test. C57 controls, 24, 48 and 72 h, n=7; IL-1R$^{-/-}$, 24 and 48 h, n=5; IL-1R$^{-/-}$, 72 h, n=4. Data are mean ± s.e.m.)

In this investigation of TBI volume in T_2-weighted MRI, there was no significant difference between IL-1R$^{-/-}$ and wild-type C57 mice between 24 and 72 h (*Figure 6.14*). A slight trend towards a slower decrease in lesion volume in knockout animals was noticeable at 72 h, but when they were calculated, the relative sizes compared with volume at 24 h (84.147% in wild-type versus 89.852% in IL-1R$^{-/-}$) were not significant, with a p value of 0.33.

In NSS tests a significant difference in performance did emerge between the two cohorts of animals (*Figure 6.15*).

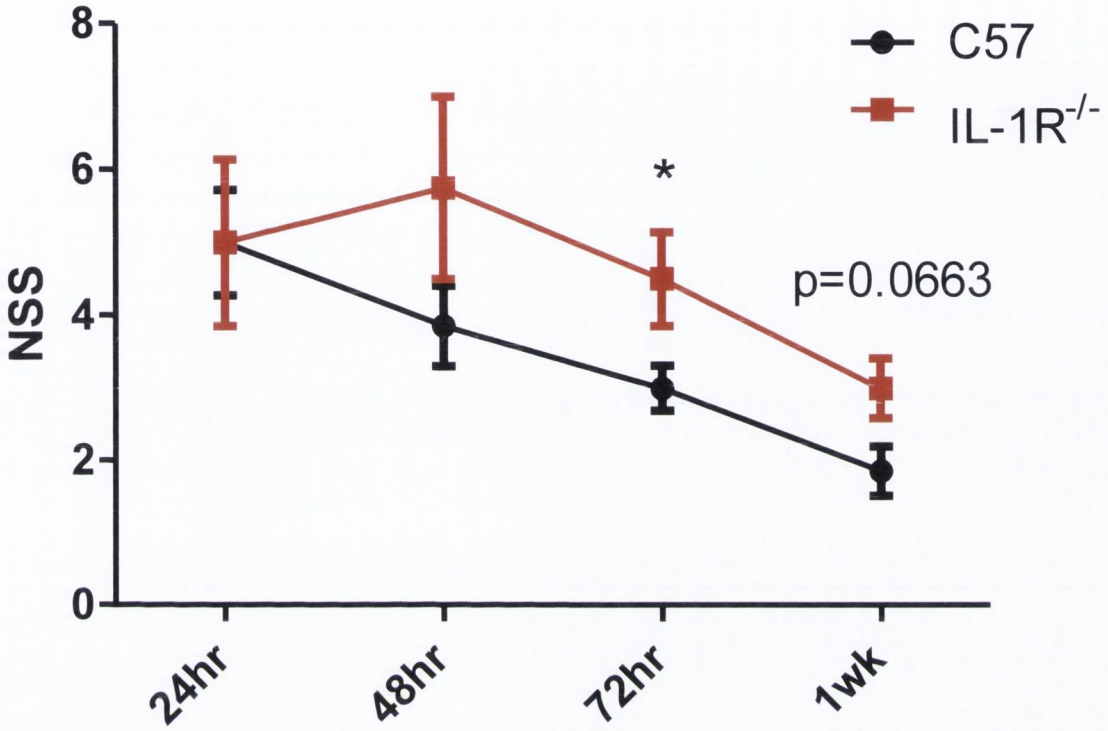

Figure 6.15: NSS results for IL-1R$^{-/-}$ mice and C57 controls after TBI. *Significantly impaired NSS performance was observed in IL-1R$^{-/-}$ animals compared with C57 controls 72 h after TBI. Worse performance in IL-1R$^{-/-}$ mice at 1 week after injury closely approached significance, at p=0.0663. NSS tests were carried out blind to treatment group throughout the timepoints to prevent bias. (*P≤0.05; Student's t-test. C57 controls, n=7; IL-1R$^{-/-}$, 24 h, n=5; IL-1R$^{-/-}$, 48 h – 1 week, n=4. Data are mean ± s.e.m.)*

Despite not having observed significant variations IL-1R$^{-/-}$ in oedema volume (*Figure 6.14*), these animals failed an average of 1.5 of the 10 NSS tests at 72 h (*Figure 6.15*). This difference narrowed slightly at 1 week after injury, with the result being on the border of statistical significance at p=0.0663.

6.3.6 Traumatic Brain Injury in IL-18 Knockout

IL-18 knockout animals were also assayed for the same outcome measures as for IL-1R$^{-/-}$ mice; firstly for differences in oedema volume following TBI (*Figure 6.16*).

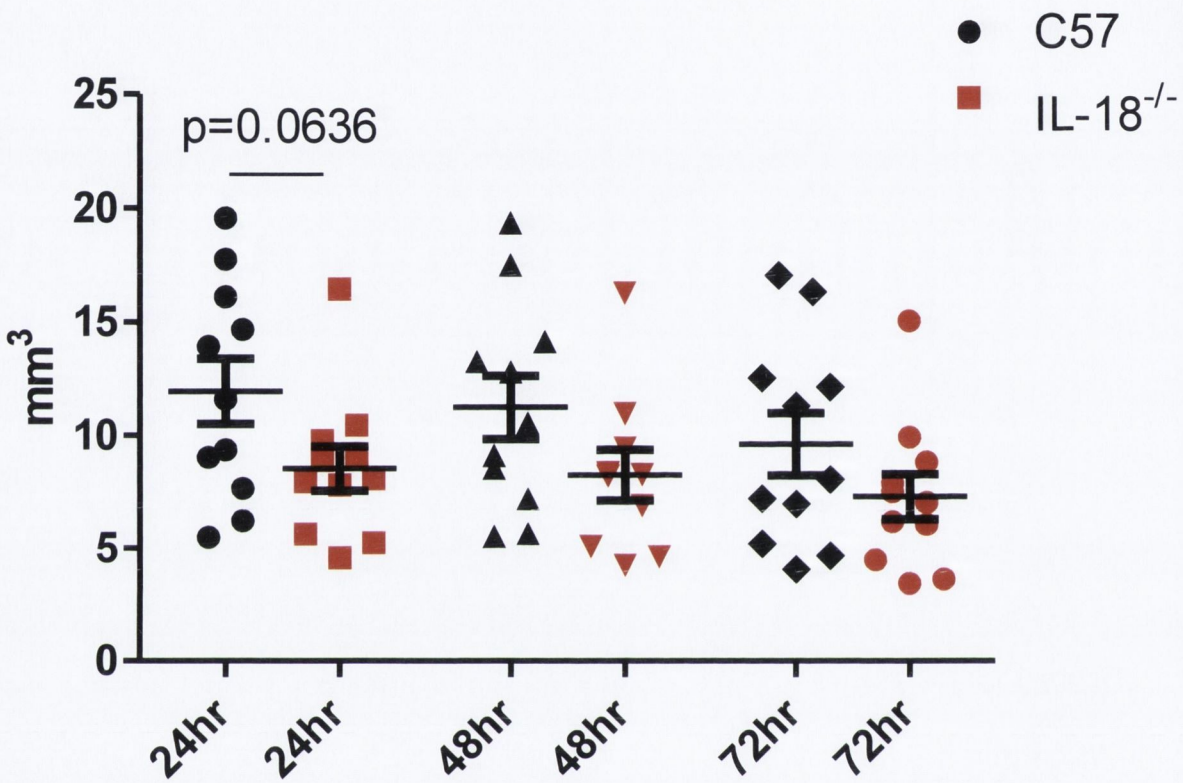

Figure 6.16: Quantification of total TBI lesion size in IL-18$^{-/-}$ mice and C57 controls.

Volumetric analyses of oedematous regions were carried out from T_2-weighted MRI images using an automatic MIPAV tool, while being blind to the treatment groups. Data illustrated here is pooled from two separate cohorts of IL-18$^{-/-}$ and wild-type C57 animals. No significant differences in lesion size were observed at any timepoint. Lower TBI volumes in IL-18$^{-/-}$ at 24 h closely approached significance, however, at p=0.0636. (P≥0.05, Student's t-test. C57 controls, 24, 48 and 72 h, n=11; IL-18$^{-/-}$, 24 and 72 h, n=11; IL-18$^{-/-}$, 48 h, n=10. Data are mean ± s.e.m.)

To generate the data shown in *Figure 6.16* two separate volumetric analyses were carried out. This was done in order to increase animal numbers after the first MRI study on this knockout, provided a tentative indication that lesion sizes were reduced in the absence of IL-18. As can be seen in *Figure 6.16* this remained the case after the addition of the second cohort of animals, with borderline significance occurring at 24 h (P=0.0636) but a lack of firm statistical clarity at any timepoint due to high TBI volume variation in both groups. The initially smaller TBIs in IL-$18^{-/-}$ animals did appear to shrink slower than those in wild-type C57 mice, reaching 78.276% and 83.277% respectively at 72 h compared to their 24 h volumes. This effect was also not statistically significant however, with a p-value of 0.1383.

NSS was carried out on one of the two cohorts of IL-18 knockout and wild-type animals, with results being shown in *Figure 6.17*.

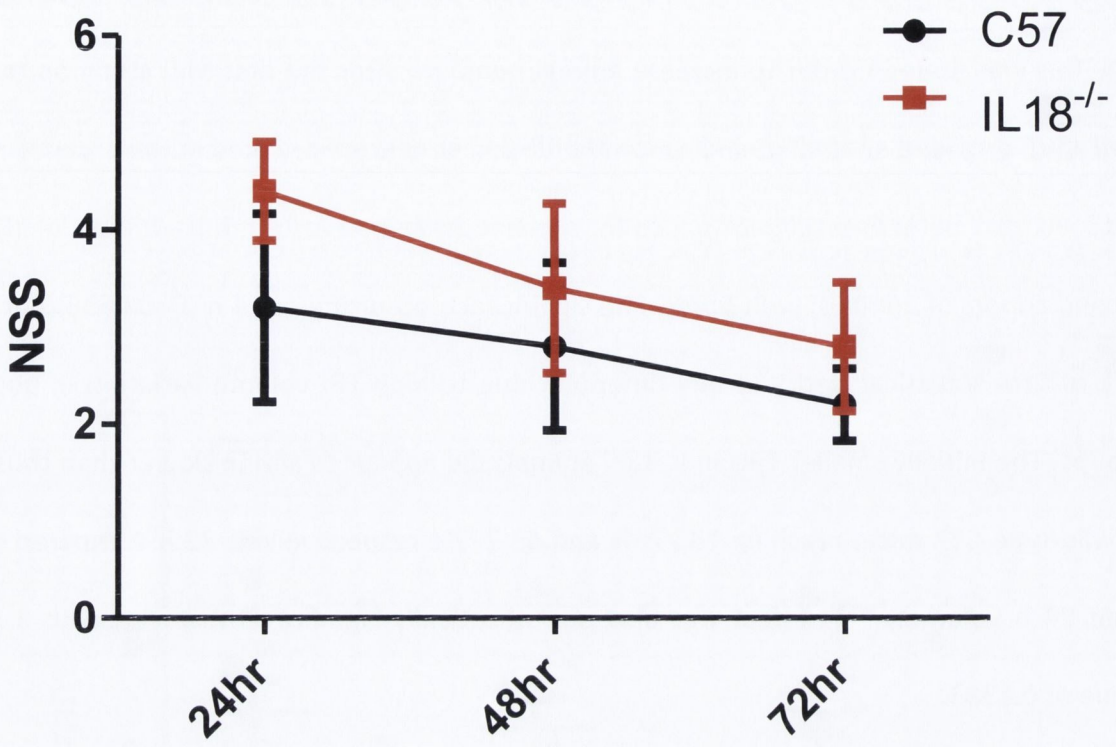

Figure 6.17: NSS results for IL-18$^{-/-}$ mice and C57 controls after TBI. *No significant differences in the number of NSS tests failed were observed at any timepoint. NSS tests were carried out blind to treatment group throughout the timepoints to prevent bias. (P≥0.05; Student's t-test. C57 controls, n=5; IL-18$^{-/-}$, n=5. Data are mean ± s.e.m.)*

As can be seen, during the NSS tests carried out IL-18$^{-/-}$ animals consistently recorded a greater number of failures (*Figure 6.17*), however these higher NSS scores were well within the margin of error and no significant differences were observed at any of the timepoints assayed.

6.3.7 Traumatic Brain Injury in NLRP3 Knockout

NLRP3 is a core component of the NLRP3 inflammasome, a major function of which is to detect and respond to DAMPs such as ATP, uric acid crystals, β-amyloid plaques and islet amyloid polypeptide (IAPP). As such the absence of this protein would be expected to have a noticeable effect on TBI recovery if the inflammasome were to play a role in this process. The results of the first assay for this potential effect are shown in *Figure 6.18*.

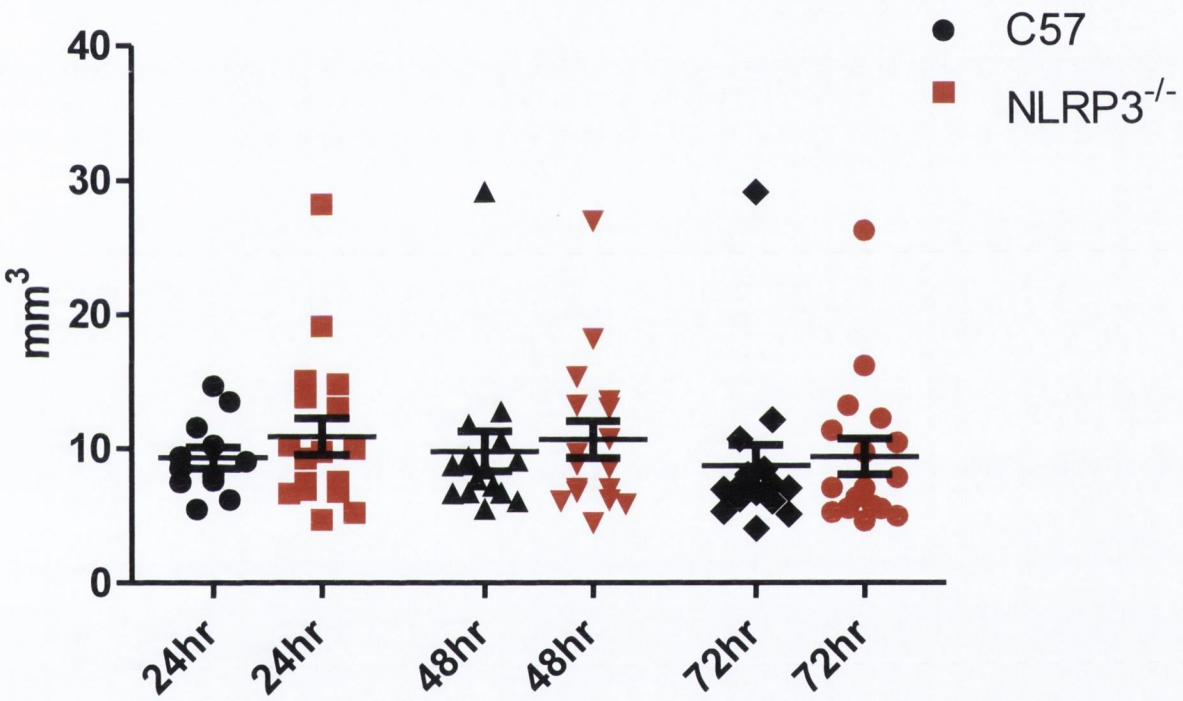

Figure 6.18: Quantification of total TBI lesion size in NLRP3$^{-/-}$ mice and C57 controls.

Volumetric analyses of oedematous regions were carried out from T_2-weighted MRI images using an automatic MIPAV tool, while being blind to the treatment groups. Data illustrated here is pooled from two separate cohorts of IL-18$^{-/-}$ and wild-type C57 animals. No significant differences in lesion size were observed at any timepoint. (P≥0.05, Student's t-test. C57 controls, 24 h, n=12; C57 controls, 48 and 72 h, n=15; NLRP3$^{-/-}$, 24 h, n=18; NLRP3$^{-/-}$, 48 and 72 h, n=17. Data are mean ± s.e.m.)

Volumetric analysis of these two experimental cohorts of animals, however, demonstrated no significant differences between NLRP3$^{-/-}$ and wild-type animals, and despite high n-numbers, average lesion sizes were very close between the strains (*Figure 6.18*).

Further tests were undertaken on one of the cohorts of NLRP3$^{-/-}$ and wild-type mice, with NSS results being displayed in *Figure 6.19*.

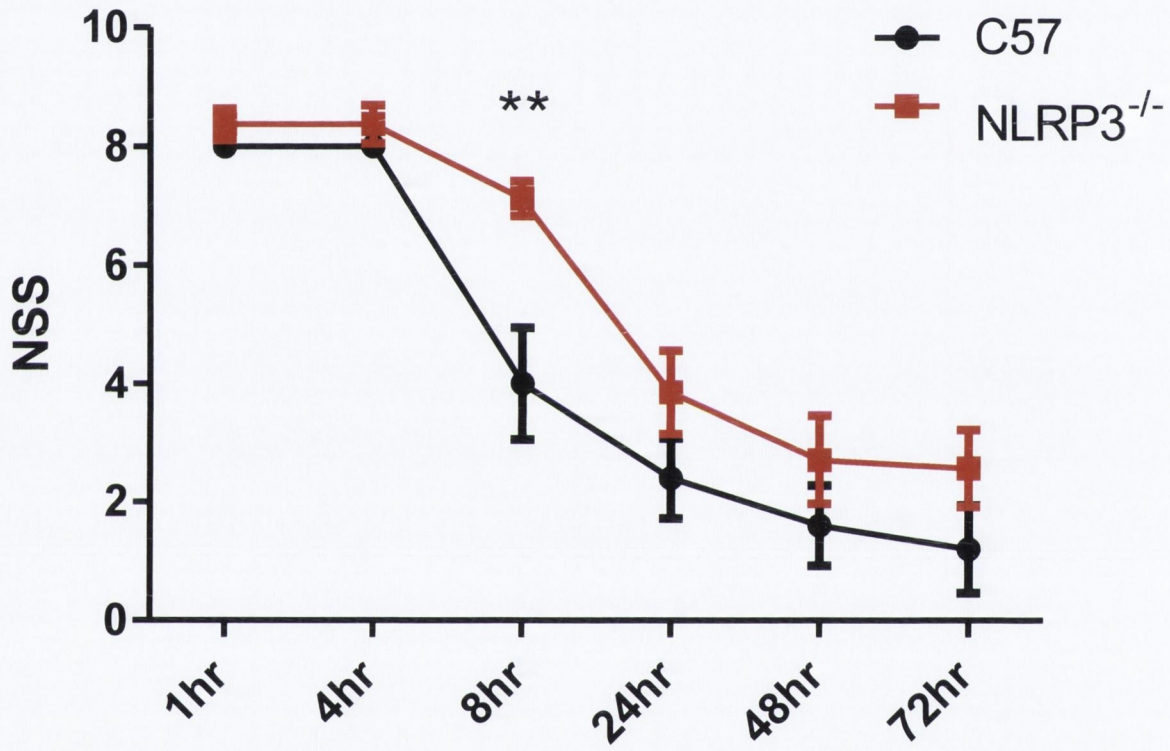

Figure 6.19: NSS results for NLRP3$^{-/-}$ mice and C57 controls after TBI. *Significantly impaired NSS performance was observed in NLRP3$^{-/-}$ animals compared with C57 controls 8 h post-injury. NSS tests were carried out blind to treatment group throughout the timepoints to prevent bias. (**P≤0.01; Student's t-test. C57 controls, n=5; NLRP3$^{-/-}$, 1 – 8 h, n=8; NLRP3$^{-/-}$, 24 – 72 h, n=7. Data are mean ± s.e.m.)*

As in the case of IL-18$^{-/-}$ (*Figure 6.17*), NLRP3$^{-/-}$ animals recorded higher numbers of failed NSS tests, however in this case there was one timepoint, 8 h post-injury, at which a

marked and significant difference from wild-type animals was observed (*Figure 6.19*). Interestingly, this is highly reminiscent of the improved NSS scores of animals given CL5 siRNA at 8 h compared with NT animals (*Figure 5.14*).

It was decided to extend the testing of this cohort of animals to include a T-maze test three weeks after injury (*Figure 6.20*).

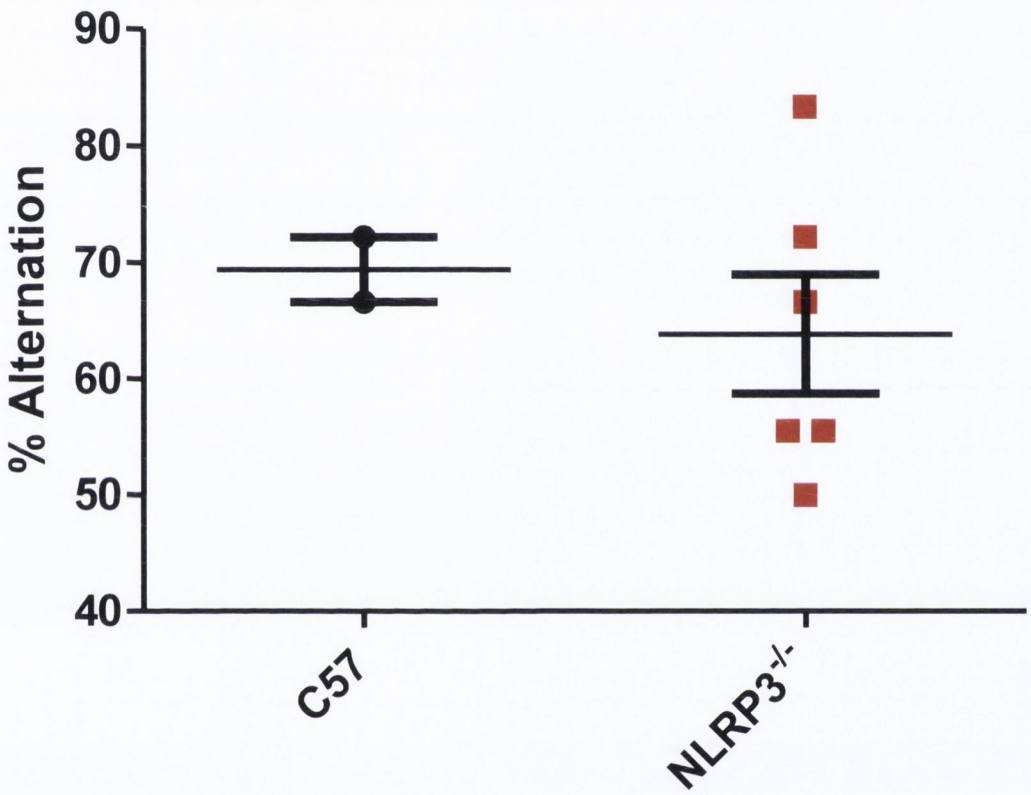

Figure 6.20: T-maze results for NLRP3$^{-/-}$ mice and C57 controls after TBI. *T-maze test was administered over the course of one week, three weeks following TBI administration. No significant difference in alternation rates was observed. (P≥0.05, Student's t-test. C57 controls, n=2; NLRP3$^{-/-}$, n=6. Data are mean ± s.e.m.)*

There was a cluster of three NLRP3$^{-/-}$ animals that demonstrated alternation rates of close to 50% over the week's testing, however, with the other three individuals performing at

or higher than the level observed in wild-type controls there was no significant impairment present in the group as a whole.

Overall results in NLRP3$^{-/-}$ animals are tentative, and do not appear to demonstrate a strong role for the NLRP3 inflammasome – the primary inflammasome believed to be involved in sterile inflammatory events – in TBI recovery.

6.3.8 Traumatic Brain Injury in ASC Knockout

The final inflammatory factor assayed was the inflammasome scaffolding protein ASC. This protein is similar to NLRP3 in so far as without it the inflammasome cannot assemble into the large, multi-protein complex which can then cleave caspase-1. The difference, however, is that ASC performs this function for a number of inflammasomes. To date the inflammasomes that are reported to be reliant on ASC are: NLRP1, NLRP3, AIM2, and possibly IPAF.

As in the case of the other inflammatory proteins studied in this way, the first step was to measure volumetric changes in TBI oedema by T_2-weighted MRI (*Figure 6.21*).

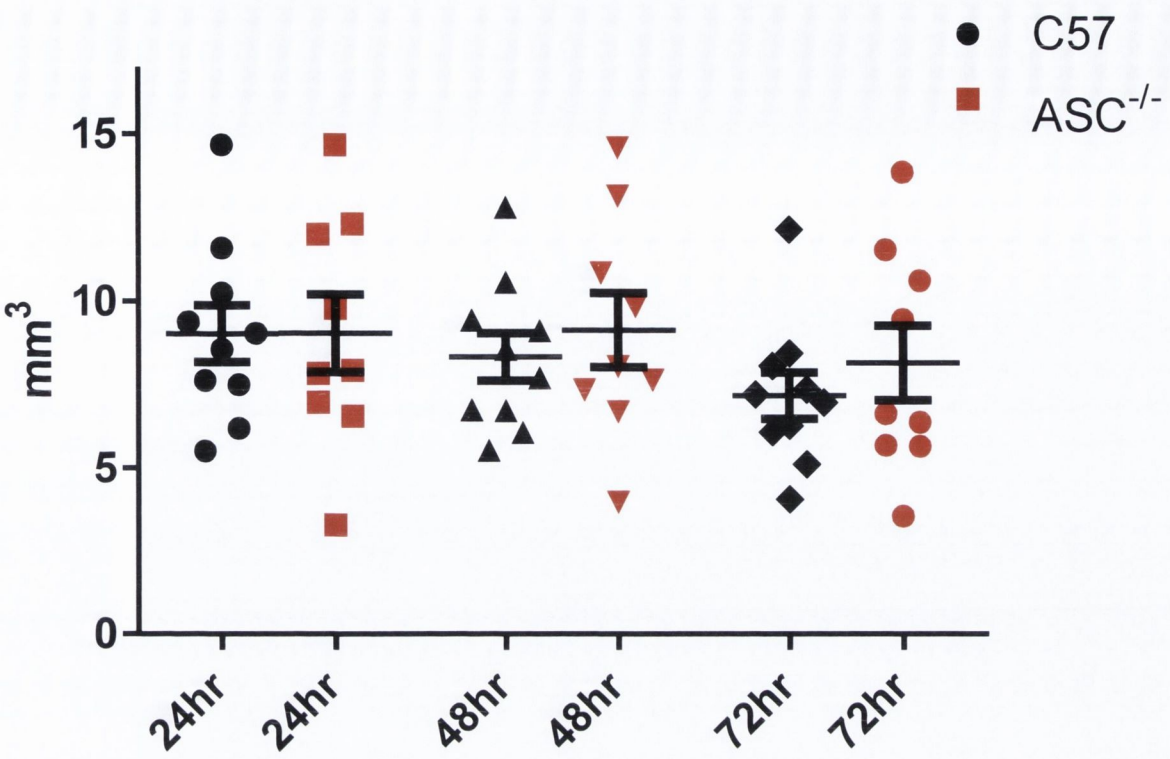

Figure 6.21: Quantification of total TBI lesion size in ASC$^{-/-}$ mice and C57 controls.

Volumetric analyses of oedematous regions were carried out from T_2-weighted MRI images using an automatic MIPAV tool, while being blind to the treatment groups. No significant differences in lesion size were observed at any timepoint. ($P \geq 0.05$, Student's t-test. C57 controls, n=10; ASC$^{-/-}$, n=9. Data are mean ± s.e.m.)

As is reported in *Figure 6.18* for NLRP3$^{-/-}$ animals there were no statistically significant differences reported between ASC$^{-/-}$ and wild-type mice in respect to total TBI lesion volume (*Figure 6.21*).

When the change in lesion volume over time, i.e. compared with the 24 h volume, is isolated and analysed independently then you do observe a significantly impaired rate of recovery in the ASC knockout animals (*Figure 6.22*).

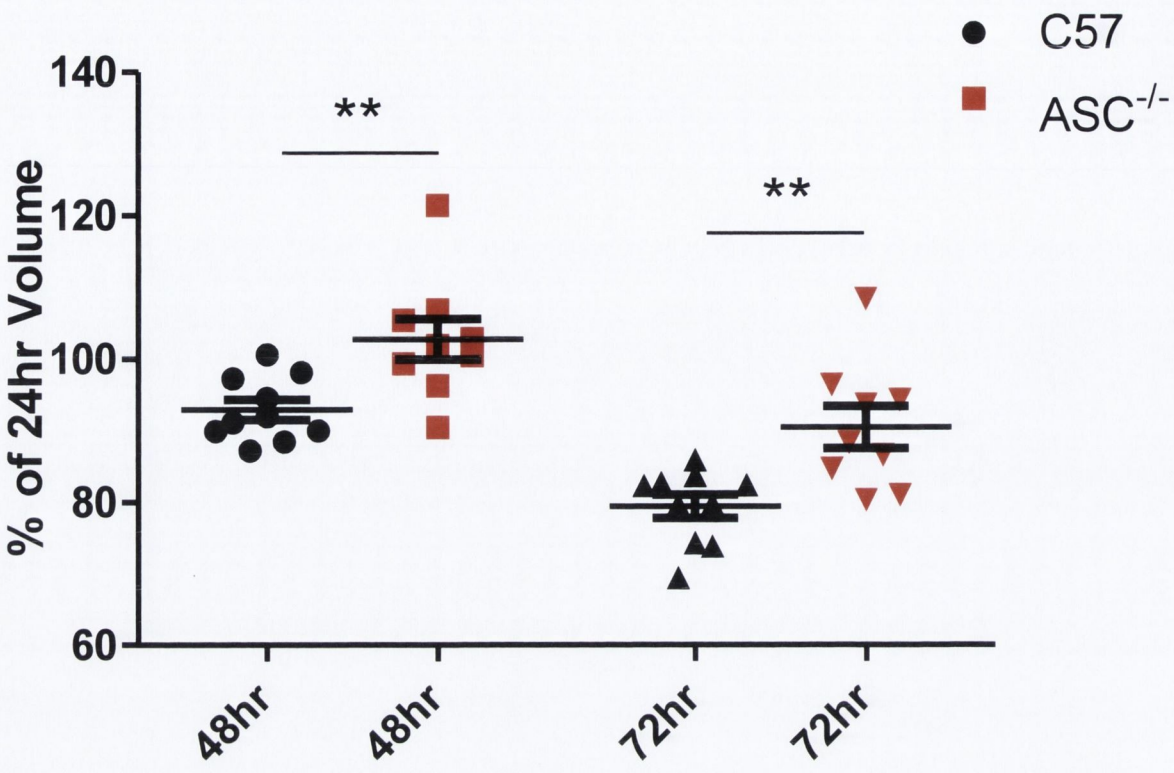

Figure 6.22: Traumatic brain injury volume over time in wild-type (C57) and ASC$^{-/-}$ mice.

*Lesions in wild-type mice shrunk significantly faster at both 48 and 72 h, compared with their size at 24 h. (**P≤0.01, Student's t-test. C57 controls, n=10; ASC$^{-/-}$, n=9. Data are mean ± s.e.m.)*

As can be seen in *Figure 6.22* the marked difference between knockout and wild-type animals emerged when the data was reanalysed to focus on change in volume over time, rather than absolute lesion size.

In order to discover if this or another effect of ASC absence effected an impact on the physiological and behavioural recovery of mice, NSS testing was carried out from the 24 h timepoint up to 1 week (*Figure 6.23*).

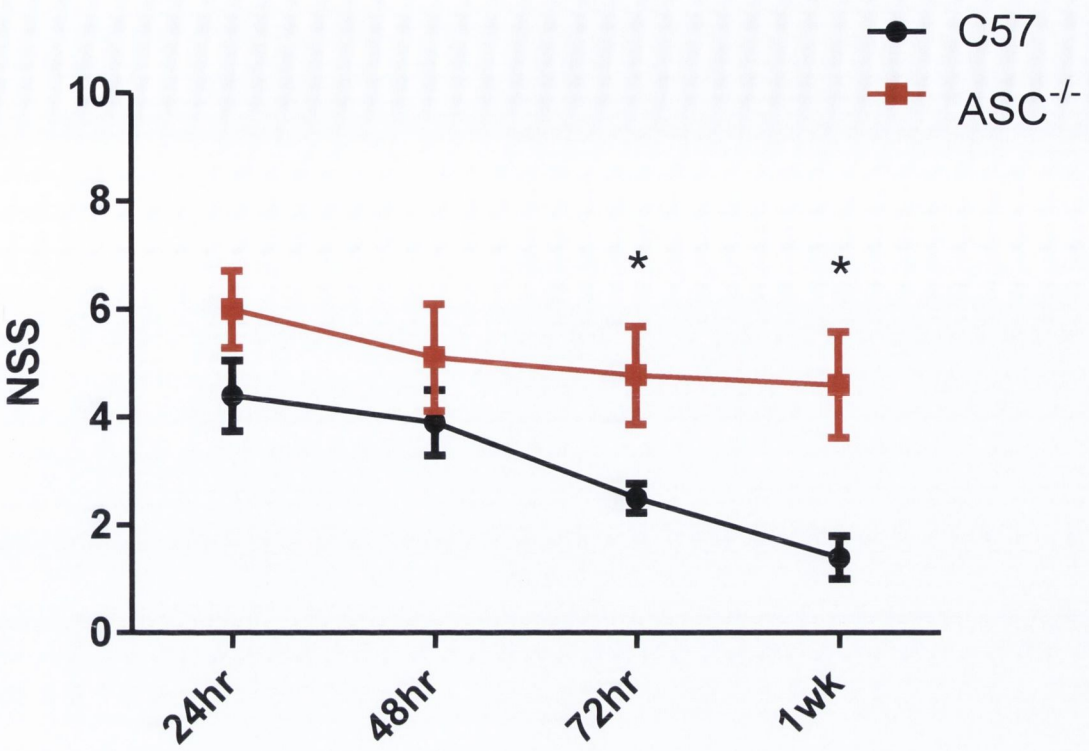

Figure 6.23: NSS results for ASC$^{-/-}$ mice and C57 controls after TBI. *Significantly impaired NSS performance was observed in ASC$^{-/-}$ animals compared with C57 controls at 72 h post-injury and remained present at 1 week. NSS tests were carried out blind to treatment group throughout the timepoints to prevent bias. (*P≤0.05; Student's t-test. C57 controls, 24 – 72 h, n=10; C57 controls, 1 week, n=5; ASC$^{-/-}$, 24 – 72 h, n=10; ASC$^{-/-}$, 1 week, n=6. Data are mean ± s.e.m.)*

NSS showed deficient recovery in ASC$^{-/-}$ animals, particularly after 48 h post-TBI. In fact from 48 h onward average NSS scores in the ASC$^{-/-}$ group only improved from 5.1 to 4.6, while during the same period wild-type mice had progressed from failing an average of 3.9 tests at 48 h to only 1.4 at 1 week following injury (*Figure 6.23*).

None of the other inflammatory factors assayed in the course of these experiments had demonstrated an effect on the rate of TBI shrinkage, and other effects were limited to

borderline significant or single timepoint differences in NSS. Therefore the clear, unambiguous results illustrated here provide a compelling case for a role for ASC in recovery from TBI.

6.4 Discussion

In the previous chapter, Chapter 5, the successful improvement in outcome in mice with cold-induced TBIs was demonstrated. Following on from this a small set of experiments was planned to ascertain whether the expression levels of a number of prominent cytokines were altered following delivery of CL5 or NT siRNA to TBIs in wild-type C57 mice.

The most notable differences between these treatment groups occur in IL-1β (*Figure 6.4*) and NGF (*Figure 6.5*) expression. IL-1β was the only cytokine to be expressed at a significantly higher level in one group compared with the other, with this occurring at 24 h in CL5-suppressed animals. IL-1β is produced in microglia and astrocytes following damage to the brain (Pearson, Rothwell et al. 1999), and the protein is an excellent example of an inflammatory molecule that demonstrates the often confusing duality of inflammation in TBI. This is observed in in vivo studies that have found improvements in the outcome of animals with TBI following IL-1β neutralisation (Clausen, Hanell et al. 2011) and also by its overexpression (Lu, Wu et al. 2007).

One interesting way in which IL-1β could have a beneficial effect in the cold-induced model of TBI in this study, if it does, is through AQP-4. AQP-4 is a water transport

expressed on glial cell membranes, particularly where they come into direct contact with blood vessels or brain meninges (Nielsen, Nagelhus et al. 1997). The highly polarized expression pattern of this transport protein means that it is positioned to regulate water flow between the brain and the blood and CSF. IL-1β leads to increased AQ-4 expression (Laird, Sukumari-Ramesh et al. 2010), and AQ-4 expression has been reported to be beneficial in cases of vasogenic oedema (Papadopoulos and Verkman 2007) – the predominant form of oedema in the cold-induced model of TBI. Another study reported that when sulforaphane was given to animals that had been administered TBI, the compound led to an increase in AQ-4 expression and a subsequent reduction in water content at the site of injury (Zhao, Moore et al. 2005). If IL-1β had a similar effect to the sulforaphane this could be highly relevant to the reduction in lesion volume and the improvement in neurological function observed, especially as IL-1β is expressed extremely early and highly following TBI.

The observation of higher IL-1β in TBI regions at 24 h in CL5 animals (*Figure 6.4*), is evidence of a further early effect of CL5 siRNA, before it is expected to have modulated the BBB for a significant period of time. This data is in addition to the previously illustrated finding that CL5 siRNA-treated mice exhibited improved NSS performance as little as 8 h after TBI and siRNA (*Figure 5.14*). These early effects could be independent of barrier modulation and instead could be due simply to the presence of the siRNA, and that the CL5 siRNA simply had a larger effect than NT siRNA in the case of certain factors. One issue with respect to this is that control animals that were given neither injuries nor siRNA were used to measure baseline expression levels of these factors in the brain. Animals given CL5 siRNA or NT siRNA in the absence of TBI would arguably have

controlled better for the effect on cytokine levels of CL5 siRNA in conjunction with TBI. However, it was felt that as it was the use of CL5 siRNA as a treatment for TBI that was being investigated, and after observing a total lack of IFN-α expression or TLR activation in response to the siRNA (*Figure 3.11* and *Figure 3.12*), it was felt that animals given NT siRNA and TBI, as well as animals lacking any treatment, were appropriate controls. As was discussed in the previous chapter, permeability to low molecular weight compounds was already observed at 24 h (*Figure 3.8*). For a molecule as small as water (18 Da) even marginal decreases in CL5 protein concentration at very early timepoints are likely to have a large effect, and this hypothesis is supported by the observed decreased in TBI region water content in CL5 animals (*Figure 5.8*). Therefore a direct relationship between the BBB modulating effects of the CL5 siRNA and the altered cytokine levels observed in these experiments is possible. Also, due to the aforementioned microarray data for CL5 siRNA, as well as histopathological screening that did not observe any inflammatory responses, CL5 siRNA is not believed to activate such a response by itself (Campbell, Nguyen et al. 2009; Campbell, Hanrahan et al. 2012).

The increase in NGF expression in CL5 animals is sharper than that observed in NT animals, demonstrating a 1.035-fold increase in the injured region, versus an increase of 0.6489-fold between 24 and 72 h, although differences between the groups do not reach significance (*Figure 6.5*). IL-1β stimulates the release of NGF by astrocytes (Juric and Carman-Krzan 2001), and therefore the observed increase in the level of IL-1β (*Figure 6.4*) could explain the greater rate of increase in NGF. A presence of higher quantities of NGF would have positive implications for neuronal survival following TBI, with the growth factor having been reported to display positive effects in a number of models of brain

injury (Tanaka, Tsukahara et al. 1994; Zhou, Chen et al. 2003; Saito, Narasimhan et al. 2004). Interestingly IL-1β and NGF have been observed to act synergistically to decrease neuronal cell death (Strijbos and Rothwell 1995). However, as mentioned the difference in the rate of change of NGF between NT and CL5 animals is not significant, and overall there is no significant difference between the groups with respect to NGF expression.

It is not clear whether higher IL-1β expression is positive or negative with respect to outcome following TBI. It is possible that neurons did undergo an increased level of damage due to higher IL-1β expression in particular in mice given CL5 siRNA, but that decreases in cerebral oedema (*Figure 5.7* and *Figure 5.8*) were sufficient to outweigh these effects and lead to the net benefits of treatment that were observed (*Figure 5.14* and *Figure 5.15*). These results of the NSS and T-maze tests indicate that any potential negative effect of increased IL-1β does not prevent CL5-suppressed animals from improving over NT animals; however the role of IL-1β and other cytokines in TBI is an interesting area and remains to be elucidated.

To some surprise this limited set of RT-PCRs for a small number of inflammatory factors had turned up at least one quite interesting difference between TBI animals that had been successfully treated with CL5 siRNA, and their controls given NT siRNA. It was decided, based on these observations, to extend this study to a wider range of cytokines. The effect of this would be to determine if the result obtained for IL-1β was part of a broad difference in inflammatory response in the treated and untreated TBIs, or if it represented an isolated response, or potentially even an error. For this purpose cytokine proteome arrays containing antibodies against 40 different cytokines were employed. The

purpose of these was to carry out a screen in order to detect the broad inflammatory trends of CL5 and NT siRNA-administered TBI animals. The nature of these cytokine arrays means that only one animal can be assayed with each array, meaning that quantification and deeper analysis are not possible. This is a major limitation of this experiment, however it was felt that the large number of cytokines being assayed for would provide an interesting overview of the inflammatory profile and their change over time.

Firstly injured and injured brain tissue was compared, in the absence of siRNA, and this analysis returned ten cytokines which appeared to be differentially regulated following TBI (*Figure 6.6*). Of these C5a is a complement component that acts as a pro-inflammatory regulator (Raby, Holst et al. 2011), Timp-1 is an inhibitor of matrix metalloproteinases (MMPs) (Gomez, Alonso et al. 1997), KC (CXCL-1) is a potent chemoattractant for dendritic cells (Lentsch, Yoshidome et al. 1998), G-CSF is a maturation and proliferation factor for granulocytes (Avalos 1996), Trem-1 is a receptor found on neutrophils and monocytes (Bouchon, Dietrich et al. 2000), JE (MCP-1/CCL-2) is a monocyte chemotactic factor (Carr, Roth et al. 1994) as is MCP-5 (CCL-12) (Sarafi, Garcia-Zepe Da et al. 1997), Mip-1α is a polymorphonuclear leukocyte attractant (Menten, Wuyts et al. 2002) as is Mip-2 (CXCL2) (Wolpe, Sherry et al. 1989), and IL-16 attracts $CD4^+$ immune cells (Cruikshank, Center et al. 1994). The cytokines with the greatest difference between the CL5 and NT TBI samples were Timp-1, KC, JE, and IL-16 – the latter of which was the only factor in any assays for inflammatory markers to demonstrate lower expression following TBI (*Figure 6.6*).

Timp-1 acts by inhibiting MMPs, and therefore increased expression would likely lead to reduced infiltration by immune cells (Gomez, Alonso et al. 1997). In contrast, however, KC attracts immune cells (Lei, Hossain et al. 2012) and JE induces the attraction and

transmigration of neutrophils and macrophages (Gregory, Morand et al. 2006; Reichel, Rehberg et al. 2009). The roles of these factors induced following TBI appear at first to contradictory, however as with many inflammatory molecules these factors have multiple effects in damaged tissue. There is evidence, for instance, that Timp-1 may also function as a growth factor for a variety of cell types (Hayakawa, Yamashita et al. 1992; Kikuchi, Kadono et al. 1997); KC, meanwhile, increases vascular permeability (Lei, Hossain et al. 2012) and inhibition of KC has been observed to result in decreased endothelial cell recovery in models of wound healing (Liehn, Schober et al. 2004) as well as preventing damage to cells from hypoxia and superoxide radicals (Morimoto, Hirose et al. 2008). Together these provide an array of reasons why their upregulation could be beneficial to damaged tissue, as well as being potentially damaging, at least in the case of KC and JE, by recruiting immune cells and heightening neuroinflammation.

As mentioned, IL-16 is the only factor to be downregulated following injury (*Figure 6.6*). This cytokine appears to be primarily associated with interferon responses to microbial invasion, not sterile inflammation, as observed in its functions as a specific chemoattractant of $CD4^+$ immune cells and as an inhibitor of viral replication (Baier, Bannert et al. 1997). The attraction of $CD4^+$ cells is undesirable in a sterile inflammatory setting, and their presence can result in inappropriate interferon production and autoinflammation (Harrington, Hatton et al. 2005; Hirota, Duarte et al. 2011). As such, it is likely that IL-16's downregulation is in response to the absence of PAMPs, indicating a sterile inflammatory environment where $CD4^+$ cells are not needed and would in fact be damaging.

Between 24 and 72 h after TBI administration a number of cytokines appear to be differentially regulated in animals treated with CL5 siRNA versus those given NT siRNA (*Figure 6.7*, *Figure 6.8*, *Figure 6.9*). Of these four factors stand out as exhibiting marked differences in protein expression level – JE, sICAM-1, MCP-5 and IP-10. Of these only JE was previously identified as being induced following TBI (*Figure 6.6*).

The first of the previously unchanged cytokines, sICAM-1, is an endothelial-produced factor that is produced in response to inflammatory signals such as IL-1α, and acts to block the translocation-aiding effect of ICAM-1 (Fonsatti, Altomonte et al. 1997). Interestingly JE and MCP-5 are homologues of each other and have similar functions, namely neutrophil and macrophage recruitment particularly in conditions of hypoxia (Mojsilovic-Petrovic, Callaghan et al. 2007).

IL-1β, identified in *Figure 6.4* as being increased in TBI animals treated with CL5 siRNA, was present on the cytokine array (*Table 6.1*), but interestingly in these cytokine arrays IL-1β expression was not observed in any of the animals. One possibility is that the increase observed for IL-1β only occurs at the transcript level, with post-transcriptional mechanisms preventing its increase at the protein level. Alternatively it can be observed that IL-1β mRNA levels rapidly return to baseline levels after 24 h (*Figure 6.4*), so it is possible that protein levels of IL-1β were elevated at earlier timepoints but that some endogenous signal or feedback result in rapid shut-off of its production and that post-transcriptional mechanisms result in a faster return to baseline levels at the protein level than at mRNA. Without further experiments on timepoints earlier than 24 h it is impossible to confirm whether there is or is not a rise in IL-1β levels following CL5 siRNA-administration after TBI.

The major positive finding of these analyses of cytokine expression in CL5 and NT animals was the greatly increased level of IP-10 protein at 24 and 48 h after injury (*Figure 6.7* and *Figure 6.8*). Particularly following the failure to find IL-1β expression in any of the cytokine arrays, it was deemed important to confirm this finding for IP-10 at the transcript level. Here a similar increase in IP-10 mRNA level was observed in a Taqman assay (*Figure 6.10*). In the brain IP-10 is expressed primarily by astrocytes (Phares, Stohlman et al. 2013), and TBI-invading immune cells (Israelsson, Bengtsson et al. 2010), most likely in response to TLR4 activation by endogenous DAMPs (Imaizumi, Murakami et al. 2013). IP-10 is a cytokine responsible largely for attracting cytotoxic $CD8^+$ T-cells (Peperzak, Veraar et al. 2013), as well as promoting the cytolytic factors perforin and granzyme B (Majumder, Bhattacharjee et al. 2012). It has been previously reported that in disease models where antibody-producing cells enter the CNS – undesirable in a sterile inflammatory context – a lack of IP-10 expression blocks their translocation into the parenchyma (Phares, Stohlman et al. 2013), and in rheumatoid arthritis IP-10 causes immune cell attraction to sites of autoinflammation, and appears to increase tissue damage in the arthritic regions (Lee, Lee et al. 2013). IP-10 even directly causes Ca^{2+}-mediated neuronal apoptosis in vitro in the absence of immune cell involvement (Nelson and Gruol 2004; Sui, Stehno-Bittel et al. 2006), as well as increasing apoptosis following spinal cord injury in vivo (Glaser, Gonzalez et al. 2004; Glaser, Gonzalez et al. 2006).

With all these reports of deleterious effects of IP-10 expression in inflammation, is IP-10 inducement a purely negative side-effect of TBI treatment with CL5 siRNA, which causes damage but is simply overcome by the positive effects that are induced (*Figure 5.7* and *Figure 5.8*)? One possibility to counter this is that high levels of serum IP-10 is a strong identifier of hemophagocytic syndrome, where macrophages phagocytose large numbers

of erythrocytes (Maruoka, Inoue et al. 2013). While in the context of this disease this has highly damaging effects, it could represent an ability for IP-10 to increase macrophage phagocytosis of body cells that they perceive to be damaged. Transported to the context of a TBI, with large quantities of necrotic and apoptotic cells that require clearance before cytokine levels and toxic cell contents rise to unmanageable levels, this could in fact represent an important mechanism to aid in damage attenuation and repair of the TBI region.

One characteristic of the 24 h Taqman data in *Figure 6.10* is that the samples from the 8 animals treated with CL5 siRNA appear to cluster in two sub-groups of 4 animals. One sub-group demonstrates greatly increased IP-10 mRNA levels, while the other matches the levels observed in NT animals almost exactly. This effect could simply be due to chance, or alternatively it could be caused by an unnoticed difference in experimental conditions. Many factors could hypothetically cause a significant difference in cytokine expression such as this, for instance different genders between sub-groups or mice being of significantly different ages. The two sub-groups could represent two cages of 4 mice each, meaning that lack of food or water, pathogenic infection, significant fighting or other environmental factors could have had an impact on one cage and not the other. Finally, errors in experimental protocol could have resulted in one cage of four animals failing to receive antisedan to reverse the effects of the anaesthetic, or TBIs could have been inflicted with too much severity due to a timing issue for instance. Despite always generating experimental cohorts of animals using gender and age-matched individuals, and maintaining good practices of protocol and animal welfare, there always remains an outside possibility of error that can lead to issues such as this. However due to the

presence of statistical significance despite the wide variation, and with the result being in support of a previous finding (*Figure 6.7*), in this case it can be safely assumed that the result was representative of a genuine difference in expression levels between CL5 and NT-treated TBIs.

The experiments on TBI severity in Caspase-1 knockout mice demonstrate the importance of having the correct background strain. Here, the significantly different performance observed between uninjured Caspase-$1^{-/-}$ animals and their Balb/c controls in T-maze tests (*Figure 6.13*) had the effect of invalidating the striking results observed in NSS (*Figure 6.12*) and in particular the greatly larger TBI lesion sizes (*Figure 6.11*) between these groups. It is possible, despite the T-maze findings, that these two earlier findings still represent a significant impairment after TBI in mice lacking Casape-1, however the lack of an appropriate control means that these results cannot be confirmed.

Caspase-$1^{-/-}$ mice were originally generated on a C57BL/6N background, so hypothetically it could have been possible to carry out the experiments using this strain as a control. There are, however, a number of problems with this. First is the difficulty in assaying performance-based tests when a knockout strain differs in coat colour from its original background strain. Even if an observer is used who lacks any knowledge of the experimental groups in relation to coat colour difference, the fact that the two separate groups of animals can be clearly differentiated from each other means that bias will inevitably be introduced. Further to this a 32 SNP analysis of the knockout strain has discovered that since their original creation on a C57BL/6N background these animals have been crossbred, and the Jackson Laboratory Repository Caspase-$1^{-/-}$ mice are now on a mixed C57BL/6J, C57BL/6N genetic background. Finally, and possibly most

significantly, it has been recently discovered that Caspase-1 knockout mice are in fact double knockout animals, also lacking Caspase-11 (Kayagaki, Warming et al. 2011). This finding has called into question the results of every study on this knockout model since its inception, and many effects attributed to Caspase-1 will no doubt be reassigned to Caspase-11 as the role of this newly discovered inflammatory enzyme is investigated over the next few years.

The majority of the other inflammatory knockout models demonstrated tentative indications of altered outcomes in the absence of an intact inflammatory response. These included significantly impaired performance in NSS in mice lacking IL-1R (*Figure 6.15*). The observation of a possible trend towards slower IL-1R$^{-/-}$ TBI lesion shrinkage in MRI analysis (*Figure 6.14*), despite not being statistically significant, may have been enough to influence this knockout's impaired performance on NSS (*Figure 6.15*). Another possibility, however, is that neuroinflammatory events effect oedema by a very different mechanism than NSS. In this latter case it would be possible to record improvement in one outcome measure without the other having altered significantly.

A similar finding was observed for NSS in NLRP3$^{-/-}$ animals, except for being present at 8 h (*Figure 6.19*) instead of at 72 h in IL-1R$^{-/-}$ mice (*Figure 6.15*). The early finding in NLRP3 knockout animals is highly reminiscent of the case of animals with TBIs the received CL5 siRNA improving at this timepoint (*Figure 5.14*). It is possible that the NLRP3 inflammasome aids in brain function in this very acute stage after TBI, and hypothetically the improvement observed at this time following CL5 delivery could be due to a boosting of this NLRP3-mediated effect. This could for instance be a result of improved transportation of DAMPs or other immunomodulating factors via BBB modulation. Alternatively it is possible that the inflammatory markers that appear to aid in recovery

following TBI and CL5 siRNA carry out their positive role by the same means – by increasing BBB permeability. In fact it has been previously reported that induction of inflammation, even in the periphery, leads to decreased TJ protein expression and increased paracellular permeability at the BBB (Huber, Witt et al. 2001; Ronaldson, Demarco et al. 2009), and in another study inhibition of CNS inflammation was observed to inhibit these changes in BBB permeability (Hooper, Scott et al. 2000).

Finally, borderline significance in lesion was also observed in IL-18$^{-/-}$ mice in comparison with wild-type C57 controls (*Figure 6.16*). This finding, if it were to be a significant result with higher animal numbers or with a change in protocol or timepoints, would be notable as it would represent the only result pointing to deleterious effects of an inflammatory factor in this study. This would be interesting also because of the indication of a minor protective role of NLRP3 discussed above, as IL-18 is produced by stimulation of the NLRP3 inflammasome (Doyle, Campbell et al. 2012). However, due the lack of significance, even with relatively high animal numbers (*Figure 6.17*), conclusions of a role for IL-18 in this model cannot be made.

The final inflammatory knockout that was assessed, ASC$^{-/-}$, returned no significant result for TBI lesion volume (*Figure 6.21*). However, upon closer inspection there is a clear trend towards faster shrinkage in wild-type animals. Average starting oedema volumes of 9.022 mm^3 in ASC$^{-/-}$ and 9.031 mm^3 in wild-type animals are nearly identical, and visually this enables clear recognition of the trend as it emerges throughout this experiment. At 48 h post-TBI volumes in the two groups of animals are now 8.321 mm^3 and 9.120 mm^3 respectively, and while control mice have lost nearly 1 mm^3 in volume, those lacking ASC have actually gained in volume (*Figure 6.21*). When this data was reanalysed to focus on

the rate of volume change over time, as in Chapter 5 (eg. *Figure 5.7*), rather than absolute lesion volumes, the resulting data appears very different (*Figure 6.22*). The size of oedematous regions, as imaged by T_2-weighted MRI, in C57 control mice shrink to an average of 92.96% at 48 h, and 79.46% at 72 h from their 24 h volumes. Meanwhile, lesions in $ASC^{-/-}$ animals are an average of 102.8% at 48 h, and 90.49% at 72 h. This demonstrated a significant impairment in oedema shrinkage in the absence of ASC (*Figure 6.22*).

The original ASC TBI volume data not being statistically significant but still providing highly interesting data, demonstrates the need to closely analyse results in order to tease out subtle effects and changes. One should attempt not to slip into an over-reliance on p-values and statistical significance, and this is particularly true for in vivo work where n-numbers can be low. Here it can be tempting to observe a lack of statistical significance and conclude that the factor being investigated matches the null hypothesis, whereas it a profound effect on experimental outcome may be occurring. This could require a change in analysis method or experimental conditions, such as timepoint assayed, in order to produce significant results.

The data on $ASC^{-/-}$ TBI oedema volume (*Figure 6.*21) and change in volume (*Figure 6.22*) was made up of two separate cohorts of animals, which were given TBIs and assayed at different times. Both of these experiments returned significant results for TBI lesion shrinkage when analysed separately, or combined as presented here. When this same recovery rate was queried in the other inflammatory knockouts no significance was observed at any timepoint.

The significant impairment in oedema reduction observed in *Figure 6.22* appears to indicate a protective role for ASC in TBI recovery. This hypothesis is strongly supported by results of NSS testing on these animals. Here $ASC^{-/-}$ mice failed an average of 4.6 of the 10 tests of behaviour and coordination, compared to an average of 1.4 tests failed among wild-type C57 controls 1 week after TBI (*Figure 6.23*). In fact remaining blind to treatment groups was challenging due to the comparative severity of phenotype among knockout animals.

So why then does ASC absence result in such a marked phenotype? As mentioned earlier ASC's established function is as a scaffolding protein for inflammasome formation, acting as an intermediary between damage-sensing proteins, such as NLRP3, and Caspase-1

One recent study on the inflammatory response to the adjuvant alum, found that stimulation of the immune system by this molecule was abated in $ASC^{-/-}$ mice, whereas $NLRP3^{-/-}$ or $Caspase\text{-}1^{-/-}$ mice remained unaffected (Ellebedy, Lupfer et al. 2011). Another report showed that addition of monosodium urate, a DAMP normally believed to be sensed solely by the NLRP3 inflammasome, to cells was observed to result in ASC dimerisation and Caspase-1 activation, independent of the involvement of other inflammasome proteins (Fernandes-Alnemri, Wu et al. 2007). This form of inflammation is referred to as pyroptosis, and formation of the purported ASC pyroptosome leads to IL-1β processing, pore formation in the cell membrane, and eventual Caspase-1-dependent cell death.

The mechanism whereby this hypothesised activity of ASC would exhibit its observed protective role following TBI is unclear as of yet. One possibility is that the type of tissue damage acquired in TBI is only, or primarily, detected by the ASC pyroptosome, for

instance due to the types of DAMPs released. This would result in a greatly reduced release of IL-1β, and other cytokines, from cells lacking ASC, and consequently a lower immune response to damaged tissue is triggered. Immune cell activation and recruitment to damaged brain tissue following TBI aids in the clearance of cell debris (Neumann, Kotter et al. 2009), release of neuroprotective growth factors (Kossmann, Hans et al. 1996), and weakening of the BBB (Adelson, Whalen et al. 1998) which may enable increased water flux out of the injured region.

The cause of the ASC-mediated improvement in outcome following TBI remains to be elucidated, as does how this might relate to the increase in inflammatory markers observed following CL5 siRNA delivery. There is even potential for part of the observed improvement following CL5 siRNA to be dependent on increases in ASC and other inflammatory activity. One thing for certain, however, is that the view that neuroinflammation is a purely damaging feature of brain injury, and other conditions, must change. This view has been strengthened by studying the many notable cases where it runs unchecked in models of chronic inflammatory damage such as experimental autoimmune encephalomyelitis (Banati, Newcombe et al. 2000; Kutzelnigg, Lucchinetti et al. 2005). Rather it should be seen that inflammation serves a vital role in tissue repair and regeneration in situations of sterile injury, and the brain is no exception.

The scapegoating of inflammation and immune activation following damage to the brain has led to the field being misdirected, and many studies single-mindedly attempt to apply anti-inflammatory compounds to models of brain injury. Certainly this approach does result in notable successes. Delivery of the anti-inflammatory agent honokiol, for instance, was recently reported to decrease inflammation as well as lower oedema in a

model of ischemic brain damage (Zhang, Liu et al. 2013). In contrast, however, reduction of neuroinflammation following TBI in rats by treatment with ibuprofen was found to worsen recovery and consequent cognitive performance (Browne, Iwata et al. 2006). Significant findings in this study indicating a strongly protective role for at least some elements of inflammation following cold-induced TBI in mice. These findings support a more open-minded approach being taken in the future towards inflammation in conditions of the brain.

6.4 Future Directions

The discovery of a number of inflammatory cytokines being upregulated following treatment of this model of TBI with CL5 siRNA could be investigated further by backing up the preliminary findings presented here with assays at the RNA and protein level. This would function to generate a more complete picture of the inflammatory profile of the injury with or without treatment by means of CL5 suppression. The next question to investigate would be where this increase in cytokine expression is coming from. For instance are more immune cells capable of infiltrating the injured region following BBB modulation? It would be important also to further rule out the possibility that the presence of CL5 siRNA is activating an immune response in the TBI region. The CL5 siRNA used here has been investigated previously for its potential to alter expression of transcripts and its delivery to the brain was not found to increase the levels of any inflammatory markers (Campbell, Nguyen et al. 2009), however that study was carried

out in the absence of the tissue damage in the current study, so cytokine expression from damaged tissue in response to siRNAs should be investigated.

The finding that $ASC^{-/-}$ mice demonstrate impaired recovery both in terms of injury shrinkage and in cognitive outcome is a significant one, suggesting that inflammation is protective in the model presented in this study. This is particularly true considering that $NLRP3^{-/-}$ animals do not demonstrate a similarly impaired recovery. To elucidate this relationship and the independent role of ASC in this inflammatory environment a number of ELISAs should be carried out on $ASC^{-/-}$, $NLRP3^{-/-}$ and wt^{+} immune cells which are primed and exposed to necrotic tissue simulating the mass release of DAMPs following TBI. Furthermore TBI regions in $ASC^{-/-}$ mice should be dissected and investigated for immune cell infiltration, the types of immune cells present, as well as they inflammatory cytokines present compared. When compared to $NLRP3^{-/-}$ and wt^{+} TBI regions these investigations should provide a large amount of information as to what unique role ASC is playing in the post-TBI inflammatory environment.

Chapter 7: Concluding Remarks

This thesis has demonstrated effective modulation of the blood-brain barrier, by means of targeted siRNA suppression of the tight junction protein CL5, delivered to cells by the carrier agent PEI. This has contributed to the field firstly by demonstrating an increase in the range of tissue reached by low-molecular weight compounds in a model of human-derived glioblastoma multiforme. This succeeded in demonstrating the first of the hypotheses in this thesis, that CL5 suppression could be used in order to aid in the delivery of compounds into the brain as it had been shown in the retina previously by this lab (Campbell, Nguyen et al. 2009; Tam, Kiang et al. 2010; Campbell, Humphries et al. 2013). Indications were presented that improved delivery of chemotherapeutic agents to this model resulted in increased survival, but these fell short of statistical significance. Nonetheless this study represented a proof-of-principal that CL5 suppression can aid in the delivery of drugs to tumours of the brain. This work is being actively pursued by the lab of Gerald Grant with whom we collaborated on during the course of this study on chemotherapeutic delivery.

Secondly, this thesis provides the first demonstration that CL5 siRNA can be used not only to deliver compounds but also to relieve the brain of damaging material. This was shown in a model of cold-induced TBI where oedema was reduced compared to control animals, and this reduction in water in the brain coincided with an improvement in cognitive outcome. This has added to the field of research into TBI, as well as other models of oedema in the brain, and we successfully published our results in Nature Communications at the beginning of 2012 (Campbell, Hanrahan et al. 2012). The demonstration of the

hypothesis that damaging material can be transported out of the brain by means of BBB modulation during the course of this thesis has resulted in a number of studies being launched by the Humphries lab. One such project underway currently is attempting to reduce intraocular pressure in a model of glaucoma by enabling water to move across the iBRB following CL5 siRNA suppression. Secondly a project is approaching publication which attempts to enable amyloid-β, the causative agent in Alzheimer's disease, to move out of the brain by means of BBB modulation.

Finally the altered inflammatory response in mice treated with siRNA targeting CL5 was investigated, as was the contribution of inflammation to TBI outcome. This study found that a number of inflammatory markers were increased in CL5 siRNA-treated animals. Subsequently it was discovered that the inflammatory protein ASC, believed to be a scaffolding protein of the NLRP3 inflammasome, is protective in cases of TBI. On its own this is a highly interesting result, suggesting in the model used in this study that inflammation is protective, at least up until 3 weeks after injury. However this result became more interesting when it was found that this change in outcome was not matched when NLRP3 was absent. This suggests that ASC is carrying out a significant role in post-injury inflammatory events that is independent of its role in formation of the NLRP3 inflammasome. The work in this study is at a preliminary stage still, but the data gathered thus far raise interesting questions as to the role of ASC and inflammation following sterile injury such as TBI.

In summary I feel that I fulfilled the aims, and successfully demonstrated the hypotheses set out for this thesis. I contributed meaningfully to my field of research, publishing a

peer-reviewed paper in the process, influenced the future course of research to be undertaken by this lab, as well as representing my work and the lab at conferences around the world.

Bibliography

Abbott, N. J. (2002). "Astrocyte-endothelial interactions and blood-brain barrier permeability." J Anat **200**(6): 629-638.

Adelson, P. D., M. J. Whalen, et al. (1998). "Blood brain barrier permeability and acute inflammation in two models of traumatic brain injury in the immature rat: a preliminary report." Acta Neurochir Suppl **71**: 104-106.

Agarwal, S., P. Manchanda, et al. (2013). "Function of the blood-brain barrier and restriction of drug delivery to invasive glioma cells: findings in an orthotopic rat xenograft model of glioma." Drug Metab Dispos **41**(1): 33-39.

Agaugue, S., E. D. Carosella, et al. (2011). "Role of HLA-G in tumor escape through expansion of myeloid-derived suppressor cells and cytokinic balance in favor of Th2 versus Th1/Th17." Blood **117**(26): 7021-7031.

Agrawal, S., P. Anderson, et al. (2006). "Dystroglycan is selectively cleaved at the parenchymal basement membrane at sites of leukocyte extravasation in experimental autoimmune encephalomyelitis." J Exp Med **203**(4): 1007-1019.

Ahlers, S. T., E. Vasserman-Stokes, et al. (2012). "Assessment of the effects of acute and repeated exposure to blast overpressure in rodents: toward a greater understanding of blast and the potential ramifications for injury in humans exposed to blast." Front Neurol **3**: 32.

Alderson, P. and I. Roberts (2005). "Corticosteroids for acute traumatic brain injury." Cochrane Database Syst Rev(1): CD000196.

Aloisi, F., G. Penna, et al. (1997). "IL-12 production by central nervous system microglia is inhibited by astrocytes." J Immunol **159**(4): 1604-1612.

Alvarez, J. I., R. Cayrol, et al. (2011). "Disruption of central nervous system barriers in multiple sclerosis." Biochim Biophys Acta **1812**(2): 252-264.

Alvarez, J. I., A. Dodelet-Devillers, et al. (2011). "The Hedgehog pathway promotes blood-brain barrier integrity and CNS immune quiescence." Science **334**(6063): 1727-1731.

Aminmansour, B., H. Nikbakht, et al. (2012). "Comparison of the administration of progesterone versus progesterone and vitamin D in improvement of outcomes in

patients with traumatic brain injury: A randomized clinical trial with placebo group." Adv Biomed Res **1**: 58.

Anders, C. K., B. Adamo, et al. (2013). "Pharmacokinetics and efficacy of PEGylated liposomal doxorubicin in an intracranial model of breast cancer." PLoS ONE **8**(5): e61359.

Anderson, J. M. and C. M. Van Itallie (2008). "Tight junctions." Curr Biol **18**(20): R941-943.

Andersson, P. B., V. H. Perry, et al. (1992). "The acute inflammatory response to lipopolysaccharide in CNS parenchyma differs from that in other body tissues." Neuroscience **48**(1): 169-186.

Anderson, J. M. and C. M. Van Itallie (2009). "Physiology and function of the tight junction." Cold Spring Harb Perspect Biol **1**(2): a002584.

Antonov, A. S., M. E. Lukashev, et al. (1986). "Morphological alterations in endothelial cells from human aorta and umbilical vein induced by forskolin and phorbol 12-myristate 13-acetate: a synergistic action of adenylate cyclase and protein kinase C activators." Proc Natl Acad Sci U S A **83**(24): 9704-9708.

Antonov, A. S., M. A. Nikolaeva, et al. (1986). "Primary culture of endothelial cells from atherosclerotic human aorta. Part 1. Identification, morphological and ultrastructural characteristics of two endothelial cell subpopulations." Atherosclerosis **59**(1): 1-19.

Argaw, A. T., B. T. Gurfein, et al. (2009). "VEGF-mediated disruption of endothelial CLN-5 promotes blood-brain barrier breakdown." Proc Natl Acad Sci U S A **106**(6): 1977-1982.

Armulik, A., G. Genove, et al. (2010). "Pericytes regulate the blood-brain barrier." Nature **468**(7323): 557-561.

Arnett, H. A., J. Mason, et al. (2001). "TNF alpha promotes proliferation of oligodendrocyte progenitors and remyelination." Nat Neurosci **4**(11): 1116-1122.

Arun, P., R. Abu-Taleb, et al. (2013). "Acute mitochondrial dysfunction after blast exposure: potential role of mitochondrial glutamate oxaloacetate transaminase." J Neurotrauma.

Asano, A., K. Asano, et al. (2003). "Claudins in Caenorhabditis elegans: their distribution and barrier function in the epithelium." Curr Biol **13**(12): 1042-1046.

Avalos, B. R. (1996). "Molecular analysis of the granulocyte colony-stimulating factor receptor." Blood **88**(3): 761-777.

Baier, M., N. Bannert, et al. (1997). "Molecular cloning, sequence, expression, and processing of the interleukin 16 precursor." Proc Natl Acad Sci U S A **94**(10): 5273-5277.

Balint, Z., I. A. Krizbai, et al. (2007). "Changes induced by hyperosmotic mannitol in cerebral endothelial cells: an atomic force microscopic study." Eur Biophys J **36**(2): 113-120.

Ballabh, P., A. Braun, et al. (2004). "The blood-brain barrier: an overview: structure, regulation, and clinical implications." Neurobiol Dis **16**(1): 1-13.

Banati, R. B., J. Newcombe, et al. (2000). "The peripheral benzodiazepine binding site in the brain in multiple sclerosis: quantitative in vivo imaging of microglia as a measure of disease activity." Brain **123 (Pt 11)**: 2321-2337.

Banks, W. A. (2006). "The CNS as a target for peptides and peptide-based drugs." Expert Opin Drug Deliv **3**(6): 707-712.

Bareyre, F., F. Wahl, et al. (1997). "Time course of cerebral edema after traumatic brain injury in rats: effects of riluzole and mannitol." J Neurotrauma **14**(11): 839-849.

Barth, R. F., W. Yang, et al. (2002). "Neutron capture therapy of intracerebral melanoma: enhanced survival and cure after blood-brain barrier opening to improve delivery of boronophenylalanine." Int J Radiat Oncol Biol Phys **52**(3): 858-868.

Bartus, R. T., N. J. Hayward, et al. (1994). "Calpain inhibitor AK295 protects neurons from focal brain ischemia. Effects of postocclusion intra-arterial administration." Stroke **25**(11): 2265-2270.

Barzo, P., A. Marmarou, et al. (1997). "Contribution of vasogenic and cellular edema to traumatic brain swelling measured by diffusion-weighted imaging." J Neurosurg **87**(6): 900-907.

Baskaya, M. K., A. M. Rao, et al. (1997). "The biphasic opening of the blood-brain barrier in the cortex and hippocampus after traumatic brain injury in rats." Neurosci Lett **226**(1): 33-36.

Bauer, H. C. and H. Bauer (2000). "Neural induction of the blood-brain barrier: still an enigma." Cell Mol Neurobiol **20**(1): 13-28.

Bazarian, J. J., J. Zhong, et al. (2007). "Diffusion tensor imaging detects clinically important axonal damage after mild traumatic brain injury: a pilot study." J Neurotrauma **24**(9): 1447-1459.

Beaumont, A., P. Fatouros, et al. (2006). "Bolus tracer delivery measured by MRI confirms edema without blood-brain barrier permeability in diffuse traumatic brain injury." Acta Neurochir Suppl **96**: 171-174.

Beaumont, A., A. Marmarou, et al. (2000). "The permissive nature of blood brain barrier (BBB) opening in edema formation following traumatic brain injury." Acta Neurochir Suppl **76**: 125-129.

Bechmann, I., I. Galea, et al. (2007). "What is the blood-brain barrier (not)?" Trends Immunol **28**(1): 5-11.

Bechmann, I., J. Goldmann, et al. (2005). "Circulating monocytic cells infiltrate layers of anterograde axonal degeneration where they transform into microglia." FASEB J **19**(6): 647-649.

Bechmann, I., G. Mor, et al. (1999). "FasL (CD95L, Apo1L) is expressed in the normal rat and human brain: evidence for the existence of an immunological brain barrier." Glia **27**(1): 62-74.

Bedi, S. S., P. A. Walker, et al. (2013). "Autologous bone marrow mononuclear cells therapy attenuates activated microglial/macrophage response and improves spatial learning after traumatic brain injury." J Trauma Acute Care Surg.

Behr, M., D. Riedel, et al. (2003). "The claudin-like megatrachea is essential in septate junctions for the epithelial barrier function in Drosophila." Dev Cell **5**(4): 611-620.

Bell, H. S., I. R. Whittle, et al. (2001). "The development of necrosis and apoptosis in glioma: experimental findings using spheroid culture systems." Neuropathol Appl Neurobiol **27**(4): 291-304.

Ben-Yosef, T., I. A. Belyantseva, et al. (2003). "Claudin 14 knockout mice, a model for autosomal recessive deafness DFNB29, are deaf due to cochlear hair cell degeneration." Hum Mol Genet **12**(16): 2049-2061.

Berditchevski, F., E. Odintsova, et al. (2002). "Expression of the palmitoylation-deficient CD151 weakens the association of alpha 3 beta 1 integrin with the tetraspanin-enriched microdomains and affects integrin-dependent signaling." J Biol Chem **277**(40): 36991-37000.

Bergsneider, M., D. A. Hovda, et al. (2001). "Metabolic recovery following human traumatic brain injury based on FDG-PET: time course and relationship to neurological disability." J Head Trauma Rehabil **16**(2): 135-148.

Betz, A. L. (1983). "Sodium transport in capillaries isolated from rat brain." J Neurochem **41**(4): 1150-1157.

Bevan, H. S., S. C. Slater, et al. (2011). "Acute laminar shear stress reversibly increases human glomerular endothelial cell permeability via activation of endothelial nitric oxide synthase." Am J Physiol Renal Physiol **301**(4): F733-742.

Blum, M. S., E. Toninelli, et al. (1997). "Cytoskeletal rearrangement mediates human microvascular endothelial tight junction modulation by cytokines." Am J Physiol **273**(1 Pt 2): H286-294.

Blumbergs, P. C., G. Scott, et al. (1994). "Staining of amyloid precursor protein to study axonal damage in mild head injury." Lancet **344**(8929): 1055-1056.

Bonnet, M. E., P. Erbacher, et al. (2008). "Systemic delivery of DNA or siRNA mediated by linear polyethylenimine (L-PEI) does not induce an inflammatory response." Pharm Res **25**(12): 2972-2982.

Borlongan, C. V. and D. F. Emerich (2003). "Facilitation of drug entry into the CNS via transient permeation of blood brain barrier: laboratory and preliminary clinical evidence from bradykinin receptor agonist, Cereport." Brain Res Bull **60**(3): 297-306.

Borlongan, C. V., D. F. Emerich, et al. (2002). "Bradykinin receptor agonist facilitates low-dose cyclosporine-A protection against 6-hydroxydopamine neurotoxicity." Brain Res **956**(2): 211-220.

Bouchon, A., J. Dietrich, et al. (2000). "Cutting edge: inflammatory responses can be triggered by TREM-1, a novel receptor expressed on neutrophils and monocytes." J Immunol **164**(10): 4991-4995.

Brabb, T., P. von Dassow, et al. (2000). "In situ tolerance within the central nervous system as a mechanism for preventing autoimmunity." J Exp Med **192**(6): 871-880.

Browne, K. D., A. Iwata, et al. (2006). "Chronic ibuprofen administration worsens cognitive outcome following traumatic brain injury in rats." Exp Neurol **201**(2): 301-307.

Bsibsi, M., C. Persoon-Deen, et al. (2006). "Toll-like receptor 3 on adult human astrocytes triggers production of neuroprotective mediators." Glia **53**(7): 688-695.

Buki, A., D. O. Okonkwo, et al. (2000). "Cytochrome c release and caspase activation in traumatic axonal injury." J Neurosci **20**(8): 2825-2834.

Buki, A., R. Siman, et al. (1999). "The role of calpain-mediated spectrin proteolysis in traumatically induced axonal injury." J Neuropathol Exp Neurol **58**(4): 365-375.

Butt, A. M., H. C. Jones, et al. (1990). "Electrical resistance across the blood-brain barrier in anaesthetized rats: a developmental study." J Physiol **429**: 47-62.

Byram, S. C., M. J. Carson, et al. (2004). "CD4-positive T cell-mediated neuroprotection requires dual compartment antigen presentation." J Neurosci **24**(18): 4333-4339.

Campbell, M., F. Hanrahan, et al. (2012). "Targeted suppression of claudin-5 decreases cerebral oedema and improves cognitive outcome following traumatic brain injury." Nat Commun **3**: 849.

Campbell, M., M. M. Humphries, et al. (2011). "Systemic low-molecular weight drug delivery to pre-selected neuronal regions." EMBO Mol Med **3**(4): 235-245.

Campbell, M., A. S. Kiang, et al. (2008). "RNAi-mediated reversible opening of the blood-brain barrier." J Gene Med **10**(8): 930-947.

Campbell, M., A. T. Nguyen, et al. (2009). "An experimental platform for systemic drug delivery to the retina." Proc Natl Acad Sci U S A **106**(42): 17817-17822.

Carr, M. W., S. J. Roth, et al. (1994). "Monocyte chemoattractant protein 1 acts as a T-lymphocyte chemoattractant." Proc Natl Acad Sci U S A **91**(9): 3652-3656.

Carthew, R. W. and E. J. Sontheimer (2009). "Origins and Mechanisms of miRNAs and siRNAs." Cell **136**(4): 642-655.

Castillo, M. R. and J. R. Babson (1998). "Ca(2+)-dependent mechanisms of cell injury in cultured cortical neurons." Neuroscience **86**(4): 1133-1144.

Caudy, A. A., M. Myers, et al. (2002). "Fragile X-related protein and VIG associate with the RNA interference machinery." Genes Dev **16**(19): 2491-2496.

Cekic, M., S. J. Johnson, et al. (2012). "Progesterone treatment alters neurotrophin/proneurotrophin balance and receptor expression in rats with traumatic brain injury." Restor Neurol Neurosci **30**(2): 115-126.

Cernak, I., Z. Wang, et al. (2001). "Cognitive deficits following blast injury-induced neurotrauma: possible involvement of nitric oxide." Brain Inj **15**(7): 593-612.

Cernak, I., Z. Wang, et al. (2001). "Ultrastructural and functional characteristics of blast injury-induced neurotrauma." J Trauma **50**(4): 695-706.

Centers for Disease Control and Prevention (2010). "Traumatic Brain Injury in the United States: Emergency Department Visits, Hospitalizations and Deaths 2002–2006." Atlanta (GA): Centers for Disease Control and Prevention, National Center for Injury Prevention and Control. (www.cdc.gov/traumaticbraininjury/pdf/blue_book.pdf)

Chauvet, A. E., P. P. Kesava, et al. (1998). "Selective intraarterial gene delivery into a canine meningioma." J Neurosurg **88**(5): 870-873.

Chen, X. H., V. E. Johnson, et al. (2009). "A lack of amyloid beta plaques despite persistent accumulation of amyloid beta in axons of long-term survivors of traumatic brain injury." Brain Pathol **19**(2): 214-223.

Chen, X. H., R. Siman, et al. (2004). "Long-term accumulation of amyloid-beta, beta-secretase, presenilin-1, and caspase-3 in damaged axons following brain trauma." Am J Pathol **165**(2): 357-371.

Cho, J., H. Chang, et al. (2012). "LIN28A is a suppressor of ER-associated translation in embryonic stem cells." Cell **151**(4): 765-777.

Cho, W. G., R. J. Albuquerque, et al. (2009). "Small interfering RNA-induced TLR3 activation inhibits blood and lymphatic vessel growth." Proc Natl Acad Sci U S A **106**(17): 7137-7142.

Christensen, J., M. G. Pedersen, et al. (2009). "Long-term risk of epilepsy after traumatic brain injury in children and young adults: a population-based cohort study." Lancet **373**(9669): 1105-1110.

Christman, C. W., M. S. Grady, et al. (1994). "Ultrastructural studies of diffuse axonal injury in humans." J Neurotrauma **11**(2): 173-186.

Clausen, F., A. Hanell, et al. (2011). "Neutralization of interleukin-1beta reduces cerebral edema and tissue loss and improves late cognitive outcome following traumatic brain injury in mice." Eur J Neurosci **34**(1): 110-123.

Clifton, G. L., E. R. Miller, et al. (2001). "Lack of effect of induction of hypothermia after acute brain injury." N Engl J Med **344**(8): 556-563.

Colegio, O. R., C. M. Van Itallie, et al. (2002). "Claudins create charge-selective channels in the paracellular pathway between epithelial cells." Am J Physiol Cell Physiol **283**(1): C142-147.

Colgan, N. C., M. M. Cronin, et al. (2010). "Quantitative MRI analysis of brain volume changes due to controlled cortical impact." J Neurotrauma **27**(7): 1265-1274.

Colombo, F., M. Zanusso, et al. (1997). "Gene stereotactic neurosurgery for recurrent malignant gliomas." Stereotact Funct Neurosurg **68**(1-4 Pt 1): 245-251.

Cooper, D. J., P. S. Myles, et al. (2004). "Prehospital hypertonic saline resuscitation of patients with hypotension and severe traumatic brain injury: a randomized controlled trial." JAMA **291**(11): 1350-1357.

Cruikshank, W. W., D. M. Center, et al. (1994). "Molecular and functional analysis of a lymphocyte chemoattractant factor: association of biologic function with CD4 expression." Proc Natl Acad Sci U S A **91**(11): 5109-5113.

Daneman, R., D. Agalliu, et al. (2009). "Wnt/beta-catenin signaling is required for CNS, but not non-CNS, angiogenesis." Proc Natl Acad Sci U S A **106**(2): 641-646.

Daneman, R., L. Zhou, et al. (2010). "The mouse blood-brain barrier transcriptome: a new resource for understanding the development and function of brain endothelial cells." PLoS ONE **5**(10): e13741.

Das, S. K., T. Hashimoto, et al. (2005). "Fucoxanthin induces cell cycle arrest at G0/G1 phase in human colon carcinoma cells through up-regulation of p21WAF1/Cip1." Biochim Biophys Acta **1726**(3): 328-335.

Davalos, D., J. Grutzendler, et al. (2005). "ATP mediates rapid microglial response to local brain injury in vivo." Nat Neurosci **8**(6): 752-758.

Davson, H. and E. Spaziani (1959). "The blood-brain barrier and the extracellular space of brain." J Physiol **149**: 135-143.

Deacon, R. M. and J. N. Rawlins (2006). "T-maze alternation in the rodent." Nat Protoc **1**(1): 7-12.

Diaz-Arrastia, R., K. K. Wang, et al. (2013). "Acute biomarkers of traumatic brain injury: Relationship between plasma levels of ubiquitin C-terminal hydrolase-L1 (UCH-L1) and glial fibrillary acidic protein (GFAP)." J Neurotrauma.

Dixon, C. E., G. L. Clifton, et al. (1991). "A controlled cortical impact model of traumatic brain injury in the rat." J Neurosci Methods **39**(3): 253-262.

Dixon, C. E., J. W. Lighthall, et al. (1988). "Physiologic, histopathologic, and cineradiographic characterization of a new fluid-percussion model of experimental brain injury in the rat." J Neurotrauma **5**(2): 91-104.

Dolecek, T. A., J. M. Propp, et al. (2012). "CBTRUS statistical report: primary brain and central nervous system tumors diagnosed in the United States in 2005-2009." Neuro Oncol **14 Suppl 5**: v1-49.

Doyle, S. L., M. Campbell, et al. (2012). "NLRP3 has a protective role in age-related macular degeneration through the induction of IL-18 by drusen components." Nat Med **18**(5): 791-798.

Dua, R. K., B. I. Devi, et al. (2010). "Increased expression of Aquaporin-4 and its correlation with contrast enhancement and perilesional edema in brain tumors." Br J Neurosurg **24**(4): 454-459.

Egen, J. G., M. S. Kuhns, et al. (2002). "CTLA-4: new insights into its biological function and use in tumor immunotherapy." Nat Immunol **3**(7): 611-618.

Eisenberg, H. M., H. E. Gary, Jr., et al. (1990). "Initial CT findings in 753 patients with severe head injury. A report from the NIH Traumatic Coma Data Bank." J Neurosurg **73**(5): 688-698.

Elbashir, S. M., J. Harborth, et al. (2001). "Duplexes of 21-nucleotide RNAs mediate RNA interference in cultured mammalian cells." Nature **411**(6836): 494-498.

Elbashir, S. M., J. Martinez, et al. (2001). "Functional anatomy of siRNAs for mediating efficient RNAi in Drosophila melanogaster embryo lysate." EMBO J **20**(23): 6877-6888.

Ellebedy, A. H., C. Lupfer, et al. (2011). "Inflammasome-independent role of the apoptosis-associated speck-like protein containing CARD (ASC) in the adjuvant effect of MF59." Proc Natl Acad Sci U S A **108**(7): 2927-2932.

Elliott, P. J., N. J. Hayward, et al. (1996). "Intravenous RMP-7 selectively increases uptake of carboplatin into rat brain tumors." Cancer Res **56**(17): 3998-4005.

Emerich, D. F., P. Snodgrass, et al. (1998). "Central analgesic actions of loperamide following transient permeation of the blood brain barrier with Cereport (RMP-7)." Brain Res **801**(1-2): 259-266.

Farkas, A., E. Szatmari, et al. (2005). "Hyperosmotic mannitol induces Src kinase-dependent phosphorylation of beta-catenin in cerebral endothelial cells." J Neurosci Res **80**(6): 855-861.

Feliers, D., X. Chen, et al. (2005). "VEGF regulation of endothelial nitric oxide synthase in glomerular endothelial cells." Kidney Int **68**(4): 1648-1659.

Fernandes-Alnemri, T., J. Wu, et al. (2007). "The pyroptosome: a supramolecular assembly of ASC dimers mediating inflammatory cell death via caspase-1 activation." Cell Death Differ **14**(9): 1590-1604.

Fine, H. F., I. Zhitomirsky, et al. (2009). "Bevacizumab (avastin) and ranibizumab (lucentis) for choroidal neovascularization in multifocal choroiditis." Retina **29**(1): 8-12.

Finsen, B. R., T. Sorensen, et al. (1991). "Leukocyte infiltration and glial reactions in xenografts of mouse brain tissue undergoing rejection in the adult rat brain. A light and electron microscopical immunocytochemical study." J Neuroimmunol **32**(2): 159-183.

Fleminger, S., D. L. Oliver, et al. (2003). "Head injury as a risk factor for Alzheimer's disease: the evidence 10 years on; a partial replication." J Neurol Neurosurg Psychiatry **74**(7): 857-862.

Flierl, M. A., P. F. Stahel, et al. (2009). "Mouse closed head injury model induced by a weight-drop device." Nat Protoc **4**(9): 1328-1337.

Floyd, C. L., K. M. Golden, et al. (2002). "Craniectomy position affects morris water maze performance and hippocampal cell loss after parasagittal fluid percussion." J Neurotrauma **19**(3): 303-316.

Foda, M. A. and A. Marmarou (1994). "A new model of diffuse brain injury in rats. Part II: Morphological characterization." J Neurosurg **80**(2): 301-313.

Fonsatti, E., M. Altomonte, et al. (1997). "Tumour-derived interleukin 1alpha (IL-1alpha) up-regulates the release of soluble intercellular adhesion molecule-1 (sICAM-1) by endothelial cells." Br J Cancer **76**(10): 1255-1261.

Fox, G. B., R. A. LeVasseur, et al. (1999). "Behavioral responses of C57BL/6, FVB/N, and 129/SvEMS mouse strains to traumatic brain injury: implications for gene targeting approaches to neurotrauma." J Neurotrauma **16**(5): 377-389.

Furuse, M., M. Hata, et al. (2002). "Claudin-based tight junctions are crucial for the mammalian epidermal barrier: a lesson from claudin-1-deficient mice." J Cell Biol **156**(6): 1099-1111.

Furuse, M. and S. Tsukita (2006). "Claudins in occluding junctions of humans and flies." Trends Cell Biol **16**(4): 181-188.

Galea, I., I. Bechmann, et al. (2007). "What is immune privilege (not)?" Trends Immunol **28**(1): 12-18.

Gantier, M. P., S. Tong, et al. (2008). "TLR7 is involved in sequence-specific sensing of single-stranded RNAs in human macrophages." J Immunol **180**(4): 2117-2124.

Gennarelli, T. A., L. E. Thibault, et al. (1982). "Diffuse axonal injury and traumatic coma in the primate." Ann Neurol **12**(6): 564-574.

Giacino, J. T., J. Whyte, et al. (2012). "Placebo-controlled trial of amantadine for severe traumatic brain injury." N Engl J Med **366**(9): 819-826.

Gilley, J. and M. P. Coleman (2010). "Endogenous Nmnat2 is an essential survival factor for maintenance of healthy axons." PLoS Biol **8**(1): e1000300.

Gimsa, U., O. R. A, et al. (2004). "Astrocytes protect the CNS: antigen-specific T helper cell responses are inhibited by astrocyte-induced upregulation of CTLA-4 (CD152)." J Mol Med (Berl) **82**(6): 364-372.

Glaser, J., R. Gonzalez, et al. (2004). "Neutralization of the chemokine CXCL10 enhances tissue sparing and angiogenesis following spinal cord injury." J Neurosci Res **77**(5): 701-708.

Glaser, J., R. Gonzalez, et al. (2006). "Neutralization of the chemokine CXCL10 reduces apoptosis and increases axon sprouting after spinal cord injury." J Neurosci Res **84**(4): 724-734.

Glenn, T. C., D. F. Kelly, et al. (2003). "Energy dysfunction as a predictor of outcome after moderate or severe head injury: indices of oxygen, glucose, and lactate metabolism." J Cereb Blood Flow Metab **23**(10): 1239-1250.

Golarai, G., A. C. Greenwood, et al. (2001). "Physiological and structural evidence for hippocampal involvement in persistent seizure susceptibility after traumatic brain injury." J Neurosci **21**(21): 8523-8537.

Gomez, D. E., D. F. Alonso, et al. (1997). "Tissue inhibitors of metalloproteinases: structure, regulation and biological functions." Eur J Cell Biol **74**(2): 111-122.

Goodchild, A., N. Nopper, et al. (2009). "Sequence determinants of innate immune activation by short interfering RNAs." BMC Immunol **10**: 40.

Goodrich, G. S., A. Y. Kabakov, et al. (2013). "Ceftriaxone treatment after traumatic brain injury restores expression of the glutamate transporter GLT-1, reduces regional gliosis, and reduces posttraumatic seizures in the rat." J Neurotrauma.

Gow, A., C. M. Southwood, et al. (1999). "CNS myelin and sertoli cell tight junction strands are absent in Osp/claudin-11 null mice." Cell **99**(6): 649-659.

Grasl-Kraupp, B., B. Ruttkay-Nedecky, et al. (1995). "In situ detection of fragmented DNA (TUNEL assay) fails to discriminate among apoptosis, necrosis, and autolytic cell death: a cautionary note." Hepatology **21**(5): 1465-1468.

Gregory, J. L., E. F. Morand, et al. (2006). "Macrophage migration inhibitory factor induces macrophage recruitment via CC chemokine ligand 2." J Immunol **177**(11): 8072-8079.

Gumerlock, M. K., B. D. Belshe, et al. (1992). "Osmotic blood-brain barrier disruption and chemotherapy in the treatment of high grade malignant glioma: patient series and literature review." J Neurooncol **12**(1): 33-46.

Guo, D., L. Zeng, et al. (2013). "Rapamycin attenuates the development of posttraumatic epilepsy in a mouse model of traumatic brain injury." PLoS ONE **8**(5): e64078.

Guo, Z., L. A. Cupples, et al. (2000). "Head injury and the risk of AD in the MIRAGE study." Neurology **54**(6): 1316-1323.

Guskiewicz, K. M., S. W. Marshall, et al. (2005). "Association between recurrent concussion and late-life cognitive impairment in retired professional football players." Neurosurgery **57**(4): 719-726; discussion 719-726.

Hadj-Rabia, S., L. Baala, et al. (2004). "Claudin-1 gene mutations in neonatal sclerosing cholangitis associated with ichthyosis: a tight junction disease." Gastroenterology **127**(5): 1386-1390.

Hamazaki, Y., M. Itoh, et al. (2002). "Multi-PDZ domain protein 1 (MUPP1) is concentrated at tight junctions through its possible interaction with claudin-1 and junctional adhesion molecule." J Biol Chem **277**(1): 455-461.

Hamstra, D. A., B. A. Moffat, et al. (2005). "Intratumoral injection of BCNU in ethanol (DTI-015) results in enhanced delivery to tumor--a pharmacokinetic study." J Neurooncol **73**(3): 225-238.

Handa, O., J. Stephen, et al. (2008). "Role of endothelial nitric oxide synthase-derived nitric oxide in activation and dysfunction of cerebrovascular endothelial cells during early onsets of sepsis." Am J Physiol Heart Circ Physiol **295**(4): H1712-1719.

Hara, H., P. L. Huang, et al. (1996). "Reduced brain edema and infarction volume in mice lacking the neuronal isoform of nitric oxide synthase after transient MCA occlusion." J Cereb Blood Flow Metab **16**(4): 605-611.

Harrington, L. E., R. D. Hatton, et al. (2005). "Interleukin 17-producing CD4+ effector T cells develop via a lineage distinct from the T helper type 1 and 2 lineages." Nat Immunol **6**(11): 1123-1132.

Hawkins, B. T. and T. P. Davis (2005). "The blood-brain barrier/neurovascular unit in health and disease." Pharmacol Rev **57**(2): 173-185.

Hawkins, B. T. and R. D. Egleton (2006). "Fluorescence imaging of blood-brain barrier disruption." J Neurosci Methods **151**(2): 262-267.

Hayakawa, T., K. Yamashita, et al. (1992). "Growth-promoting activity of tissue inhibitor of metalloproteinases-1 (TIMP-1) for a wide range of cells. A possible new growth factor in serum." FEBS Lett **298**(1): 29-32.

Hayashi, Y., M. Nomura, et al. (1997). "Induction of various blood-brain barrier properties in non-neural endothelial cells by close apposition to co-cultured astrocytes." Glia **19**(1): 13-26.

He, L. and G. J. Hannon (2004). "MicroRNAs: small RNAs with a big role in gene regulation." Nat Rev Genet **5**(7): 522-531.

Hegi, M. E., A. C. Diserens, et al. (2005). "MGMT gene silencing and benefit from temozolomide in glioblastoma." N Engl J Med **352**(10): 997-1003.

Heil, F., H. Hemmi, et al. (2004). "Species-specific recognition of single-stranded RNA via toll-like receptor 7 and 8." Science **303**(5663): 1526-1529.

Higashida, T., C. W. Kreipke, et al. (2011). "The role of hypoxia-inducible factor-1alpha, aquaporin-4, and matrix metalloproteinase-9 in blood-brain barrier disruption and brain edema after traumatic brain injury." J Neurosurg **114**(1): 92-101.

Higgins, S. C. and G. J. Pilkington (2010). "The in vitro effects of tricyclic drugs and dexamethasone on cellular respiration of malignant glioma." Anticancer Res **30**(2): 391-397.

Hirota, K., J. H. Duarte, et al. (2011). "Fate mapping of IL-17-producing T cells in inflammatory responses." Nat Immunol **12**(3): 255-263.

Hoek, R. M., S. R. Ruuls, et al. (2000). "Down-regulation of the macrophage lineage through interaction with OX2 (CD200)." Science **290**(5497): 1768-1771.

Hong, R. L., C. J. Huang, et al. (1999). "Direct comparison of liposomal doxorubicin with or without polyethylene glycol coating in C-26 tumor-bearing mice: is surface coating with polyethylene glycol beneficial?" Clin Cancer Res **5**(11): 3645-3652.

Hooper, D. C., G. S. Scott, et al. (2000). "Uric acid, a peroxynitrite scavenger, inhibits CNS inflammation, blood-CNS barrier permeability changes, and tissue damage in a mouse model of multiple sclerosis." FASEB J **14**(5): 691-698.

Hornung, V., M. Guenthner-Biller, et al. (2005). "Sequence-specific potent induction of IFN-alpha by short interfering RNA in plasmacytoid dendritic cells through TLR7." Nat Med **11**(3): 263-270.

Hoshi, A., T. Yamamoto, et al. (2011). "Chemical preconditioning-induced reactive astrocytosis contributes to the reduction of post-ischemic edema through aquaporin-4 downregulation." Exp Neurol **227**(1): 89-95.

Houkin, K., H. Abe, et al. (1996). "Magnetic resonance imaging of cold injury-induced brain edema in rats." Neurol Med Chir (Tokyo) **36**(2): 72-77.

Hsieh, C. H., Y. F. Chen, et al. (2005). "Evaluation of pharmacokinetics of 4-borono-2-(18)F-fluoro-L-phenylalanine for boron neutron capture therapy in a glioma-bearing rat model with hyperosmolar blood-brain barrier disruption." J Nucl Med **46**(11): 1858-1865.

Huang, Z., P. L. Huang, et al. (1996). "Enlarged infarcts in endothelial nitric oxide synthase knockout mice are attenuated by nitro-L-arginine." J Cereb Blood Flow Metab **16**(5): 981-987.

Huang, Z., P. L. Huang, et al. (1994). "Effects of cerebral ischemia in mice deficient in neuronal nitric oxide synthase." Science **265**(5180): 1883-1885.

Huber, J. D., K. A. Witt, et al. (2001). "Inflammatory pain alters blood-brain barrier permeability and tight junctional protein expression." Am J Physiol Heart Circ Physiol **280**(3): H1241-1248.

Hukkelhoven, C. W., E. W. Steyerberg, et al. (2002). "Regional differences in patient characteristics, case management, and outcomes in traumatic brain injury: experience from the tirilazad trials." J Neurosurg **97**(3): 549-557.

Hurst, R. D. and I. B. Fritz (1996). "Properties of an immortalised vascular endothelial/glioma cell co-culture model of the blood-brain barrier." J Cell Physiol **167**(1): 81-88.

Hutvagner, G., J. McLachlan, et al. (2001). "A cellular function for the RNA-interference enzyme Dicer in the maturation of the let-7 small temporal RNA." Science **293**(5531): 834-838.

Hutvagner, G. and P. D. Zamore (2002). "A microRNA in a multiple-turnover RNAi enzyme complex." Science **297**(5589): 2056-2060.

Igarashi, H., V. J. Huber, et al. (2011). "Pretreatment with a novel aquaporin 4 inhibitor, TGN-020, significantly reduces ischemic cerebral edema." Neurol Sci **32**(1): 113-116.

Imaizumi, T., K. Murakami, et al. (2013). "MDA5 and ISG56 mediate CXCL10 expression induced by Toll-like receptor 4 activation in U373MG human astrocytoma cells." Neurosci Res **76**(4): 195-206.

Ishibashi, S., T. Kuroiwa, et al. (2007). "Galectin-1 regulates neurogenesis in the subventricular zone and promotes functional recovery after stroke." Exp Neurol **207**(2): 302-313.

Ishihara, H., H. Kubota, et al. (2008). "Endothelial cell barrier impairment induced by glioblastomas and transforming growth factor beta2 involves matrix metalloproteinases and tight junction proteins." J Neuropathol Exp Neurol **67**(5): 435-448.

Israelsson, C., H. Bengtsson, et al. (2008). "Distinct cellular patterns of upregulated chemokine expression supporting a prominent inflammatory role in traumatic brain injury." J Neurotrauma **25**(8): 959-974.

Israelsson, C., H. Bengtsson, et al. (2010). "Appearance of Cxcl10-expressing cell clusters is common for traumatic brain injury and neurodegenerative disorders." Eur J Neurosci **31**(5): 852-863.

Itoh, M., M. Furuse, et al. (1999). "Direct binding of three tight junction-associated MAGUKs, ZO-1, ZO-2, and ZO-3, with the COOH termini of claudins." J Cell Biol **147**(6): 1351-1363.

Ivens, S., D. Kaufer, et al. (2007). "TGF-beta receptor-mediated albumin uptake into astrocytes is involved in neocortical epileptogenesis." Brain **130**(Pt 2): 535-547.

Iwamoto, Y., T. Yamaki, et al. (1997). "Investigation of morphological change of lateral and midline fluid percussion injury in rats, using magnetic resonance imaging." Neurosurgery **40**(1): 163-167.

Iwata, A., P. K. Stys, et al. (2004). "Traumatic axonal injury induces proteolytic cleavage of the voltage-gated sodium channels modulated by tetrodotoxin and protease inhibitors." J Neurosci **24**(19): 4605-4613.

Jack, C. S., N. Arbour, et al. (2005). "TLR signaling tailors innate immune responses in human microglia and astrocytes." J Immunol **175**(7): 4320-4330.

Johansson, P. A., K. M. Dziegielewska, et al. (2006). "Blood-CSF barrier function in the rat embryo." Eur J Neurosci **24**(1): 65-76.

Johnston, A. J., L. A. Steiner, et al. (2005). "Effect of cerebral perfusion pressure augmentation on regional oxygenation and metabolism after head injury." Crit Care Med **33**(1): 189-195; discussion 255-187.

Joly, E., L. Mucke, et al. (1991). "Viral persistence in neurons explained by lack of major histocompatibility class I expression." Science **253**(5025): 1283-1285.

Joosen, M. J., M. J. van der Schans, et al. (2011). "Increasing oxime efficacy by blood-brain barrier modulation." Toxicol Lett.

Judge, A. D., V. Sood, et al. (2005). "Sequence-dependent stimulation of the mammalian innate immune response by synthetic siRNA." Nat Biotechnol **23**(4): 457-462.

Juric, D. M. and M. Carman-Krzan (2001). "Interleukin-1 beta, but not IL-1 alpha, mediates nerve growth factor secretion from rat astrocytes via type I IL-1 receptor." Int J Dev Neurosci **19**(7): 675-683.

Kacem, K., P. Lacombe, et al. (1998). "Structural organization of the perivascular astrocyte endfeet and their relationship with the endothelial glucose transporter: a confocal microscopy study." Glia **23**(1): 1-10.

Kanasty, R. L., K. A. Whitehead, et al. (2012). "Action and reaction: the biological response to siRNA and its delivery vehicles." Mol Ther **20**(3): 513-524.

Kang, J. H., Y. Tachibana, et al. (2010). "Liver-targeted siRNA delivery by polyethylenimine (PEI)-pullulan carrier." Bioorg Med Chem **18**(11): 3946-3950.

Karakotchian, M. and I. S. Fraser (2007). "An ultrastructural study of microvascular inter-endothelial tight junctions in normal endometrium." Micron **38**(6): 632-636.

Kariko, K., M. Buckstein, et al. (2005). "Suppression of RNA recognition by Toll-like receptors: the impact of nucleoside modification and the evolutionary origin of RNA." Immunity **23**(2): 165-175.

Kariko, K., P. Bhuyan, et al. (2004). "Exogenous siRNA mediates sequence-independent gene suppression by signaling through toll-like receptor 3." Cells Tissues Organs **177**(3): 132-138.

Katayama, Y. and T. Kawamata (2003). "Edema fluid accumulation within necrotic brain tissue as a cause of the mass effect of cerebral contusion in head trauma patients." Acta Neurochir Suppl **86**: 323-327.

Kawai, N., M. Kawanishi, et al. (2003). "Treatment of cold injury-induced brain edema with a nonspecific matrix metalloproteinase inhibitor MMI270 in rats." J Neurotrauma **20**(7): 649-657.

Kawamata, T., Y. Katayama, et al. (2000). "Heterogeneous mechanisms of early edema formation in cerebral contusion: diffusion MRI and ADC mapping study." Acta Neurochir Suppl **76**: 9-12.

Kawamata, T., T. Mori, et al. (2007). "Tissue hyperosmolality and brain edema in cerebral contusion." Neurosurg Focus **22**(5): E5.

Kayagaki, N., S. Warming, et al. (2011). "Non-canonical inflammasome activation targets caspase-11." Nature **479**(7371): 117-121.

Kelly, D. F., N. A. Martin, et al. (1997). "Cerebral blood flow as a predictor of outcome following traumatic brain injury." J Neurosurg **86**(4): 633-641.

Ketroussi, F., M. Giuliani, et al. (2011). "Lymphocyte cell-cycle inhibition by HLA-G is mediated by phosphatase SHP-2 and acts on the mTOR pathway." PLoS ONE **6**(8): e22776.

Ketting, R. F., S. E. Fischer, et al. (2001). "Dicer functions in RNA interference and in synthesis of small RNA involved in developmental timing in C. elegans." Genes Dev **15**(20): 2654-2659.

Kevil, C. G., N. Okayama, et al. (1998). "Expression of zonula occludens and adherens junctional proteins in human venous and arterial endothelial cells: role of occludin in endothelial solute barriers." Microcirculation **5**(2-3): 197-210.

Kikuchi, K., T. Kadono, et al. (1997). "Tissue inhibitor of metalloproteinase 1 (TIMP-1) may be an autocrine growth factor in scleroderma fibroblasts." J Invest Dermatol **108**(3): 281-284.

Kim, D. H., M. Longo, et al. (2004). "Interferon induction by siRNAs and ssRNAs synthesized by phage polymerase." Nat Biotechnol **22**(3): 321-325.

Kim, J., J. Whyte, et al. (2010). "Resting cerebral blood flow alterations in chronic traumatic brain injury: an arterial spin labeling perfusion FMRI study." J Neurotrauma **27**(8): 1399-1411.

Kim, J. Y., S. Choung, et al. (2007). "Immune activation by siRNA/liposome complexes in mice is sequence- independent: lack of a role for Toll-like receptor 3 signaling." Mol Cells **24**(2): 247-254.

Kim, K. S. (2008). "Mechanisms of microbial traversal of the blood-brain barrier." Nat Rev Microbiol **6**(8): 625-634.

Kim, W. J., J. W. Yockman, et al. (2006). "Anti-angiogenic inhibition of tumor growth by systemic delivery of PEI-g-PEG-RGD/pCMV-sFlt-1 complexes in tumor-bearing mice." J Control Release **114**(3): 381-388.

Kinsella, P., M. Clynes, et al. (2011). "Imatinib and docetaxel in combination can effectively inhibit glioma invasion in an in vitro 3D invasion assay." J Neurooncol **101**(2): 189-198.

Kitajiri, S., T. Miyamoto, et al. (2004). "Compartmentalization established by claudin-11-based tight junctions in stria vascularis is required for hearing through generation of endocochlear potential." J Cell Sci **117**(Pt 21): 5087-5096.

Klasa, R. J., A. M. Gillum, et al. (2002). "Oblimersen Bcl-2 antisense: facilitating apoptosis in anticancer treatment." Antisense Nucleic Acid Drug Dev **12**(3): 193-213.

Kleihues, P., P. C. Burger, et al. (1993). "The new WHO classification of brain tumours." Brain Pathol **3**(3): 255-268.

Klein, P., D. Herr, et al. (2012). "Results of phase 2 safety and feasibility study of treatment with levetiracetam for prevention of posttraumatic epilepsy." Arch Neurol **69**(10): 1290-1295.

Kleinman, M. E., H. Kaneko, et al. (2012). "Short-interfering RNAs induce retinal degeneration via TLR3 and IRF3." Mol Ther **20**(1): 101-108.

Kleinman, M. E., K. Yamada, et al. (2008). "Sequence- and target-independent angiogenesis suppression by siRNA via TLR3." Nature **452**(7187): 591-597.

Klingler, C., U. Kniesel, et al. (2000). "Disruption of epithelial tight junctions is prevented by cyclic nucleotide-dependent protein kinase inhibitors." Histochem Cell Biol **113**(5): 349-361.

Knott, J. C., A. J. Edwards, et al. (1990). "A human glioma cell line retaining expression of GFAP and gangliosides, recognized by A2B5 and LB1 antibodies, after prolonged passage." Neuropathol Appl Neurobiol **16**(6): 489-500.

Kossmann, T., V. Hans, et al. (1996). "Interleukin-6 released in human cerebrospinal fluid following traumatic brain injury may trigger nerve growth factor production in astrocytes." Brain Res **713**(1-2): 143-152.

Koto, T., K. Takubo, et al. (2007). "Hypoxia disrupts the barrier function of neural blood vessels through changes in the expression of claudin-5 in endothelial cells." Am J Pathol **170**(4): 1389-1397.

Kroll, R. A., M. A. Pagel, et al. (1994). "Differential permeability of the blood-tumour barrier in intracerebral tumour-bearing rats: antidrug antibody to achieve systemic drug rescue." Ther Immunol **1**(6): 333-341.

Krueger, G. G., D. D. Manning, et al. (1975). "Long-term maintenance of psoriatic human skin on congenitally athymic (nude) mice." J Invest Dermatol **64**(5): 307-312.

Kuchler-Bopp, S., J. P. Delaunoy, et al. (1999). "Astrocytes induce several blood-brain barrier properties in non-neural endothelial cells." Neuroreport **10**(6): 1347-1353.

Kutzelnigg, A., C. F. Lucchinetti, et al. (2005). "Cortical demyelination and diffuse white matter injury in multiple sclerosis." Brain **128**(Pt 11): 2705-2712.

Laird, M. D., S. Sukumari-Ramesh, et al. (2010). "Curcumin attenuates cerebral edema following traumatic brain injury in mice: a possible role for aquaporin-4?" J Neurochem **113**(3): 637-648.

Larsson, H. B., M. Stubgaard, et al. (1990). "Quantitation of blood-brain barrier defect by magnetic resonance imaging and gadolinium-DTPA in patients with multiple sclerosis and brain tumors." Magn Reson Med **16**(1): 117-131.

Lazana, I., A. Zoudiari, et al. (2012). "Identification of a novel HLA-G+ regulatory population in blood: expansion after allogeneic transplantation and de novo HLA-G expression at graft-versus-host disease sites." Haematologica **97**(9): 1338-1347.

Lee, E. Y., Z. H. Lee, et al. (2013). "The interaction between CXCL10 and cytokines in chronic inflammatory arthritis." Autoimmun Rev **12**(5): 554-557.

Lee, J. H., N. A. Martin, et al. (1997). "Hemodynamically significant cerebral vasospasm and outcome after head injury: a prospective study." J Neurosurg **87**(2): 221-233.

Lee, R. C., R. L. Feinbaum, et al. (1993). "The C. elegans heterochronic gene lin-4 encodes small RNAs with antisense complementarity to lin-14." Cell **75**(5): 843-854.

Lee, Y., C. Ahn, et al. (2003). "The nuclear RNase III Drosha initiates microRNA processing." Nature **425**(6956): 415-419.

Lefranc, F., J. Brotchi, et al. (2005). "Possible future issues in the treatment of glioblastomas: special emphasis on cell migration and the resistance of migrating glioblastoma cells to apoptosis." J Clin Oncol **23**(10): 2411-2422.

Leggas, M., M. Adachi, et al. (2004). "Mrp4 confers resistance to topotecan and protects the brain from chemotherapy." Mol Cell Biol **24**(17): 7612-7621.

Lei, X., M. Hossain, et al. (2012). "Different microvascular permeability responses elicited by the CXC chemokines MIP-2 and KC during leukocyte recruitment: role of LSP1." Biochem Biophys Res Commun **423**(3): 484-489.

Lentsch, A. B., H. Yoshidome, et al. (1998). "Chemokine involvement in hepatic ischemia/reperfusion injury in mice: roles for macrophage inflammatory protein-2 and KC." Hepatology **27**(4): 1172-1177.

Li, L., J. Yang, et al. (2012). "Pigment epithelium-derived factor gene loaded in cRGD-PEG-PEI suppresses colorectal cancer growth by targeting endothelial cells." Int J Pharm **438**(1-2): 1-10.

Li, X., J. Gao, et al. (2013). "Aquaporin-4 expression contributes to decreases in brain water content during mouse postnatal development." Brain Res Bull **94**: 49-55.

Liebner, S., A. Fischmann, et al. (2000). "Claudin-1 and claudin-5 expression and tight junction morphology are altered in blood vessels of human glioblastoma multiforme." Acta Neuropathol **100**(3): 323-331.

Liebner, S., M. Corada, et al. (2008). "Wnt/beta-catenin signaling controls development of the blood-brain barrier." J Cell Biol **183**(3): 409-417.

Liehn, E. A., A. Schober, et al. (2004). "Blockade of keratinocyte-derived chemokine inhibits endothelial recovery and enhances plaque formation after arterial injury in ApoE-deficient mice." Arterioscler Thromb Vasc Biol **24**(10): 1891-1896.

Lim, S. W., C. C. Wang, et al. (2013). "Microglial activation induced by traumatic brain injury is suppressed by postinjury treatment with hyperbaric oxygen therapy." J Surg Res.

Ling, V. (1995). "P-glycoprotein: its role in drug resistance." Am J Med **99**(6A): 31S-34S.

Loane, D. J. and A. I. Faden (2010). "Neuroprotection for traumatic brain injury: translational challenges and emerging therapeutic strategies." Trends Pharmacol Sci **31**(12): 596-604.

Lockman, P. R., R. K. Mittapalli, et al. (2010). "Heterogeneous blood-tumor barrier permeability determines drug efficacy in experimental brain metastases of breast cancer." Clin Cancer Res **16**(23): 5664-5678.

Logan, C. Y. and R. Nusse (2004). "The Wnt signaling pathway in development and disease." Annu Rev Cell Dev Biol **20**: 781-810.

Loh, Y. H., A. Christoffels, et al. (2004). "Extensive expansion of the claudin gene family in the teleost fish, Fugu rubripes." Genome Res **14**(7): 1248-1257.

Lu, K. T., C. Y. Wu, et al. (2007). "Bumetanide administration attenuated traumatic brain injury through IL-1 overexpression." Neurol Res **29**(4): 404-409.

Lu, L. F., E. F. Lind, et al. (2006). "Mast cells are essential intermediaries in regulatory T-cell tolerance." Nature **442**(7106): 997-1002.

Lyck, R., Y. Reiss, et al. (2003). "T-cell interaction with ICAM-1/ICAM-2 double-deficient brain endothelium in vitro: the cytoplasmic tail of endothelial ICAM-1 is necessary for transendothelial migration of T cells." Blood **102**(10): 3675-3683.

Ma, D., L. Wang, et al. (2012). "Foxn1 maintains thymic epithelial cells to support T-cell development via mcm2 in zebrafish." Proc Natl Acad Sci U S A **109**(51): 21040-21045.

Maas, A. I., G. Murray, et al. (2006). "Efficacy and safety of dexanabinol in severe traumatic brain injury: results of a phase III randomised, placebo-controlled, clinical trial." Lancet Neurol **5**(1): 38-45.

Maas, A. I., N. Stocchetti, et al. (2008). "Moderate and severe traumatic brain injury in adults." Lancet Neurol **7**(8): 728-741.

Macpherson, P. and D. I. Graham (1978). "Correlation between angiographic findings and the ischaemia of head injury." J Neurol Neurosurg Psychiatry **41**(2): 122-127.

Maguen, S., E. Madden, et al. (2012). "The impact of head injury mechanism on mental health symptoms in veterans: do number and type of exposures matter?" J Trauma Stress **25**(1): 3-9.

Majumder, S., S. Bhattacharjee, et al. (2012). "CXCL10 is critical for the generation of protective CD8 T cell response induced by antigen pulsed CpG-ODN activated dendritic cells." PLoS ONE **7**(11): e48727.

Malinski, T., F. Bailey, et al. (1993). "Nitric oxide measured by a porphyrinic microsensor in rat brain after transient middle cerebral artery occlusion." J Cereb Blood Flow Metab **13**(3): 355-358.

Manley, G. T., M. Fujimura, et al. (2000). "Aquaporin-4 deletion in mice reduces brain edema after acute water intoxication and ischemic stroke." Nat Med **6**(2): 159-163.

Maolood, N. and B. Meister (2009). "Protein components of the blood-brain barrier (BBB) in the brainstem area postrema-nucleus tractus solitarius region." J Chem Neuroanat **37**(3): 182-195.

Marchi, N., G. Betto, et al. (2009). "Blood-brain barrier damage and brain penetration of antiepileptic drugs: role of serum proteins and brain edema." Epilepsia **50**(4): 664-677.

Marmarou, A., P. P. Fatouros, et al. (2000). "Contribution of edema and cerebral blood volume to traumatic brain swelling in head-injured patients." J Neurosurg **93**(2): 183-193.

Marmarou, A., M. A. Foda, et al. (1994). "A new model of diffuse brain injury in rats. Part I: Pathophysiology and biomechanics." J Neurosurg **80**(2): 291-300.

Marmarou, A., S. Signoretti, et al. (2006). "Predominance of cellular edema in traumatic brain swelling in patients with severe head injuries." J Neurosurg **104**(5): 720-730.

Marmarou, C. R. and J. T. Povlishock (2006). "Administration of the immunophilin ligand FK506 differentially attenuates neurofilament compaction and impaired axonal transport in injured axons following diffuse traumatic brain injury." Exp Neurol **197**(2): 353-362.

Maruoka, H., D. Inoue, et al. (2013). "IP-10/CXCL10 and MIG/CXCL9 as novel markers for the diagnosis of lymphoma-associated hemophagocytic syndrome." Ann Hematol.

Masliah, E. and E. Diez-Tejedor (2012). "The pharmacology of neurotrophic treatment with Cerebrolysin: brain protection and repair to counteract pathologies of acute and chronic neurological disorders." Drugs Today (Barc) **48 Suppl A**: 3-24.

Martinez, J., A. Patkaniowska, et al. (2002). "Single-stranded antisense siRNAs guide target RNA cleavage in RNAi." Cell **110**(5): 563-574.

Masocha, W., M. E. Rottenberg, et al. (2007). "Migration of African trypanosomes across the blood-brain barrier." Physiol Behav **92**(1-2): 110-114.

Mason, J. L., K. Suzuki, et al. (2001). "Interleukin-1beta promotes repair of the CNS." J Neurosci **21**(18): 7046-7052.

Matsumoto, K., E. H. Lo, et al. (1995). "Role of vasogenic edema and tissue cavitation in ischemic evolution on diffusion-weighted imaging: comparison with multiparameter MR and immunohistochemistry." AJNR Am J Neuroradiol **16**(5): 1107-1115.

Matyszak, M. K. and V. H. Perry (1996). "The potential role of dendritic cells in immune-mediated inflammatory diseases in the central nervous system." Neuroscience **74**(2): 599-608.

Mayhan, W. G. (1999). "VEGF increases permeability of the blood-brain barrier via a nitric oxide synthase/cGMP-dependent pathway." Am J Physiol **276**(5 Pt 1): C1148-1153.

McKee, A. C., R. C. Cantu, et al. (2009). "Chronic traumatic encephalopathy in athletes: progressive tauopathy after repetitive head injury." J Neuropathol Exp Neurol **68**(7): 709-735.

McLendon, R., A. Friedman, et al. (2008). "Comprehensive genomic characterization defines human glioblastoma genes and core pathways." Nature **455**(7216): 1061-1068.

McRobbie, D. W. (2007). MRI from picture to proton. Cambridge, UK ; New York, Cambridge University Press.

Mecklenburg, L., R. Paus, et al. (2004). "FOXN1 is critical for onycholemmal terminal differentiation in nude (Foxn1) mice." J Invest Dermatol **123**(6): 1001-1011.

Medawar, P. B. (1948). "Immunity to homologous grafted skin; the fate of skin homografts transplanted to the brain, to subcutaneous tissue, and to the anterior chamber of the eye." Br J Exp Pathol **29**(1): 58-69.

Menten, P., A. Wuyts, et al. (2002). "Macrophage inflammatory protein-1." Cytokine Growth Factor Rev **13**(6): 455-481.

Mohan, P. and N. Rapoport (2010). "Doxorubicin as a molecular nanotheranostic agent: effect of doxorubicin encapsulation in micelles or nanoemulsions on the ultrasound-mediated intracellular delivery and nuclear trafficking." Mol Pharm **7**(6): 1959-1973.

Mojsilovic-Petrovic, J., D. Callaghan, et al. (2007). "Hypoxia-inducible factor-1 (HIF-1) is involved in the regulation of hypoxia-stimulated expression of monocyte

chemoattractant protein-1 (MCP-1/CCL2) and MCP-5 (Ccl12) in astrocytes." J Neuroinflammation **4**: 12.

Morimoto, H., M. Hirose, et al. (2008). "MCP-1 induces cardioprotection against ischaemia/reperfusion injury: role of reactive oxygen species." Cardiovasc Res **78**(3): 554-562.

Morita, K., H. Sasaki, et al. (1999). "Endothelial claudin: claudin-5/TMVCF constitutes tight junction strands in endothelial cells." J Cell Biol **147**(1): 185-194.

Mott, F.W. (1913). "The Late Professor Edwin Goldmann's Investigations on the Central Nervous System by Vital Staining." Br Med J **2**(2753): 871-873.

Mott, R. T., G. Ait-Ghezala, et al. (2004). "Neuronal expression of CD22: novel mechanism for inhibiting microglial proinflammatory cytokine production." Glia **46**(4): 369-379.

Muldoon, L. L., G. Nilaver, et al. (1995). "Comparison of intracerebral inoculation and osmotic blood-brain barrier disruption for delivery of adenovirus, herpesvirus, and iron oxide particles to normal rat brain." Am J Pathol **147**(6): 1840-1851.

Murakami, K., T. Kondo, et al. (1999). "Cold injury in mice: a model to study mechanisms of brain edema and neuronal apoptosis." Prog Neurobiol **57**(3): 289-299.

Murakami, K., M. Kawase, et al. (1998). "Cellular accumulation of extravasated serum protein and DNA fragmentation following vasogenic edema." J Neurotrauma **15**(10): 825-835.

Nadeau, S. and S. Rivest (2003). "Glucocorticoids play a fundamental role in protecting the brain during innate immune response." J Neurosci **23**(13): 5536-5544.

Navarro, G., R. R. Sawant, et al. (2012). "P-glycoprotein silencing with siRNA delivered by DOPE-modified PEI overcomes doxorubicin resistance in breast cancer cells." Nanomedicine (Lond) **7**(1): 65-78.

Nelson, T. E. and D. L. Gruol (2004). "The chemokine CXCL10 modulates excitatory activity and intracellular calcium signaling in cultured hippocampal neurons." J Neuroimmunol **156**(1-2): 74-87.

Ness, T., N. Feltgen, et al. (2010). "Toxic vitreitis outbreak after intravitreal injection." Retina **30**(2): 332-338.

Neumann, H., M. R. Kotter, et al. (2009). "Debris clearance by microglia: an essential link between degeneration and regeneration." Brain **132**(Pt 2): 288-295.

Neumann, J., S. Sauerzweig, et al. (2008). "Microglia cells protect neurons by direct engulfment of invading neutrophil granulocytes: a new mechanism of CNS immune privilege." J Neurosci **28**(23): 5965-5975.

Neuwelt, E. A., D. L. Goldman, et al. (1991). "Primary CNS lymphoma treated with osmotic blood-brain barrier disruption: prolonged survival and preservation of cognitive function." J Clin Oncol **9**(9): 1580-1590.

Nielsen, S., E. A. Nagelhus, et al. (1997). "Specialized membrane domains for water transport in glial cells: high-resolution immunogold cytochemistry of aquaporin-4 in rat brain." J Neurosci **17**(1): 171-180.

Nimmerjahn, A., F. Kirchhoff, et al. (2005). "Resting microglial cells are highly dynamic surveillants of brain parenchyma in vivo." Science **308**(5726): 1314-1318.

Nitta, T., M. Hata, et al. (2003). "Size-selective loosening of the blood-brain barrier in claudin-5-deficient mice." J Cell Biol **161**(3): 653-660.

Nittby, H., G. Grafstrom, et al. (2008). "Radiofrequency and extremely low-frequency electromagnetic field effects on the blood-brain barrier." Electromagn Biol Med **27**(2): 103-126.

Noch, E. and K. Khalili (2009). "Molecular mechanisms of necrosis in glioblastoma: the role of glutamate excitotoxicity." Cancer Biol Ther **8**(19): 1791-1797.

Noell, S., D. Mayer, et al. (2011). "Selective enrichment of hypericin in malignant glioma: pioneering in vivo results." Int J Oncol **38**(5): 1343-1348.

Nottebaum, A. F., G. Cagna, et al. (2008). "VE-PTP maintains the endothelial barrier via plakoglobin and becomes dissociated from VE-cadherin by leukocytes and by VEGF." J Exp Med **205**(12): 2929-2945.

Obermeier, B., R. Daneman, et al. (2013). "Development, maintenance and disruption of the blood-brain barrier." Nat Med **19**(12): 1584-1596.

Ohtsuki, S., S. Sato, et al. (2007). "Exogenous expression of claudin-5 induces barrier properties in cultured rat brain capillary endothelial cells." J Cell Physiol **210**(1): 81-86.

Oldendorf, W. H., M. E. Cornford, et al. (1977). "The large apparent work capability of the blood-brain barrier: a study of the mitochondrial content of capillary endothelial cells in brain and other tissues of the rat." Ann Neurol **1**(5): 409-417.

Olivecrona, M., M. Rodling-Wahlstrom, et al. (2009). "Prostacyclin treatment in severe traumatic brain injury: a microdialysis and outcome study." J Neurotrauma **26**(8): 1251-1262.

Ose, A., M. Ito, et al. (2009). "Limited brain distribution of [3R,4R,5S]-4-acetamido-5-amino-3-(1-ethylpropoxy)-1-cyclohexene-1-carboxyl ate phosphate (Ro 64-0802), a pharmacologically active form of oseltamivir, by active efflux across the blood-brain barrier mediated by organic anion transporter 3 (Oat3/Slc22a8) and multidrug resistance-associated protein 4 (Mrp4/Abcc4)." Drug Metab Dispos **37**(2): 315-321.

Oubaha, M. and J. P. Gratton (2009). "Phosphorylation of endothelial nitric oxide synthase by atypical PKC zeta contributes to angiopoietin-1-dependent inhibition of VEGF-induced endothelial permeability in vitro." Blood **114**(15): 3343-3351.

Oury, T. D., C. A. Piantadosi, et al. (1993). "Cold-induced brain edema in mice. Involvement of extracellular superoxide dismutase and nitric oxide." J Biol Chem **268**(21): 15394-15398.

Papadopoulos, M. C. and A. S. Verkman (2007). "Aquaporin-4 and brain edema." Pediatr Nephrol **22**(6): 778-784.

Pardridge, W. M. (2003). "Blood-brain barrier drug targeting: the future of brain drug development." Mol Interv **3**(2): 90-105, 151.

Pardridge, W. M. (2005). "The blood-brain barrier: bottleneck in brain drug development." NeuroRx **2**(1): 3-14.

Pardridge, W. M. (2007). "Blood-brain barrier delivery." Drug Discov Today **12**(1-2): 54-61.

Pardridge, W. M. and W. H. Oldendorf (1975). "Kinetics of blood-brain transport of hexoses." Biochim Biophys Acta **382**(3): 377-392.

Park, K., S. W. Hong, et al. (2011). "Target specific systemic delivery of TGF-beta siRNA/(PEI-SS)-g-HA complex for the treatment of liver cirrhosis." Biomaterials **32**(21): 4951-4958.

Pau, E., Y. H. Cheung, et al. (2012). "TLR tolerance reduces IFN-alpha production despite plasmacytoid dendritic cell expansion and anti-nuclear antibodies in NZB bicongenic mice." PLoS ONE **7**(5): e36761.

Pearson, V. L., N. J. Rothwell, et al. (1999). "Excitotoxic brain damage in the rat induces interleukin-1beta protein in microglia and astrocytes: correlation with the progression of cell death." Glia **25**(4): 311-323.

Peperzak, V., E. A. Veraar, et al. (2013). "CD8+ T Cells Produce the Chemokine CXCL10 in Response to CD27/CD70 Costimulation To Promote Generation of the CD8+ Effector T Cell Pool." J Immunol.

Perry, C. M. and J. A. Balfour (1999). "Fomivirsen." Drugs **57**(3): 375-380; discussion 381.

Phares, T. W., S. A. Stohlman, et al. (2013). "Astrocyte-derived CXCL10 drives accumulation of antibody-secreting cells in the central nervous system during viral encephalomyelitis." J Virol **87**(6): 3382-3392.

Polderman, K. H., R. Tjong Tjin Joe, et al. (2002). "Effects of therapeutic hypothermia on intracranial pressure and outcome in patients with severe head injury." Intensive Care Med **28**(11): 1563-1573.

Prados, M. D., S. J. S. Schold, et al. (2003). "A randomized, double-blind, placebo-controlled, phase 2 study of RMP-7 in combination with carboplatin administered intravenously for the treatment of recurrent malignant glioma." Neuro Oncol **5**(2): 96-103.

Qiu, W., Y. Zhang, et al. (2007). "Effects of therapeutic mild hypothermia on patients with severe traumatic brain injury after craniotomy." J Crit Care **22**(3): 229-235.

Quagliarello, V. J., B. Wispelwey, et al. (1991). "Recombinant human interleukin-1 induces meningitis and blood-brain barrier injury in the rat. Characterization and comparison with tumor necrosis factor." J Clin Invest **87**(4): 1360-1366.

Qureshi, N. H., K. S. Bankiewicz, et al. (2000). "Multicolumn infusion of gene therapy cells into human brain tumors: technical report." Neurosurgery **46**(3): 663-668; discussion 668-669.

Raby, A. C., B. Holst, et al. (2011). "TLR activation enhances C5a-induced pro-inflammatory responses by negatively modulating the second C5a receptor, C5L2." Eur J Immunol **41**(9): 2741-2752.

Rahman, A., D. Carmichael, et al. (1986). "Comparative pharmacokinetics of free doxorubicin and doxorubicin entrapped in cardiolipin liposomes." Cancer Res **46**(5): 2295-2299.

Rainov, N. G. and C. M. Kramm (2001). "Vector delivery methods and targeting strategies for gene therapy of brain tumors." Curr Gene Ther **1**(4): 367-383.

Rajagopal, R. and J. W. Harbour (2011). "Diagnostic testing and treatment choices in primary vitreoretinal lymphoma." Retina **31**(3): 435-440.

Rajesh, M., K. N. Sulochana, et al. (2004). "Iron chelation abrogates excessive formation of hydroxyl radicals and lipid peroxidation products in monocytes of patients with Eales' disease: direct evidence using electron spin resonance spectroscopy." Curr Eye Res **28**(6): 399-407.

Rapoport, S. I. (2000). "Osmotic opening of the blood-brain barrier: principles, mechanism, and therapeutic applications." Cell Mol Neurobiol **20**(2): 217-230.

Rascher, G., A. Fischmann, et al. (2002). "Extracellular matrix and the blood-brain barrier in glioblastoma multiforme: spatial segregation of tenascin and agrin." Acta Neuropathol **104**(1): 85-91.

Reeves, T. M., L. L. Phillips, et al. (2007). "Preferential neuroprotective effect of tacrolimus (FK506) on unmyelinated axons following traumatic brain injury." Brain Res **1154**: 225-236.

Reeves, T. M., L. L. Phillips, et al. (2005). "Myelinated and unmyelinated axons of the corpus callosum differ in vulnerability and functional recovery following traumatic brain injury." Exp Neurol **196**(1): 126-137.

Reichel, C. A., M. Rehberg, et al. (2009). "Ccl2 and Ccl3 mediate neutrophil recruitment via induction of protein synthesis and generation of lipid mediators." Arterioscler Thromb Vasc Biol **29**(11): 1787-1793.

Reis, M., C. J. Czupalla, et al. (2012). "Endothelial Wnt/beta-catenin signaling inhibits glioma angiogenesis and normalizes tumor blood vessels by inducing PDGF-B expression." J Exp Med **209**(9): 1611-1627.

Rejman, J., A. Bragonzi, et al. (2005). "Role of clathrin- and caveolae-mediated endocytosis in gene transfer mediated by lipo- and polyplexes." Mol Ther **12**(3): 468-474.

Reneer, D. V., R. D. Hisel, et al. (2011). "A multi-mode shock tube for investigation of blast-induced traumatic brain injury." J Neurotrauma **28**(1): 95-104.

Reynolds, A., E. M. Anderson, et al. (2006). "Induction of the interferon response by siRNA is cell type- and duplex length-dependent." RNA **12**(6): 988-993.

Rigau, V., M. Morin, et al. (2007). "Angiogenesis is associated with blood-brain barrier permeability in temporal lobe epilepsy." Brain **130**(Pt 7): 1942-1956.

Robbins, M., A. Judge, et al. (2007). "2'-O-methyl-modified RNAs act as TLR7 antagonists." Mol Ther **15**(9): 1663-1669.

Roberts, I., D. Yates, et al. (2004). "Effect of intravenous corticosteroids on death within 14 days in 10008 adults with clinically significant head injury (MRC CRASH trial): randomised placebo-controlled trial." Lancet **364**(9442): 1321-1328.

Ronaldson, P. T., K. M. Demarco, et al. (2009). "Transforming growth factor-beta signaling alters substrate permeability and tight junction protein expression at the blood-brain barrier during inflammatory pain." J Cereb Blood Flow Metab **29**(6): 1084-1098.

Rooprai, H. K., I. Kyriazis, et al. (2007). "Inhibition of invasion and induction of apoptosis by selenium in human malignant brain tumour cells in vitro." Int J Oncol **30**(5): 1263-1271.

Rose, J. C., T. A. Neill, et al. (2006). "Continuous monitoring of the microcirculation in neurocritical care: an update on brain tissue oxygenation." Curr Opin Crit Care **12**(2): 97-102.

Rosenfeld, J. V., A. C. McFarlane, et al. (2013). "Blast-related traumatic brain injury." Lancet Neurol.

Rosenfeld, P. J., J. S. Heier, et al. (2006). "Tolerability and efficacy of multiple escalating doses of ranibizumab (Lucentis) for neovascular age-related macular degeneration." Ophthalmology **113**(4): 623 e621.

Ross, J. S., R. Delamarter, et al. (1989). "Gadolinium-DTPA-enhanced MR imaging of the postoperative lumbar spine: time course and mechanism of enhancement." AJR Am J Roentgenol **152**(4): 825-834.

Rousselle, C., P. Clair, et al. (2000). "New advances in the transport of doxorubicin through the blood-brain barrier by a peptide vector-mediated strategy." Mol Pharmacol **57**(4): 679-686.

Rubin, L. L., D. E. Hall, et al. (1991). "A cell culture model of the blood-brain barrier." J Cell Biol **115**(6): 1725-1735.

Saito, A., P. Narasimhan, et al. (2004). "Neuroprotective role of a proline-rich Akt substrate in apoptotic neuronal cell death after stroke: relationships with nerve growth factor." J Neurosci **24**(7): 1584-1593.

Sarafi, M. N., E. A. Garcia-Zepeda, et al. (1997). "Murine monocyte chemoattractant protein (MCP)-5: a novel CC chemokine that is a structural and functional homologue of human MCP-1." J Exp Med **185**(1): 99-109.

Schinkel, A. H., J. J. Smit, et al. (1994). "Disruption of the mouse mdr1a P-glycoprotein gene leads to a deficiency in the blood-brain barrier and to increased sensitivity to drugs." Cell **77**(4): 491-502.

Seabrook, T. J., M. Johnston, et al. (1998). "Cerebral spinal fluid lymphocytes are part of the normal recirculating lymphocyte pool." J Neuroimmunol **91**(1-2): 100-107.

Seidel, C., N. Dorner, et al. (2011). "Does age matter? - A MRI study on peritumoral edema in newly diagnosed primary glioblastoma." BMC Cancer **11**: 127.

Seiffert, E., J. P. Dreier, et al. (2004). "Lasting blood-brain barrier disruption induces epileptic focus in the rat somatosensory cortex." J Neurosci **24**(36): 7829-7836.

Shahbazi-Gahrouei, D., M. Williams, et al. (2001). "In vitro study of relationship between signal intensity and gadolinium-DTPA concentration at high magnetic field strength." Australas Radiol **45**(3): 298-304.

Shakeri, M., M. R. Boustani, et al. (2013). "Effect of progesterone administration on prognosis of patients with diffuse axonal injury due to severe head trauma." Clin Neurol Neurosurg.

Sharma, A., A. Tandon, et al. (2011). "Polyethylenimine-conjugated gold nanoparticles: Gene transfer potential and low toxicity in the cornea." Nanomedicine **7**(4): 505-513.

Shaw, K., M. A. MacKinnon, et al. (2001). "TUNEL-positive staining in white and grey matter after fatal head injury in man." Clin Neuropathol **20**(3): 106-112.

Shen, J., H. Sun, et al. (2013). "Simultaneous inhibition of metastasis and growth of breast cancer by co-delivery of twist shRNA and paclitaxel using pluronic P85-PEI/TPGS complex nanoparticles." Biomaterials **34**(5): 1581-1590.

Sherriff, F. E., L. R. Bridges, et al. (1994). "Early detection of axonal injury after human head trauma using immunocytochemistry for beta-amyloid precursor protein." Acta Neuropathol **87**(1): 55-62.

Schinkel, A. H. and J. W. Jonker (2003). "Mammalian drug efflux transporters of the ATP binding cassette (ABC) family: an overview." Adv Drug Deliv Rev **55**(1): 3-29.

Silbergeld, D. L. and M. R. Chicoine (1997). "Isolation and characterization of human malignant glioma cells from histologically normal brain." J Neurosurg **86**(3): 525-531.

Simon, D. B., Y. Lu, et al. (1999). "Paracellin-1, a renal tight junction protein required for paracellular Mg2+ resorption." Science **285**(5424): 103-106.

Simet, S. M., T. A. Wyatt, et al. (2012). "Alcohol increases the permeability of airway epithelial tight junctions in Beas-2B and NHBE cells." Alcohol Clin Exp Res **36**(3): 432-442.

Sioud, M. (2005). "Induction of inflammatory cytokines and interferon responses by double-stranded and single-stranded siRNAs is sequence-dependent and requires endosomal localization." J Mol Biol **348**(5): 1079-1090.

Skaer, H. B., S. H. Maddrell, et al. (1987). "The permeability properties of septate junctions in Malpighian tubules of Rhodnius." J Cell Sci **88 (Pt 2)**: 251-265.

Skold, M. K., C. von Gertten, et al. (2005). "VEGF and VEGF receptor expression after experimental brain contusion in rat." J Neurotrauma **22**(3): 353-367.

Smith, A. M., H. M. Gibbons, et al. (2013). "M-CSF increases proliferation and phagocytosis while modulating receptor and transcription factor expression in adult human microglia." J Neuroinflammation **10**: 85.

Smith, D. H., X. H. Chen, et al. (1999). "Accumulation of amyloid beta and tau and the formation of neurofilament inclusions following diffuse brain injury in the pig." J Neuropathol Exp Neurol **58**(9): 982-992.

Smith, D. H., X. H. Chen, et al. (1997). "Characterization of diffuse axonal pathology and selective hippocampal damage following inertial brain trauma in the pig." J Neuropathol Exp Neurol **56**(7): 822-834.

Smith, D. H., M. Nonaka, et al. (2000). "Immediate coma following inertial brain injury dependent on axonal damage in the brainstem." J Neurosurg **93**(2): 315-322.

Society of British Neurological Surgeons (2010). "Proceedings of the 155th meeting of the Society of British Neurological Surgeons." British Journal of Neurosurgery **24**(2): 108–147.

Song, S. W., G. N. Fuller, et al. (2003). "IIp45, an insulin-like growth factor binding protein 2 (IGFBP-2) binding protein, antagonizes IGFBP-2 stimulation of glioma cell invasion." Proc Natl Acad Sci U S A **100**(24): 13970-13975.

Sridharan, A., C. Patel, et al. (2013). "Voltage Preconditioning Allows Modulated Gene Expression in Neurons Using PEI-complexed siRNA." Mol Ther Nucleic Acids **2**: e82.

Staub, F., J. Peters, et al. (1997). "Swelling and damage of glial cells by lactacidosis and glutamate: effect of alpha-trinositol." Brain Res **766**(1-2): 285-288.

Steiner, O., C. Coisne, et al. (2010). "Differential roles for endothelial ICAM-1, ICAM-2, and VCAM-1 in shear-resistant T cell arrest, polarization, and directed crawling on blood-brain barrier endothelium." J Immunol **185**(8): 4846-4855.

Stenman, J. M., J. Rajagopal, et al. (2008). "Canonical Wnt signaling regulates organ-specific assembly and differentiation of CNS vasculature." Science **322**(5905): 1247-1250.

Stiefel, M. F., Y. Tomita, et al. (2005). "Secondary ischemia impairing the restoration of ion homeostasis following traumatic brain injury." J Neurosurg **103**(4): 707-714.

Stork, T., D. Engelen, et al. (2008). "Organization and function of the blood-brain barrier in Drosophila." J Neurosci **28**(3): 587-597.

Strijbos, P. J. and N. J. Rothwell (1995). "Interleukin-1 beta attenuates excitatory amino acid-induced neurodegeneration in vitro: involvement of nerve growth factor." J Neurosci **15**(5 Pt 1): 3468-3474.

Stuhr, C. M., P. E. Miller, et al. (1998). "Effect of intracameral administration of carbachol on the postoperative increase in intraocular pressure in dogs undergoing cataract extraction." J Am Vet Med Assoc **212**(12): 1885-1888.

Stumm, R. K., J. Rummel, et al. (2002). "A dual role for the SDF-1/CXCR4 chemokine receptor system in adult brain: isoform-selective regulation of SDF-1 expression modulates CXCR4-dependent neuronal plasticity and cerebral leukocyte recruitment after focal ischemia." J Neurosci **22**(14): 5865-5878.

Stupp, R., W. P. Mason, et al. (2005). "Radiotherapy plus concomitant and adjuvant temozolomide for glioblastoma." N Engl J Med **352**(10): 987-996.

Sugiyama, Y., H. Kusuhara, et al. (1999). "Kinetic and biochemical analysis of carrier-mediated efflux of drugs through the blood-brain and blood-cerebrospinal fluid

barriers: importance in the drug delivery to the brain." J Control Release **62**(1-2): 179-186.

Sui, Y., L. Stehno-Bittel, et al. (2006). "CXCL10-induced cell death in neurons: role of calcium dysregulation." Eur J Neurosci **23**(4): 957-964.

Szeto, W., W. Jiang, et al. (2001). "Overexpression of the retinoic acid-responsive gene Stra6 in human cancers and its synergistic induction by Wnt-1 and retinoic acid." Cancer Res **61**(10): 4197-4205.

Taddei, A., C. Giampietro, et al. (2008). "Endothelial adherens junctions control tight junctions by VE-cadherin-mediated upregulation of claudin-5." Nat Cell Biol **10**(8): 923-934.

Tagliaferri, F., C. Compagnone, et al. (2006). "A systematic review of brain injury epidemiology in Europe." Acta Neurochir (Wien) **148**(3): 255-268; discussion 268.

Takahashi, H., R. Obata, et al. (2006). "A novel vascular endothelial growth factor receptor 2 inhibitor, SU11248, suppresses choroidal neovascularization in vivo." J Ocul Pharmacol Ther **22**(4): 213-218.

Takahashi, H., F. Yamaguchi, et al. (2005). "Long-term outcome and reconsideration of intracystic chemotherapy with bleomycin for craniopharyngioma in children." Childs Nerv Syst **21**(8-9): 701-704.

Tam, L. C., A. S. Kiang, et al. (2010). "Prevention of autosomal dominant retinitis pigmentosa by systemic drug therapy targeting heat shock protein 90 (Hsp90)." Hum Mol Genet **19**(22): 4421-4436.

Tam, L. C., A. S. Kiang, et al. (2008). "Therapeutic benefit derived from RNAi-mediated ablation of IMPDH1 transcripts in a murine model of autosomal dominant retinitis pigmentosa (RP10)." Hum Mol Genet **17**(14): 2084-2100.

Tan, B. T., K. H. Foong, et al. (2008). "Polyethylenimine-mediated cochlear gene transfer in guinea pigs." Arch Otolaryngol Head Neck Surg **134**(8): 884-891.

Tanaka, K., T. Tsukahara, et al. (1994). "Effect of nerve growth factor on delayed neuronal death after cerebral ischaemia." Acta Neurochir (Wien) **129**(1-2): 64-71.

Tang-Schomer, M. D., V. E. Johnson, et al. (2012). "Partial interruption of axonal transport due to microtubule breakage accounts for the formation of periodic varicosities after traumatic axonal injury." Exp Neurol **233**(1): 364-372.

Tang, M. X. and F. C. Szoka (1997). "The influence of polymer structure on the interactions of cationic polymers with DNA and morphology of the resulting complexes." Gene Ther **4**(8): 823-832.

Taylor, A., W. Butt, et al. (2001). "A randomized trial of very early decompressive craniectomy in children with traumatic brain injury and sustained intracranial hypertension." Childs Nerv Syst **17**(3): 154-162.

Taylor, A. W. and N. Kitaichi (2008). "The diminishment of experimental autoimmune encephalomyelitis (EAE) by neuropeptide alpha-melanocyte stimulating hormone (alpha-MSH) therapy." Brain Behav Immun **22**(5): 639-646.

Terpolilli, N. A., S. W. Kim, et al. (2013). "Inhaled nitric oxide reduces secondary brain damage after traumatic brain injury in mice." J Cereb Blood Flow Metab **33**(2): 311-318.

Thal, S. C., C. Luh, et al. (2012). "Volatile anesthetics influence blood-brain barrier integrity by modulation of tight junction protein expression in traumatic brain injury." PLoS ONE **7**(12): e50752.

Thibault, L. E., D. F. Meaney, et al. (1992). "Biomechanical aspects of a fluid percussion model of brain injury." J Neurotrauma **9**(4): 311-322.

Thibeault, I., N. Laflamme, et al. (2001). "Regulation of the gene encoding the monocyte chemoattractant protein 1 (MCP-1) in the mouse and rat brain in response to circulating LPS and proinflammatory cytokines." J Comp Neurol **434**(4): 461-477.

Timofeev, I., J. Nortje, et al. (2013). "Extracellular brain pH with or without hypoxia is a marker of profound metabolic derangement and increased mortality after traumatic brain injury." J Cereb Blood Flow Metab **33**(3): 422-427.

Tinsley, J. H., M. H. Wu, et al. (1999). "Activated neutrophils induce hyperpermeability and phosphorylation of adherens junction proteins in coronary venular endothelial cells." J Biol Chem **274**(35): 24930-24934.

Toft-Hansen, H., R. Buist, et al. (2006). "Metalloproteinases control brain inflammation induced by pertussis toxin in mice overexpressing the chemokine CCL2 in the central nervous system." J Immunol **177**(10): 7242-7249.

Tompkins, P., Y. Tesiram, et al. (2013). "Brain Injury: Neuro-Inflammation, Cognitive Deficit & MRI in a Model of Blast Induced TBI." J Neurotrauma.

Toscano, M. A., A. G. Commodaro, et al. (2006). "Galectin-1 suppresses autoimmune retinal disease by promoting concomitant Th2- and T regulatory-mediated anti-inflammatory responses." J Immunol **176**(10): 6323-6332.

Tran, N. D., S. Kim, et al. (2010). "Aquaporin-1-mediated cerebral edema following traumatic brain injury: effects of acidosis and corticosteroid administration." J Neurosurg **112**(5): 1095-1104.

Trapp, B. D., J. R. Wujek, et al. (2007). "Evidence for synaptic stripping by cortical microglia." Glia **55**(4): 360-368.

Turksen, K. and T. C. Troy (2001). "Claudin-6: a novel tight junction molecule is developmentally regulated in mouse embryonic epithelium." Dev Dyn **222**(2): 292-300.

Ueki, K., Y. Ono, et al. (1996). "CDKN2/p16 or RB alterations occur in the majority of glioblastomas and are inversely correlated." Cancer Res **56**(1): 150-153.

Ueno, M., T. Nakagawa, et al. (2010). "Transporters in the brain endothelial barrier." Curr Med Chem **17**(12): 1125-1138.

Unterberg, A. W., R. Stroop, et al. (1997). "Characterisation of brain edema following "controlled cortical impact injury" in rats." Acta Neurochir Suppl **70**: 106-108.

Uryu, K., X. H. Chen, et al. (2007). "Multiple proteins implicated in neurodegenerative diseases accumulate in axons after brain trauma in humans." Exp Neurol **208**(2): 185-192.

Vajda, Z., M. Pedersen, et al. (2002). "Delayed onset of brain edema and mislocalization of aquaporin-4 in dystrophin-null transgenic mice." Proc Natl Acad Sci U S A **99**(20): 13131-13136.

Valli, A., J. C. Oliveros, et al. (2011). "The specific binding to 21-nt double-stranded RNAs is crucial for the anti-silencing activity of Cucumber vein yellowing virus P1b and perturbs endogenous small RNA populations." RNA **17**(6): 1148-1158.

Van Itallie, C. M. and J. M. Anderson (2004). "The molecular physiology of tight junction pores." Physiology (Bethes Da) **19**: 331-338.

Van Itallie, C. M., O. R. Colegio, et al. (2004). "The cytoplasmic tails of claudins can influence tight junction barrier properties through effects on protein stability." J Membr Biol **199**(1): 29-38.

Van Itallie, C. M., T. M. Gambling, et al. (2005). "Palmitoylation of claudins is required for efficient tight-junction localization." J Cell Sci **118**(Pt 7): 1427-1436.

van Landeghem, F. K., J. F. Stover, et al. (2001). "Early expression of glutamate transporter proteins in ramified microglia after controlled cortical impact injury in the rat." Glia **35**(3): 167-179.

Van Meir, E. G., P. J. Polverini, et al. (1994). "Release of an inhibitor of angiogenesis upon induction of wild type p53 expression in glioblastoma cells." Nat Genet **8**(2): 171-176.

Van Meter, T. E., W. C. Broaddus, et al. (2004). "Induction of membrane-type-1 matrix metalloproteinase by epidermal growth factor-mediated signaling in gliomas." Neuro Oncol **6**(3): 188-199.

Veitch, D. P., E. K. Friedl, et al. (2013). "Military Risk Factors for Cognitive Decline, Dementia and Alzheimer's Disease." Curr Alzheimer Res.

Wakabayashi, T., J. Yoshida, et al. (2001). "Intratumoral microinfusion of nimustine (ACNU) for recurrent glioma." Brain Tumor Pathol **18**(1): 23-28.

Wang, H., W. Shen, et al. (2003). "Insulin-like growth factor binding protein 2 enhances glioblastoma invasion by activating invasion-enhancing genes." Cancer Res **63**(15): 4315-4321.

Weber, M., P. Grolimund, et al. (1990). "Evaluation of posttraumatic cerebral blood flow velocities by transcranial Doppler ultrasonography." Neurosurgery **27**(1): 106-112.

Wiendl, H., U. Feger, et al. (2005). "Expression of the immune-tolerogenic major histocompatibility molecule HLA-G in multiple sclerosis: implications for CNS immunity." Brain **128**(Pt 11): 2689-2704.

Wightman, B., I. Ha, et al. (1993). "Posttranscriptional regulation of the heterochronic gene lin-14 by lin-4 mediates temporal pattern formation in C. elegans." Cell **75**(5): 855-862.

Willis, C. L. (2012). "Imaging in vivo astrocyte/endothelial cell interactions at the blood-brain barrier." Methods Mol Biol **814**: 515-529.

Willis, C. L., L. Leach, et al. (2004). "Reversible disruption of tight junction complexes in the rat blood-brain barrier, following transitory focal astrocyte loss." Glia **48**(1): 1-13.

Wolburg, H., K. Wolburg-Buchholz, et al. (2003). "Localization of claudin-3 in tight junctions of the blood-brain barrier is selectively lost during experimental autoimmune encephalomyelitis and human glioblastoma multiforme." Acta Neuropathol **105**(6): 586-592.

Wolf, J. A., P. K. Stys, et al. (2001). "Traumatic axonal injury induces calcium influx modulated by tetrodotoxin-sensitive sodium channels." J Neurosci **21**(6): 1923-1930.

Wolpe, S. D., B. Sherry, et al. (1989). "Identification and characterization of macrophage inflammatory protein 2." Proc Natl Acad Sci U S A **86**(2): 612-616.

Wu, V. M., J. Schulte, et al. (2004). "Sinuous is a Drosophila claudin required for septate junction organization and epithelial tube size control." J Cell Biol **164**(2): 313-323.

Wu, Y., S. W. Song, et al. (2010). "IIp45 inhibits cell migration through inhibition of HDAC6." J Biol Chem **285**(6): 3554-3560.

Yamasaki, Y., N. Matsuura, et al. (1995). "Interleukin-1 as a pathogenetic mediator of ischemic brain damage in rats." Stroke **26**(4): 676-680; discussion 681.

Yamauchi, K., T. Rai, et al. (2004). "Disease-causing mutant WNK4 increases paracellular chloride permeability and phosphorylates claudins." Proc Natl Acad Sci U S A **101**(13): 4690-4694.

Yan, N., A. D. Regalado-Magdos, et al. (2010). "The cytosolic exonuclease TREX1 inhibits the innate immune response to human immunodeficiency virus type 1." Nat Immunol **11**(11): 1005-1013.

Yang, Z., C. Stratton, et al. (2008). "Toll-like receptor 3 and geographic atrophy in age-related macular degeneration." N Engl J Med **359**(14): 1456-1463.

Yoshino, A., D. A. Hovda, et al. (1991). "Dynamic changes in local cerebral glucose utilization following cerebral conclusion in rats: evidence of a hyper- and subsequent hypometabolic state." Brain Res **561**(1): 106-119.

You, S. J., S. H. Lee, et al. (2010). "Kinetic analysis of RNA interference for lamin A/C in HeLa cells." Acta Biochim Biophys Sin (Shanghai) **42**(9): 623-627.

Zerangue, N. and M. P. Kavanaugh (1996). "Flux coupling in a neuronal glutamate transporter." Nature **383**(6601): 634-637.

Zhang, M. and Y. Olsson (1997). "Hematogenous metastases of the human brain--characteristics of peritumoral brain changes: a review." J Neurooncol **35**(1): 81-89.

Zhang, P., X. Liu, et al. (2013). "Honokiol inhibits the inflammatory reaction during cerebral ischemia reperfusion by suppressing NF-kappaB activation and cytokine production of glial cells." Neurosci Lett **534**: 123-127.

Zhang, R. D., J. E. Price, et al. (1992). "Differential permeability of the blood-brain barrier in experimental brain metastases produced by human neoplasms implanted into nude mice." Am J Pathol **141**(5): 1115-1124.

Zhao, J., A. N. Moore, et al. (2005). "Sulforaphane enhances aquaporin-4 expression and decreases cerebral edema following traumatic brain injury." J Neurosci Res **82**(4): 499-506.

Zhou, Z., H. Chen, et al. (2003). "Protective effect of nerve growth factor on neurons after traumatic brain injury." J Basic Clin Physiol Pharmacol **14**(3): 217-224.

Zlokovic, B. V. (2008). "The blood-brain barrier in health and chronic neurodegenerative disorders." Neuron **57**(2): 178-201.

Zlotnik, A., A. Leibowitz, et al. (2012). "Effect of estrogens on blood glutamate levels in relation to neurological outcome after TBI in male rats." Intensive Care Med **38**(1): 137-144.